Università degli Studi di Napoli Federico II

Doctorate Course in Chemical Sciences – XXXI Cycle

Polyolefins by hydrogenation of stereoregular poly(1,3-diene)s and chain-walking polymerization: synthesis, structure and mechanical properties

Ivana Pierro

Supervisor:
Prof. Claudio De Rosa (UniNA)
Co-supervisor:
Dr. Giovanni Ricci (CNR-ISMAC)

Coordinator:
Prof. Luigi Paduano (UniNA)

2015 - 2018

Abstract

A deep understanding of the structure-property relationship of polymeric materials is essential if you want to design the synthesis of new olefin homo- and copolymers with improved properties.

In this regard, the aim of this study was to develop new methods for the synthesis of stereoregular polyolefins with a controlled microstructure and tunable level of branching, subsequently carrying out a complete characterization of the thermal, structural and mechanical properties of the polymers obtained.

In particular, two different synthetic strategies were developed:

1) the first one is related to the synthesis of highly stereoregular poly(1,3-diene)s having different structures and their successive hydrogenation with diimide, formed in situ by thermal decomposition of *p*-toluenesulfonyl hydrazide;

2) the second one regards the synthesis of branched and hyperbranched polyolefins through the chain-walking (co)polymerization of long chain α-olefins. These polyolefins were obtained by using a series of traditional α-diimine Ni(II) complexes with methyl ligand backbone and different substituents in *ortho*- and *para*- aryl positions as catalyst components, in combination with different aluminum alkyls.

All the obtained polymers were fully characterized, in order to establish correlations between their structures and properties, and to evaluate their possible applications as thermoplastic and/or elastomeric materials.

As concern the first synthetic strategy highly stereoregular poly(1,3-diene)s having different structures (*i.e.*, *cis*-1,4; *trans*-1,4; 1,2; 3,4; iso-and syndiotactic) were synthesized by polymerizing various 1,3-dienes with catalytic systems based on transition metal and lanthanide organometallic compounds. The polymers obtained were successively hydrogenated for producing a whole series of stereoregular olefin homopolymers and perfectly alternating copolymers which, in most cases, were not obtainable through the simple stereospecific polymerization of the corresponding monomers.

In particular, I obtained *i)* highly stereoregular polyolefins from 1,2 and 3,4 polydienes and *ii)* perfectly alternating ethylene/α-olefin copolymers from 1,4 (*cis* and *trans*) poly(1,3-diene)s.

Some of the polymers obtained exhibited interesting properties for possible application as thermoplastic and elastomeric materials. Moreover, their use as model polymers, is useful for evaluating similar polymers.

As concern the second synthetic strategy I reported a systematic investigation on the chain-walking polymerization of higher linear α-olefins (1-octene, 1-decene, 1-octadecene) catalyzed by traditional α-diimine Ni(II) complexes with methyl α-diimine backbone and different aryl *ortho*- (H, Me, Et, ^{i}Pr, ^{t}Bu) and *para*- (H, Me) substituents. The effect of ligand steric and electronic perturbation on the catalytic behavior, monomer enchainment, and polymer properties is discussed.

Unlike 1-octene and 1-decene polymers, which behave as elastomers, long chain 1-octadecene polymers behave as plastomers, showing evident yielding phenomena and plastic deformation.

These polyolefins show different properties depending on the branching level and branches-type distribution.

These systems prove great prospect due to the low cost and accessibility of starting reagents and monomer feedstocks, the high turnovers/h together with the reusability of the resulting polymers that retain excellent mechanical properties even after being melted and reprocessed several times.

Index

Pag.

Chapter III

Chain-walking: An Approach to Control Polymer Microstructure

Chapter IV

Chain-Walking Polymerization of α-Olefins by α-Diimine Ni(II) Complexes

Introduction

POLYOLEFINS: AN INTEGRAL PART OF DAILY LIFE

Poly(olefin)s (POs), the generic name for synthetic polymers based on ethylene, propylene, and α-olefins, have become the world's most common synthetic polymers. The current trend suggests that POs global installed capacity growth is expected to increase by 4-5% over the next few years. This growth will be powered by a series of breakthroughs in development of different classes of well-defined transition metal complexes[1-3], living insertion/coordination polymerization[4], and synthesis of differentiated and more complex polymers and crystalline structures.[5,6]

Polyolefins (LDPE, LLDPE, HDPE and PP) account for more than 50% of global plastics materials demand (Figure 1).

The global production of plastics is a sector in continuous growth for more than 50 years, and still nowadays. In 2016 the global production of plastic materials (thermoplastics and polyurethanes) and other plastics (thermosets, adhesives, coatings and sealants) was of 335 millions of tons.[7]

Polyolefins are used in a wide variety of applications, including engineering plastics, containers, toys, adhesives, grocery bags, home appliances, automotive parts, medical applications, and prosthetic implants.

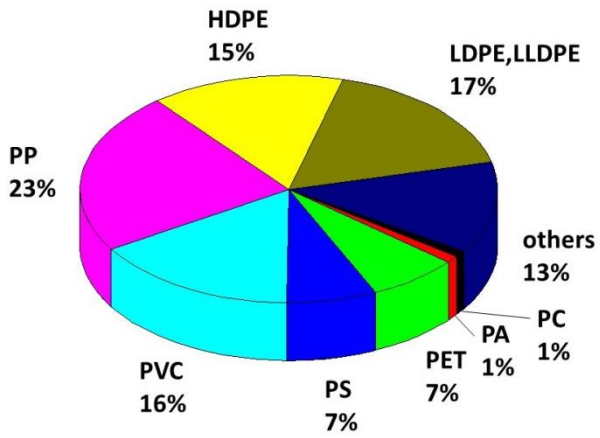

Figure 1. *World Plastics Materials Demand 2015 by Types (Source: Plastic Europe Market Research Group).*

Polymeric materials can be classified as thermosets and thermoplastics.

Thermoset is a polymer which is irreversibly cured by heat or chemical reaction. It results in cross-linking between polymer chains to give an infusible and insoluble material. The polymerization is controlled to result in strongly cross linked short chains for rigid product and lightly cross linked long chains for flexible products.

Thermoplastic is a polymer which softens above a specific temperature and hardens when cooled. Thermoplastic materials are made of linear molecular chains. Thermoplastics may be reshaped by heating and are typically used to produce parts by various polymer processing techniques such as injection molding, compression molding, calendering, and extrusion.[8] The most important physical property of a thermoplastic is its glass transition temperature at which it begins to soften.

The thermoplastic polymers can be amorphous or semi-crystalline. The difference between the two lies in their molecular structure.

Thermoplastics semi-crystalline are usually opaque and include polypropylene (PP), polyethylene (PE). They have a highly ordered molecular structure with characteristics such as sharp melt points, better strength, improved fatigue performance, good chemical resistance and improved wear resistance.

Thermoplastics amorphous are usually translucent. They have a randomly ordered molecular structure that gives them a wider range of temperatures over which they soften. Examples are polycarbonate (PC), polymethylmethacrylate (PMMA), polystyrene (PS), polyphenylene oxide (PPO), acrylonitrile butadiene styrene (ABS).

Polyolefin thermoplastic elastomers (TPEs) are another important class of materials. TPEs combine the processing advantages (*i.e.*, they can be processed by injection molding, extrusion, and blow molding) and recycling potential of thermoplastics with the flexibility, low modulus, and soft touch of elastomers.[9,10] A two-phase molecular structure usually gives TPEs their combination of strength and flexibility: amorphous domains in the polymer are soft and provide its elastomeric nature, while the hard crystalline segments, usually dispersed throughout the amorphous matrix, form physical cross-links that give tensile strength, resistance to chemicals, and produce recoverable elasticity after strain-induced deformation.[11] Physical properties and elasticity of TPEs strongly depend on the distribution of crystalline and amorphous regions and polymer microstructure.[12-14]

It is therefore fundamental to understand the structure-property relationships of polymeric materials at the molecular level, from which we can get an idea of what may be possible in the future.

A possibility to achieve this objective is offered by the development of novel methods of controlled synthesis of polymers that have increased our control over the molecular structure of the produced macromolecules, in terms of molecular masses and their distribution, stereo- and regio-regularity, type and distribution of defects and molecular architecture, such as stereospecific polymerization by organometallic catalysis, controlled radical and anionic polymerizations and strategies of combined polymerizations.

Catalyst design is behind the success of modern industrial olefin polymerization processes because the catalyst determines how the monomers will be linked in the polymer chain, effectively defining the polymer microstructure and properties. Industrial and academic research on olefin polymerization catalysis have been very dynamic since the original discoveries of Ziegler and Natta (Ziegler–Natta catalysts) and Hogan and Banks (Phillips catalysts), with many catalyst families being developed and optimized at a rapid pace.[15] There are basically four main types of olefin polymerization catalysts: (*i*) Ziegler–Natta catalysts, (*ii*) Phillips catalysts, (*iii*) metallocene catalysts, and (i*v*) late transition metal catalysts.

Ziegler–Natta and Phillips catalyst were discovered in the early 1950s, initiating a paradigm shift in olefin polymerization processes, while metallocene and late transition metal catalysts (sometimes called post-metallocenes) were developed in the 1980s and 1990s, respectively.

These systems have afforded a unique opportunity for controlling the final physical properties.

Precise control over product structure is the goal of all chemical synthesis. In particular in the field of polymer synthesis, the structure of the resultant macromolecules are intimately linked to their material properties, which ultimately determine their potential applications of it.

Scope and outline of this thesis

The research activity of my PhD project concerns the synthesis of innovative polyolefins with thermoplastic and/or elastomeric properties, through two different approaches. The first one involves the preparation of stereoregular poly(1,3-diene)s, obtained by polymerizing the corresponding 1,3-dienes with transition metal and lanthanide based catalysts, and successive hydrogenation. The second approach involves the preparation of branched polyolefins through the chain-walking polymerization of α-olefins catalyzed by α-diimine late transition metal complexes.

This thesis is divided into four chapter.

- **Chapter I** introduces the recent developments in the field of catalytic systems for the stereospecific polymerization of 1,3-dienes and the basic principles of hydrogenation method, allowing to synthesize a whole series of olefin homopolymers and copolymers which, in most cases, are not obtainable through the simple stereospecific polymerization of the corresponding monomers.
- In **Chapter II**, the synthesis of polydienes with a 1,4 structure and of ethylene-α-olefin alternating copolymers obtained through hydrogenation reaction of the 1,4-polydienes is described. The synthesis of polydienes with a 1,2 or 3,4 structure, and of the branched polyolefins resulting from their hydrogenation, is also reported. All the polymers obtained were studied by structural and thermal analysis, and their mechanical properties were examined in order to evaluate the potential for elastomeric and thermoplastic applications.
- **Chapter III** introduces the chain-walking mechanism involved in the polymerization of ethylene and long chain α-olefins to produce polyolefins with short and long branches.
- In **Chapter IV** the synthesis and characterization of homo- and copolymers from 1-octene, 1-decene, 1-octadecene and cyclopentene are described. All the (co)polymers were obtained with catalysts based on a series of α-diimine Nickel(II) complexes with methyl ligand backbone and different substituents in the *ortho* and *para* aryl positions. The effect of ligand steric and electronic perturbation on the catalytic behavior, monomer enchainment, and polymer properties is discussed.

References

[1] Klosin, J. ; Fontaine, P.P.; Figueroa, R. *Acc. Chem. Res.* **2015***, 48,* 2004-2016*.*

[2] Baier, M.C.; Zuideveld, M.A.; Mecking, S. *Angew. Chem. Int. Ed.* **2014,** *53,* 9722-9744.

[3] McInnis, J.P.; Delferro, M.; Marks, T.J. *Acc. Chem. Res.* **2014***, 47,* 2545-2557.

[4] Coates*, G.W.; Hustad, P.D.; Reinartz, S. Angew. Chem. Int. Ed.* **2002***, 41,* 2236-2257.

[5] Stürzel, M.; Mihan, S.; Mülhaupt, R. *Chem. Rev*. **2016**, *116*, 1398-1433.

[6] Chen, Y.; Wang, L.; Yu, H.; Zhao, Y.; Sun, R.; Jing, G.; Huang, J.; Khalid, H.; Abbasi, M. Akram, N.M*. Prog. Polym. Sci.* **2015**, *45*, 23-43.

[7] Plastics – the Facts 2017, PlasticsEurope.

[8] https://en.wikipedia.org/wiki/Thermoplastic

[9] Holden, G.; Kricheldorf, H. R.; Quirk, R. P. Thermoplastic Elastomers, 3rd ed.; Hanser Publishers: Munich, **2004**.

[10] Drobny, J. G. Handbook of Thermoplastic Elastomers; William Andrews: New York, **2007**.

[11] Deplace, F.; Scholz, A. K.; Fredrickson, G. H.; Kramer, E. J.; Shin, Y.-W.; Shimizu, F.; Zuo, F.; Rong, L.; Hsiao, B. S.; Coates, G. W. *Macromolecules* **2012**, *45*, 5604−5618.

[12] De Rosa, C.; Auriemma, F.; Perretta, C. *Macromolecules* **2004**, *37*, 6843−6855.

[13] Hong, K.; Strobl, G. *Macromolecules* **2006**, *39,* 268−273.

[14] Hiss, R.; Hobeika, S.; Lynn, C.; Strobl, G. *Macromolecules* **1999**, *32*, 4390−4403.

[15] Polyolefin Reaction Engineering, First Edition. João B. P. Soares and Timothy F. L. McKenna. © **2012** Wiley-VCH Verlag GmbH & Co. KGaA.

Chapter I

1,3-Dienes Polymerization and Hydrogenation Method

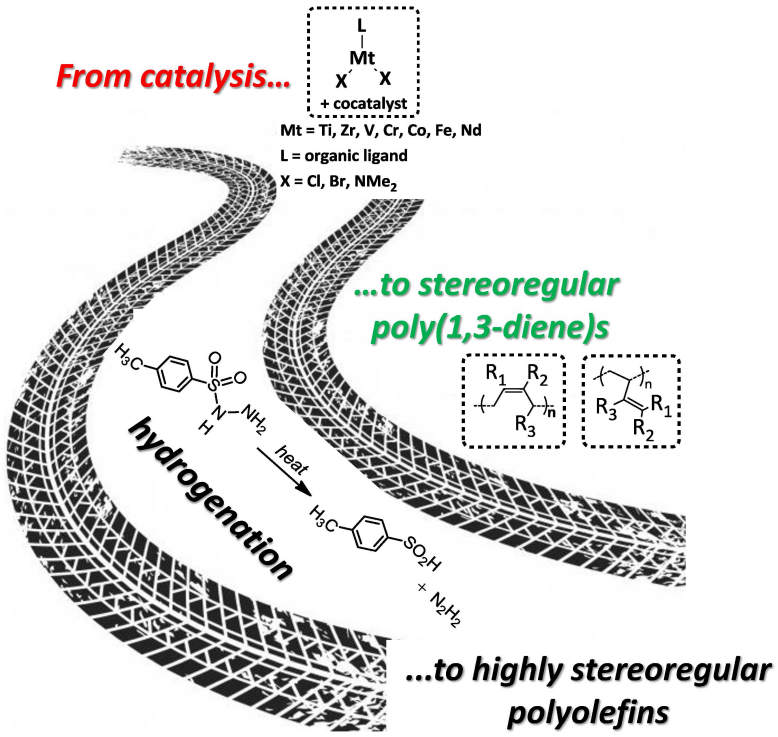

1.1 Catalytic systems for the stereospecific polymerization of 1,3-dienes

The stereospecific polymerization of conjugated dienes began in 1954 with the first catalysts obtained by combining $TiCl_4$ or $TiCl_3$ with aluminum-alkyls, *i.e*. the catalytic systems previously employed for ethylene and propylene polymerizations. Subsequently, many other catalytic systems were obtained and examined by a combination of transition metal or lanthanide compounds with appropriate alkylating agents.[1-3] With the advent of MAO (methylaluminoxane) as alkylating agent, at the beginning of the 1980s,[4,5] new catalytic systems were introduced, in some cases much more active and stereospecific than those based on common aluminum-alkyls.[6-12] In particular, MAO allowed the use of catalyst precursors such as cyclopentadienyl derivatives of transition metals (*e.g*., $CpTiCl_3$, Cp_2TiCl_2, $CpVCl_2$),[13-18] practically inactive in combination with the normal aluminum-alkyls, providing highly active and stereospecific catalytic systems, also capable of polymerizing monomers such as (*Z*)-1,3-pentadiene [19-21] and 4-methyl-1,3-pentadiene,[13,16-18,22] which could not be polymerized with the common Ziegler-Natta catalysts.

Starting from the 2000s, in the wake of what happened in the case of mono-olefins, [23-40] a new generation of catalysts based on complexes of transition metals and lanthanides with various ligands containing donor atoms such as P, N, O (*e.g.*, phosphines, imines, imino-pyridines, cheto-imines) has been introduced. These systems have proved particularly active and able to provide polymers with controlled microstructure (*i.e.*, *cis*-1,4; 1,2; mixed *cis*-1,4/1,2 with a variable 1,2 content) [41-52] from several types of 1,3-dienes (*i.e*., isoprene, 2,3-dimethyl-1,3-butadiene, 1,3-pentadiene, 1,3-hexadiene, 3-methyl-1,3-pentadiene, 1,3-heptadiene, 1,3-octadiene, and 5-methyl-1,3-hexadiene).

In general, the regio- and stereo-selectivity in the polymerization of 1,3-dienes with transition metal complexes-based catalysts were strongly affected by the catalyst structure (*i.e*., type of ligand bonded to the metal atom) and by the monomer structure.[41,43,44,47,48,51]

By using the appropriate combination of catalyst structure (*i.e.*, type of metal, type of ligand, and type of alkylating agent) and monomer structure (different types of substituted 1,3-butadienes) we were able to obtain several highly stereoregular 1,4 and 1,2 (or 3,4), iso- and syndiotactic, polydienes useful for the preparation of stereoregular polyolefins and perfectly alternating ethylene/α-

olefin copolymers through their hydrogenation. The transition metal and lanthanide catalysts used and the different stereoregular polydienes with them obtained are listed below.

Cobalt catalyst

Cobalt catalysts are probably the most versatile among the various catalytic system based on transition metals for the polymerization of 1,3-dienes. In recent years, new catalytic systems have been developed by combination of MAO with phosphine $CoCl_2$ complexes. [4,5,44,49,50,53-55]

The peculiarity of such novel systems lies in their ability to allow the formation of poly(diene)s with controlled microstructure (*cis*-1,4; 1,2; and *cis*-1,4/1,2 mixed structure) depending on the type of ligand coordinated to the Co atom.[56]

For example, the system $CoCl_2(P^tBu_2Me)_2$-MAO gave highly syndiotactic *cis*-1,4 polymers (Figure 1.1) from different types of terminally substituted 1,3-dienes such as (*E*)-1,3-pentadiene, (*E*)-1,3-hexadiene, (*E*)-3-methyl-1,3-pentadiene, (*E*)-1,3-heptadiene and (*E*)-1,3-octadiene, while highly 1,2 polymers, iso- or syndiotactic depending on the monomer structure, were obtained with the system $CoCl_2(P^iPrPh_2)_2$-MAO from the same monomers (Figure 1.2). A particular structure, perfectly alternating *cis*-1,4-*alt*-3,4, definitely uncommon in the field of stereospecific polymerization, was obtained from isoprene (Figure 1.2).

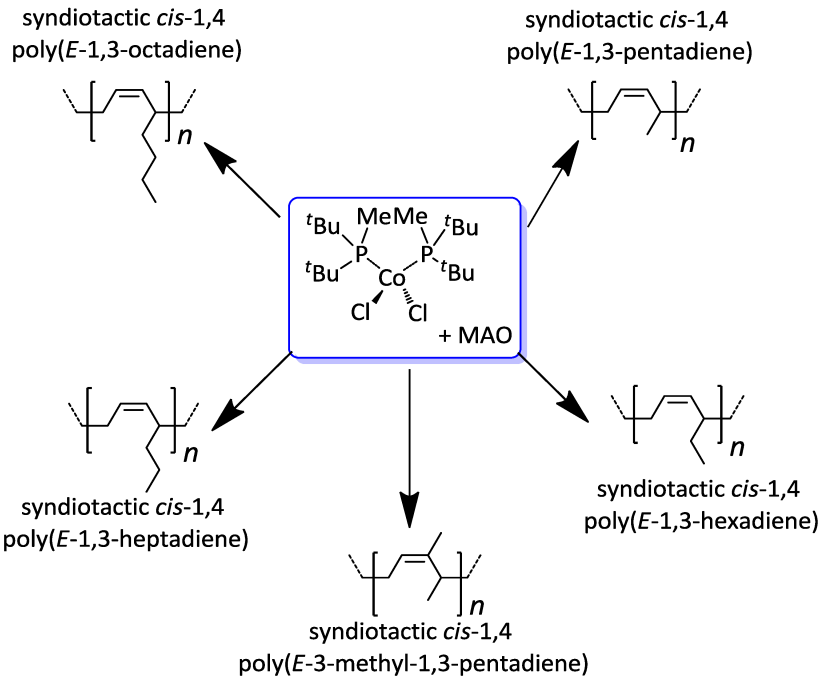

Figure 1.1. *Example of syndiotactic cis-1,4 polymers obtained by system $CoCl_2(P^tBu_2Me)_2$-MAO.*

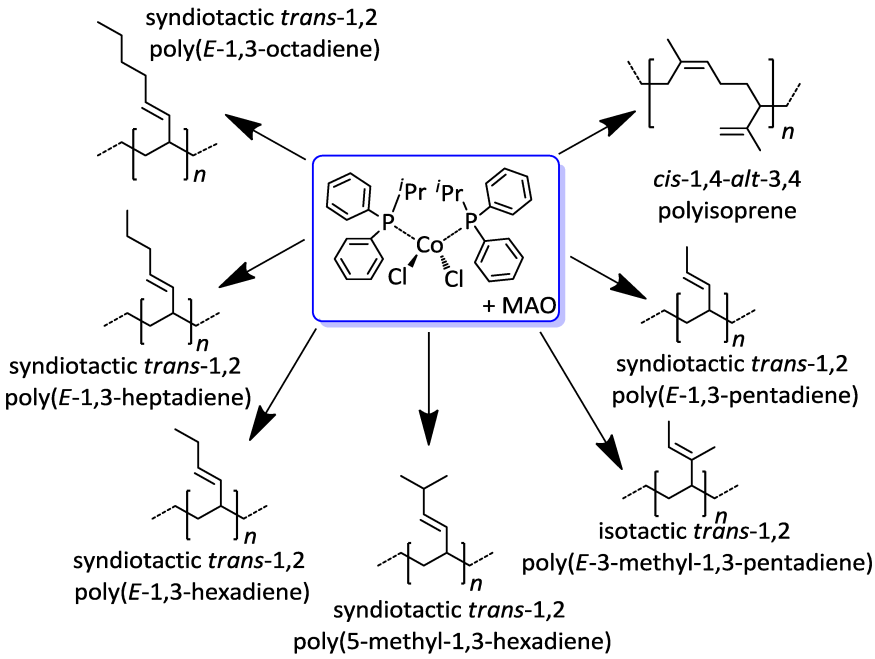

Figure 1.2. *Example of 1,2 polymers, iso- or syndiotactic, obtained by system $CoCl_2(P^iPrPh_2)_2$-MAO.*

Iron catalyst

Extremely active catalysts were obtained by combining Fe(II) complexes such as $FeCl_2(bipy)_2$ or $FeCl_2(phen)_2$ (bipy = bipyridine; phen = phenantroline) with aluminum-alkyls (*e.g.*, $Al(^iBu)_3$, $AlEt_3$, MAO). [43-45,57]

These systems gave predominantly syndiotactic 1,2 polymers from butadiene, highly syndiotactic 3,4 polymers from isoprene, highly syndiotactic 1,2 polymers from 3-methyl-1,3-pentadiene, but exclusively *cis*-1,4 polymers from 2,3-dimethyl-1,3-butadiene, pointing out the strong influence of the monomer structure on the polymerization regio-selectivity.

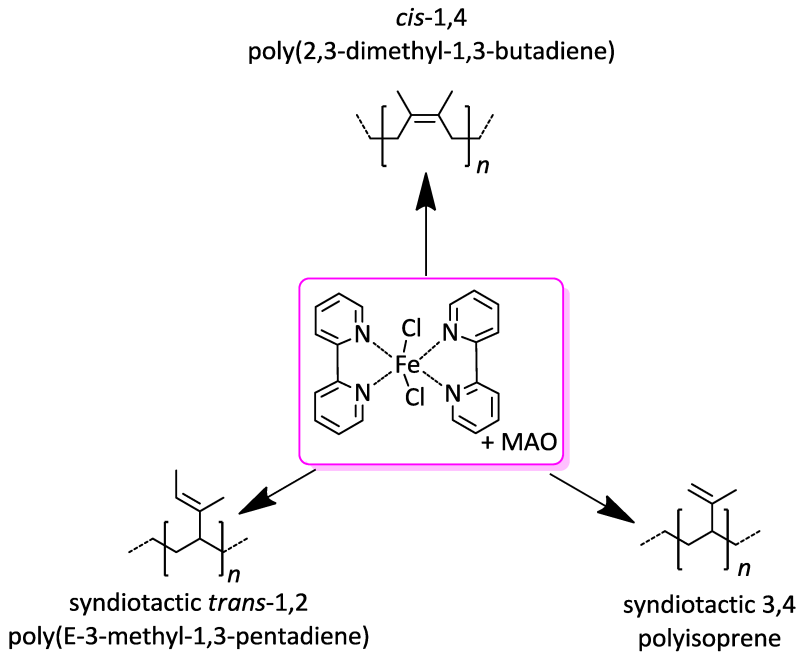

Figure 1.3. *Example of polymers, obtained by system $FeCl_2(bipy)_2$.*

Nickel catalyst

A wide variety of Ni based catalysts (*e.g.*, $Ni(naph)_2$-$AlEt_2Cl$-H_2O, naph = naphthenate; $NiCp_2$-MAO; $Ni(acac)_2$-MAO) has been reported in the literature as active catalysts in the butadiene polymerization.[1,2,54,58- 60]

Some of them exhibit activity and stereospecificity comparable with those of Co.

The system $Ni(acac)_2$-MAO in particular was able to polymerize different types of substituted 1,3-butdienes, and in case of (*E*)-3-methyl-1,3-pentadiene a highly syndiotactic *cis*-1,4 polymer was obtained[11] (Figure 1.4).

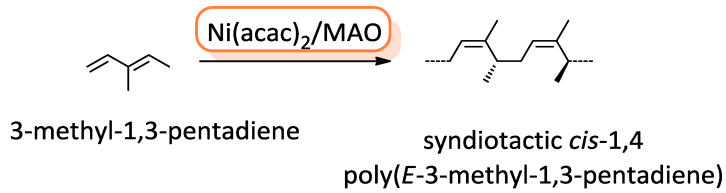

Figure 1.4. *Example of polymer, obtained by system $Ni(acac)_2$-MAO.*

Lanthanide catalyst

Lanthanide catalysts are known to be specific for the *cis* polymerization of 1,3-dienes, butadiene in particular.[1-3,58] Conventional lanthanide catalysts, Nd in particular, are typically obtained by reacting a Nd-compound (*e.g.*, $Nd(acac)_3$; $Nd(OCOC_7H_{15})_3$) with a chlorine donor (*e.g.*, Et_2AlCl; $Al_2Et_3Cl_3$, *tert*-butyl chloride) and an aluminum alkyl (*e.g.*, Al^iBu_3, Al^iBu_2H). [61-65]

The ternary system $AlEt_2Cl$-$Nd(OCOR)_3$-Al^iBu_3 (R = alkyl group) so obtained is actually used for the commercial production of *cis* poly(butadiene).

The same system was able to polymerize various types of terminally substituted 1,3-butadienes giving polymers with a very high isotactic *cis*-1,4 structure, with the exception of (*E,E*)-2,4-hexadiene, which gave diisotactic *trans*-1,4 polymers (Figure 1.5).

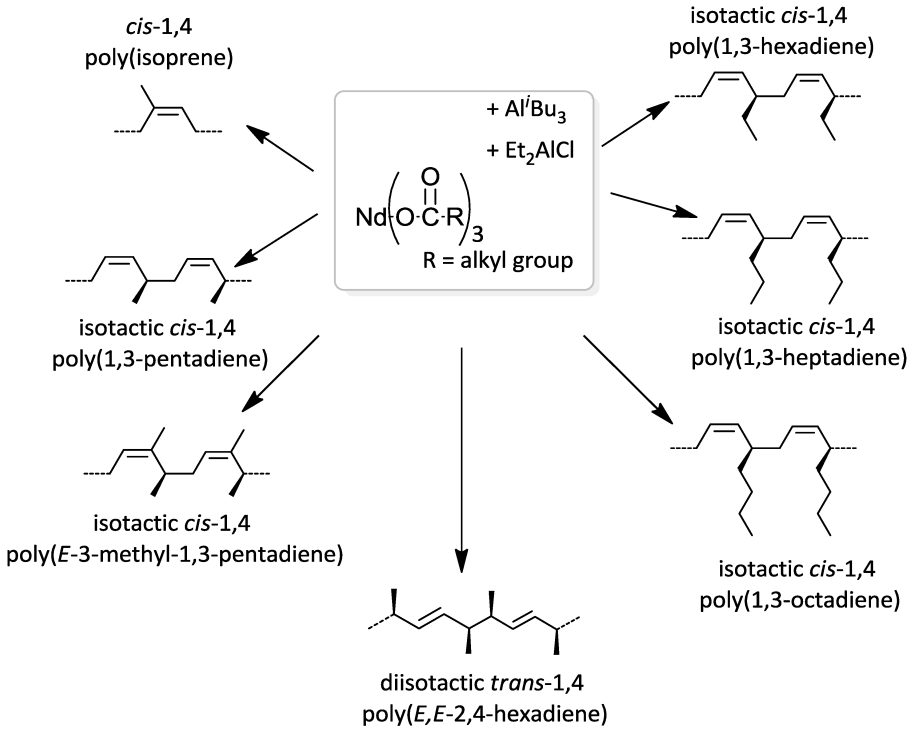

Figure 1.5. *Example of polymers, obtained by system Et_2AlCl-$Nd(OCOR)_3$-$Al^{i}Bu_3$.*

The results obtained in the polymerization of 1,3-dienes (*i.e.*, 1,3-butadiene and substituted 1,3-dienes) with various type of catalysts, that is polymers having different structure (*cis*-1,4; *trans*-1,4; 1,2; 3,4; iso- and syndiotactic) from the different monomers, were very important from a scientific point of view, since they permitted to improve our knowledge on the diene polymerization mechanism, in particular pointing out the fundamental role played by the catalyst structure (*i.e.*, nature of the ligand on the metal atom), the monomer structure (*i.e.*, presence of substituents on the monomeric unit) and definitely the combination of these two factors, on the polymerization regio- and stereo-selectivity.

At the same time, the availability of all these highly stereoregular polymers may allow, at least in principle, to synthesize, via hydrogenation reactions, a whole series of olefin homopolymers and copolymers which, in most cases, are not obtainable through the simple stereospecific polymerization of the corresponding monomers.

In particular, by hydrogenation of iso- and syndiotactic *cis*-1,4 polydienes, it is possible to obtain ethylene-α-olefin perfectly alternating copolymers (Figure 1.6),

while through hydrogenation of highly stereoregular 1,2 or 3,4 polydienes, isotactic and syndiotactic, novel stereoregular branched polyolefins can be obtained (Figure 1.7).

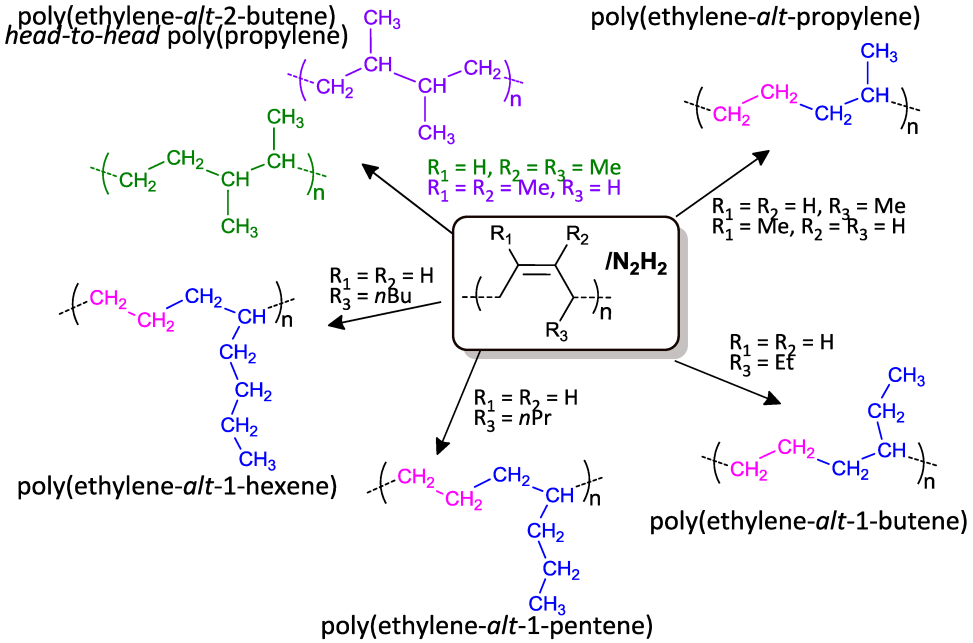

Figure 1.6. *Saturated olefin copolymers which can be obtained by hydrogenation of poly(1,3-diene)s with a 1,4 structure.*

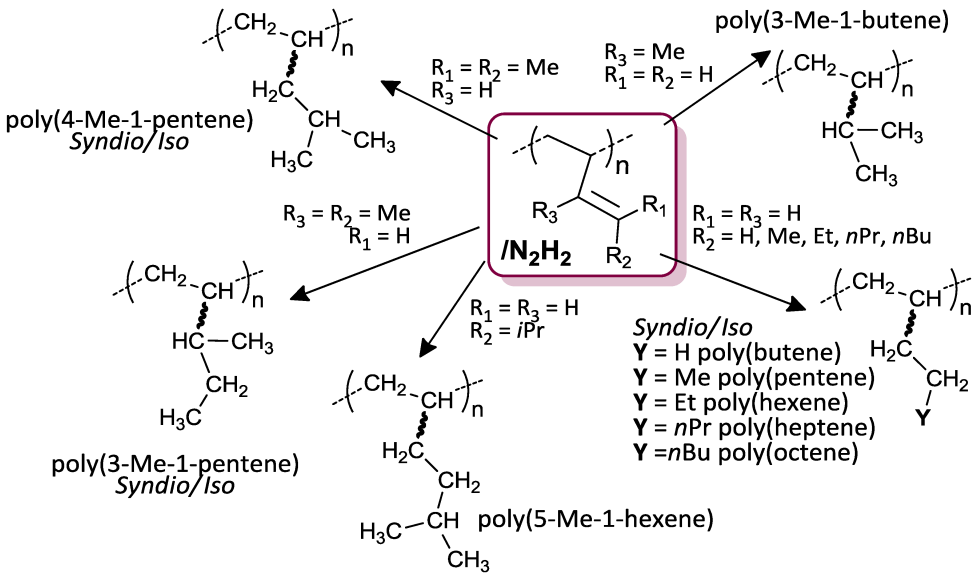

Figure 1.7. *Saturated olefin polymers which can be obtained by hydrogenation of poly(1,3-diene)s with a 1,2 structure.*

In the following paragraph some of the fundamental of the non-catalytic hydrogenation are reported.

1.2 Diimide hydrogenation

Chemical modification of existing polymers has been an active field of research as it leads to polymers with altered and improved properties or production of new materials.[66] Unsaturated polymers, especially diene rubbers, are useful target for chemical modification, because the double bond in the polymer chains are prone to chemical reactions such as epoxidation, halogenation, and maleinization.[67] However, the polymers containing olefinic units have a tendency to be low-heat-resistant materials. Hydrogenation, one type of chemical modification of unsaturated polymers, is an important method to reduce the amount of unsaturation and produce a saturated structure, which is resistant to oxidation and degradation. Therefore, the hydrogenation reaction is expected to improve the thermal and physical properties of polymers. The hydrogenation is also a potential method offering a polymer that cannot be prepared by a simple conventional polymerization reaction. [68-70]

There are many methods to hydrogenate polydienes which involve catalytic and non-catalytic processes.[68,70-72] Catalytic hydrogenation has been the conventional process to hydrogenate polydienes, but some problems are reported, such as high cost of equipment and catalyst, as well as low efficiencies resulting from limited solubility.[82] Hence, some studies investigated the non-catalytic procedure as an alternative to substitute catalytic hydrogenation in unsaturated polymers.[70,72,73,75,76]

The diimide hydrogenation has been drawing much attention since Wideman reported the first diimide hydrogenation of diene-based polymers in 1984.[77] The hydrogenation of diene polymers by diimide is an attractive alternative to the conventional catalytic hydrogenation due to the fact that it could circumvent the requirements for specialized hydrogenation apparatus.

Diimide hydrogenation is a non-catalytic process, in which the hydrogenated polymers are formed through the reduction reaction between the diimide and C=C. The diimide molecule (N_2H_2), the hydrogenation agent, is generated in situ from the thermal decomposition of *p*-toluenesulfonyl hydrazide (*p*-T*s*NH) as shown in equation (1) in Figure 1.9. The decomposition of *p*-T*s*NH also generates a byproduct, the *p*-toluenesulfinic acid. The diimide molecule (N_2H_2) can then

release a hydrogen molecule directly to the carbon-carbon double bonds of isoprene units as represented in equation (2) in Figure 1.8.

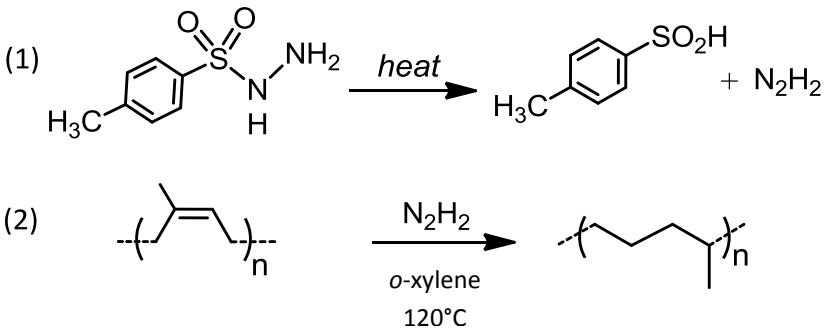

Figure 1.8. *Diimide generation by thermal decomposition of p-TsNH.*

The *p*-toluenesulfinic acid can undergo an ionic or radical addition to yield sulfones and sulfides or, still, it can react with the double bond of pendant vinyl groups or unsaturated bonds along the polymer structure.[71,78-80] Their presence can be monitored by FTIR and ^{1}H-NMR analysis.[78,79,81,82] Typical bands in FTIR analysis are visualized at 1318 cm^{-1} and 1145 cm^{-1}, corresponding to the asymmetric and symmetric stretching of the SO_2 group, at 811 cm^{-1} associated with C-H rocking vibration, and at 1020 cm^{-1} , attributed to the *p*-tolyl aromatic ring. Peaks are detected at 2.4 ppm by ^{1}H-NMR, due to the methyl group attached to an aromatic ring, and at 7.70 ppm due to the hydrogens from the aromatic ring of the *p*-toluenesulfinic group.

References

[1] Porri, L.; Giarrusso, A. Part II: Conjugated Diene Polymerization. In *Comprehensive Polymer Science*; Pergamon: Oxford, UK, 1989; Volume 4, pp. 53–108.

[2] Thiele, S.K.H.; Wilson, D.R. *J. Macromol. Sci, Polym. Rev. C* **2003,** *43*, 581-628.

[3] Friebe, L.; Nuyken, O.; Obrecht, W. *Adv. Polym. Sci.* **2006**, *204*, 1-154.

[4] Sinn, H.; Bliemeister, J.; Clausnitzer, D.; Winter, L.; Zarncke, O. In: Kaminsky W, Sinn H (eds) Transition metals and organometallics as catalysts for olefin polymerization. Springer-Verlag, Berlin Heidelberg, New York, **1998**, 257-268

[5] Bliemeister J, Hagendorf W, Harder A, Heitmann B, Schimmel I, Schmedt E, Schnuchel W, Sinn H, Tikwe L, von Thiene N, Urlass K, Winter H, Zarncke O. In: Fink

G, Mülhaupt R, Brintzinger HH (eds) Ziegler catalysts. Springer- Verlag, Berlin Heidelberg, New York, **1995**, 57-82.
[6] Ricci, G.; Italia, S.; Comitani, C.; Porri, L. *Polym. Commun*. **1991**, *32*, 514-517.
[7] Ricci, G.; Italia, S.; Porri, L. *Macromol. Chem. Phys.* **1994**, *195*, 1389-1397.
[8] Ricci, G.; Porri, L. *Polymer,* **1997**, *38*, 4499-4503.
[9] Ricci, G.; Zetta, L.; Alberti, E.; Motta, T.; Canetti, M.; Bertini, F. *J. Polym. Sci. Part A: Polym.Chem.* **2007**, *45*, 4635-4646.
[10] Zambelli, A.; Ammendola, P.; Proto, A. *Macromolecules*, **1989**, *22*, 2126-2128.
[11] Oliva, L.; Longo, P.; Grassi, A.; Ammendola, P.; Pellecchia, C. *Die Makromol. Chem. Rapid Commun.* **1990,** *11*, 519-524.
[12] Venditto, V.; De Rosa, C.; Guerra, G.; Napolitano, R. *Polymer* **1992**, *33*, 3547-3551.
[13] Ricci, G.; Italia, S.; Giarrusso, A.; Porri, L*. J. Organomet. Chem*. **1993**, *451*, 67-72.
[14] Ricci, G.; Panagia, A.; Porri, L. *Polymer* **1996**, *37,* 363-365.
[15] Ricci, G.; Bosisio, C.; Porri, L. *Macromol. Chem. Rapid Commun.* **1996**, *17*, 781-785.
[16] Porri L, Ricci G, Giarrusso A. In: Kaminsky W (ed) Metal organic catalysts for synthesis and polymerization. Springer-Verlag, Berlin, Heidelberg, **1999**, 519-530.
[17] Porri, L.; Giarrusso, A.; Ricci, G. In: Scheirs J, Kaminsky W (eds) Metallocene-based polyolefins. John Wiley, New York, **2000**, 115-141.
[18] Longo, P.; Oliva, P.; Proto, A.; Zambelli, A. *Gazzetta Chimica italiana*, **1996,** *126,* 377-382.
[19] Ricci, G.; Italia, S.; Porri, L. *Macromolecules*, **1994,** *27*, 868-869.
[20] Ricci, G.; Alberti, E.; Zetta, L.; Motta, T.; Bertini, F.; Mendichi, R.; Arosio, P.; Famulari, A.; Meille, S.V. *Macromolecules,* **2005**, *38*, 8353-8361.
[21] Longo, P.; Guerra, G.; Grisi, F.; Pizzuti, S. Zambelli, A. *Macromol. Chem. Phys.* **1998**, *199*, 149-154.
[22] Ricci, G.; Porri, L. *Macromol. Chem. Phys.* **1997**, *198,* 3647-3650.
[23] Johnson, L.K.; Killian, C.M.; Brookhart, M. *J.Am.Chem.Soc*.**1995**, *117*, 6414-6415.
[24] Killian, C.M.; Tempel, D.J.; Johnson, L.K.; Brookhart, M. *J. Am. Chem. Soc*. **1996,** *118*, 11664-11665.
[25] Killian, C.M.; Johnson, L.K.; Brookhart, M. *Organometallics* **1997**, *16*, 2005-2007.

[26] Mecking, S.; Johnson, L.K.; Wang, L.; Brookhart, M. *J. Am. Chem. Soc.* **1998**, *120*, 888-899.
[27] Svejda, S.A.; Johnson, L.K.; Brookhart, M. *J. Am. Chem. Soc*. **1999**, *121*, 10634-10635.
[28] Ittel, S.D.; Johnson, L.K.; Brookhart, M. *Chem. Rev.* **2000**, *100*, 1169-1203.
[29] Gate, D.P.; Svejda, S.A.; Oñate, E.; Killian, C.M.; Johnson, L.K.; White, P.S. Brookhart, M. *Macromolecules* **2000**, *33*, 2320-2324.
[30] Tempel, D.J.; Johnson, L.K.; Huff, P.S.; Brookhart, M. *J. Am. Chem. Soc*. **2000**, *122*, 6686-6700.
[31] Shultz, L.H.; Tempel, D.J.; Brookhart, M. *J. Am. Chem. Soc.* **2001**, *123*, 11539-11555.
[32] Shultz, L.H.; Brookhart, M. *Organometallics* **2001**, *20,* 3975-3982.
[33] Leatherman, M.D.; Svejda, S.A.; Johnson, L.K.; Brookhart, M. *J. Am. Chem. Soc*. **2003,** *125*, 3068-3081.
[34] Mecking, S. *Angew. Chem. Int. Ed.* **2001**, *40*, 534-540.
[35] Britovsek, G.J.P.; Gibson, V.C.; Kimberley, B.S.; Maddox, P.J.; McTavish, S.J.; Solan, G.A.; White, A.J.P.; Williams, D.J. *Chem. Commun.* **1998**, *7*, 849-850.
[36] Small, B.L., Brookhart, M.; Bennett, A.M.A. *J. Am. Chem. Soc*. **1998**, *120*, 4049-4050.
[37] Small, B.L.; Brookhart, M. **1998,** *120*, 7143-7144.
[38] Bennet, A.M.A. *Chem. Tech*. **1999,** *29*, 24-28.
[39] Britovsek, G.J.P.; Bruce, M.; Gibson, V.C.; Kimberley, B.S.; Maddox, P.J.; Mastroianni, S.; McTavish S.J.; Redshaw, C.; Solan, G.A.; Stromberg, S.; White, A.J.P.; Williams, D.J. *J. Am. Chem. Soc.* **1999**, *121,* 8728-8740.
[40] Britovsek, G.J.P.; Mastroianni, S.; Solan, G.A.; Baugh, S.P.D.; Redshaw, C.; Gibson, V.C.; White, A.J.P.; Williams, A.J.P.; Elsegood, M.R.J. *Chem. Eur. J.* **2000,** *6*, 2221-2231.
[41] Ricci, G.; Battistella, M.; Porri, L. *Macromolecules* **2001,** *34*, 5766-5769.
[42] Ricci, G.; Battistella, M.; Bertini, F.; Porri, L. *Polym. Bull.* **2002**, *48*, 25-31.
[43] Bazzini, C.; Giarrusso, A.; Porri, L *Macromol. Rapid Commun.* **2002**, *23*, 922-927.
[44] Ricci, G.; Morganti, D.; Sommazzi, A.; Santi, R.; Masi, F. *J. Mol. Cat. A: Chem.* **2003**, *204/205*, 287-293.
[45] Bazzini, C.; Giarrusso, A.; Porri, L.; Pirozzi, B.; Napolitano, R. *Polymer*, **2004**, *45,* 2871-2875.

[46] Pirozzi, B.; Napolitano, R.; Petraccone, V.; Esposito, S. *Macromol. Chem. Phys.* **2004,** *205*, 1343-1350.
[47] Ricci, G.; Forni, A.; Boglia, A.; Sonzogni, M. *Organometallics* **2004**, *23*, 3727-3732.
[48] Ricci, G.; Forni, A.; Boglia, A.; Motta, T. *J. Mol. Cat. A: Chem.* **2005**, *226*, 235-241.
[49] Ricci, G.; Forni, A.; Boglia, A.; Motta, T.; Zannoni, G.; Canetti, M.; Bertini, F. *Macromolecules* **2005,** *38,* 1064-1070.
[50] Ricci, G.; Forni, A.; Boglia, A.; Sommazzi, A.; Masi, F. *J. Organomet. Chem.* **2005,** *690*, 1845-1854.
[51] Ricci, G.; Boglia, A.; Motta, T. *J. Mol. Cat. A: Chem*. **2007**, *267*, 102-107.
[52] Ricci, G.; Boglia, A.; Boccia, A.C.; Zetta, L. *Macromol. Symp.* **2007**, *260*, 172–178.
[53] Ricci, G.; Boglia, A.; Santi, R.; Sommazzi, A.; Masi, F. Procedimento per la preparazione di polybutadiene a contenuto variabile cis-1,4/1,2, **2003**, Italian Patent MI03A 001807.
[54] Ricci, G.; Boglia, A.; Forni, A.; Santi, R.; Sommazzi, A.; Masi, F. Complessi fosfinici di cobalto e procedimento per la loro preparazione, **2003,** Italian Patent MI 03A 001808.
[55] Ricci, G.; Boglia, A.; Santi, R.; Sommazzi, A.; Masi, F. Procedimento per la preparazione di polibutadiene ad alto contenuto in unità 1,2, Italian Patent MI03A 001809.
[56] Ricci, G.; Boccia, A.C.; Leone, G.; Forni, A. *Catalysts* **2017**, 7*,* 381.
[57] Ricci, G.; Leone, G.; Masi, F.; Sommazzi, A. In: Phillips ES (ed) Ferrocenes: compounds, properties and applications. *Nova Science*, USA, **2011**, 273-313.
[58] Osakada, K.; Takeuchi, D. *Adv. Polym. Sci.* **2004**, *171*, 137–194.
[59] Sato, H.; Yagi, Y. *Bull. Chem. Soz. Jpn.* **1992**, *65*, 1299-1302.
[60] Longo, P.; Grisi, F.; proto, A.; Zambelli, A. *Macromol. Rapid. Commun*. **1998,** *19*, 31-34.
[61] Cabassi, F.; Italia, S., Ricci, g., Porri, L. In: *Quirk RP(ed)* Transition metal catalyzed polymerization. Cambridge Univ, Ma, USA, 1988, 655-670.
[62] Ricci, G.; Italia, S.; Cabassi, F.; Porri, L. *Polym. Commun.* **1987,** *28,* 223-226.
[63] Wilson, D.J.; Jenkins, D.K. *Polym. Bull*. **1992**, *27*, 407-411.
[64] Porri, L.; Ricci, G.; Shubin, N. *Macromol. Symp.* **1998**, *128*, 53-61.

[65] Porri, L.; Ricci, G.; Giarrusso, A.; Shubin, N.; Lu, Z. In: Arjuan, P.; McGrath, J.C.; Hanlon, T. (eds) *ACS Symposium Series 749* - Olefin polymerization: emerging frontiers. Oxford University, USA, 15-30.
[66] Samran, J.; Phinyocheep, P.; Daniel, P.; Kittipoom, S. *J. App. Pol. Sc.* **2005**, *95*,16-27.
[67] Schulz, D. N.; Turner, S. R.; Golub, M. A. *Rubber Chem. Technol*. **1982**, *55*, 809.
[68] Singha, N.K.; Bhattacharjee, S.; Sivaram, S. *Rubber Chem. Technol.* **1997**, *70*, 309–367.
[69] McManus, N.T.; Rempel, G.L. *J. Macromole. Sci. Part C-Polym. Rev.* **1995**, *35*, 239–285.
[70] Mango, L. A.; Lenz, R. W. *Makromol. Chem*. **1973,** *163*, 13.
[71] Wang, I. C.; Minton, R. J.; McGrath, J. E. *Polym. Prep. Am. Chem. Soc. Div. Polym. Chem.* **1983,** *24*, 28.
[72] Luo, Y. *J. Appl. Polym.Sci.* **1995,** *56,* 721.
[73] C-Jiménez, C. M.; P-Blas, M. M.; F-Gòmez, Martinez, T. M. *Int. J. Adhes. Adhes* **2001**, *21*, 161.
[74] He, Y.; Daniels, E. S.; Klein, A.; El-Aasser, M. S. *J. App. Polym. Sci*. **1996**, *25*, 2047.
[75] Phinyocheep, P.; Pasiri, S.; Tavachai, O. *J. App. Polym. Sci*. **2003**, *87*, 76.
[76] Samran, J.; Daniel, P.; Phinyocheep, P.; Kittipoom, S. *J. App. Polym. Sci.* **2005,** *95*, 16.
[77] Wideman, L.G. Process for hydrogenation of carbon-carbon double bonds in an unsaturated polymer in latex form, **1984,** US Patent 4452950.
[78] Xie, H.-Q.; Li, X.-D.; Guo, J.-S.. *J. Appl. Polym. Sci.* **2003**, *90*, 1026.
[79] Hahn, S. *J. Appl. Polym. Sci. Polym. Chem.* **1992**, *30*, 397.
[80] Harwood, H. J.; Russel, D. B.; Verthe, J. J. A.; Zymonas, J. *Die Makromolekulare Chemie.* **1973,** *163*, 1.
[81] Hashim, A. S.; Ong, S. K.; Jessy, R. S. *Nat. rubber* **2002**, *28*, 3.
[82] Edwards, H. G. M.; Farwell D. W.; Johnson, A. F.; Lewis, I. R.; Ward, N. J. *Macromolecules* **1992**, *25*, 525.

Chapter II

New Stereoregular (Co)Polymers by Hydrogenation of Poly(1,3-diene)s

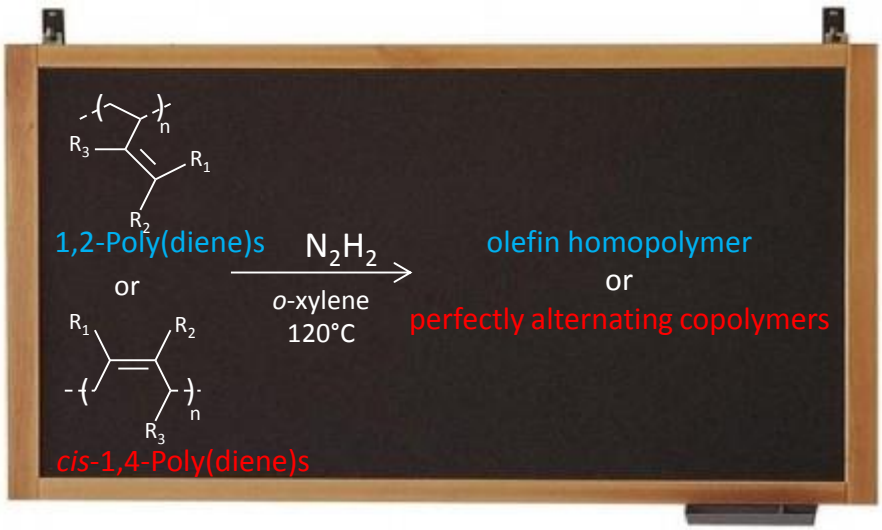

Introduction

In this Chapter, I report (*i*) on the synthesis and characterization of some stereoregular poly(1,3-diene)s obtained by polymerizing the corresponding 1,3-dienes with transition metal and lanthanide based catalysts, and (*ii*) on their successive hydrogenation giving olefin homo- and co-polymers which, in most cases, cannot be obtained through the simple stereospecific polymerization of the corresponding monomers.

All the polydienes and the hydrogenated polymers examined in this Chapter have been synthesized at the CNR-ISMAC, Milan; the NMR characterization of the polymers too has been carried out at ISMAC, while their crystalline molecular structures and their thermal and mechanical properties have been studied at the University of Naples Federico II.

I first report on the synthesis and characterization of the polydienes with a 1,4 structure and the ethylene-α-olefin alternating copolymers obtained through their hydrogenation. The polymers studied are listed in the Table 2.1.

Successively, I will describe the synthesis and characterization of polydienes with a 1,2 or 3,4 structure, and of the branched polyolefins obtained by hydrogenation of these polydienes. All these polymers are listed in Table 2.2.

Table 2.1. *Polymerized monomer, catalytic system, polydienes with a 1,4 structure obtained before hydrogenation and alternating copolymers obtained after hydrogenation reaction of the corresponding polydienes.*

Monomer	Catalytic system	Poly(1,3-diene)	Hydrogenated alternating copolymers
(*E,E*)-2,4-hexadiene	$Et_2AlCl/Nd(OCOC_7H_{15})_3/Al^iBu_3$	di-isotactic *trans*-1,4 poly(*E,E*-2,4-hexadiene)	*racemo*-di-isotactic ethylene/2-butene
3-methyl-1,3-pentadiene	$Et_2AlCl/Nd(OCOC_7H_{15})_3/Al^iBu_3$	isotactic *cis*-1,4 poly(*E*-3-methyl-1,3-pentadiene)	isotactic ethylene/2-butene
3-methyl-1,3-pentadiene	$Ni(acac)_2$/MAO	syndiotactic *cis*-1,4 poly(*E*-3-methyl-1,3-pentadiene)	syndiotactic ethylene/2-butene
2,3-dimethyl-1,3-butadiene	$FeCl_2(bipy)_2$/MAO	*cis*-1,4 poly(2,3-dimethyl-1,3-butadiene)	atactic ethylene/2-butene
E-1,3-pentadiene	$Et_2AlCl/Nd(OCOC_7H_{15})_3/Al^iBu_3$	isotactic *cis*-1,4 poly(1,3-pentadiene)	isotactic ethylene/propylene
E-1,3-pentadiene	$CoCl_2(P^tBu_2Me)_2$/MAO	syndiotactic *cis*-1,4 poly(1,3-pentadiene)	syndiotactic ethylene/propylene
isoprene	$Et_2AlCl/Nd(OCOC_7H_{15})_3/Al^iBu_3$	*cis*-1,4 poly(isoprene)	atactic ethylene/propylene
1,3-hexadiene	$Et_2AlCl/Nd(OCOC_7H_{15})_3/Al^iBu_3$	isotactic *cis*-1,4 poly(1,3-hexadiene)	isotactic ethylene/1-butene
1,3-heptadiene	$Et_2AlCl/Nd(OCOC_7H_{15})_3/Al^iBu_3$	isotactic *cis*-1,4 poly(1,3-heptadiene)	isotactic ethylene/1-pentene
1,3-heptadiene	$CoCl_2(P^tBu_2Me)_2$/MAO	syndiotactic *cis*-1,4 poly(1,3-heptadiene)	syndiotactic ethylene/1-pentene
1,3-octadiene	$Et_2AlCl/Nd(OCOC_7H_{15})_3/Al^iBu_3$	isotactic *cis*-1,4 poly(1,3-octadiene)	isotactic ethylene/1-hexene
1,3-octadiene	$CoCl_2(P^tBu_2Me)_2$/MAO	syndiotactic *cis*-1,4 poly(1,3-octadiene)	syndiotactic ethylene/1-hexene

Table 2.2. *Polymerized monomer; catalytic system; polydienes with a 1,2 or 3,4 structure obtained before hydrogenation, and branched polyolefins obtained after hydrogenation reaction of the respective polydienes.*

Monomer	**Catalytic system**	**Poly(1,3-diene)s**	**Hydrogenated branched polyolefins**
3-methyl-1,3-pentadiene	$CoCl_2(P^nPrPh_2)_2$/MAO	isotactic 1,2 poly(*E*-3-methyl-1,3-pentadiene)	isotactic poly((*R,S*)-3-methyl-1-pentene)
3-methyl-1,3-pentadiene	$FeCl_2(bipy)_2$/MAO	syndiotactic 1,2 poly(*E*-3-methyl-1,3-pentadiene)	syndiotactic poly((*R,S*)-3-methyl-1-pentene)
isoprene	$FeCl_2(bipy)_2$/MAO	syndiotactic 3,4 poly(isoprene)	syndiotactic poly(3-mehyl-1-butene)
5-methyl-1,3-hexadiene	$CoCl_2(P^iPrPh_2)_2$/MAO	syndiotactic *trans*-1,2 poly(5-methyl-1,3-hexadiene)	syndiotactic 1,2 poly(5-methyl-1-hexene)
1,3-heptadiene	$CoCl_2(P^iPrPh_2)_2$/MAO	syndiotactic *trans*-1,2 poly(1,3-heptadiene)	syndiotactic 1,2 poly(heptene)
1,3-octadiene	$CoCl_2(P^iPrPh_2)_2$/MAO	syndiotactic *trans*-1,2 poly(1,3-octadiene)	syndiotactic 1,2 poly(octene)

2.1 Perfectly alternating olefin copolymers by hydrogenation of stereoregular *cis*-1,4 iso- and syndiotactic poly(1,3-diene)s

2.2.1 Alternating ethylene/2-butene copolymers [1]

I am reporting on the synthesis and characterization of four perfectly alternating ethylene/2-butene copolymers [which can also be seen as perfectly "head-to-head" poly(propylene)s (PPs); Scheme 2.1] having different stereoregularity degree (from completely isotactic to predominantly syndiotactic).[1] The results of this work have been taken from: Pierro I. *et al. Macromolecules* **2017,** *50*, 754−761.

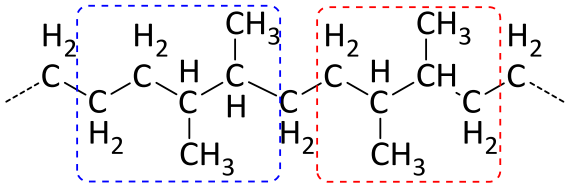

Scheme 2.1. *Hydrogenated polymers structure: ethylene-alt-2-butene or head-to-head PP.*

Polymerization

I first focused on the polymerization of (*E,E*)-2,4-hexadiene, 3-methyl-1,3-pentadiene and 2,3-dimethyl-1,3-butadiene.

By polymerizing (*E,E*)-2,4-hexadiene and 3-methyl-1,3-pentadiene with the catalyst system $Et_2AlCl/Nd(OCOC_7H_{15})_3/Al^iBu_3$ I obtained a diisotactic *trans*-1,4 poly(*E,E*-2,4-hexadiene) and an isotactic *cis*-1,4 poly(*E*-3-methyl-1,3-pentadiene), respectively.[2,3] With the catalyst $Ni(acac)_2$/MAO, I obtained from 3-methyl-1,3-pentadiene a syndiotactic *cis*-1,4 poly(*E*-3-methyl-1,3-pentadiene);[4] from 2,3-dimethyl-1,3-butadiene, with $FeCl_2(bipy)_2$/MAO, I obtained a *cis*-1,4 poly(2,3-dimethyl-1,3-butadiene)[5] (Scheme 2.2). Data concerning the polymerization of the 1,3-dienes are summarized in Table 2.3.

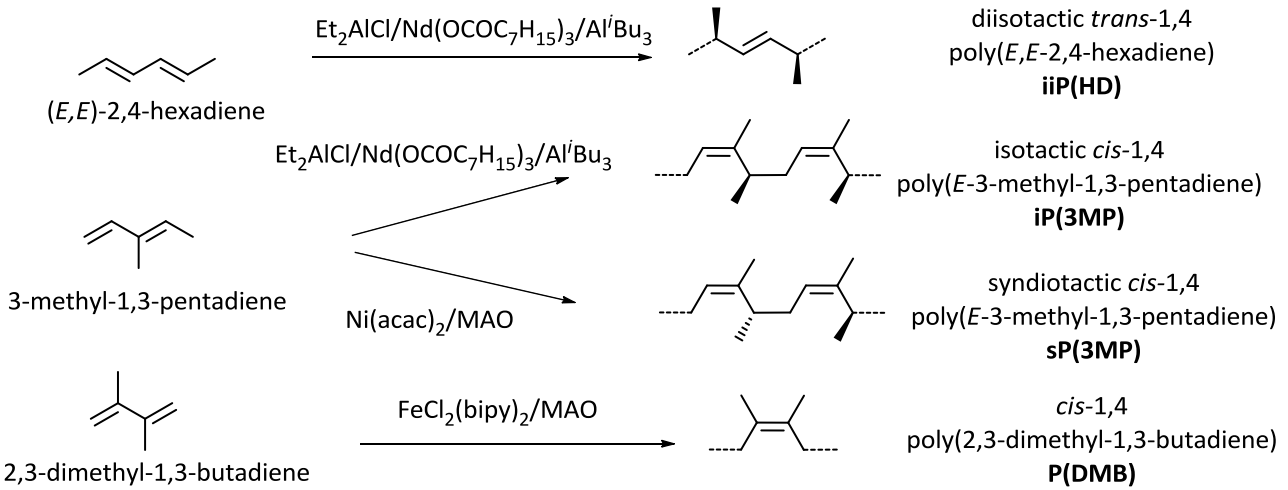

***Scheme 2.2**. Polymerization of (E,E)-2,4-hexadiene, 3-methyl-1,3-pentadiene, and 2,3-dimethyl-1,3-butadiene.*

***Table 2.3**. Polymerization of 1,3-dienes with catalysts based on Nd, Ni and Fe.[a]*

monomer	catalytic system	time(h)	Yield (%)	*cis*-1,4 [b] (%)	*trans*-1,4 [b] (%)	T_m [c] (°C)
(*E*,*E*)-2,4-hexadiene	$Et_2AlCl/Nd(OCOC_7H_{15})_3/Al^iBu_3$	360	88		>99	95
3-methyl-1,3-pentadiene	$Et_2AlCl/Nd(OCOC_7H_{15})_3/Al^iBu_3$	20	78	≥90[d]		79
3-methyl-1,3-pentadiene	$Ni(acac)_2$/MAO	60	80	>99		98
2,3-dimethyl-1,3-butadiene	$FeCl_2(bipy)_2$/MAO	1/60	100	>99		200

[a] Polymerization conditions: monomer, 2 mL; toluene as solvent (heptane with Nd based catalyst), total volume, 16 mL; 1×10^{-5} moles of Mt (Nd, Ni, Fe); temperature, 20°C; [b] determined by ^{13}C NMR; [c] determined by DSC; [d] the remaining units are essentially 1,2.

Successively, the four highly stereoregular poly(1,3-diene)s were hydrogenated with diimide, formed in situ by thermal decomposition of *p*-T*s*NH, obtaining alternating ethylene/2-butene copolymers, with different configurations (Scheme 2.3). Hereafter, we will named iiP(HD) the diisotactic *trans*-1,4 poly(*E,E*-2,4-hexadiene), iP(3MP) the isotactic *cis*-1,4 poly(3-methyl-1,3-pentadiene), sP(3MP) the syndiotactic *cis*-1,4 poly(3-methyl-1,3-pentadiene), P(DMB) the *cis*-1,4 poly(2,3-dimethyl-1,3-butadiene), and H-iiP(HD), H-iP(3MP), H-sP(3MP), and H-P(DMB) the corresponding hydrogenated polymers.

The hydrogenation reactions were carried out in boiling *o*-xylene using *p*-T*s*NH in large excess.

Specifically, for each sample the hydrogenation conditions were the following:
(i) diisotactic *trans*-1,4 poly(*E,E*-2,4-hexadiene): polymer 2.6 g, *o*-xylene 250 mL, first addition of *p*-T*s*NH, 18.0 g (9.70×10^{-2} mol), second and third addition of *p*-T*s*NH, 20.0 g (1.07×10^{-1} mol);
(ii) isotactic *cis*-1,4 poly(*E*-3-methyl-1,3-pentadiene): polymer 0.6 g, *o*-xylene 100 mL, first addition of *p*-T*s*NH, 5.2 g (2.89×10^{-2} mol); second and third addition of *p*-T*s*NH, 10.0 g (5.56 × 10–2 mol);
(iii) syndiotactic *cis*-1,4 poly(*E*-3-methyl-1,3-pentadiene): polymer 1.2 g, *o*-xylene 200 mL, first addition of *p*-T*s*NH, 8.5 g (4.72×10^{-2} mol), second and third addition of *p*-T*s*NH, 15.0 g (8.34×10^{-2} mol);
(iv) cis-1,4 poly(2,3-dimethyl-1,3-butadiene): polymer 2.8 g, *o*-xylene 200 mL, first addition of *p*-T*s*NH, 18.0 g (9.70×10^{-2} mol), second and third addition of *p*-T*s*NH, 15.0 g (8.34×10^{-2} mol).

The molecular weight and the molecular weight distribution of the obtained alternating ethylene/2-butene copolymers are reported in Table 2.4.

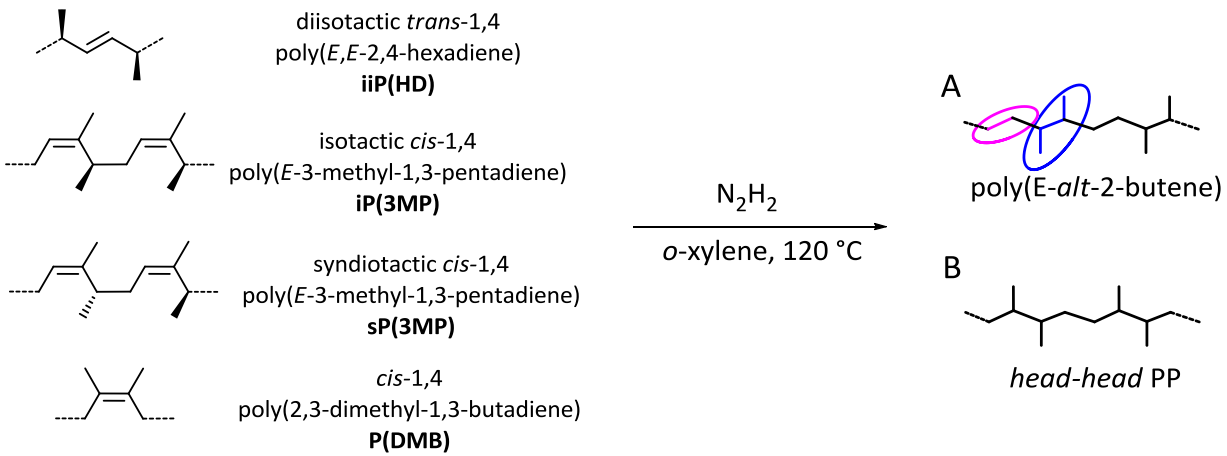

Scheme 2.3. *Scheme of hydrogenation of diisotactic trans-1,4 poly(E,E-2,4-hexadiene) (iiP(HD)), iso- and syndiotactic cis-1,4 poly(E-3-methyl-1,3-pentadiene) (iP(3MP) and sP(3MP)), and cis-1,4 poly(2,3-dimethyl-1,3-butadiene) (P(DMB).*

Table 2.4*. Molecular weight (M_w), molecular weight distribution (M_w/M_n) and glass transition temperature (T_g) of the alternating ethylene/2-butene copolymers obtained by hydrogenation of the corresponding poly(1,3-diene)s.*

ethylene/2-butene copolymers	**pristine poly(1,3-diene)**	M_w [a] **(kg/mol)**	M_w/M_n [a]	T_g [b] **(°C)**
H-iiP(HD)	*trans*-1,4 poly(*E*,*E*-2,4-hexadiene)	66.0	7.0	–29
H-iP(3MP)	isotactic *cis*-1,4 poly(*E*-3-methyl-1,3-pentadiene)	105.0	3.3	–18
H-sP(3MP)	syndiotactic *cis*-1,4 poly(*E*-3-methyl-1,3-pentadiene)	20.0	2.5	–19
H-P(DMB)	*cis*-1,4 poly(2,3-dimethyl-1,3-butadiene)	39.0	2.9	–18

[a] determined by SEC; [b] determined by DSC.

Structural and thermal analysis

All the poly(diene)s and the corresponding hydrogenated polymers have been characterized by FT-IR, NMR, and their structure, thermal and mechanical properties have been investigated.

The ^{13}C NMR spectra of the stereoregular poly(1,3-diene)s, together with the peaks attribution, are shown in Figure 2.1.

polymer/ppm	C1	C2	C3	C4	C5	C6
iiP(HD)	40.11	131.43	131.43	40.11	15.76	15.76
iP(3MP)	30.95	122.11	137.42	33.22	16.34	16.83
sP(3MP)	30.87	121.97	137.54	33.03	16.38	16.66
P(DMB)	31.65	126.51	126.51	31.65	16.60	16.60

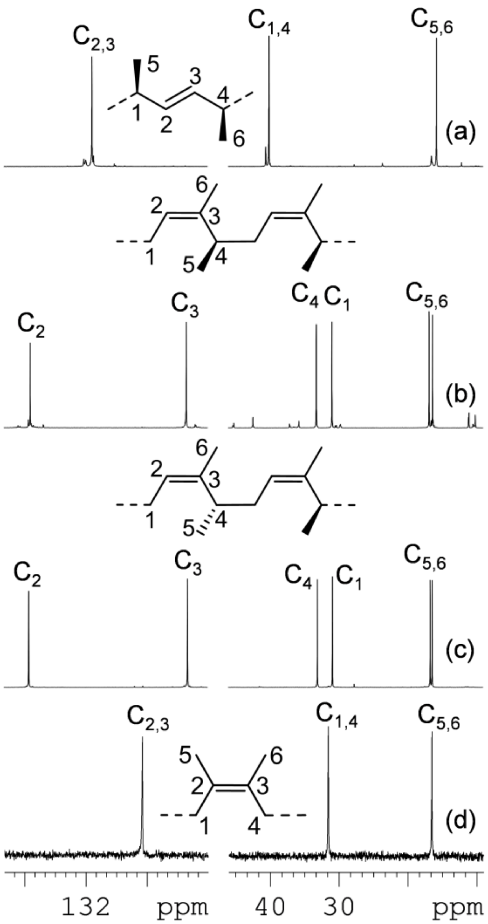

Figure 2.1. *^{13}C NMR spectra ($C_2D_2Cl_4$, 103°C, HMDS as internal standard) of iiP(HD) (a), iP(3MP) (b), sP(3MP) (c), and P(DMB) (d).*

In the ^{1}H-NMR spectra of the saturated polymers no peaks were detected in the olefinic region (from 5.2 to 5.4 ppm), confirming indeed that the hydrogenation reaction was completed, and that the poly(1,3-diene)s were totally converted into the saturated polymers (*i.e.*, ethylene/2-butene copolymers).

The copolymers microstructure was determined by means of different NMR spectroscopic techniques: ^{13}C NMR (Figure 2.2), and a two-dimensional NMR technique (2D NMR) such as ^{1}H–^{13}C HSQC (Figure 2.3).[6,7] The relative configurational regularity of subsequent monomeric units along the polymer chain is expressed in term of tacticity. The analysis of the ^{13}C NMR spectra of Figure 2.2 clearly puts in evidence a different tacticity of the saturated copolymers obtained, from perfectly isotactic (Figure 2.2 a) to slightly syndiotactic (Figure 2.2 d), passing through atactic copolymers (Figure 2.2 b,c).

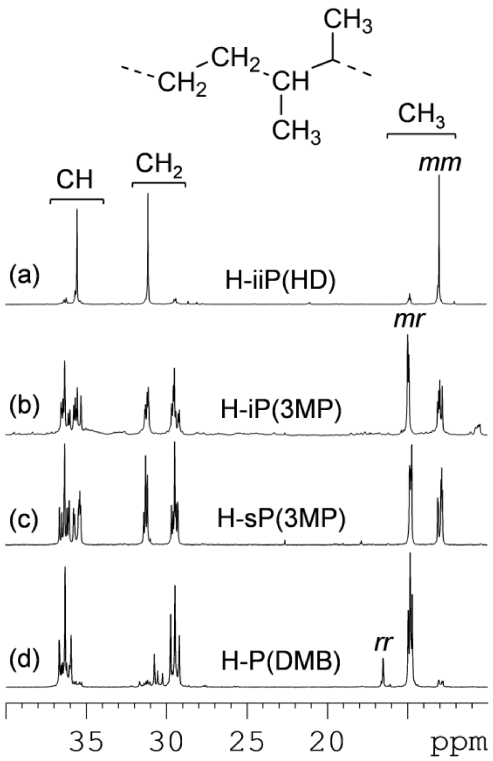

Figure 2.2. *^{13}C NMR spectra ($C_2D_2Cl_4$, 103°C, HMDS as internal standard) of the hydrogenated polymers H-iiP(HD) (a), H-iP(3MP) (b), H-sP(3MP) (c), and P(DMB) (d).*

When the hydrogenation reaction does not lead to the formation of new centers of asymmetry, as in the case of the hydrogenation of iiP(HD), the tacticity of the starting poly(1,3-diene) (*i.e.,* isotactic) is maintained in the corresponding saturated polymer; in the other cases instead, in which we have the formation of new chiral carbons [*e.g.,* iP(3MP), sP(3MP), and P(DMB)], the hydrogenated

polymers are substantially atactic, as expected, given the non catalytic nature of the hydrogenation reaction with *p*-TsNH.

The analysis of the $^{1}H-^{13}C$ HSQC correlation spectra performed on all the hydrogenated polymers, are shown in Figure 2.3.

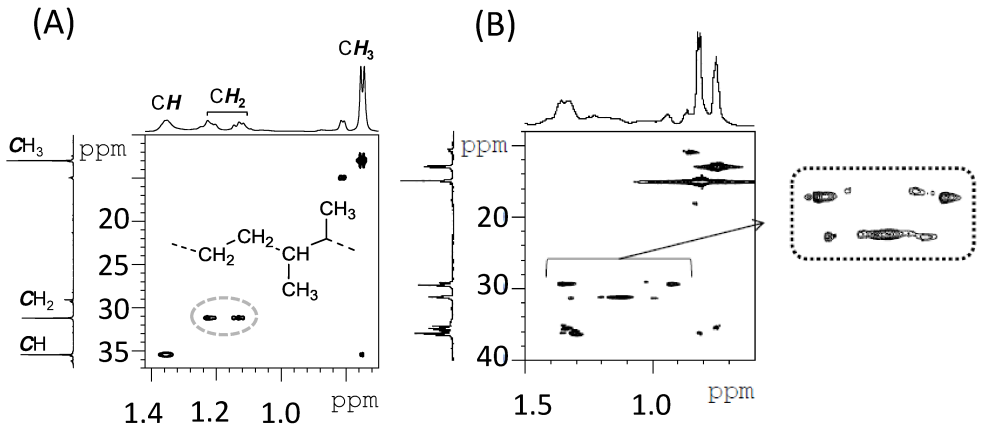

***Figure 2.3**. HSQC spectrum of (a) the isotactic head-to-head PP obtained by hydrogenation of iiP(HD) and (b) ethylene/2-butene copolymer obtained by hydrogenation of isotactic cis-1,4 poly(3-methyl-1,3-pentadiene).*

In the $^{1}H-^{13}C$ HSQC spectrum of isotactic ethylene/2-butene copolymer [H-iiP(HD)] (Figure 2.3 A) it is noted that the carbon atom at δ = 31.1 ppm correlates with two cross peaks at δ_H = 1.23 and 1.13 ppm, respectively. This carbon atom appears to be a methylene to which two magnetically non equivalent protons are linked; that is clearly indicative of an isotactic structure of the polymer.[8-10] These results are in analogy with spectroscopic data observed in the case of an isotactic PP in which the two methylene protons of a *meso* dyad, Ha and Hb, respectively, are in different environments as they give two cross-peaks at two different resonance frequencies in the 2D HSQC spectrum. The $^{1}H-^{13}C$ HSQC spectrum of ethylene/2-butene copolymer from H-iP(3MP) is shown in Figure 2.3 B, just to put in evidence the differences on copolymers microstructure. As evident from the number of cross-peaks in the spectrum, this copolymer is less stereoregular than the ethylene/2-butene copolymer from H-iiP(HD). Moreover, the cross-peak of the methylene at δ = 31.18 ppm is broad, as for a *mr* triad, supporting a random tacticity. The same tacticity is observed for ethylene/2-butene copolymer from H-sP(3MP).

The X-ray powder diffraction profiles and the DSC heating curves of the hydrogenated polymers are reported in Figures 2.4 A and 2.4 B, respectively.

All samples of alternating ethylene/2-butene copolymers are amorphous (Figure 2.4 A). The diffraction patterns do not change upon thermal treatments, and the samples do not crystallize even after annealing at relatively high temperatures. This is expected for the samples H-iP(3MP), H-sP(3MP) and H-P(DMB), due to their predominantly atactic structure, even though in the case of H-P(DMB) a non-negligible amount of syndiotactic sequences is present (Figure 2.2 d). The sample H-iiP(HD) is also amorphous (Figure 2.4 A) even though the NMR data of Figure 2.2 a indicates a perfect di-isotactic structure of the chains. According to the X-ray diffraction profiles, all DSC curves show only a glass transition (T_g) at nearly −20 °C for H-iP(3MP), H-sP(3MP), and H-P(DMB) and at −29 °C for H-iiP(HD) and absence of any endothermic signal (Table 2.4). Only the glass transition at the same temperatures is observed in the successive cooling scans with absence of exothermic signals.

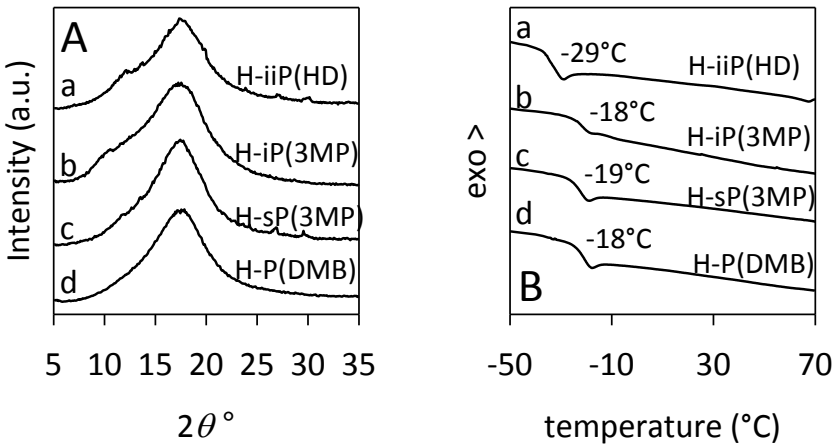

***Figure 2.4**. (A) X-ray powder diffraction profiles of as-prepared samples of alternating ethylene/2-butene copolymers corresponding to the hydrogenated polymers. (B) DSC heating curves, recorded at 10 °C/min, of as-prepared samples of alternating ethylene-2-butene copolymers corresponding to the hydrogenated polymers*.

It is worth reminding that the alternating ethylene/2-butene copolymer [P(E/2B)] prepared with Ziegler−Natta catalysts from the copolymerization of ethylene with *cis*-2-butene is a crystalline polymer melting at 130−135°C.[11-15]

The presence of this slight crystallinity was taken as indicative of a regularity of the chemical and steric structure.[13,14] Four different regular configurations, shown in Figure 2.5, are possible for the chains of alternating ethylene/2-butene copolymer according to the relative *meso* (erythro) or *racemo* (threo) configurations of two adjacent tetrahedral stereoisomeric centers,[16,17] and the

relative configuration, isotactic or syndiotactic, of successive monomeric units along the chain. [11,15]

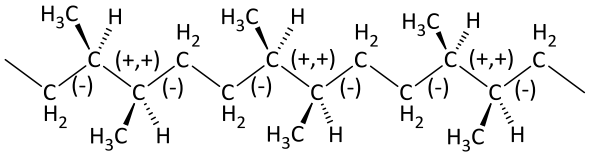

Racemo di-isotactic

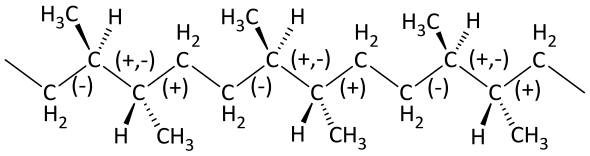

Meso di-isotactic

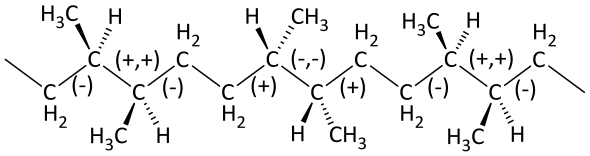

Racemo di-syndiotactic

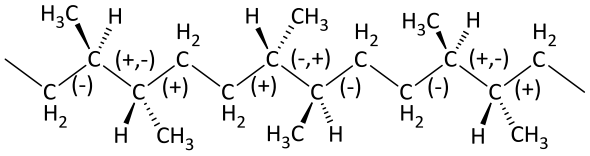

Meso di-syndiotactic

Figure 2.5. *Four possible configurations of the chain of the alternating ethylene/2-butene copolymer. The inherent asymmetry of the skeletal bonds is represented with the configurational (+) and (–) signs.[16] Note that in ref. 18 the relative configurations racemo and meso were defined as threo and erythro, respectively.[11,16]*

The complete determination of the crystal structure by X-ray diffraction has indicated that the chains of P(E/2B) have a *meso*-di-isotactic structure with $(T_3G^+T_3G^-)_n$ conformation [11,12] and are packed in a monoclinic unit cell with axes a = 10.92 Å, b = 5.94 Å, c = 9.10 Å, and α = 90°, according to the space group $P2_1/b$.[11] The gauche bonds of opposite signs G^+ and G^- in the two consecutive structural units are those connecting the two methine carbon atoms $CH(CH_3)–CH(CH_3)$.[11,12] The result that the sample H-iiP(HD) of alternating ethylene/2-butene copolymer (Figure 2.4 a), obtained by hydrogenation of the di-isotactic *trans*-1,4-poly(*E,E*-2,4-hexadiene), is not able to crystallize notwithstanding the regular isotactic structure, indicates that a polymer with a

molecular structure different from that of the *meso*-di-isotactic P(E/2B) copolymer prepared with Ziegler–Natta catalyst,[11] has been obtained by the hydrogenation route. In fact, the polymerization of (*E,E*)-2,4-hexadiene with the catalytic system $Et_2AlCl/Nd(OCOC_7H_{15})_3/Al(^{i}Bu)_3$ produces a di-isotactic *trans*-1,4-poly(*E,E*-2,4-hexadiene) (Scheme 2.2) with a relative *racemo* configuration of two adjacent tetrahedral stereoisomeric centers. The successive hydrogenation of the *racemo*-di-isotactic *trans*-1,4-poly(*E,E*-2,4-hexadiene) produces the alternating ethylene/2-butene copolymer where the configurations of the adjacent stereoisomeric centers in the starting poly(1,3-diene) are maintained in the saturated polymer, resulting in a *racemo* di-isotactic structure of the alternating ethylene/2-butene copolymer (Figure 2.5). The *racemo*-di-isotactic alternating ethylene/2-butene copolymer produced by hydrogenation of the di-isotactic *trans*-1,4-poly(*E,E*-2,4-hexadiene) is a novel stereoregular polymer never reported before. Based on the structures of Figure 2.5 and Figure 1.6 (in Chapter I) and Scheme 2.2 of synthesis and hydrogenation, the molecular structures of the hydrogenated polymers H-iiP(HD), H-iP(3MP), H-sP(3MP), and H-P(DMB), and corresponding definition of stereochemistry, are reported in Figure 2.6.

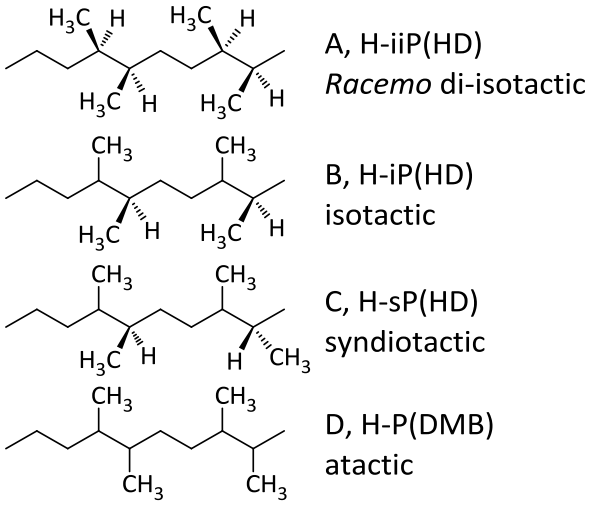

Figure 2.6*. Molecular structures of the hydrogenated polymers and corresponding stereochemistry: A) H-iiP(HD) is racemo-di-isotactic; B) H-iP(3MP) is isotactic for one of the two adjacent tetrahedral stereoisomeric centers and atactic for the second one; C) H-sP(3MP) is syndiotactic for one of the two adjacent tetrahedral stereoisomeric centers and atactic for the second one; D) H-P(DMB) is atactic for both the two adjacent tetrahedral stereoisomeric centers.*

The sample H-iiP(HD) is *racemo*-di-isotactic, the samples H-iP(3MP) and H-sP(3MP) are isotactic and syndiotactic, respectively, for one of the two adjacent tetrahedral stereoisomeric centers and atactic for the second one, and H-P(DMB) is atactic for both the two adjacent tetrahedral stereoisomeric centers. As expected from the structures of Figure 2.6, the atactic polymers [*i.e.,* H-P(DMB), H-iP(3MP), and H-sP(3MP)] are not able to crystallize, even when one of the two adjacent tetrahedral stereoisomeric centers has a regular succession of configurations, isotactic [H-iP(3MP)] or syndiotactic [(H-sP(3MP)]. Contrary to the crystalline *meso*-di-isotactic alternating ethylene/2-butene copolymer prepared with Ziegler–Natta catalysts,[11-14] the *racemo*-di-isotactic ethylene/2-butene copolymer [sample H-iiP(HD)] is not able to crystallize, notwithstanding the regular relative configurations of two adjacent tetrahedral stereoisomeric centers (*racemo*), and the regular succession of configurations, di-isotactic, of successive monomeric units along the chain. This is probably related to the fact that the conformation of the *racemo*-di-isotactic copolymer is different from the $(T_3G^+T_3G^-)_n$ of the *meso*-diisotactic copolymer, although this conformation is energetically feasible also for the *racemo*-di-isotactic structure.[11,15,16] In fact, in the *racemo*-di-isotactic configuration, with succession of configurational (+) and (−) signs of the bonds of the type ...(−)(+,+)(−)... (Figure 2.5), the torsion angles of bonds connecting the tertiary carbon atoms $C(CH_3)–C(CH_3)$ of consecutive monomeric units (bonds (+,+) in Figure 2.5) should be gauche with the same sign (G^+ for (+,+) bonds).[15,16] Therefore, the conformation of the *racemo*-di-isotactic alternating ethylene/2-butene copolymer would be helical with succession of torsion angles $(TTTG^+)_n$, that is probably not able to crystallize for packing or kinetics reasons.

Mechanical properties

The mechanical properties under tensile deformation of the four samples of the alternating ethylene/2-butene copolymers, having the different microstructures defined in Figure 2.6, have also been studied. The stress–strain curves recorded at room temperature of compression-molded films of the samples of the hydrogenated polymers H-iiP(HD), H-iP(3MP), H-sP(3MP) and H-P(DMB) are shown in Figure 2.7.

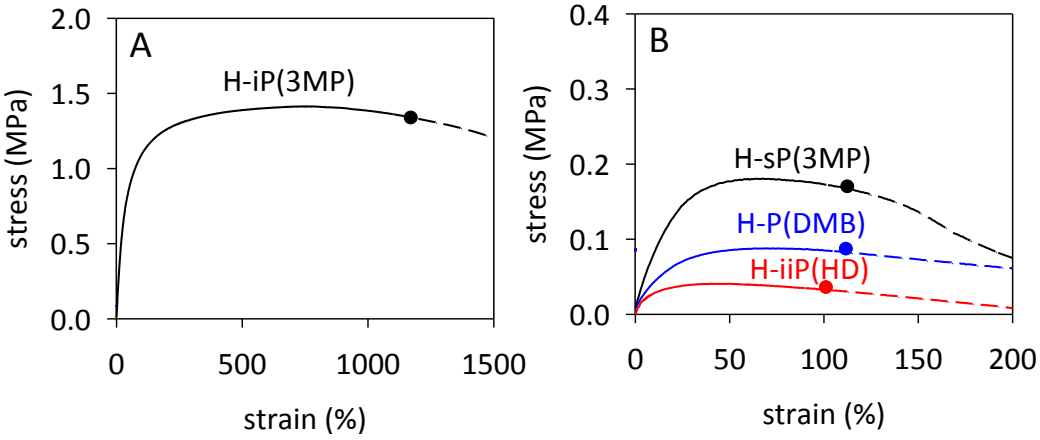

***Figure 2.7**. Stress-strain curves recorded at room temperature of compression-molded films of alternating ethylene/2-butene copolymers corresponding to the hydrogenated polymers.*

According to the absence of crystallinity, all samples show low values of the Young modulus and low values of the stress at any strain, easy deformability, and viscous flow at high deformations. The isotactic sample H-iP(3MP) (Figure 2.7 A) shows slight higher values of modulus (1.9 MPa) and strength and deformation up to high value of strain, up to 1000%, before undergoing viscous flow without breaking. The *racemo* diisotactic sample H-iiP(HD), the syndiotactic sample H-sP(3MP), and the atactic sample H-P(DMB) show instead lower modulus (0.1−0.2 MPa) and strength, and viscous flow already at low deformations, as low as 100% (Figure 2.7 B). The different behavior of the sample H-iP(3MP) is related to the higher molecular mass (Table 2.4). For the isotactic sample H-iP(3MP) that shows higher strength up to very high degree of deformation, elastic behavior has been observed in the range of deformations lower than the maximum strain at which viscous flow begins (1000%). To quantify the elastic properties, mechanical cycles of stretching and relaxation have been recorded at room temperature on the compression-molded films measuring the values of tension set and elastic recovery and the corresponding hysteresis. Three successive stress−strain hysteresis cycles of the sample H-iP(3MP), obtained by stretching compression-molded films up to the deformation of 200% and then relaxing at controlled rate, are reported in Figure 2.8. It is apparent that the sample shows good elastic behavior with low values of tension set, that is, the residual deformation after relaxation at the end of the cycle (t_s = 20% after the first cycle, 10% after the second cycle, and 7% after the third cycle). However, during mechanical cycles a

certain viscous flow occurs as demonstrated by the decrease of the values of stress after each cycle.

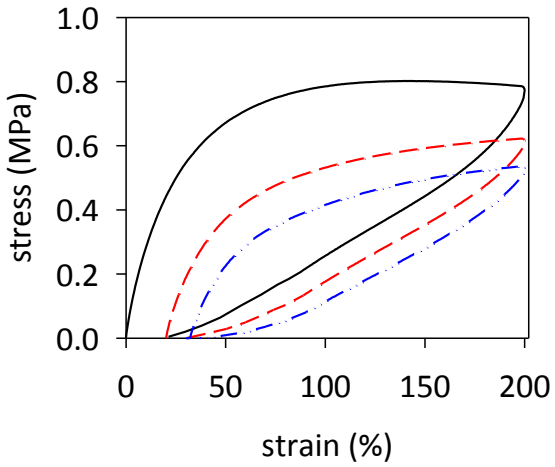

Figure 2.8. *Stress–strain hysteresis cycles, composed of stretching and relaxation steps of compression-molded films of the sample H-iP(3MP). The first hysteresis (solid lines), second (dashed lines), and third (dotted lines) cycles are reported.*

2.1.2 Alternating ethylene/propylene copolymers [19]

Nowadays ethylene/propylene (E/P) copolymers are one of the most important families of polymeric materials, with endless applications. The performance of E/P copolymers can be easily tuned by varying the comonomer composition, comonomer distribution and chain stereoregularity. When the comonomers are randomly distributed, amorphous polymers (E/P rubbers and E/P/diene rubbers), emerging as a new class of thermoplastic elastomers, can be obtained.[20] If the comonomer is isolated, crystalline copolymers result, which are widely used as impact-strength modifiers in blends with isotactic poly(propylene).[21]

The synthesis of alternating E/P copolymers has been one of the challenging subjects of both practical and fundamental interest in recent years.[22] The development of metallocene,[23] and post-metallocene complexes[24] for olefin polymerization has opened new opportunities for the synthesis of alternating copolymers with controlled microstructure and properties. Alternating E/P copolymers have been obtained by the copolymerization of ethylene with propylene with some *ansa*-zirconocenes-based catalysts,[25-27] and by living polymerization of 1-pentene with an α-diimine Ni(II) catalyst through a controlled chain-walking mechanism.[28]

An alternative route for the synthesis of perfectly alternating ethylene/α-olefin copolymers in general, and of E/P copolymers in particular, is the one taking advantage of the hydrogenation of stereoregular poly(1,3-diene)s with a 1,4 structure (*cis*-1,4 and *trans*-1,4-poly(1,3-pentadiene) and poly(isoprene)s in case of E/P copolymers).

I report the preparation and characterization of perfectly alternating ethylene/propylene iso- and syndiotactic copolymers, obtained by hydrogenation of the following three highly stereoregular poly(1,3-diene)s: isotactic *cis*-1,4 poly(1,3-pentadiene), syndiotactic *cis*-1,4 poly(1,3-pentadiene), and *cis*-1,4 poly(isoprene). The results of this work have been taken from: Pierro I. *et al. Molecules* **2017**, *22*, 755.

Polymerization

I first focused on the polymerization of (*E*)-1,3-pentadiene and isoprene. By polymerizing (*E*)-1,3-pentadiene and isoprene with the catalyst system $Et_2AlCl/Nd(OCOC_7H_{15})_3/Al^iBu_3$ I obtained an isotactic *cis*-1,4 poly(1,3-pentadiene) [iP(EP)] and a *cis*-1,4 poly(isoprene) (PI), respectively;[29-31] by polymerizing (*E*)-1,3-pentadiene with the catalyst system $CoCl_2(P^tBu_2Me)_2$/MAO I obtained a syndiotactic *cis*-1,4 poly(1,3-pentadiene) [sP(EP)][32] (Scheme 2.4).

The polymerization data are summarized in Table 2.5.

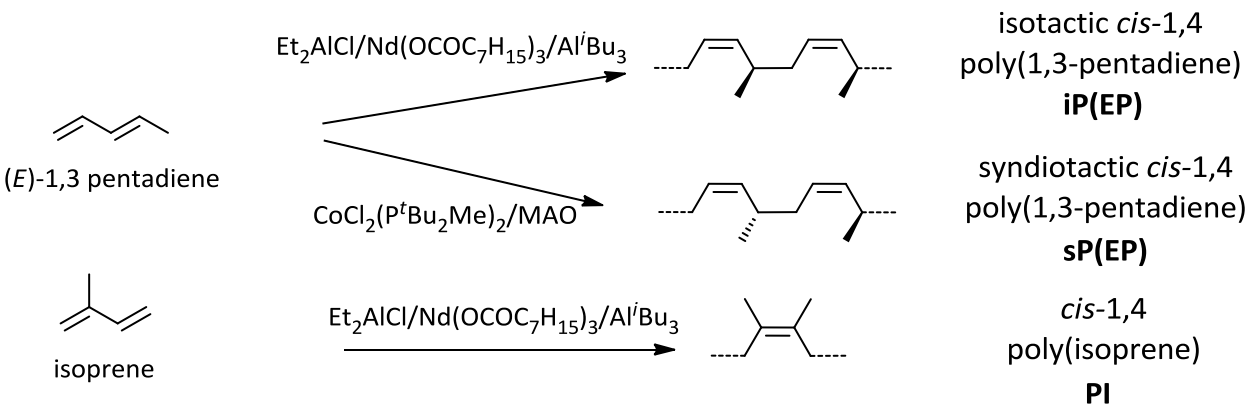

Scheme 2.4. *Polymerization of (E)-1,3-pentadiene and isoprene.*

Table 2.5. *Polymerization of (E)-1,3-pentadiene and isoprene with catalysts based on Nd and Co.*[a]

Sample	Monomer	Catalyst	Time (min)	Yield (%)	*cis*-1,4 [b] (%)	T_g [c] (°C)
iP(EP)	(*E*)-1,3-pentadiene	$Et_2AlCl/Nd(OCOC_7H_{15})_3/Al^iBu_3$	60	87	≥90	−66
sP(EP)	(*E*)-1,3-pentadiene	$CoCl_2(P^tBu_2Me)_2/MAO$	144	69	≥99	−66
PI	isoprene	$Et_2AlCl/Nd(OCOC_7H_{15})_3/Al^iBu_3$	30	100	≥97	−65

[a] *Polymerization conditions: monomer (2 mL); heptane (total volume 16 mL) (or toluene in the case of sP(EP)), Co or Nd complex, 2 × 10^{-5} mol; temperature, 22 °C;* [b] *Percentage of cis-1,4 units, determined by NMR analysis;* [c] *determined by DSC.*

Successively, the above three highly stereoregular poly(1,3-diene)s were hydrogenated with diimide, formed in situ by thermal decomposition of *p*-toluenesulfonyl hydrazide,[22] obtaining perfectly alternating ethylene/propylene[23] copolymers (Scheme 2.5) having isotactic or syndiotactic structures depending on the starting unsaturated polymer. Hereafter, we will name the alternating E/P copolymers from the hydrogenation of the corresponding 1,3-diene polymers as H-sP(EP), H-iP(EP) and H-PI, respectively.

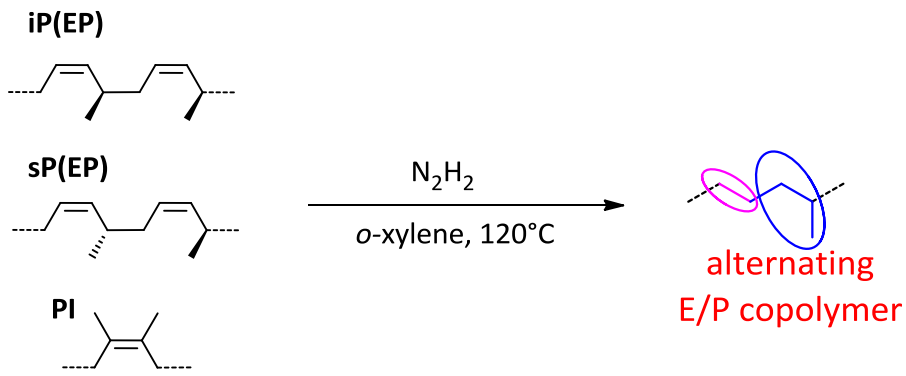

Scheme 2.5. *Scheme of hydrogenation of iso- and syndiotactic cis-1,4 poly(1,3-pentadiene) (iP(EP) and sP(EP)), and cis-1,4 poly(isoprene) (PI).*

Specifically, for each sample the hydrogenation conditions were the following:
(*i*) isotactic *cis*-1,4 poly(1,3-pentadiene): polymer 2.9 g; *o*-xylene, 300 mL; first addition of *p*-T*s*NH, 20.0 g (1.07×10^{-1} mol); second and third addition of *p*-T*s*NH, 30.0 g (1.87×10^{-1} mol);
(*ii*) syndiotactic *cis*-1,4 poly(1,3-pentadiene): polymer 0.5 g; *o*-xylene, 70 mL; first addition of *p*-T*s*NH, 9.0 g (5.0×10^{-2} mol); second and third addition of *p*-T*s*NH, 10.0 g (5.56×10^{-2} mol);
(*iii*) *cis*-1,4 poly(isoprene): polymer 0.5 g; *o*-xylene, 100 mL; first addition of *p*-T*s*NH, 8.0 g (4.44×10^{-2} mol); second and third addition of *p*-T*s*NH, 9.0 g (5.0×10^{-2} mol).

The obtained copolymers were characterized by ^{1}H-, ^{13}C-, 2D NMR spectroscopy and XRD. Thermal and mechanical properties were also investigated.

Structural and thermal analysis

The complete hydrogenation of the diene polymers was confirmed by comparison of FT-IR and ^{1}H-NMR spectra of the starting *cis*-1,4 poly(1,3-diene)s and of the corresponding hydrogenated products (Figures 2.9 and 2.10, respectively).

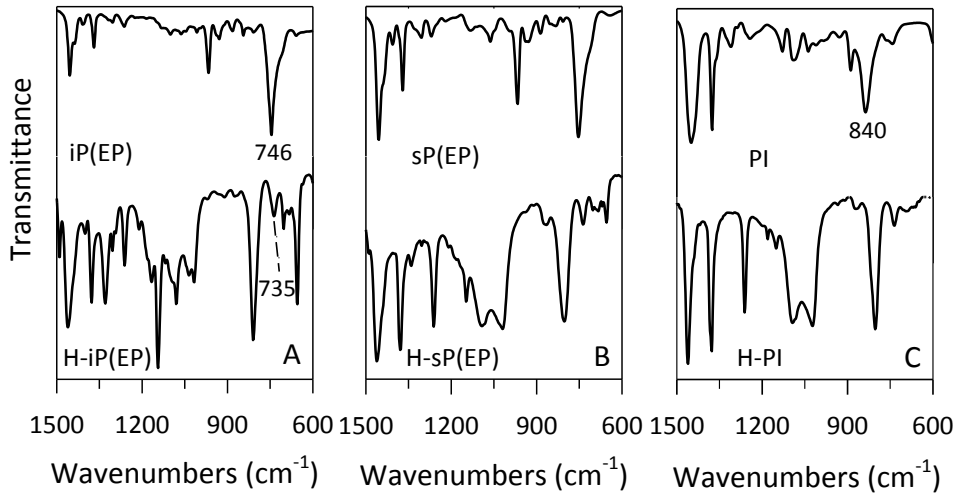

Figure 2.9. *FTIR spectra of (A) isotactic cis-1,4 poly(1,3-pentadiene) (top) and its saturated polymers (bottom), (B) syndiotactic cis -1,4 poly(1,3-pentadiene) (top) and its saturated polymers (bottom) and (C) cis-1,4 poly(isoprene)(top) and its saturated polymers (bottom).*

The typical bands observed at 746 cm^{-1} in the FT-IR spectra of *cis*-1,4 poly(1,3-pentadiene)s and 840 cm^{-1} in the FTIR spectra of *cis*-1,4 poly(isoprene), ascribed to the out-of-plane vibration of the hydrogen atoms adjacent to the double bond in a *cis*-1,4 unit, are completely absent in the FT-IR spectra of the corresponding saturated polymers; besides, a new band at 735 cm^{-1} was observed in the FT-IR spectra of the hydrogenated polymers, ascribed to the vibration of a $–CH_2–$ unit, typical of saturated polyolefins (Figure 2.9).

The ^{1}H NMR spectra of sP(EP), iP(EP), PI and those of the corresponding hydrogenated products H-sP(EP), H-iP(EP) and H-PI, are shown in Figure 2.10.

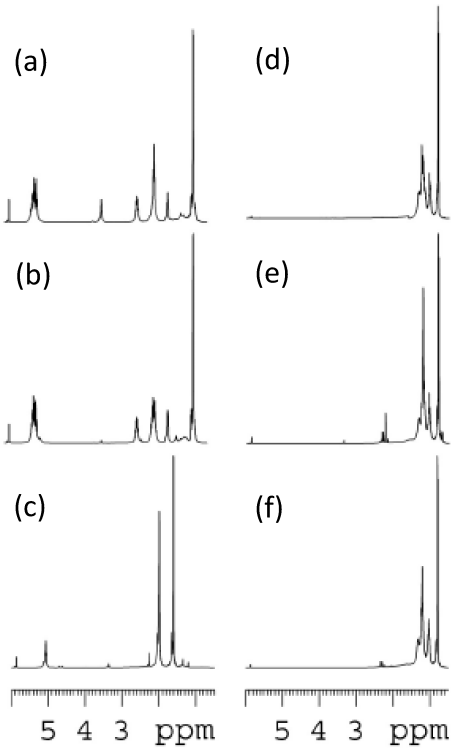

Figure 2.10. *^{1}H-NMR spectra ($C_2D_2Cl_4$, 103°C, HMDS) of the unsaturated iP(EP) (a), sP(EP) (b) and (PI) (c), and saturated H-iP(EP) (d), H-sP(EP) (e) and H-PI (f).*

As it is clearly evident the peaks in the olefinic region (from 5.2 to 5.4 ppm), observed in the ^{1}H-NMR spectra of the diene polymers, and due to the olefinic hydrogen atoms, are not observed in the ^{1}H-NMR spectra of the hydrogenated polymers, confirming indeed the complete hydrogenation of the diene polymers. The structure and tacticity of the resulting E/P copolymers were investigated by means of ^{1}H NMR and ^{13}C NMR, 2D NMR experiments [*i.e.*, Heteronuclear Single Quantum Correlation (HSQC)] and X-ray diffraction analysis. Figure 2.11 shows the ^{13}C NMR spectra of the diene polymers; the peaks were assigned as already reported.[33]

polymer/ppm	C1	C2	C3	C4	C5
PI	30.44	123.35	133.30	24.60	21.38
sP(EP)	33.37	124.62	134.75	30.31	18.73
iP(EP)	33.38	124.73	134.72	30.42	18.84

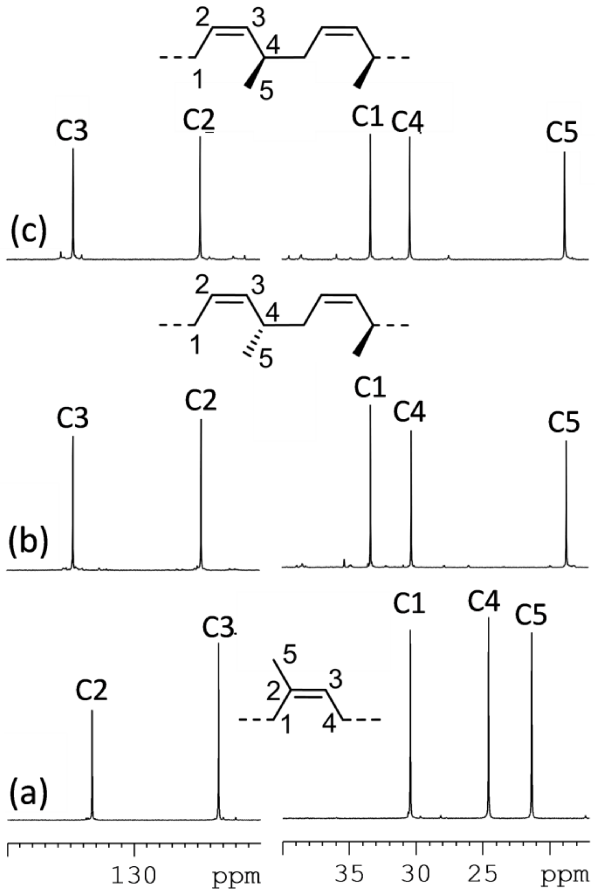

Figure 2.11. *^{13}C-NMR spectra ($C_2D_2Cl_4$, 103°C, HMDS) of the unsaturated polymer: (a) PI, (b) sP(EP) and (c) iP(EP).*

The ^{13}C-NMR spectra of the hydrogenated polymers (E/P copolymers) are shown in Figure 2.12 and exhibit four major resonances around 17.9 (C5), 22.6 (C2), 31.0 (C4), and 35.7 (C1,C3) ppm likely corresponding to the four unique signals of a perfectly alternating E/P copolymer structure.

Polymer/ppm	C1/C3	C2	C4	C5
H-PI	35.72	22.60	30.96	17.92
	35.69			17.88
	35.66			17.84
	35.63			
H-sP(EP)	35.69	22.61	30.96	17.82
H-iP(EP)	35.66	22.59	30.98	17.92

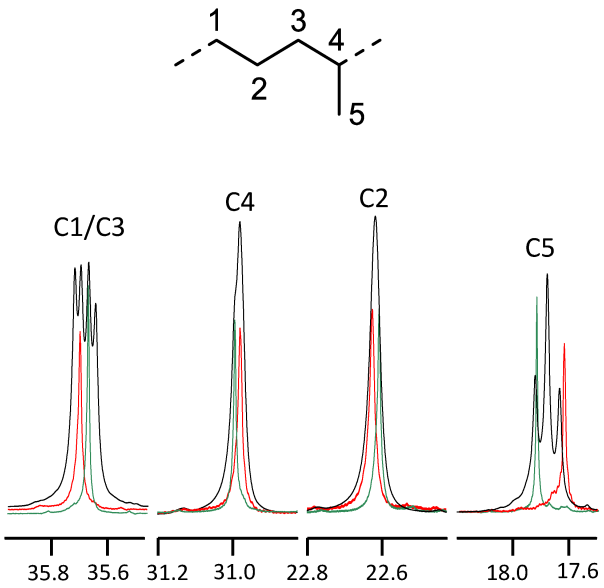

Figure 2.12. *^{13}C-NMR spectra of the hydrogenated polymers: H-PI in black, H-sP(EP) in red, and H-iP(EP) in green.*

The chemical shifts are very close for the three hydrogenated polymers so that, on the basis of the ^{13}C-NMR spectra only, it is not possible to distinguish the tacticity of the copolymers obtained with the hydrogenation reaction. In principle, however, since the hydrogenation reaction in the case of poly(1,3-pentadiene)s does not lead to the formation of new asymmetric carbon atoms, it is reasonable to assume that the tacticity of the diene polymer precursors is maintained in the alternating resulting E/P copolymers, that is isotactic for H-iP(EP) and syndiotactic for H-sP(EP). This assumption was confirmed by means of the two-dimensional correlation spectroscopy, HSQC experiment, as the presence of a cross peak is indicative of protons and carbons directly linked through $^{1}J_{CH}$, and was able to give

information about the different tacticity of the E/P copolymers. Results of these experiments are shown in Figure 2.13. Specifically, the signal at about 22.6 ppm, corresponding to the Sββ methylene carbon, has proved to be diagnostic of the tacticity of the copolymer, as it is influenced by the arrangement of the methyl substituents, although not adjacent to the carbon atom bearing the methyl.

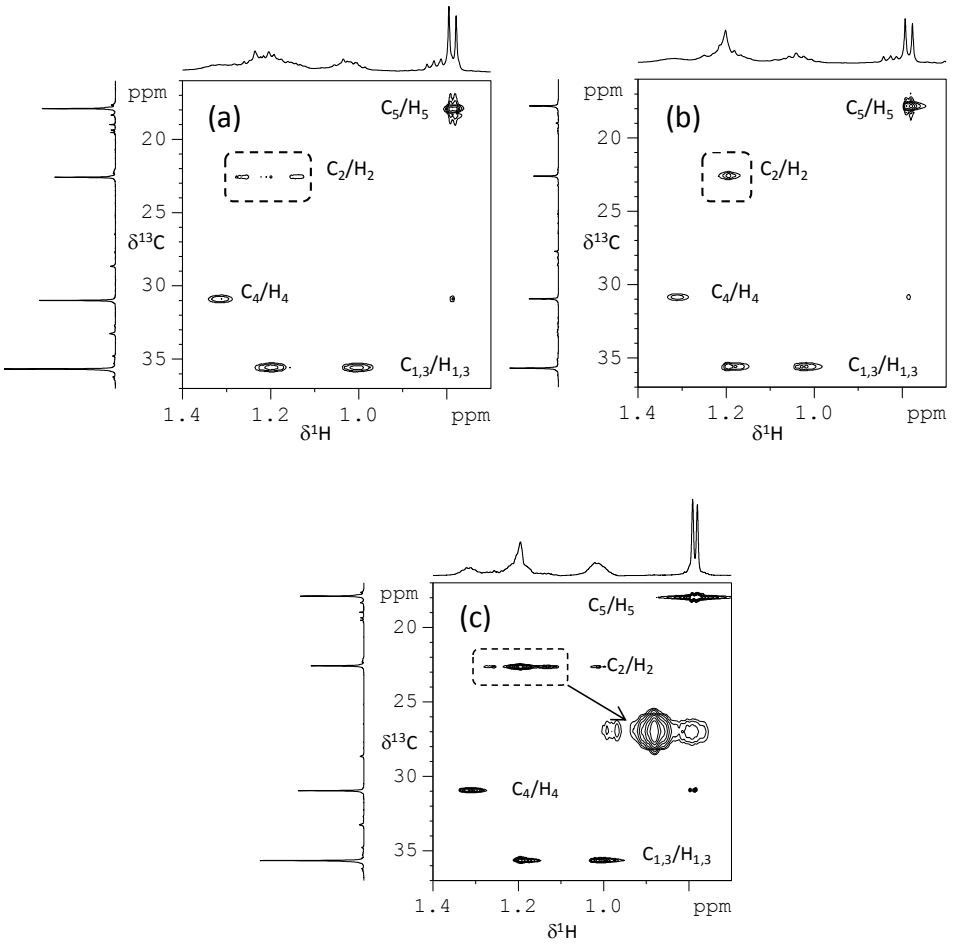

Figure 2.13. *^1H- ^{13}C HSQC of H-iP(EP) (a), H-sP(EP) (b) and H-PI (c), at 330 K in $C_2D_2Cl_4$.*

In the HSQC spectrum of the product of the hydrogenation of isotactic *cis*-1,4 poly(1,3-pentadiene) (Figure 2.13 a, iP(EP)), the C2 carbon at δ = 22.59 ppm correlates with two cross peaks at δ_H= 1.25 and 1.14 ppm, respectively. This is indicative of a methylene to which two magnetically non-equivalent protons are linked, as they display two different resonance frequencies "like in a different environment", thus suggesting that the E/P copolymer obtained by hydrogenation of iP(EP) has an isotactic structure. [9,34]

In the case of sP(EP) (Figure 2.13 b), the methylene at δ= 22.61 ppm showed a single correlation peak at δ_H =1.19 ppm, meaning a linking with two magnetic equivalent, in agreement with the syndiotactic structure of H-sP(EP). Finally, for the H-PI, the 2D HSQC experiment suggest the coexistence of isotactic and syndiotactic stereoregularities (Figure 2.13 c). The syndiotacticity (associated to the single cross peak for δ_C= 22.6 ppm, δ_H = 1.19 ppm) seems to be slightly preferred with respect to the isotacticity (two cross peaks for δ_C= 22.6 ppm, δ_H = 1.13 and 1.27 ppm), being the single cross peak intensity more pronounced in the 2D spectrum. Once the tacticity was established, the peaks multiplicity observed for the ^{13}C-NMR resonances in the ^{13}C-NMR spectrum of H-PI (Figure 2.12, black line; 35.72, 35.69, 35.66, 35.63 ppm for C1/C3 carbons; 17.92, 17.88, 17.84 for C5 carbon; some enlargement of the peaks at 22.60 and 30.96 ppm corresponding to carbons C2 and C4, respectively), could be reasonably related to the sensitivity of the carbon atoms up to triad level (in case of C5) and tetrads level (C1/C3 carbons).

The X-ray powder diffraction profiles of the hydrogenated polymers H-iP(EP), H-sP(EP), and H-PI are shown in Figure 2.14 A. It is apparent that all samples show broad diffraction profiles with an absence of Bragg reflections, indicating that all samples are amorphous. The diffraction profiles do not change upon thermal treatments and the samples do not crystallize even after annealing at relatively high temperatures or upon aging at room and low temperatures. Moreover, in the case of sample iP(EP), that can be stretched at relatively high deformations, crystallization does not take place by stretching up to high degrees of deformation and even keeping the sample under tension at low temperature for long time. The NMR data of Figures 2.12 and 2.13 as well as the diffraction data of Figure 2.14 A indicate that the E/P alternating copolymers have a regular stereochemical structure, isotactic and syndiotactic for H-iP(EP) and H-sP(EP), respectively, and a statistical atactic structure for H-PI; the regular copolymers are however not able to crystallize. The DSC heating curves of samples H-iP(EP), H-sP(EP) and H-PI are shown in Figure 2.14 B. According to the X-ray diffraction profiles of Figure 2.14 A, all DSC curves show only a T_g at about −60 °C and the absence of any endothermic signal (Table 2.6). Only the glass transition at the same temperatures is observed in the successive cooling scans with absence of exothermic signals.

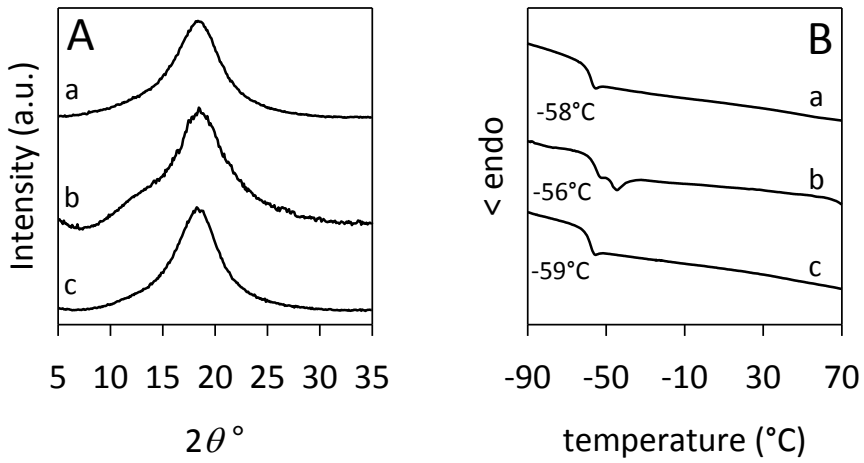

Figure 2.14. *(A) X-ray powder diffraction profiles of as-prepared samples of E/P alternating copolymers corresponding to the hydrogenated polymers H-iP(EP) (a), H-sP(EP) (b), and H-PI (c). (B) DSC heating curves, recorded at 10 °C/min, of as-prepared samples of alternating E/P copolymers corresponding to the hydrogenated polymers H-iP(EP) (a), H-sP(EP) (b), and H-PI (c).*

Table 2.6 *Values of M_n, M_w/M_n and T_g of samples of E/P alternating copolymers obtained by hydrogenation of the corresponding polydienes.*

E/P Copolymers	**Corresponding Poly(1,3-diene)**	M_w **(kg/mol)** [a]	M_w/M_n [a]	T_g [b] **(°C)**
H-iP(EP)	isotactic *cis*-1,4 poly(1,3-pentadiene)	194.8	2.8	–58
H-sP(EP)	syndiotactic *cis*-1,4 poly(1,3-pentadiene)	60.5	3.1	–56
H-PI	*cis*-1,4 isoprene	249.3	2.8	–59

[a] *determined by SEC;* [b] *determined by DSC.*

Mechanical properties

The mechanical properties under tensile deformation of the three E/P alternating copolymers of different stereochemical structure have also been studied. The stress-strain curves recorded at room temperature of compression-molded films of the hydrogenated polymers are shown in Figure 2.15. According to the absence of crystallinity, all samples show low values of the Young modulus (0.6–1.0 MPa) and of the stress at any strain and viscous flow already at relatively low deformations. The differences in the stress-strain curves are mainly related to the different molecular masses of the three alternating copolymers. Higher values of the stress are, indeed, shown by the sample H-PI of higher molecular mass.

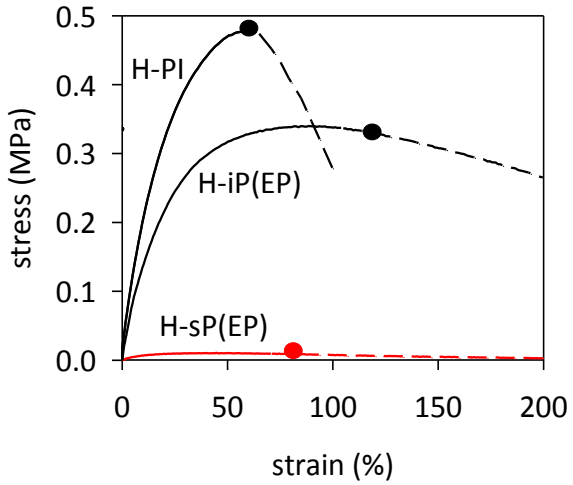

Figure 2.15. *Stress-strain curves of alternating E/P copolymers corresponding to the hydrogenated polymers H-iP(EP), H-sP(EP), and H-PI. The dashed portions of the stress-strain curves indicate the deformation at which viscous flow without breaking occurs.*

2.1.3 Alternating ethylene/1-butene copolymers

Now, I describe the synthesis and characterization of perfectly alternating isotactic ethylene/1-butene copolymer, obtained by hydrogenation of isotactic *cis*-1,4 poly(1,3-hexadiene).[35,36]

Polymerization

The highly stereoregular poly(1,3-diene) on which this study focused was: isotactic *cis*-1,4 poly(1,3-hexadiene) [iP(HEX)]. The isotactic *cis*-1,4 polymer has been obtained with the ternary catalyst system $Et_2AlCl/Nd(OCOC_7H_{15})_3/Al^iBu_3$, as described in reference[6,35,36] (Scheme 2.6). The polymerization data are summarized in Table 2.7.

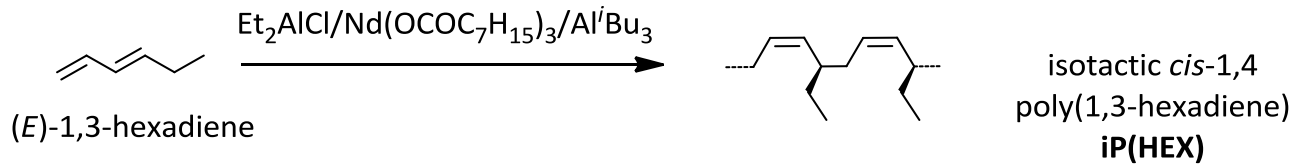

Scheme 2.6. *Polymerization of (E)-1,3-hexadiene.*

Table 2.7. *Polymerization of (E)-1,3-hexadiene with catalysts based on Nd* [a]

Sample	Monomer (type)	Catalyst (type)	Time (min)	Yield (%)	*cis*-1,4 [b] (%)	T_g [c] (°C)	M_w [d] (kg/mol)	M_w/M_n [d]
iP(HEX)	(*E*)-1,3-hexadiene	$Et_2AlCl/Nd(OCOC_7H_{15})_3/Al^iBu_3$	60	87	≥90	–66	270	3.8

[a] *Polymerization Conditions: monomer, 2 mL; heptane, total volume, 16 mL, Nd complex, 2×10^{-5} mol; temperature, 21°C;* [b] *Percentage of cis-1,4 units, determined by NMR analysis;* [c] *glass transition temperature, determined by DSC;* [d] *determined by SEC.*

The hydrogenation process converted isotactic *cis*-1,4 poly(1,3-hexadiene)s into perfectly alternating ethylene/1-butene copolymers (E/1B), having isotactic structure as a function of the starting diene polymer (Scheme 2.7). Hereafter we will call H-iP(HEX) the alternating E/1B copolymer arising from the hydrogenation of isotactic *cis*-1,4 poly(1,3-hexadiene).

Specifically, for isotactic *cis*-1,4 poly(1,3-hexadiene)s the hydrogenation conditions were:

(i) isotactic *cis*-1,4 poly(1,3-hexadiene): polymer 0.543 g; *o*-xylene, 80 mL; first addition of *p*-TsNH, 4.2 g (2.25×10^{-2} mol); second and third addition of *p*-TsNH, 7 g (3.74×10^{-2} mol).

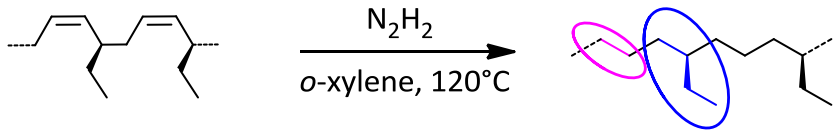

isotactic *cis*-1,4 poly(1,3-hexadiene) **iP(HEX)**

alternating E/1B copolymer

Scheme 2.7*. Scheme of hydrogenation of isotactic cis-1,4 poly(1,3-hexadiene) (iP(HEX)).*

Structural and thermal analysis

The successful complete hydrogenation of the diene polymer was confirmed by comparison of the Fourier transform infrared (FT-IR) (Figure 2.16) and ^{1}H NMR spectra (Figure 2.17) of the starting *cis*-1,4 poly(1,3-diene) and of the corresponding hydrogenated product.

The typical bands observed at 751 cm^{-1} in the FTIR spectra of *cis*-1,4 poly(1,3-hexadiene) ascribed to the out-of-plane vibration of the hydrogen atoms adjacent to the double bond in a *cis*-1,4 unit, are completely absent in the FT-IR spectra of the corresponding hydrogenated polymer; besides, a new band at 735 cm^{-1} is observed in the FT-IR spectra of the hydrogenated polymer, ascribed to the vibration of a $–CH_2–$ unit, typical of saturated polyolefins (Figure 2.16).

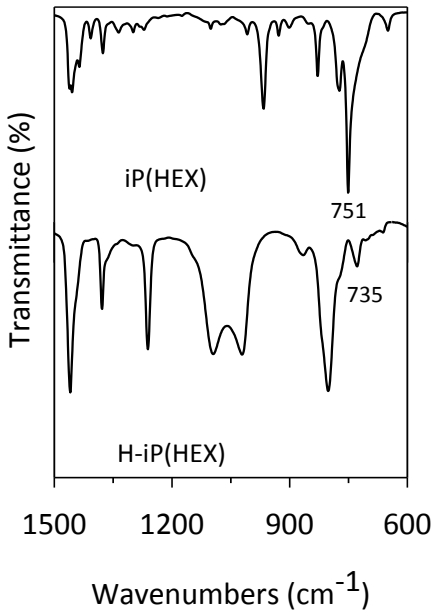

***Figure 2.16**. FTIR spectra of isotactic cis-1,4 poly(1,3-hexadiene) (top) and its saturated polymer (bottom).*

The ^{1}H NMR spectra of the isotactic *cis*-1,4 poly(1,3-hexadiene) and of the corresponding hydrogenated product are shown in Figure 2.17. As it is clearly evident, peaks in the olefinic region (from 5.2 to 5.4 ppm), observed in the ^{1}H NMR spectra of the diene polymer and due to the olefinic hydrogen atoms, are not observed in the ^{1}H NMR spectra of the hydrogenated polymer, confirming indeed the complete hydrogenation of the diene polymer.

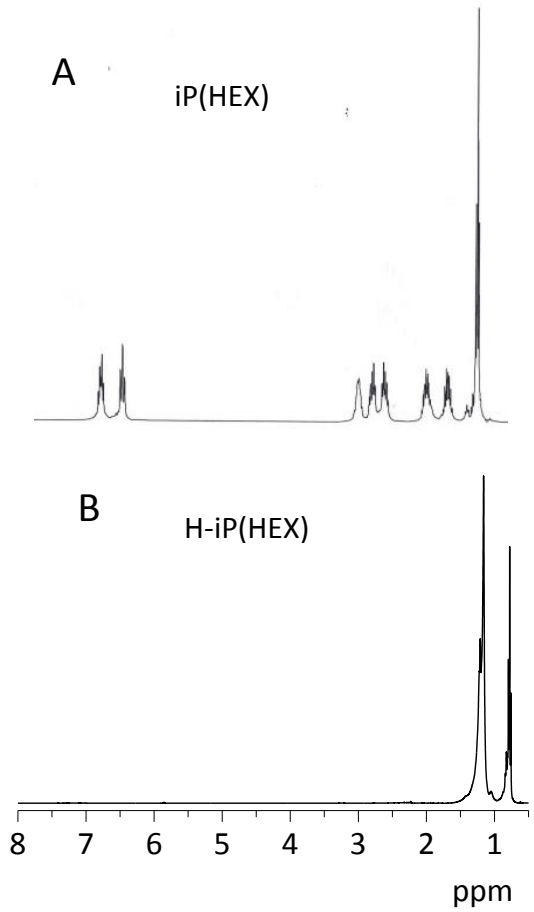

Figure 2.17. *^{1}H NMR spectra ($C_2D_2Cl_4$, 103°C, HMDS) of isotactic cis-1,4 poly(1,3-hexadiene) (A) and its saturated polymer (B).*

The structure and tacticity of the resulting E/1B copolymer were studied by means of ^{1}H and ^{13}C NMR, and X-ray diffraction analysis.

Figure 2.18 shows the ^{13}C NMR spectra of the isotactic *cis*-1,4 poly(1,3-hexadiene) and its saturated polymer; the peaks were assigned as already reported.[6,35,36]

polymer/ppm	C1	C2	C3	C4	C5	C6
iP(HEX)	31.63	126.12	133.00	37.53	26.10	9.67
H-iP(HEX)	32.29	22.33	32.29	37.36	24.48	9.07

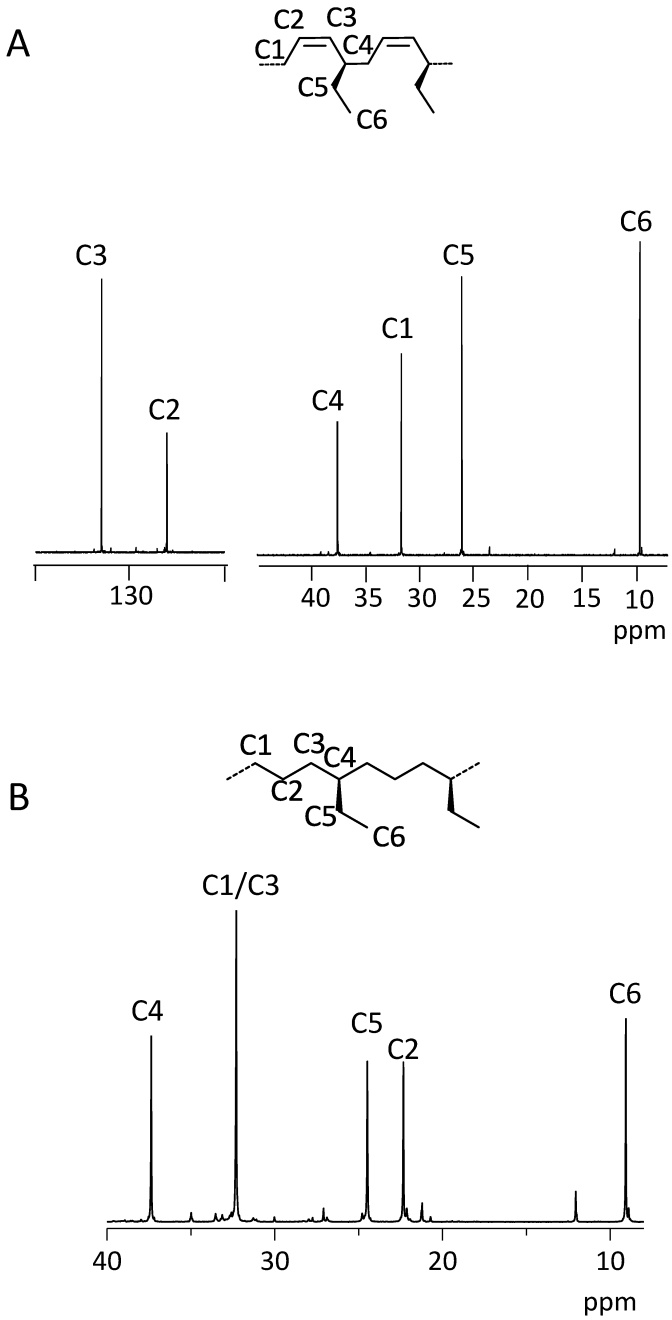

Figure 2.18. *^{13}C NMR spectra ($C_2D_2Cl_4$, 103°C, HMDS) of the iP(HEX) (A) and of the hydrogenated polymer H-iP(HEX) (B).*

The X-ray diffraction profile of the alternating isotactic ethylene/1-butene copolymer is shown in Figure 2.19 A, and the DSC curves recorded during first heating, successive cooling from the melt and second heating of the melt crystallized sample are reported in Figure 2.19 B.

Both X-ray diffraction and DSC data indicate the absence in this sample of a crystallinity. The alternating isotactic ethylene/1-butene copolymer does not crystallize after annealing or cooling from high temperature as confirmed from the absence of exothermic peaks or endothermic peaks in the DSC cooling and heating curves.

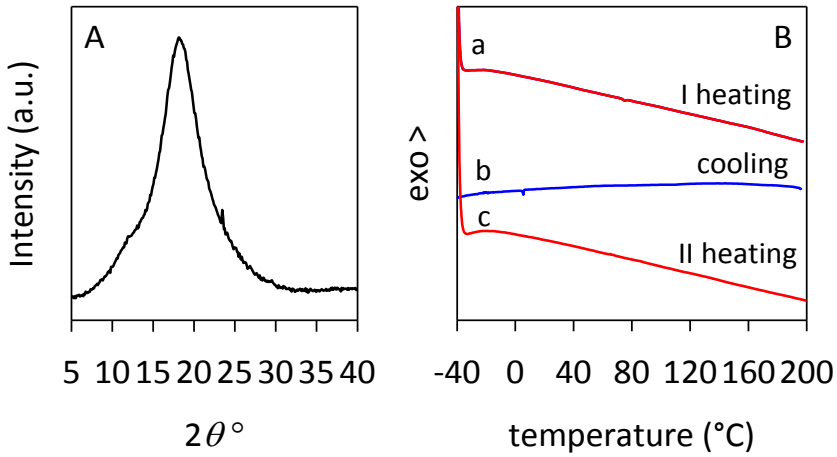

***Figure 2.19**. (A) X-ray powder diffraction profile of alternating E/1B copolymer.(B) DSC curves recorded during first heating (a), successive cooling (b) and second heating scans (c) of alternating E/1B copolymer.*

2.1.4 Alternating ethylene/1-pentene copolymers

Polymerization

I describe the synthesis and characterization of alternating ethylene/1-pentene copolymers, iso- and syndiotactic, obtained by hydrogenation of *cis*-1,4 poly(1,3-heptadiene), iso- and syndiotactic. The highly stereoregular poly(1,3-diene)s on which this study focused were: syndiotactic *cis*-1,4 poly(1,3-heptadiene) (hereafter named sP(HEP)), isotactic *cis*-1,4 poly(1,3-hexadiene) (iP(HEP)). The syndiotactic *cis*-1,4 poly(1,3-heptadiene) has been synthesized with the catalyst system $CoCl_2(P^tBuMe)_2$/MAO as described in references; [6,35,36] the isotactic *cis*-1,4 polymer has been obtained with the ternary catalyst system $Et_2AlCl/Nd(OCOC_7H_{15})_3/Al^iBu_3$, as described in reference[6,35,36] (Scheme 2.8). The polymerization data are summarized in Table 2.8.

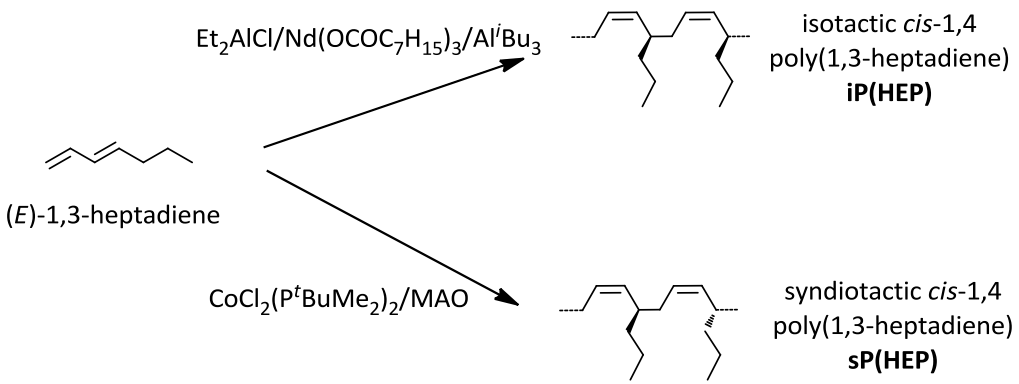

Scheme 2.8. *Polymerization of (E)-1,3-heptadiene.*

Table 2.8. *Polymerization of (E)-1,3-heptadiene with catalysts based on Nd and Co.*[a]

Sample	Monomer (type)	Catalyst (type)	Time (min)	Yield (%)	*cis*-1,4[b] (%)	M_w (kg/mol)	T_g [c] (°C)
iP(HEP)	(*E*)-1,3-heptadiene	$Et_2AlCl/Nd(OCOC_7H_{15})_3/Al^iBu_3$	30	100	≥97	78.7	–65
sP(HEP)	(*E*)-1,3-heptadiene	$CoCl_2(P^tBu_2Me)_2$/MAO	20160	73	100	29	–63

[a] *Polymerization Conditions: monomer, 2 mL; heptane for isotactic polymer and toluene for syndiotactic polymer, total volume, 16 mL, Co or Nd complex, 2×10^{-5} mol; temperature, 21°C;* [b] *Percentage of cis-1,4 units, determined by NMR analysis;* [c] *Glass transition temperature, determined by DSC.*

The hydrogenation process converted *cis*-1,4 poly(1,3-heptadiene)s into perfectly alternating ethylene/1-pentene copolymers (E/1P), having isotactic or syndiotactic structure as a function of the starting diene polymers (Scheme 2.9).

Hereafter, we will name the alternating E/1P copolymers from the hydrogenation of the corresponding 1,3-diene polymers as H-iP(EP), H-sP(EP).

Specifically, for each sample the hydrogenation conditions were the following:
(*i*) isotactic *cis*-1,4 poly(1,3-heptadiene): polymer 0.730 g; *o*-xylene, 80 mL; first addition of *p*-T*s*NH, 5.3 g (2.84×10^{-2} mol); second and third addition of *p*-T*s*NH, 9.0 g (4.83×10^{-2} mol);
(*ii*) syndiotactic *cis*-1,4 poly(1,3-heptadiene): polymer 0.460 g; *o*-xylene, 80 mL; first addition of *p*-T*s*NH, 3.5 g (1.88×10^{-2} mol); second and third addition of *p*-T*s*NH, 7.0 g (3.76×10^{-2} mol).

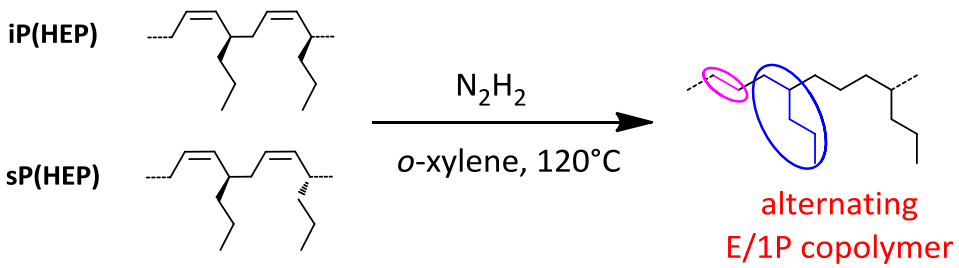

Scheme 2.9*. Scheme of hydrogenation of iP(HEP) and sP(HEP).*

Structural analysis

The successful complete hydrogenation of the diene polymers was confirmed by ^{1}H NMR spectra (Figure 2.20) of the starting *cis*-1,4 poly(1,3-diene)s and of the corresponding hydrogenated products.

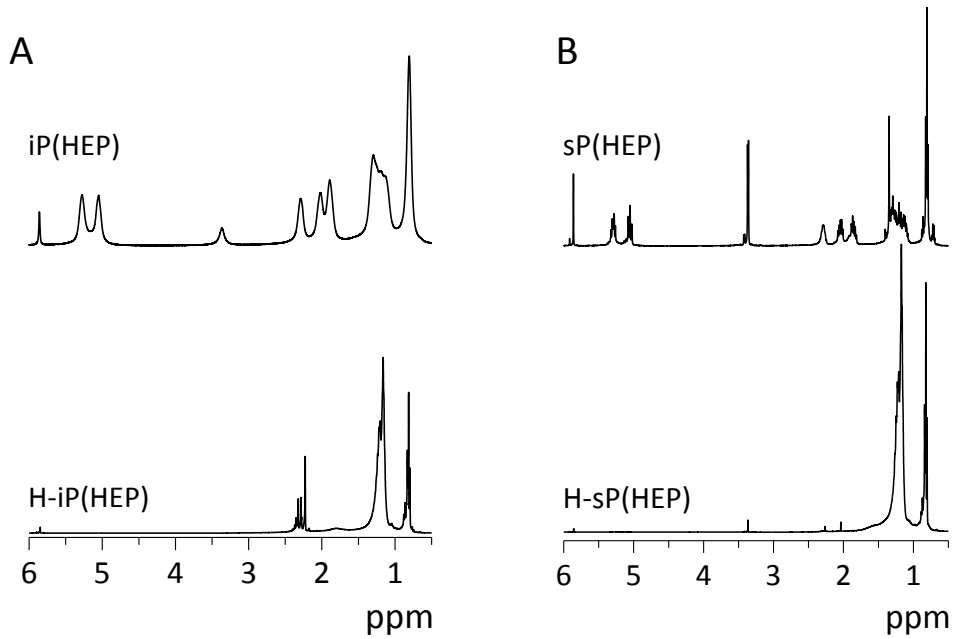

Figure 2.20. *^{1}H NMR spectra ($C_2D_2Cl_4$, 103°C, HMDS) of (A) isotactic cis-1,4 poly(1,3-heptadiene) (top) and its saturated polymer (bottom); (B) syndiotactic cis-1,4 poly(1,3-heptadiene) (top) and its saturated polymers (bottom).*

The structure and tacticity of the resulting E/1P copolymers were studied by means of ^{1}H and ^{13}C NMR.

Figure 2.21 shows the ^{13}C NMR spectra of the isotactic *cis*-1,4 poly(1,3-heptadiene) and its saturated polymer; Figure 2.22 shows the ^{13}C NMR spectra of the syndiotactic *cis*-1,4 poly(1,3-heptadiene) and its saturated polymer together with the peaks attribution.

polymer/ppm	C1	C2	C3	C4	C5	C6	C7
iP(HEP)	31.99	125.88	133.36	35.65	35.86	18.44	12.29
H-iP(HEP)	32.77	22.24	32.77	35.57	34.69	18.08	12.54

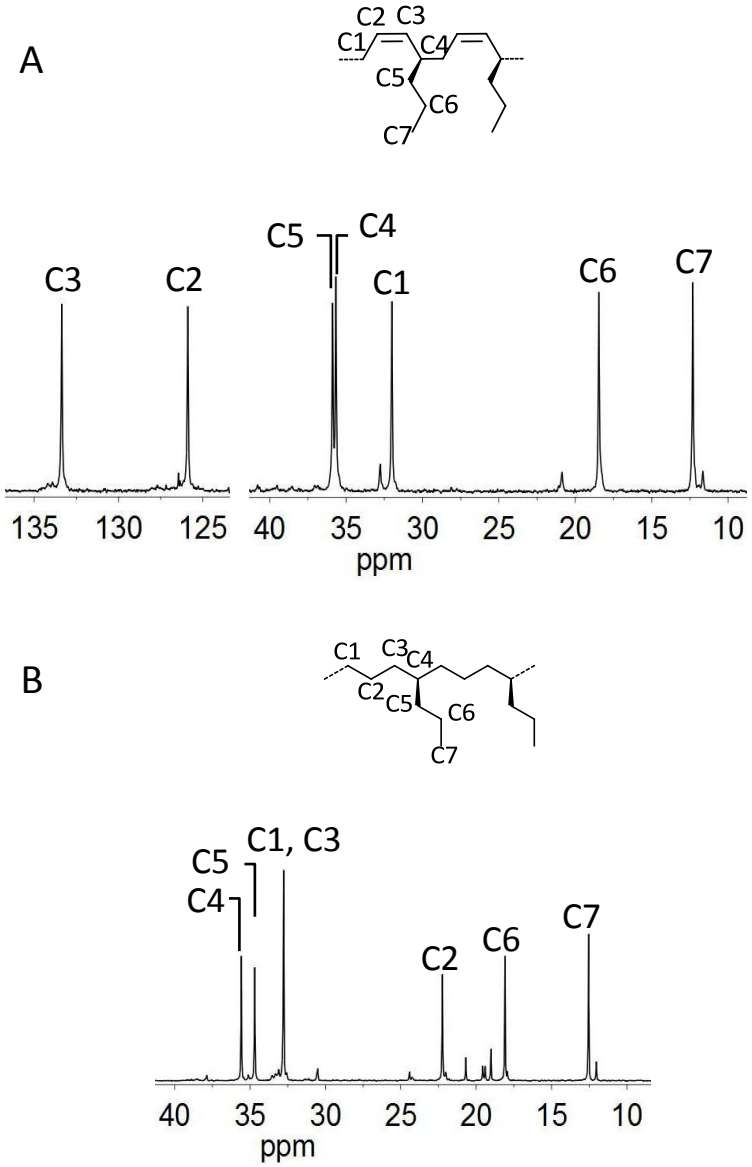

Figure 2.21. *^{13}C NMR spectra ($C_2D_2Cl_4$, 103°C, HMDS) of the iP(HEP) (A) and of the hydrogenated polymer H-iP(HEP)(B).*

polymer/ppm	C1	C2	C3	C4	C5	C6	C7
sP(HEP)	31.91	125.81	133.30	35.56	35.84	18.47	12.27
H-sP(HEP)	32.79	22.24	32.79	35.61	34.68	18.08	12.53

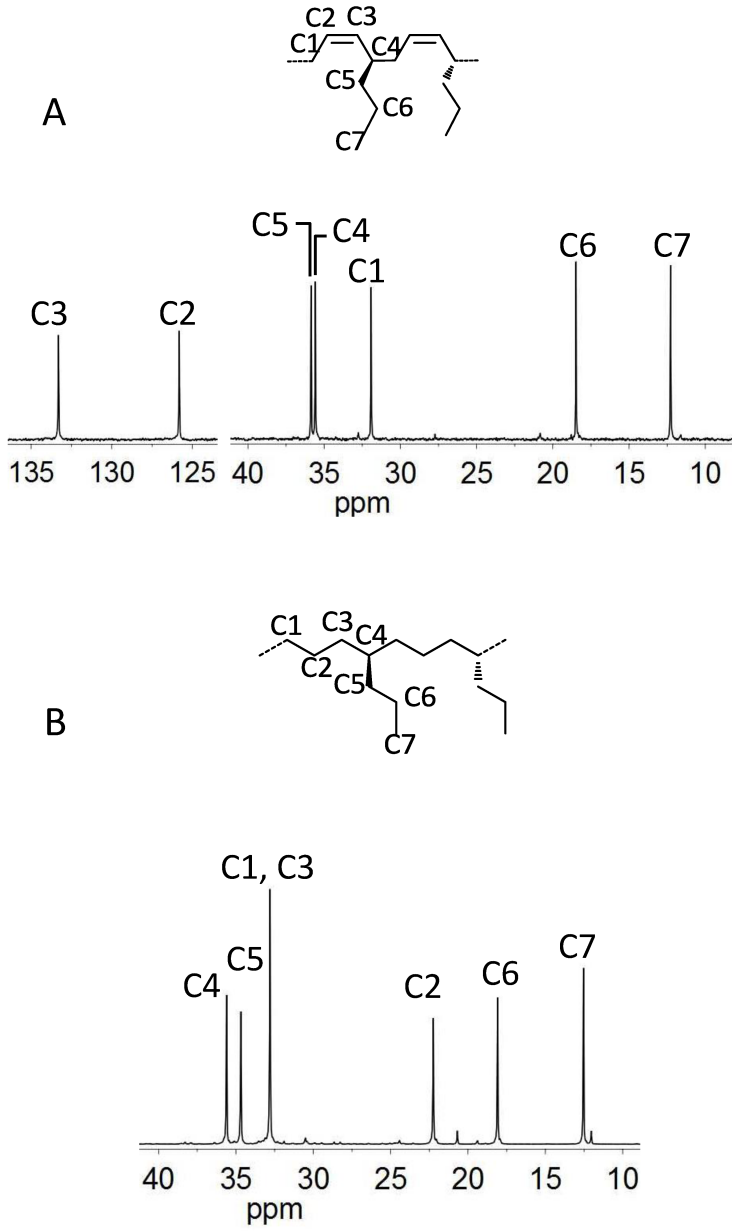

Figure 2.22. *^{13}C NMR spectra ($C_2D_2Cl_4$, 103°C, HMDS) of the sP(HEP) (A) and of the hydrogenated polymer H-sP(HEP)(B).*

2.1.5 Alternating ethylene/1-hexene copolymers

Polymerization

I describe the synthesis and characterization of alternating ethylene/1-hexene copolymers, iso- and syndiotactic, obtained by hydrogenation of *cis*-1,4 poly(1,3-octadiene), iso- and syndiotactic. The highly stereoregular poly(1,3-diene)s on which this study focused were: syndiotactic *cis*-1,4 poly(1,3-octadiene) (hereafter named sP(OCT)), isotactic *cis*-1,4 poly(1,3-octadiene) [iP(OCT)]. The syndiotactic *cis*-1,4 poly(1,3-octadiene) has been synthesized with the catalyst system $CoCl_2(P^tBu_2Me)_2$/MAO as described in references; [6,35,36] the isotactic *cis*-1,4 polymer has been obtained with the ternary catalyst system $Et_2AlCl/Nd(OCOC_7H_{15})_3/Al^iBu_3$, as described in reference [6,35,36] (Scheme 2.10). The polymerization data are summarized in Table 2.9.

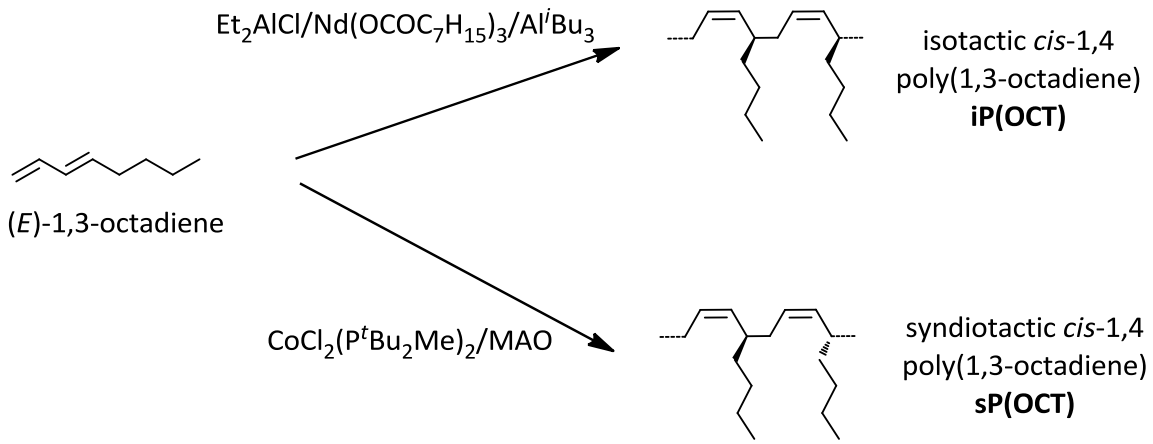

Scheme 2.10. *Polymerization of 1,3-octadiene.*

Table 2.7. *Polymerization of (E)-1,3-octadiene with catalysts based on Nd and Co.*[a]

Sample	Monomer (type)	Catalyst (type)	Time (min)	Yield (%)	*cis*-1,4[b] (%)	M_w (kg/mol)	M_w/M_n	T_g[c] (°C)
iP(OCT)	1,3-octadiene	$Et_2AlCl/Nd(OCOC_7H_{15})_3/Al^iBu_3$	1080	75	90	1100	10.0	-52
sP(OCT)	1,3-octadiene	$CoCl_2(P^tBu_2Me)_2$/MAO	24480	66	≥99	20	1.8	-53

[a] *Polymerization Conditions: monomer, 2 mL; heptane for iso-polymer and toluene for syndio polymer, total volume, 16 mL, Co or Nd complex, 2×10^{-5} mol; temperature, 21°C;* [b] *Percentage of cis-1,4 units, determined by NMR analysis;* [c] *Glass transition temperature, determined by DSC.*

The hydrogenation process converted *cis*-1,4 poly(1,3-octadiene)s into perfectly alternating ethylene/1-hexene copolymers (E/1H), having isotactic or syndiotactic structure as a function of the starting diene polymers (Scheme 2.11).

Hereafter, we will name the alternating ethylene/1-hexene copolymers from the hydrogenation of the corresponding 1,3-diene polymers as H-iP(OCT), H-sP(OCT).

Specifically, for each sample the hydrogenation conditions were the following:
(*i*) isotactic *cis*-1,4 poly(1,3-octadiene): polymer 1.08 g; *o*-xylene, 150 mL; first addition of *p*-T*s*NH, 7.66 g (4.76×10^{-2} mol); second and third addition of *p*-T*s*NH, 7.7 g (4.76×10^{-2} mol);
(*ii*) syndiotactic *cis*-1,4 poly(1,3-octadiene): polymer 0.608 g; *o*-xylene, 80 mL; first addition of *p*-T*s*NH, 4.3 g (2.3×10^{-2} mol); second and third addition of *p*-T*s*NH, 9.0 g (4.83×10^{-2} mol).

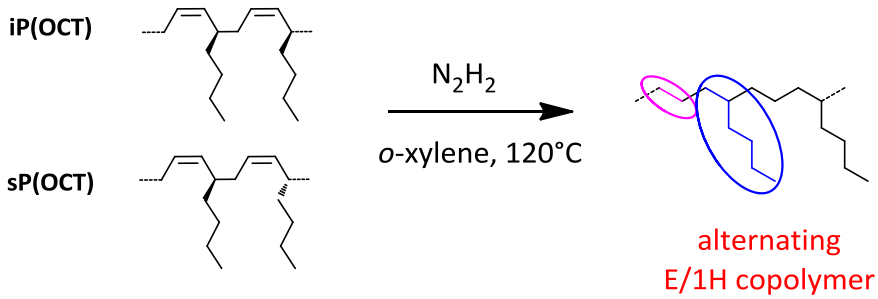

Scheme 2.11. *Scheme of hydrogenation of isotactic cis-1,4 poly(1,3-octadiene) (iP(OCT)) and syndiotactic cis-1,4 poly(1,3-octadiene) (sP(OCT)).*

Structural analysis

The successful complete hydrogenation of the diene polymers was confirmed by FT-IR (Figure 2.23) and by ^{1}H NMR spectra of the starting *cis*-1,4 poly(1,3-diene)s and of the corresponding hydrogenated products. The peaks in the olefinic region (from 5.2 to 5.4 ppm), observed in the ^{1}H NMR spectra of the diene polymers and due to the olefinic hydrogen atoms, are not observed in the ^{1}H NMR spectra of the hydrogenated polymer, confirming indeed the complete hydrogenation of the diene polymer.

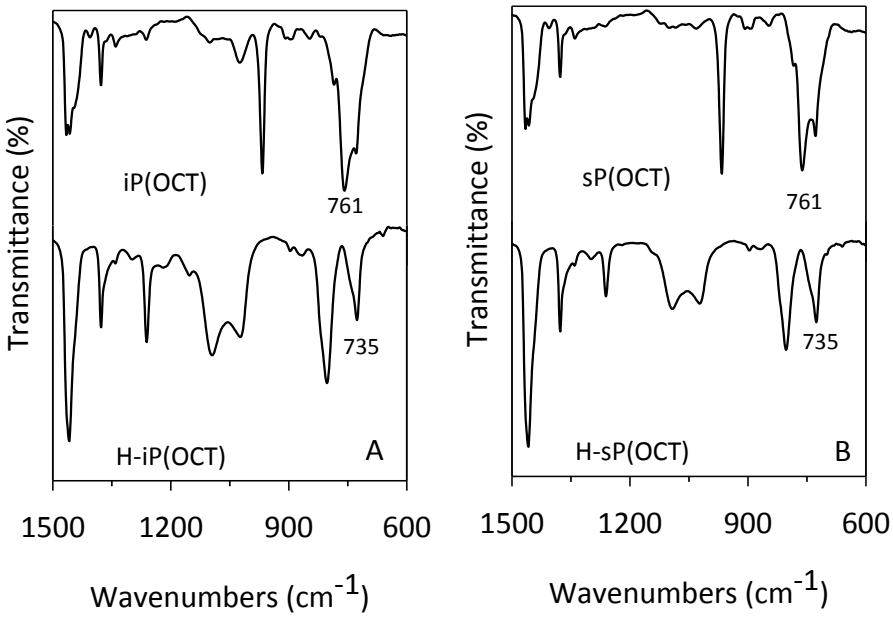

Figure 2.23. *FTIR spectra of (A) isotactic cis-1,4 poly(1,3-octadiene) (top) and its saturated polymers (bottom), (B) syndiotactic cis -1,4 poly(1,3-octadiene) (top) and its saturated polymers (bottom).*

The structure and tacticity of the resulting ethylene-1-hexene copolymers were studied by means of ^{1}H and ^{13}C NMR.

Figure 2.24 shows the ^{13}C NMR spectra of the isotactic *cis*-1,4 poly(1,3-octadiene) and its saturated polymer. Figure 2.25 shows the ^{13}C NMR spectra of the syndiotactic *cis*-1,4 poly(1,3-octadiene) and its saturated polymer together with the peaks attribution.

polymer/ppm	C1	C2	C3	C4	C5	C6	C7	C8
iP(OCT)	32.02	125.88	133.43	35.86	33.16	27.64	20.95	11.98
H-iP(OCT)	32.79	22.26	32.79	35.80	31.84	27.25	21.18	12.05

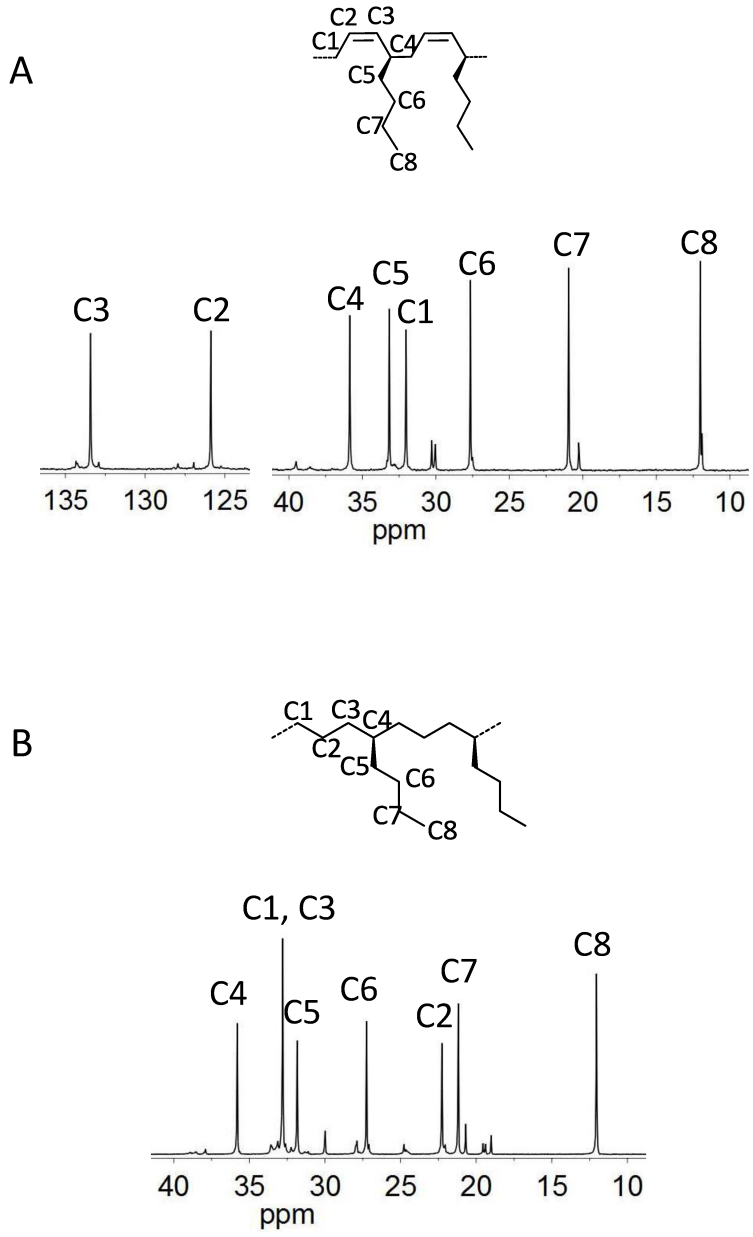

Figure 2.24. *^{13}C NMR spectra ($C_2D_2Cl_4$, 103°C, HMDS) of the iP(OCT) (A) and of the hydrogenated polymer H-iP(OCT)(B).*

polymer/ppm	C1	C2	C3	C4	C5	C6	C7	C8
sP(OCT)	31.96	125.83	133.34	35.80	33.17	27.68	20.92	11.98
H-sP(OCT)	32.81	22.27	32.81	35.83	31.83	27.25	21.18	12.05

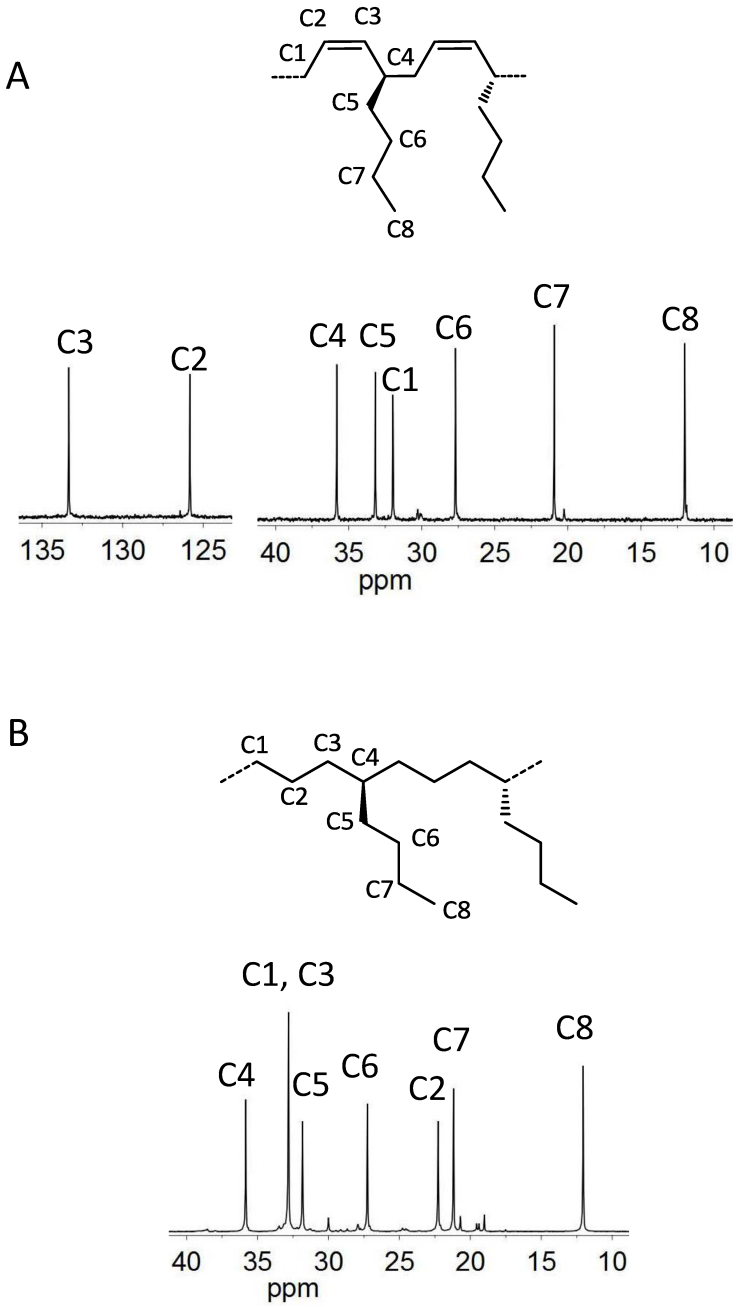

Figure 2.25. *^{13}C NMR spectra ($C_2D_2Cl_4$, 103°C, HMDS) of the sP(OCT) (A) and of the hydrogenated polymer H-sP(OCT)(B).*

The structural and thermal characterization have already been reported in the thesis of Chiara Santillo.[37] The isotactic alternating ethylene/1-hexene copolymer show broad diffraction profile with absence of Bragg reflections, indicating that the sample is amorphous. The X-ray diffraction profile of the alternating syndiotactic ethylene/1-hexene copolymer presents reflections due probably only to the presence of impurities in the sample.

2.2 Poly(α-olefins) by hydrogenation of stereoregular poly(1,3-diene)s with a 1,2 (3,4) structure

2.2.1. 1,2 poly(E-3-methyl-1,3-pentadiene) and isotactic poly(3-methyl-1-pentene)

Polymerization

In case of 3-methyl-1,3-pentadiene, among the 12 different possible stereoregular polymers,[7] the new isotactic 1,2-poly((*E*)-3-methyl-1,3-pentadiene) (iPE3MPD) has been prepared with the catalysts $CoCl_2(PRPh_2)_2$.[7] The polymer obtained with the catalytic systems having minimally hindered ligands (*e.g.*, $PMePh_2$, $PEtPh_2$, P^nPrPh_2) is highly isotactic (with isotactic triad *mm* content higher than 90%) and highly crystalline.[7] This new polymer is the third known example of crystalline isotactic 1,2-polydiene. The other two cases are the isotactic 1,2-polybutadiene[38,39] and the isotactic 1,2 poly(4-methyl-1,3-pentadiene),[40-42] besides the isotactic 3,4 polyisoprene.[43]

By polymerizing 3-methyl-1,3-pentadiene (mixture of *E* and *Z*) with the catalyst system $FeCl_2(bipy)_2$/MAO, Ricci *et al*.[44] obtained the syndiotactic 1,2 poly(*E*-3-methyl-1,3-pentadiene), a novel highly crystalline polymer. With the catalyst $CoCl_2(PRPh_2)_2$/MAO (R = methyl, ethyl, *n*-propyl, isopropyl and cyclohexyl),[45] the isotactic 1,2 poly(*E*-3-methyl-1,3-pentadiene) was instead obtained (Scheme 2.12).

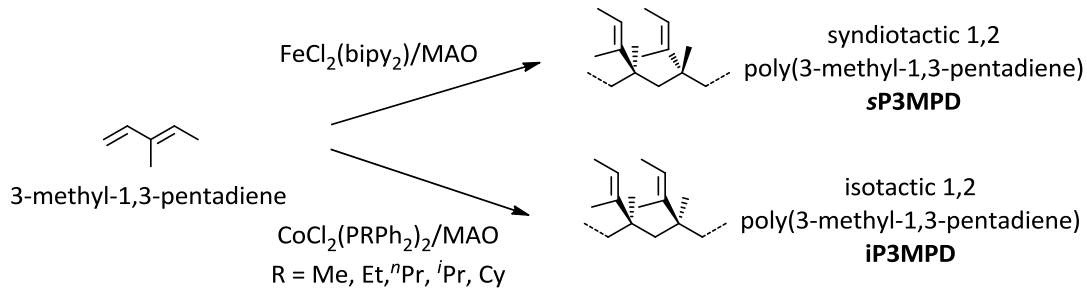

Scheme 2.12. *Polymerization of 3-methyl-1,3-pentadiene.*

Isotactic 1,2 poly(*E*-3-methyl-1,3-pentadiene) (iP3MPD) is a new crystalline polymer that could not be synthesized with the classic stereospecific Ziegler-Natta catalysts but can be synthesized with catalysts based on cobalt complexes with various phosphines in combination with methylaluminoxane (MAO).[7,45-47] The

isotactic content was found to depend on the type of catalyst used (*i.e.*, type of phosphine ligand bonded the cobalt atom), increasing with decreasing the bulkiness of the phosphine ligand. iPE3MPD was prepared with the catalyst obtained by combining the cobalt complex $CoCl_2(P^nPrPh_2)_2$ (^{n}Pr = *n*-propyl and Ph = phenyl) with methylaluminoxane (MAO),[7,29,45-47] as described in ref 7. The sample presents mass average molecular mass M_w = 81 000 g/ mol and polydispersity index M_w / M_n = 1.2 and is highly isotactic. In a previous paper we have reported the crystalline structure of iP3MPD and an exploratory analysis of the mechanical properties.[48] The crystalline structure of iP3MPD has also been reported in the thesis of Chiara Santillo.[37] This new polymer is one of the very few examples of crystalline isotactic 1,2-polydienes described in the literature. It does not crystallize by cooling from the melt but crystallizes by aging the amorphous samples at room temperature for several days and successive annealing. The stretching of amorphous or low crystalline compression-molded samples gives oriented fibers of a highly disordered mesomorphic form. Well-oriented fibers of the ordered crystalline form of iPE3MPD have been prepared by stretching amorphous or low crystalline compression-molded samples and successive annealing at 60−70 °C under tension. The crystalline structure of iPE3MPD is characterized by macromolecules in 7/2 helical conformation packed in an orthorhombic unit cell with parameters a = 17.4 Å, b = 16.5 Å, c = 15.3Å according to the space group $P2_1ab$ (Figure 2.26). iPE3MPD has shown interesting mechanical properties of high deformability with elastic behavior associated with the crystallization during deformation of the mesophase that melts upon relaxation.

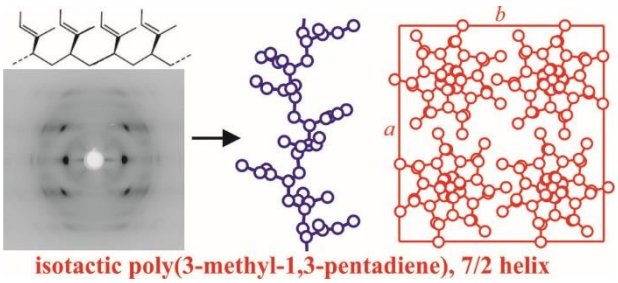

Figure 2.26. *Crystalline structure of isotactic 1,2 poy(3-methyl-1,3-pentadiene).*

Structural, thermal and mechanical analysis

I report here a summary of the study of mechanical behavior of the amorphous iP3MPD reported in the *Macromolecules* **2018**, *51*, 488–496.[49] Our results have indicated that iP3MPD is a crystalline polymer with glass-transition temperature of ≈35 °C. It crystallizes from the amorphous by aging at 25 °C (Figure 2.27). The large peaks $2\theta \approx 10°$ and 19° in the diffraction pattern of the amorphous specimens obtained by compression-molding and cooling the melt to 25 °C (Figure 2.27 a) transform into narrow reflections at $2\theta \approx 10°$ and 16.2° by aging at 25 °C for several weeks (Figure 2.27 b), indicating crystallization during aging.

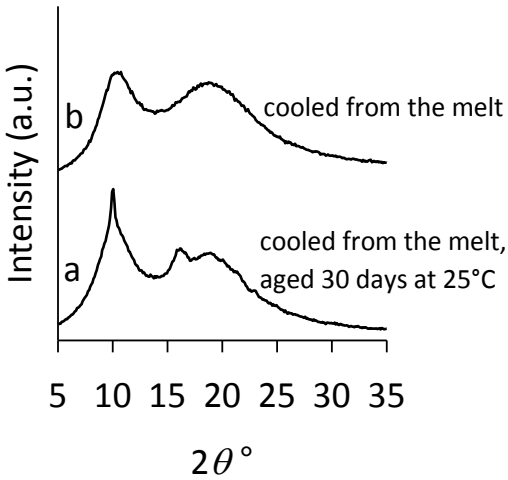

***Figure 2.27**. X-ray diffraction curves of a compression-molded sample of iP3MPD (a) and after aging at 25 °C for 4 weeks (b).*

An endothermic peak near to the glass transition, typical of hysteresis behavior of glasses,[50-52] is observed in the DSC heating curves of amorphous samples (Figure 2.28 b).

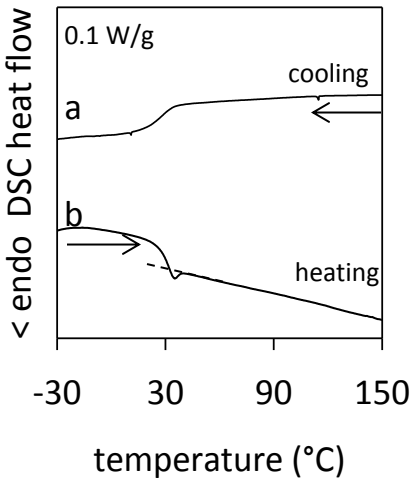

***Figure 2.28**. DSC cooling curve down to low temperature at 10 °C/min of iP3MPD (a) and successive heating curve at 10 °C/min (b).*

In the former case the endothermic effect in the heating scan increases with decreasing cooling rate,[51] whereas in the latter case annealing at temperatures below the glass-transition changes the glass to a more stable state otherwise produced on slow cooling without stress and increase of the endothermic hysteresis with increase of the annealing time has been observed.[50,52] Similar behavior was found for iP3MPD in the DSC heating curves of Figure 2.29 recorded at the same heating rate of 10 °C/min of samples cooled at different cooling rates. It is apparent that the endothermic peak is almost absent in the sample cooled at the highest cooling rate (by quenching at low temperature, curve a of Figure 2.29) and increases with decreasing cooling rate (curves b-f of Figure 2.29).

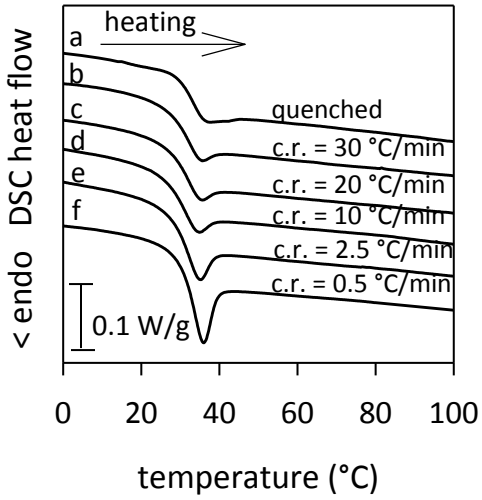

Figure 2.29. *Heating curves recorded always at 10 °C/min of samples cooled at the indicated different cooling rates (c.r.). The endothermic enthalpy overshoot near to the glass transition in the second heating scan is evidenced. The scale bar of the heat flow in W/g is indicated.*

The elasticity of iP3MPD is an unusual case of a polymer that shows rubbery elastomeric properties below the glass-transition temperature.

The stress-strain curve of the amorphous iP3MPD prepared by compression-molding is shown in Figure 2.30. The stress-strain curves of the same amorphous sample aged at 20°C for different aging time are also shown in Figure 2.30.

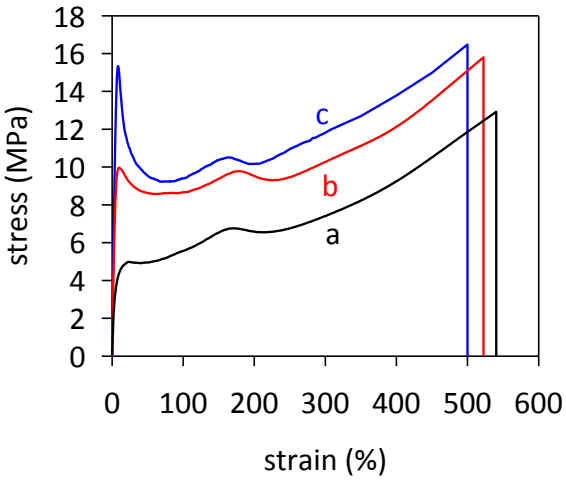

Figure 2.30*. Stress–strain curves of compression-molded samples of iP3MPD cooled from the melt to 25 °C (a) and aged at 20 °C for different aging times of 3 h (b) and 3 days (c).*

The stress-strain curves of Figure 2.30 of non-aged and aged samples present a second maximum at strain of nearly 200% after the yield point observed at low deformation of 10-20%. To explain this unusual second maximum, the structural evolution of iP3MPD during deformation has been followed recording wide- and small-angle X-ray diffraction patterns during stretching.[49] This results suggest that a mesophase of iP3PMD, characterized by structural disorder and, probably, slight order in the chain conformation, crystallizes by deforming the amorphous sample. This could explain that in the stress-strain curves of Figure 2.30, the second maximum at strain of nearly 200% after the yield point could be interpreted as a second yielding. Therefore, this non common mechanical behavior with a double yielding may be interpreted as a result of events typical of yielding at low deformation $\varepsilon_y \approx 10\%$ that involve alignment of amorphous chains and softening, followed by stress-induced crystallization of the mesophase at higher deformation (200−300%) and successive strain hardening.[49]

However, this new polymer could not be used as a synthetic rubber because of the high glass transition temperature, but as other 1,2 poly(1,3-diene)s, it could find application as a thermoplastic material with improved toughness.[49]

Ricci *et al*.[53] reported the synthesis of a purely random achiral copolymer iP(*R,S*)3MP by hydrogenation of isotactic 1,2 poly(*E*-3-methyl-1,3-pentadiene). The obtained polymer iP(*R,S*)3MP is highly isotactic and crystalline and the crystal structure was resolved by X-ray diffraction analysis.[53] De Rosa *et al*.[53] found that the crystal structure of iP(R,S)3MP is different from that of chiral iP(*S*)3MP. The reasons for the different crystallization behaviours has been discussed in terms of entropic effects related to the presence of different types of disorder involved in the crystals of the chiral and achiral polymers.

Isotactic poly(3-methyl-1-pentene) (iP3MP) is the ideal example of a polyolefin which can be either chiral, containing a “true” asymmetric atom on the side group, with corresponding optical activity, or not chiral when the two enantiomeric R and S monomeric units are randomly enchained with compensation of the chirality of the lateral groups. This allows the effect of the chirality of the lateral groups and the effect of intramolecular chirality compensation on the conformation of the chains and the packing of chains in the crystals to be studied and compared. Both the chiral monomer (*S*)-3-methyl-1-pentene ((*S*)3MP) and the racemic mixture (*R,S*)-3-methyl-1-pentene ((*R,S*)3MP) polymerize to isotactic polymers in the presence of Ziegler–Natta or metallocene catalysts.[54,55] The polymerization of the chiral monomer (*S*)3MP produces a chiral

isotactic polymer, poly((*S*)-3-methyl-1-pentene) (iP(*S*)3MP). The polymerization of the racemic mixture (*R,S*)3MP gives an isotactic copolymer, poly((*R,S*)-3-methyl-1-pentene) (iP(*R,S*)3MP), where the two enantiomeric monomers (*R*)3MP and (*S*)3MP should be enchained.[55] However, the polymer produced with a Ziegler–Natta catalyst was separated into fractions having optical activity of opposite sign by adsorption chromatography on highly crystalline iP(*S*)3MP.[55] This indicated that copolymers of the two enantiomeric monomeric units, with prevalence of S or R monomeric units in the optically active polymers, were obtained,[55] due to the stereoselectivity of the polymerization by heterogeneous catalysts which gives rise to the dominant formation of macromolecules by one single monomeric antipode.[55] The same polymer was also obtained with single center homogeneous metallocene catalysts.[56] Therefore, a purely statistical copolymer of the two monomeric antipodes was not obtained with heterogeneous or homogeneous stereoselective catalysts.

A different route for the synthesis of a purely random achiral copolymer iP(*R,S*)3MP could be the stereospecific polymerization of 3-methyl-1,3-pentadiene to isotactic 1,2-poly(3-methyl-1,3-pentadiene) and successive hydrogenation. The isotactic stereoregularity could be preserved after hydrogenation and a purely statistical copolymer of the two enantiomeric monomers with intramolecular compensation of chirality could be obtained with this procedure.[53]

2.2.2. Syndiotactic poly(3-methyl-1-butene)

Syndiotactic poly(3-methyl-1-butene) (sP3MP) has been obtained for the first time by hydrogenation of syndiotactic 3,4-poly(isoprene), which in turn has been synthesized with the catalyst $FeCl_2$(2,2'-bipyridine)$_2$ activated with methylaluminoxane.[57] The synthesized sample of sP3MB is amorphous and does not crystallize by annealing or cooling from high temperature, but crystallizes by stretching and annealing of the oriented amorphous at 60-70 °C. [58]

In the case of 3-methyl-1-butene (3MB), polymerization with the C_s symmetric catalyst (Me)(Ph)C(Cp)(9-Flu)$ZrCl_2$ (Ph = Phenyl) gave a polymer showing X-ray powder diffraction profile of isotactic poly(3-methyl-1-butene) (iP3MB) with low crystallinity.[59] The ^{13}C-NMR analysis of the obtained polymer indicated the presence of 3MB monomeric units with 4,1 enchainment arising from isomerization of secondary 2,1 last inserted unit,[59] according to a mechanism similar to the isomerization of 2,1 to 3,1 propene units and of 2,1 to 4,1 butene

units in isotactic polybutene.[59-64] Moreover, the 2D NMR spectrum confirmed that the methylene groups of the main chains are largely in meso (*m*) diads, that is the regioregular 1,2 sequences of 3MB units are largely isotactic.[59] The formation of isotactic poly(3MB) with C_s symmetric metallocene catalysts, which are syndiospecific in propene, butene and 4-methyl pentene polymerization, has not been completely explained so far and seems to be related with the accepted chain migratory polymerization mechanism involving skipped insertion of the monomer for these C_s catalysts.[59,65,66] For slow monomer insertion, as in the case of 3MB, skipped insertion may prevail and the change of the steric control from chain migratory syndiotactic to chain-end (prevailingly) isotactic could explain the formation of isotactic instead of syndiotactic poly(3MB) with C_s-symmetric metallocene catalysts.[59] However, no clear evidences are available to support this hypothesis, as for example (from ^{13}C NMR) the presence of a single *r* diad stereodefect in isotactic sequences (..*mmrmmm*..), typical of chain-end mechanism, or the effect of temperature on the isotacticity of the polymer.[59]

Now, I report a different strategy for the preparation of syndiotactic poly(3-methyl-1-butene) (sP3MB) based on the synthesis of syndiotactic 3,4-poly(isoprene) with the catalytic system $FeCl_2(bipy)_2$-MAO,[57] and successive hydrogenation, is presented. The syndiotactic stereoregularity is preserved after hydrogenation of the double bonds on the side groups (the hydrogenation reaction does not lead to the formation of new stereocenters) and samples of sP3MB able to crystallize have been obtained for the first time.

Polymerization

The hydrogenation was carried out in a round-bottom flask equipped with a reflux condenser, a nitrogen inlet port, and a temperature controller.[67,68] Typically, 4.8 g of the syndiotactic 3,4-poly(isoprene) was dissolved in *o*-xylene. The mixture was continuously stirred at room temperature until the polymer was completely dissolved. *p*-Ts*N*H (30 g, 0.16 mol) was then added and the mixture was refluxed by slowly heating to 120°C. After 3 days the mixture was allowed to cool spontaneously to room temperature and *p*-Ts*N*H (30 g, 0.16 mol) was added. This operation is repeated once again. Upon completion of the reaction, the hydrogenated sample was hot-filtered, the volume of the filtered solution was reduced under vacuum, and the dissolved polymer precipitated with methanol and collected by filtration. The polymer was dried under vacuum at room

temperature, and then it was extracted with acetone through a Soxhlet method for 10 h in order to remove any excess of *p*-TsNH and byproducts originating from *p*-TsNH decomposition. The residual polymer (*i.e.*, poly(3-methyl-1-butene) sP3MB) was finally dried under vacuum, dissolved in toluene, precipitated into methanol, and dried again under vacuum at room temperature to constant weight. (Yield = 4.4 g (91.6%), M_w = 392700 g/mol, M_w/M_n = 2.8).

The syndiotactic 3,4-poly(isoprene) was synthesized by polymerizing isoprene with the catalytic system $(bipy)_2FeCl_2$/MAO, in toluene at –30°C (Scheme 2.13).[57]

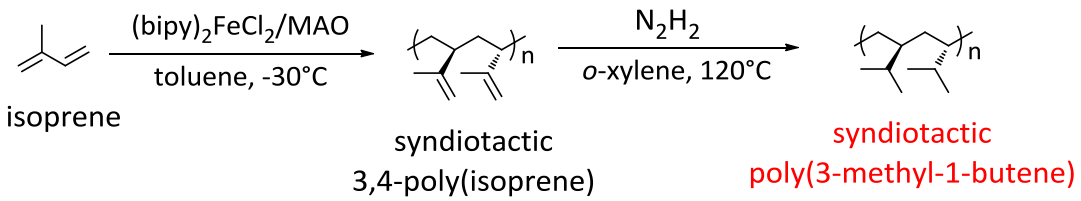

Scheme 2.13. *Polymerization of isoprene catalyzed by $(bipy)_2FeCl_2$/MAO and successive hydrogenation of the obtained syndiotactic 3,4-poly(isoprene) to give a fully saturated syndiotactic poly(3-methyl-1-butene) (sP3MB).*

Structural and thermal analysis

The ^{13}C NMR spectrum of the stereoregular syndiotactic 3,4-poly(isoprene) together with the peaks attribution is shown in Figure 2.31 A. The hydrogenation of the syndiotactic 3,4-poly(isoprene) was then performed by a non-catalytic way (Scheme 2.13).[67,68] As recently shown, this procedure is an attractive process and extremely efficient in the case of 1,3-diene polymers.[1,19,69]

polymer/ppm	C1	C2	C3	C4	C5
sP(PI)	109.99	145.31	40.86	37.10	16.37
*s*P(3MB)	16.63	26.47	33.36	30.98	16.63

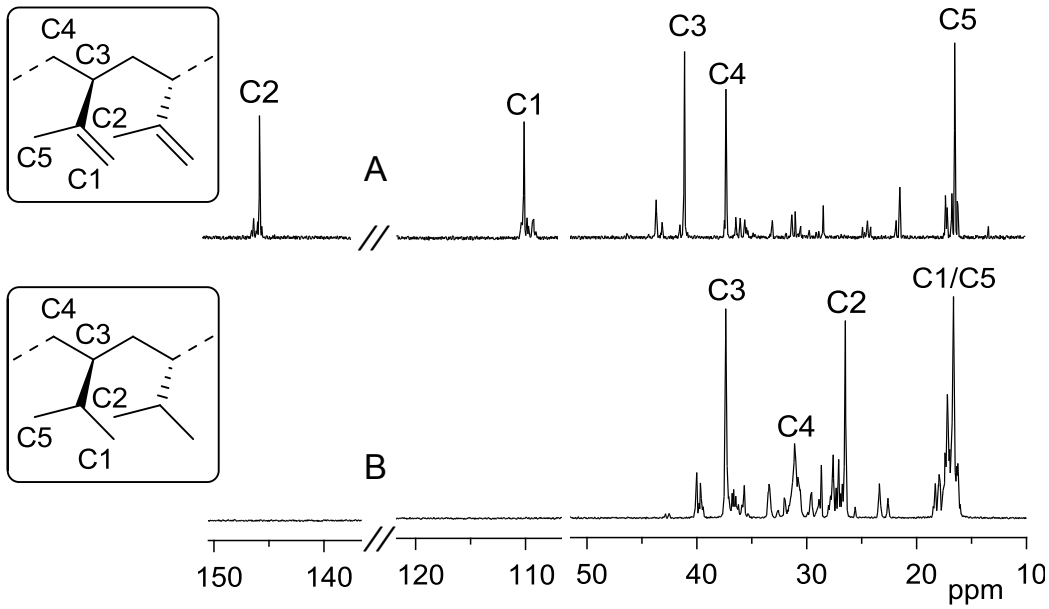

Figure 2.31. *^{13}C NMR spectra ($C_2D_2Cl_4$, 103°C, HMDS) of syndiotactic 3,4-poly(isoprene) (A) and syndiotactic poly(3-methyl-1-butene) (sP3MB) (B).*

The complete hydrogenation of the pristine 3,4-poly(isoprene) was confirmed by FT-IR and NMR (^{1}H and ^{13}C) spectroscopy. The ^{13}C NMR spectrum of the saturated polymer sP3MB, together with the peaks attribution, is shown in Figure 2.31 B: four major resonances are observed at 16.63 (C1/C5), 26.47 (C2), 30.98 (C4), and 33.36 (C3) ppm. As it is clearly evident, the peaks in the olefinic region (from 100 to 150 ppm), observed in the ^{13}C NMR spectrum of the diene polymer (Figure 2.32 A), and due to the olefinic carbon atoms, are completely absent in the ^{13}C NMR spectrum of sP3MB, confirming indeed the complete hydrogenation of the diene polymer.

Moreover, the syndiotactic stereoregularity of 3,4-poly(isoprene) is preserved after hydrogenation of the double bonds on the side groups (the hydrogenation reaction does not lead to the formation of new stereocenters) and syndiotactic poly(3-methyl-1-butene) (sP3MB) has been obtained for the first time.

The X-ray diffraction profile of the as-polymerized sample of sP3MB, shown in Figure 2.32 (profile a), presents two large peaks at 2θ = 12° and 19°. This suggests that the sample is basically amorphous. However, a shoulder at $2\theta \approx 10°$ of the first broad peak is evident (indicated by the arrow in Figure 2.32 a), indicating that some weak crystalline reflections hidden by the amorphous haloes are probably present.

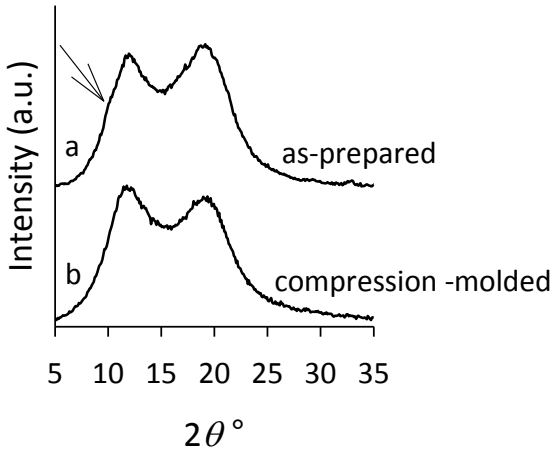

***Figure 2.32**. X-ray diffraction profiles of the as-polymerized (a) and compression-moulded (b) samples of sP3MB.*

The DSC thermograms recorded at scanning rate of 10 °C/min during heating of the as-polymerized sample up to 200°C, successive cooling down to -40 °C and second heating are reported in Figure 2.33. It is apparent that very small and large endothermic signals at 70 and 110 °C are present in the first heating scan (Figure 2.33 a), indicating the presence of small crystallinity in the as-polymerized sample. Crystallization is not observed during cooling from the amorphous state at high temperature, as shown by the absence of exothermic peaks in the thermogram of Figure 2.33 b and the absence of endothermic peaks in the successive second heating scan (Figure 2.33 c). Only the glass transition at nearly 20 °C is observed in both heating and cooling scans (Figure 2.33). The diffraction profile of a compression-moulded sample of sP3MB, obtained by cooling the as polymerized sample from 100 °C to 25 °C under a press, shows only the two amorphous halos at 2θ = 12° and 19° without shoulders, confirming that the sample is amorphous (profile b of Figure 2.32). Both as polymerized and compression-moulded samples do not crystallize by annealing at relatively high temperature (80 °C).

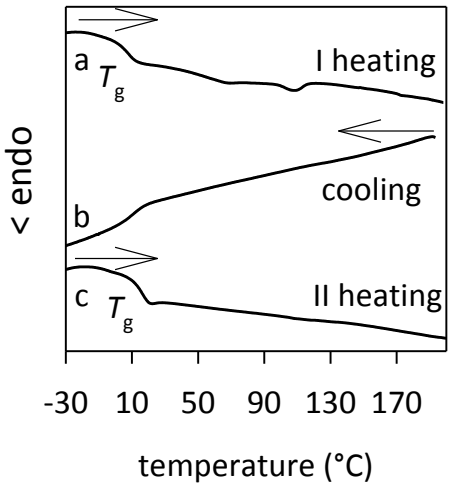

***Figure 2.33**. DSC thermograms recorded at 10 °C/min during heating of as-polymerized sample (a), cooling from 200 °C down to -40 °C (b) and successive second heating (c).*

Crystallization of sP3MB has been achieved by stretching the amorphous compression-moulded sample of Figure 2.32 b and annealing at 60-70 °C of the fibers kept in tension. The X-ray fiber diffraction pattern, and the corresponding intensity equatorial profile, of fibers of sP3MB stretched at 250% deformation and annealed at 70 °C for 30 min, are shown in Figure 2.34. The stretching at 250% strain of the amorphous sample produces only orientation of the amorphous phase, whereas annealing at 70 °C allows crystallization, as indicated by the development in the diffraction pattern of Figure 2.34 A of sharp reflections on the equator and a clear sharp reflection on the meridian. The diffraction pattern of Figure 2.34 B is different from the diffraction pattern of the isotactic poly(3-methyl-1-butene) reported in the literature,[59,70] confirming the syndiotacticity of sP3MP obtained after hydrogenation.

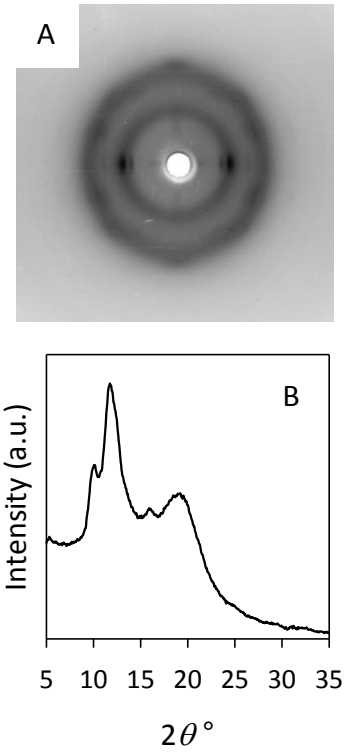

***Figure 2.34**. Bidimensional X-ray fiber diffraction image (A), and corresponding equatorial profile as a function of the Bragg angle 2θ (B), of fibers of crystalline sP3MB obtained by deformation at 250% strain the amorphous compression-moulded sample and annealing at 70 °C for 30 min.*

A model of the conformation of the chains of sP3MB was proposed by De Rosa *et al.*[58] The chains of sP3MB assume in the crystalline phase a 3/1 helical conformation, providing the first example of a syndiotactic polymer with 3-fold helical chains.[58] Crystallization of sP3MB has been achieved by stretching of compression-moulded samples at 250% deformation and annealing of the oriented amorphous at 60-70 °C. The data, obtained from the X-ray fiber diffraction pattern of the annealed crystalline fibers, indicate a highly disordered crystal structure. However, the fiber diffraction data indicate that the chains of sP3MB assumes an ordered 3/1 helical conformation. This hypothesis is supported by calculations of conformational energy.[58] sP3MB represents the first case of syndiotactic polymers with chains in 3/1 helical conformation. High degree of disorder is present in the crystals so that the structure can be described by a disordered arrangement of parallel conformationally ordered 3/1 helical chains without long-range lateral correlations between the chains (Figure 2.35). Accordingly, the distribution of the diffracted intensities along the layer lines is

well reproduced by the calculated Fourier transform of the single 3/1 helical chain of sP3MB.

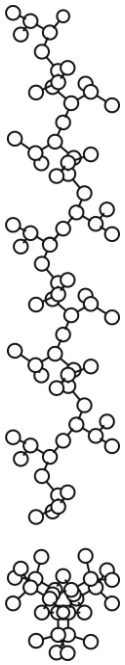

***Figure 2.35**. Model of 3/1 helical conformation for the chains of sP3MB.*

2.2.3. Syndiotactic 1,2 poly(5-methyl-1-hexene)

Polymerization

By polymerizing 5-methyl-1,3-hexadiene with the catalyst system $Et_2AlCl/Nd(OCOC_7H_{15})_3/Al^iBu_3$, Ricci *et al.*[6] obtained poly(5-methyl-1,3-hexadiene) with a mixed *cis*-1,4/1,2 structure. With the catalyst $CoCl_2(P^iPrPh_2)_2/MAO$,[6] obtained syndiotactic *trans*-1,2 poly(5-methyl-1,3-hexadiene).

I describe the synthesis and characterization of syndiotactic 1,2 poly(5-methyl-1-hexene), obtained by hydrogenation of syndiotactic *trans*-1,2 poly(5-methyl-1,3-hexadiene) (Scheme 2.14).

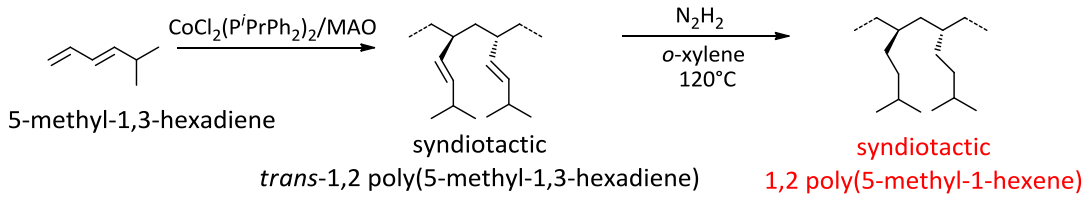

Scheme 2.14. *Polymerization of 5-methyl-1,3-hexadiene and hydrogenation of syndiotactic trans-1,2 poly(5-methyl-1,3-hexadiene).*

Specifically, the hydrogenation conditions were the following:
(*i*) syndiotactic *trans*-1,2 poly(5-methyl-1,3-hexadiene): polymer 1 g; *o*-xylene, 250 mL; first addition of *p*-T*s*NH, 9.0 g (4.8×10^{-2} mol); second and third addition of *p*-T*s*NH, 11 g (5.9×10^{-2} mol).

Upon completion of the reaction, the hydrogenated sample was hot-filtered, the volume of the filtered solution was reduced under vacuum, and the dissolved polymer precipitated with methanol and collected by filtration. The polymer was dried under vacuum at room temperature, and then it was extracted with acetone through a Soxhlet method for 10 h in order to remove any excess of *p*-T*s*NH and byproducts originating from *p*-T*s*NH decomposition. The residual polymer (*i.e.*, syndiotactic *trans*-1,2 poly(5-methyl-1-hexene) was finally dried under vacuum, dissolved in toluene, precipitated into methanol, and dried again under vacuum at room temperature to constant weight. (Yield = 0.500 g (50%), M_w = 20000 g/mol, M_w/M_n = 1.9).

Structural analysis

The successful complete hydrogenation of the diene polymer was confirmed by FT-IR (Figure 2.36) and by ^{1}H NMR spectra of the starting syndiotactic *trans*-1,2 poly(1,3-diene) and of the corresponding hydrogenated product. The peaks in the olefinic region (from 5.2 to 5.4 ppm), observed in the ^{1}H NMR spectra of the diene polymer and due to the olefinic hydrogen atoms, are not observed in the ^{1}H NMR spectra of the hydrogenated polymer, confirming indeed the complete hydrogenation of the diene polymer.

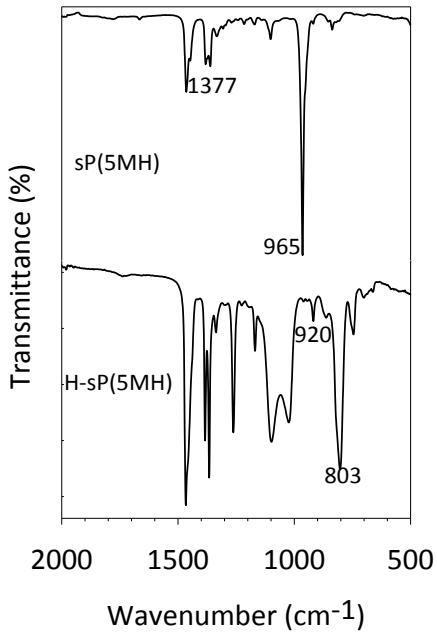

Figure 2.36. *FTIR spectra of (A) syndiotactic trans-1,2 poly(5-methyl-1,3-hexadiene) (sP(5MH)) (top) and its saturated polymers syndiotactic 1,2 poly(5-methyl-1-hexene) (H-sP(5MH)) (bottom).*

In the FT-IR spectrum of the polymer (Figure 2.36) no bands were detected around 911, 760, and 730 cm^{-1} , indicating that 3,4, *cis*-1,4 and *cis*-1,2 units, respectively, are not present along the polymer chain.[71] The strong band observed at 965 cm^{-1} is instead indicative of a *trans* configuration of the double bond,[71] but it does not allow to distinguish between a *trans* 1,4 and a *trans*-1,2 structure.[71,72] The band observed at 1377 cm^{-1} is however in agreement with a 1,2 structure.

The structure and tacticity of the resulting syndiotactic 1,2 poly(5-methyl-1-hexene) were studied by means of ^{1}H and ^{13}C NMR. Figure 2.37 shows the ^{13}C NMR spectra of the syndiotactic *trans*-1,2 poly(5-methyl-1,3-hexadiene) and its saturated polymer together with the peaks attribution.

polymer/ppm	C1	C2	C3	C4	C5	C6	C7
sP(5MP)	40.97	35.69	129.90	135.71	29.05	20.95	20.95
H-sP(5MP)	39.47	30.04	31.29	34.05	26.58	20.77	20.77

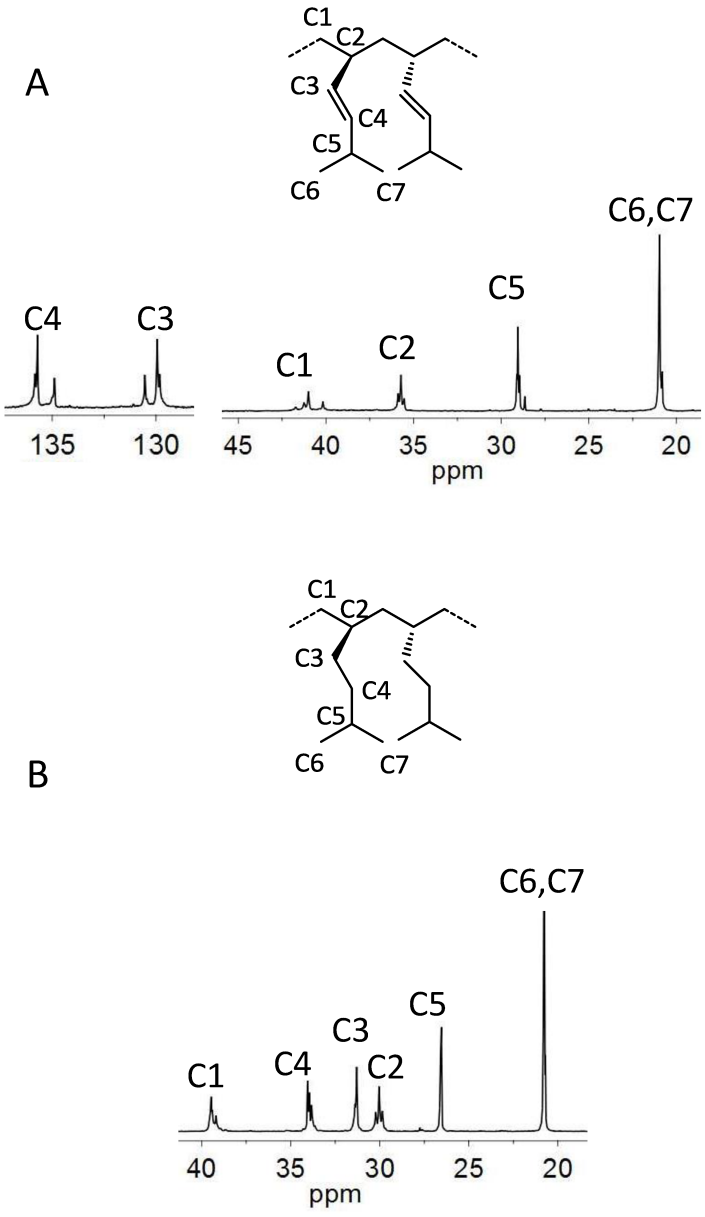

Figure 2.37. *^{13}C NMR spectra ($C_2D_2Cl_4$, 103°C, HMDS) of the sP(5MP) (A) and of the hydrogenated polymer H-sP(5MP)(B).*

2.2.4. Syndiotactic 1,2 poly(heptene)

Polymerization

By polymerizing 1,3-heptadiene with the catalyst system $Et_2AlCl/Nd(OCOC_7H_{15})_3/Al^iBu_3$, Ricci *et al.*[6] obtained isotactic *cis*-1,4 poly(1,3-heptadiene). With the catalyst $CoCl_2(P^iPrPh_2)_2$/MAO, obtained syndiotactic *trans*-1,2 poly(1,3-heptadiene).[6]

I describe the synthesis and characterization of syndiotactic 1,2 poly(heptene) (H-sP(HP)), obtained by hydrogenation of syndiotactic *trans*-1,2 poly(1,3-heptadiene) (sP(HP)) (Scheme 2.15).

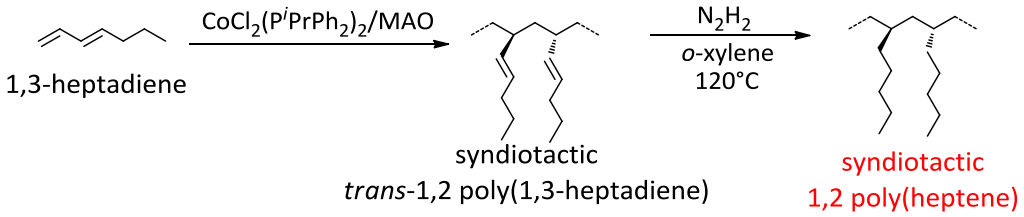

Scheme 2.15. *Polymerization of 1,3-heptadiene and hydrogenation of syndiotactic trans-1,2 poly(1,3-heptadiene).*

Specifically, the hydrogenation conditions were the following:

(*i*) syndiotactic *trans*-1,2 poly(1,3-heptadiene): polymer 0.935 g; *o*-xylene, 80 mL; first addition of *p*-T*s*NH, 6.6 g (3.5×10^{-2} mol); second and third addition of *p*-T*s*NH, 13 g (6.9×10^{-2} mol).

Upon completion of the reaction, the hydrogenated sample was hot-filtered, the volume of the filtered solution was reduced under vacuum, and the dissolved polymer precipitated with methanol and collected by filtration. The polymer was dried under vacuum at room temperature, and then it was extracted with acetone through a Soxhlet method for 10 h in order to remove any excess of *p*-TsNH and byproducts originating from *p*-T*s*NH decomposition. The residual polymer (*i.e.*, syndiotactic 1,2 poly(heptene)) was finally dried under vacuum, dissolved in toluene, precipitated into methanol, and dried again under vacuum at room temperature to constant weight (Yield = 0.550 g (60%)).

Structural analysis

The successful complete hydrogenation of the diene polymers was confirmed by ^{1}H NMR spectra of the starting syndiotactic *trans*-1,2 poly(1,3-diene) and of the corresponding hydrogenated product. The peaks in the olefinic region (from 5.2 to 5.4 ppm), observed in the ^{1}H NMR spectra of the diene polymer and due to the olefinic hydrogen atoms, are not observed in the ^{1}H NMR spectra of the hydrogenated polymer, confirming indeed the complete hydrogenation of the diene polymer.

The structure and tacticity of the resulting syndiotactic 1,2 poly(heptene) were studied by means of ^{1}H and ^{13}C NMR. Figure 2.38 shows the ^{13}C NMR spectra of the syndiotactic *trans*-1,2 poly(heptadiene) and its saturated polymer together with the peaks attribution.

polymer/ppm	C1	C2	C3	C4	C5	C6	C7
sP(HP)	40.88	35.81	133.50	127.88	32.80	20.97	11.65
H-sP(HP)	39.72	31.36	32.86	24.26	30.60	20.70	12.01

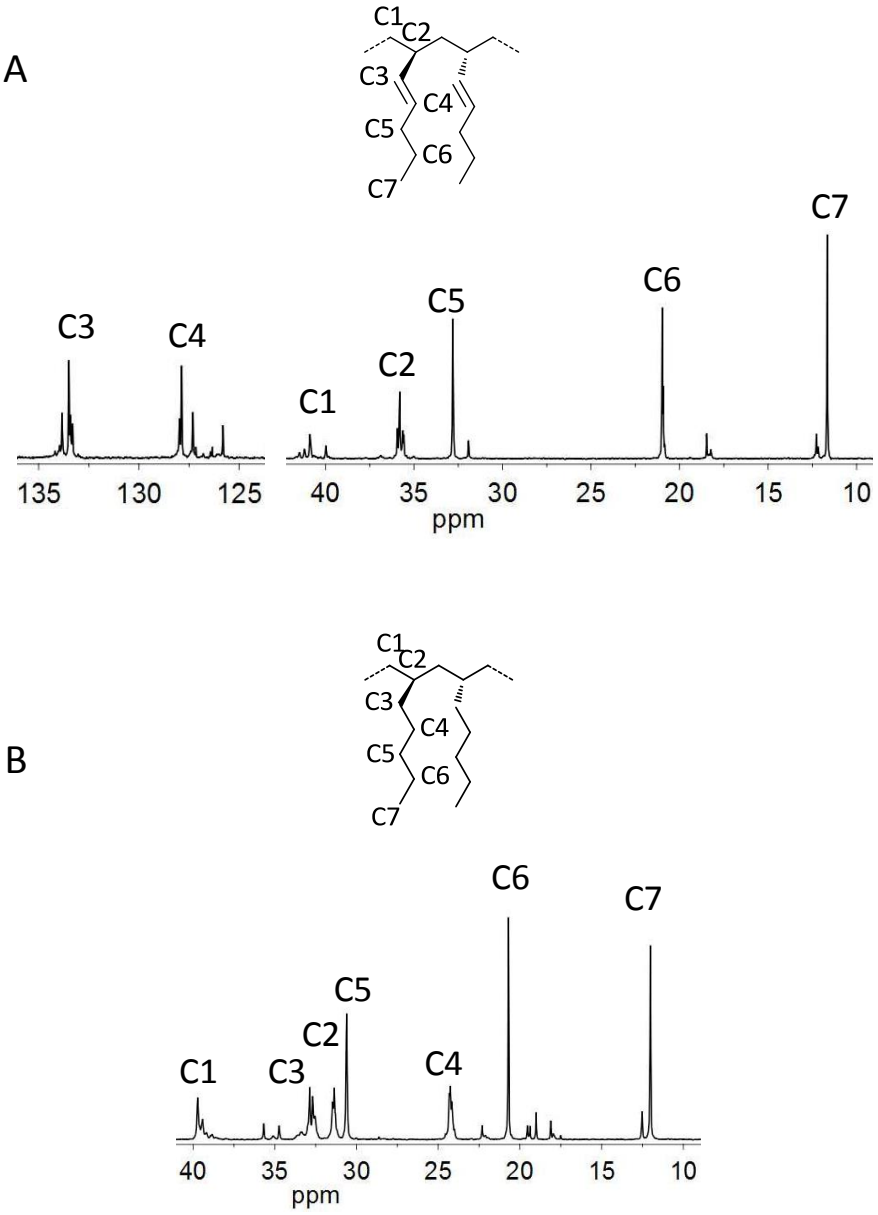

Figure 2.38. *^{13}C NMR spectra ($C_2D_2Cl_4$, 103°C, HMDS) of the sP(HP) (A) and of the hydrogenated polymer H-sP(HP)(B).*

2.2.5. Syndiotactic 1,2 poly(octene)

Polymerization

By polymerizing 1,3-heptadiene with the catalyst system $Et_2AlCl/Nd(OCOC_7H_{15})_3/Al^iBu_3$, Ricci *et al*.[6] obtained isotactic *cis*-1,4 poly(1,3-octadiene). With the catalyst $CoCl_2(P^iPrPh_2)_2$/MAO, obtained syndiotactic *trans*-1,2 poly(1,3-octadiene).[6]

I describe the synthesis and characterization of syndiotactic 1,2 poly(octane) (H-sPO), obtained by hydrogenation of syndiotactic *trans*-1,2 poly(1,3-octadiene) (sPO) (Scheme 2.16).

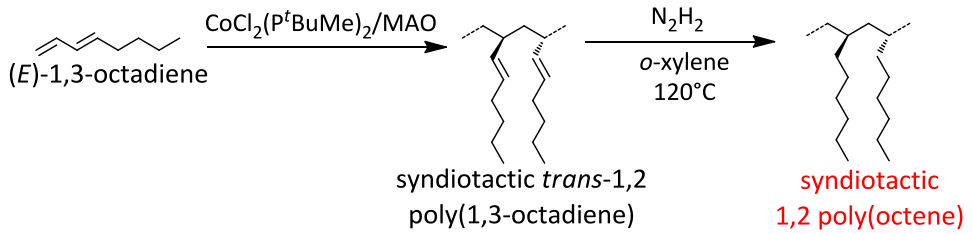

Scheme 2.16. *Polymerization of 1,3-octadiene and hydrogenation of syndiotactic trans-1,2 poly(1,3-octadiene).*

Specifically, the hydrogenation conditions were the following:
(*i*) syndiotactic *trans*-1,2 poly(1,3-octadiene): polymer 1.18 g; *o*-xylene, 250 mL; first addition of *p*-T*s*NH, 9.6 g (5.1×10^{-2} mol); second and third addition of *p*-T*s*NH, 10 g (5.4×10^{-2} mol).

Upon completion of the reaction, the hydrogenated sample was hot-filtered, the volume of the filtered solution was reduced under vacuum, and the dissolved polymer precipitated with methanol and collected by filtration. The polymer was dried under vacuum at room temperature, and then it was extracted with acetone through a Soxhlet method for 10 h in order to remove any excess of *p*-T*s*NH and byproducts originating from *p*-T*s*NH decomposition. The residual polymer (*i.e*., syndiotactic 1,2 poly(octene)) was finally dried under vacuum, dissolved in toluene, precipitated into methanol, and dried again under vacuum at room temperature to constant weight. (Yield = 0.831 g (70%) M_w = 479714 g/mol, M_w/M_n = 1.68)

Structural analysis

The successful complete hydrogenation of the diene polymer was confirmed by FT-IR (Figure 2.39) and by ^{1}H NMR spectra of the starting syndiotactic *trans*-1,2 poly(1,3-diene) (Figure 2.40 A) and of the corresponding hydrogenated product (Figure 2.40 B). The peaks in the olefinic region (from 5.2 to 5.4 ppm), observed in the ^{1}H NMR spectra of the diene polymers and due to the olefinic hydrogen atoms, are not observed in the ^{1}H NMR spectra of the hydrogenated polymer, confirming indeed the complete hydrogenation of the diene polymer.

In the FT-IR spectrum of the syndiotactic *trans*-1,2 poly(1,3-octadiene)[6] (Figure 2.39) no bands were detected at 911, 760, and 730 cm^{-1} , indicating that 3,4, *cis*-1,4, and *cis*-1,2 units, respectively, are not present, or practically negligible, along the polymer chain.[71,72] The strong band observed at 968 cm^{-1} is instead clearly indicative of a *trans* configuration of the double bond, but it does not allow to distinguish between a *trans* 1,4 and a *trans*-1,2 structure.[71,72] The band observed at 1377 cm^{-1} is however in agreement with a 1,2 structure. The 1,2 structure was also confirmed by the NMR analysis of the polymer.[6] In a Figure 2.39 a new band at 735 cm^{-1} was observed in the FT-IR spectra of the hydrogenated polymers, ascribed to the vibration of a –CH_2– unit, typical of saturated polyolefins.

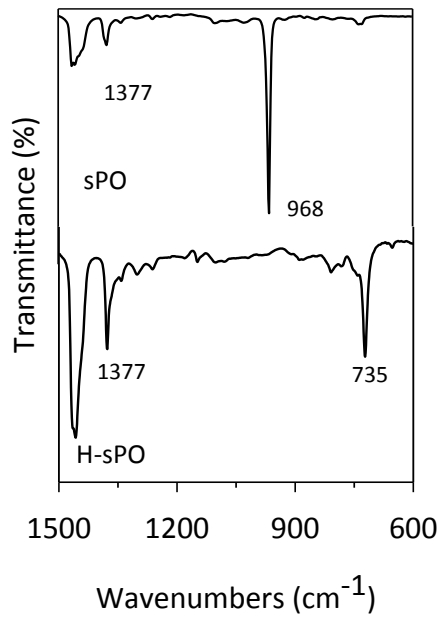

Figure 2.39. *FTIR spectra of syndiotactic trans-1,2 poly(octadiene) (H-sPO)(top) and its saturated polymer (H-sPO)(bottom).*

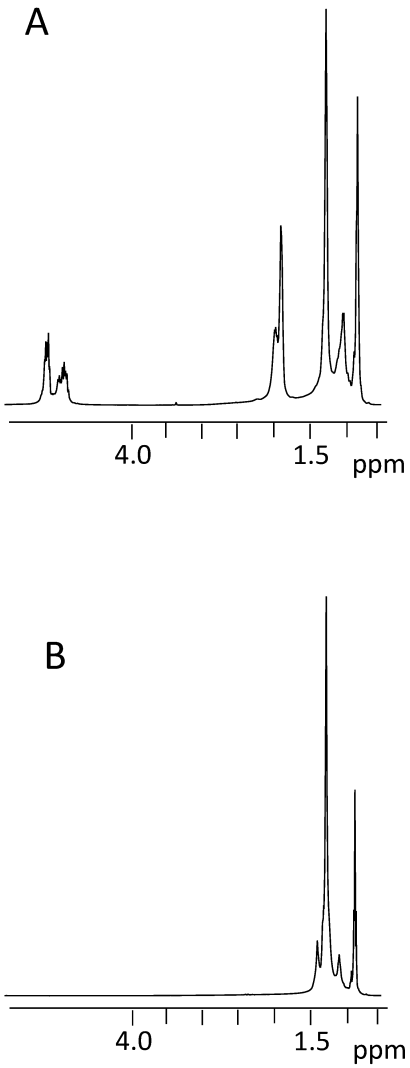

Figure 2.40. *^{1}H-NMR spectra ($C_2D_2Cl_4$, 103°C, HMDS) of the unsaturated sPO (A), and saturated H-sPO (B).*

The structure and tacticity of the resulting syndiotactic 1,2 poly(octene) were studied by means of ^{1}H and ^{13}C NMR. Figure 2.41 shows the ^{13}C NMR spectra of the syndiotactic *trans*-1,2 poly(octadiene) and its saturated polymer together with the peaks attribution.

polymer/ppm	C1	C2	C3	C4	C5	C6	C7	C8
sPO	40.81	35.79	133.27	128.05	30.29	30.14	20.25	11.85
H-sPO	39.61	31.20	32.66	24.62	27.98	30.02	20.72	11.99

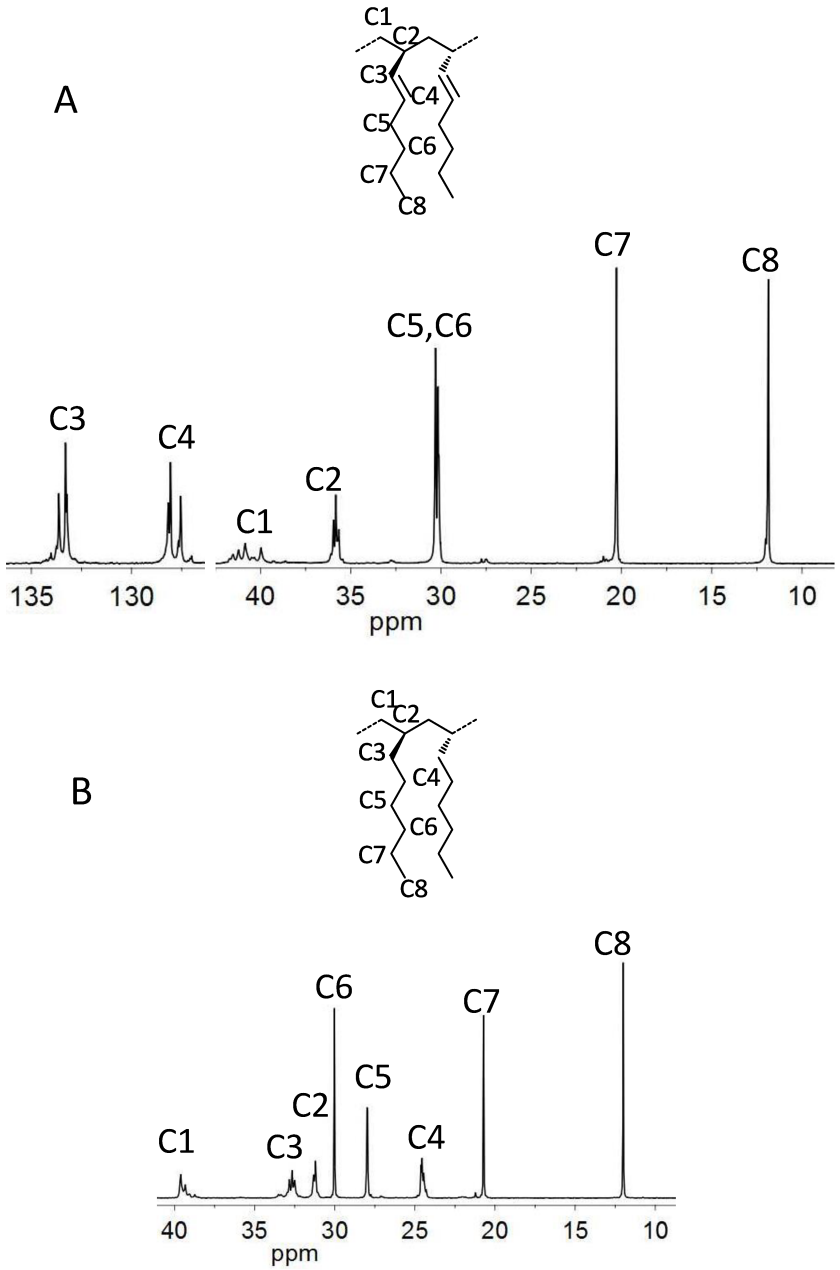

Figure 2.41. *^{13}C NMR spectra ($C_2D_2Cl_4$, 103°C, HMDS) of the sPO (A) and of the hydrogenated polymer H-sPO(B).*

References

[1] Ricci, G.; Leone, G.; Boccia, A. C.; Pierro, I.; Zanchin, G.; Mauri, M.; Scoti, M.; Malafronte, A.; Auriemma, F.; De Rosa, C. *Macromolecules* **2017,** *50*, 754−761.

[2] Wang, F.; Bolognesi, A.; Immirzi, A.; Porri, L. *Makromol. Chem.* **1981**, *182*, 3617 −3623.

[3] Meille, S. V.; Capelli, S.; Allegra, G.; Ricci, G. *Macromol. Rapid Commun*. **1995**, *16*, 329−335.

[4] Oliva, L.; Longo, P.; Grassi, A.; Ammendola, P.; Pellecchia, C. *Makromol. Chem., Rapid Commun.* **1990**, *11*, 519−524.

[5] Bazzini, C.; Giarrusso, A.; Porri, L. *Macromol. Rapid Commun*. **2002**, *23*, 922−927.

[6] Boccia, A. C.; Leone, G.; Boglia, A.; Ricci, G. *Polymer* **2013**, *54*, 3492−3503.

[7] Ricci, G.; Leone, G.; Boglia, A.; Bertini, F.; Boccia, A. C.; Zetta, L. *Macromolecules* **2009**, *42*, 3048−3056.

[8] Brar, A. S.; Singh, G.; Shankar, R. *J. Mol. Struct*. **2004**, *703*, 69−81.

[9] Markova, N.; Ivanova, G.; Enchev, V.; Simeonova, M. *Struct. Chem*. **2012**, *23*, 815−824.

[10] Busico, V.; Cipullo, R. *Prog.Polym. Sci.* **2001,** *26*, 443−533.

[11] Corradini, P.; Ganis, P. *Makromol. Chem.* **1963**, *62*, 97−107.

[12] Natta, G.; Allegra, G.; Bassi, I. W.; Corradini, P.; Ganis, P. *Makromol. Chem*. **1962**, *58*, 242−243.

[13] Natta, G.; Dall'Asta, G.; Mazzanti, G.; Pasquon, I.; Valvassori, A.; Zambelli, A. *J. Am. Chem. Soc*. **1961**, *83*, 3343−3344.

[14] Natta, G.; Dall' Asta, G.; Mazzanti, G.; Pasquon, I.; Valvassori, A.; Zambelli, A. *Makromol. Chem*. **1962**, *54*, 95−101.

[15] Auriemma, F.; De Rosa, C.; Corradini, P. *Macromol. Chem. Phys*. **2004**, *205*, 390−396.

[16] De Rosa, C.; Auriemma, F. Crystal and Crystallinity in Polymers-Diffraction Analysis of Ordered and Disordered Crystals; Wiley: 2014.

[17] De Rosa, C. Chain Conformation, Crystal Structures, and Structural Disorder in Stereoregular Polymers. Topics in Stereochemistry **2003**, *24*, 71.

[18] Ricci, G.; Forni, A.; Boglia, A.; Sonzogni, M. *Organometallics* **2004,** *23*, 3727−3732.

[19] Ricci, G.; Boccia, A.C.; Leone, G.; Pierro, I.; Zanchin, G.; Scoti, M.; Auriemma, F.; De Rosa, C. *Molecules* **2017**, *22*, 755.
[20] Kravchenko, R.; Waymouth, R.M. *Macromolecules* **1998**, *31*, 1–6.
[21] D'Orazio, L.; Mancarella, C.; Martuscelli, E.; Sticotti, G.; Massari, P. *Polymer* **1993**, *34,* 3671–3676.
[22] Kaminsky, W. Trends in Polyolefin Chemistry. *Macromol. Chem. Phys.* **2008**, *209*, 459–466.
[23] Resconi, L.; Cavallo, L.; Fait, A.; Piemontesi, F. *Chem. Rev.* **2000**, *100,* 1253–1345.
[24] Ittel, S.D.; Johnson, L.K.; Brookhart, M. *Chem. Rev*. **2000,** *100,* 1169–1203.
[25] Fan, W.; Waymouth, R.M. *Macromolecules* **2001**, *34*, 8619–8625.
[26] Leclerc, M.K.; Waymouth, R.M. *Angew. Chem. Int. Ed*. **1998**, *37,* 922–925.
[27] Jin, J.; Uozumi, T.; Sano, T.; Teranishi, T.; Soga, K.; Shiono, T. *Macromol. Rapid. Commun*. **1998**, *19,* 337–339.
[28] Rose, J.M.; Cherian, A.E.; Coates, G.W. *J. Am. Chem. Soc.* **2006**, *128,* 4186–4187.
[29] Ricci, G.; Motta, T.; Boglia, A.; Alberti, E.; Zetta, L.; Bertini, F.; Arosio, P.; Famulari, A.; Meille, S.V. *Macromolecules* **2005**, *38,* 8345–8352.
[30] Ricci, G.; Boffa, G.; Porri, L. *Makromol. Chem. Rapid Commun.* **1986,** *7*, 355–359.
[31] Ricci, G.; Italia, S.; Cabassi, F.; Porri, L. *Polymer Commun*. **1987***, 28*, 223–226.
[32] Ricci, G.; Forni, A.; Boglia, A.; Motta, T. *J. Mol. Catal. A: Chem*. **2005**, *226*, 235–241.
[33] Zetta, L.; Gatti, G.; Audisio, G. *Macromolecules* **1978,** *11*, 763–766.
[34] Busico, V.; Cipullo, R. *Prog. Polym. Sci.* **2001**, *26*, 443–533.
[35] Ricci, G.; Zetta, L.; Meille, S. V. *Gazz. Chim. Ital*. **1996**, *126,* 401-4.
[36] Pirozzi, B.; Napolitano, R.; Giusto, G.; Ricci, G. *Macromol. Chem. Phys.* **2008,** *209*, 1012-1020.
[37] http://www.fedoa.unina.it/11802/ Santillo, C. " *A molecular approach to study structure and properties of polymers"*.
[38] Natta, G.; Porri, L.; Zanini, G.; Palvarini, A. *Chem. Ind.* (Milan) **1959**,*41*, 1163. *Chem. Abstr*. **1961**, *55*, 20906.
[39] Natta, G.; Corradini, P.; Bassi, I. W. *Rend. Fis. Accad. Lincei* **1957**, *23*, 363.
[40] Porri, L.; Gallazzi, M. C. *Eur. Polym. J.* **1966**, *2*, 189.
[41] Natta, G.; Corradini, P.; Bassi, I. W.; Fagherazzi, G. *Eur. Polym. J.* **1968***, 4*, 297.
[42] Ricci, G.; Porri, L. *Polymer* **1997***, 38*, 4499.

[43] Zhang, L.; Luo, Y.; Hou, Z. *J. Am. Chem. Soc.* **2005**, *127*, 14562.
[44] Ricci, G.; Bertini, B.; Boccia, A.C.; Zetta, L.; Alberti, E.; Pirozzi, B.; Giarrusso, A.; Porri, L. *Macromolecules* **2007***, 40*, 7238-7243.
[45] Ricci, G.; Forni, A.; Boglia, A.; Motta, T.; Zannoni, G.; Canetti, M.; Bertini, F. *Macromolecules* **2005**, *38,* 1064.
[46] Ricci, G.; Forni, A.; Boglia, A.; Sommazzi, A.; Masi, F. *J. Organomet. Chem.* **2005**, *690*, 1845.
[47] Ricci, G.; Leone, G.; Boglia, A.; Boccia, A. C.; Zetta, L. *Macromolecules* **2009**, *42*, 9263.
[48] De Rosa, C.; Auriemma, F.; Santillo, C.; Scoti, M.; Malafronte, A.; Zanchin, G.; Pierro, I.; Leone, G.; Ricci, G. *Macromolecules* **2017**, *50*, 5412.
[49] De Rosa, C.; Scoti, M.; Auriemma , F.; Malafronte , A.; Santillo, C.; Zanchin, G.; Pierro, I.; Leone, G.; Ricci, G. *Macromolecules* **2018,** *51*, 488−496.
[50] Wunderlich, B. *Macromolecular Physics; Academic Press:* **1976**, *2*, 362
[51] Wunderlich, B. *Polymer* **1964,** *5*, 125.
[52] Weitz, A.; Wunderlich, B. *J. Polym. Sci., Polym. Phys. Ed.* **1974**, *12*, 2473.
[53] De Rosa, C.; Auriemma, F. ; Santillo, C. ; Di Girolamo, R. ; Leone, G. ; Ricci, G. *Cryst.Eng.Comm.* **2015,** *17*, 6006–6013.
[54] Petraccone, V.; Ganis, P.; Corradini, P.; Montagnoli, G. *Eur. Polym. J.,* **1972**, *8*, 99.
[55] Pino, P.; Ciardelli, F.; Montagnoli, G. *J. Polym. Sci., Part C: Polym. Symp.* **1968**, *16*, 3265.
[56] Oliva, L.; Longo, P., Zambelli*,* A. *Macromolecules*, **1996**, *29*, 6383.
[57] Ricci, G.; Morganti, D.; Sommazzi, A.; Santi, R.; Masi, F. *Journal of Molecular Catalysis A: Chemical* **2003**, *287,* 204.
[58] De Rosa C.; Malafronte A.; Scoti M.; Auriemma F.; Pierro I.; Leone G.; Ricci G. *Macromolecules* **2018**, *51*, 8574-8584 .
[59] Borriello, A.; Busico, V.; Cipullo, R.; Chadwick, J. C.; Sudmeijer, O. *Macromol. Rapid Commun.* **1996**, *17*, 589.
[60] Busico, V.; Cipullo, R.; Chadwick, J. C.; Modder, J. F.; Sudmeijer O. *Macromolecules* **1994**, *27,* 7538.
[61] Busico, V.; Cipullo, R.; Borriello, A. *Macromol. Rapid. Commun.* **1995**, *16*, 269.
[62] Grassi, A.; Zambelli, A.; Resconi, L.; Albizzati, E. *Macromolecules* **1988,** *21*, 617.
[63] Busico, V.; Cipullo, R. *J. Organomet. Chem.* **1995**, *497,* 113.
[64] Resconi, L.; Camurati, I.; Malizia, F. *Macromol. Chem. Phys.* **2006***, 207*, 2257.

[65] Ewen, J. A.; Jones, R. L.; Razavi, A.; Ferrara, J. D. *J. Am. Chem. Soc.* **1988,** *110*, 6255.
[66]Corradini, P.; Busico, V.; Guerra, G. "Monoalkene polymerization: stereospecificity" in Comprehensive Polymer Science, Pergamon Press, Oxford, UK, 1989, Vol. 4, Chapt. 3, pp. 29-50.
[67] Samran, J.; Phinyocheep, P.; Daniel, P.; Kittipoom, S. *J. Appl. Polym. Sci*. **2005**, *95,* 16.
[68] Mango, L. A.; Lenz, R.W. *Makromol. Chem.* **1973**, *163*, 13.
[69] De Rosa, C.; Auriemma, F.; Santillo, C.; Di Girolamo, R.; Leone, G.; Boccia, A.C.; Ricci, G. *Macromolecules* **2015,** *48*, 5251.
[70] Corradini, P.; Ganis, P.; Petraccone, V. *Eur. Polym. J.* ***1970,*** *6,* 281.
[71] Ciampelli, F.; Lachi, M.P.; Tacchi Venturi, M.; Porri, L. *Eur. Polym. J*. **1967**; *3(3)*, 353-66.
[72] Beebe, D.H.; Gordon, C.E.; Thudium, R.N.; Throckmorton, M.C.; Hanlon, T.L. *J. Polym. Sci. Polym. Chem. Ed.* **1978**, *16(9)*, 2285-301.
[73] Ricci,G.; Sommazzi, A.; Masi, F.; Ricci, M.; Boglia, A.; Leone, G. *Coord. Chem. Rev.* **2010**, *254*, 661-676

Chapter III

Chain-Walking: An Approach to Control Polymer Microstructure

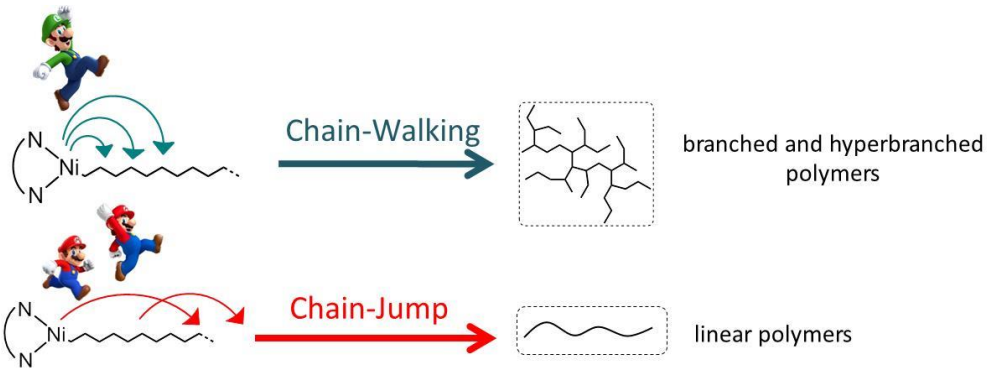

Introduction

As already mentioned in the introduction of this thesis, the performance of polyolefins strongly depends on the polymer microstructure,[1,2] which includes three major aspects: molecular weight (M_w) and molecular weight distribution (M_w/M_n), branching content, and branches-type distribution. Therefore, the tailor design of polyolefins requires at least good control of these structure elements.[3]

For this purpose, many strategies have been developed to modulate the polyolefin microstructure. For example, low-density polyethylene (LDPE) could be produced by radical polymerization. The intermolecular and intramolecular chain transfer reactions lead to the formation of both long chain branching and short chain branching.[4] In transition metal catalyzed olefin coordination polymerization, long chain branching can be generated by Dow's constrained geometry catalysts. In this case, macromonomers were produced from ethylene polymerization and subsequently incorporated in the polymer backbone.[5] Short chain branching can be generated by transition metal catalyzed copolymerization of ethylene with α-olefins. Alternatively, branched and hyperbranched polyolefins can be obtained using only ethylene as the feedstock by combining one ethylene oligomerization catalyst and one copolymerization catalyst.[6,7] In addition, Sen et *al*. synthesized low molecular weight hyperbranched PEs by combining ethylene coordination oligomerization and subsequent α-olefin cationic oligomerization.[8,9]

Conceptually different from the above-mentioned strategies, "chain-walking" polymerization represents a unique approach to modulate the polyolefin microstructure. The chain-walking mechanism was first presented by Fink *et al*. and developed by Brookhart *et al.*[10-14] Furthermore, a chain-straightening phenomenon in α-olefin polymerization was observed.[10-15]

The chain-walking mechanism was proposed and validated both experimentally and theoretically.[10-17] Here, a processing involving β-hydride elimination and reinsertion with the opposite regiochemistry is operative in addition to the common insertion, chain transfer, and termination processes. The degree of the polymer branching can be easily modulated by changing the polymerization conditions and the catalyst steric and electronic features. Since then, tremendous efforts have been devoted to chain-walking olefin polymerization and copolymerization reactions.[18,19-28] This strategy has been applied for the convenient synthesis of PEs with properties varied from thermoplastics to elastomers, and amorphous hyperbranched oils (with branch-on-branch

structures). Moreover, thermoplastic elastomers (TPEs) can be also obtained thanks to the numerous combinations of chain-walking and chain-straightening pathways.

3.1 Chain-walking mechanism

Polyolefin TPEs can be obtained through the copolymerization of ethylene with α-olefins catalyzed by a metallocene catalyst.[29] Elsewhere, late-transition-metal catalysts have shown great potential in their ability to afford branched and hyperbranched polymers that are related in structure to TPEs. A milestone in this field was the discovery of α-diimine Ni(II) and Pd(II) complexes by Brookhart in the 1990s.[20] Cationic Nickel(II) and Palladium(II) α-diimine complexes are capable of producing polyolefins from ethylene and α-olefins with variable branching densities and microstructures. This diversity allows access to materials with a broad range of thermal, mechanical, and rheological properties. [24,27,30-37]

The structural diversity stems primarily from a competitive reaction between the olefin insertion and the isomerization event known as "chain-walking". Chain walking involves β-hydride elimination followed by metal hydride reinsertion into the growing polymer chain with opposite regiochemistry (Scheme 3.1).

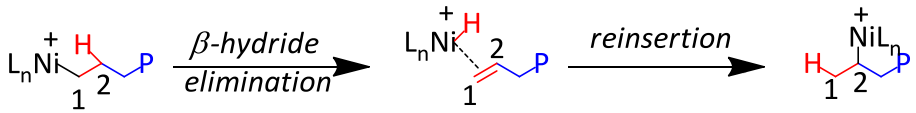

Scheme 3.1. *Chain Walking Isomerization Pathway.*

Metal migration along the polymer backbone allows propagation to occur at sites beyond the position generated in the initial insertion.[19] For α-olefin polymerization, the regiochemistry of the initial olefin insertion paired with the position of the subsequent insertion event determines the overall branching structure (Scheme 3.2). Thus, performing a 2,1-insertion followed by complete chain-walking and a new insertion to the terminal carbon (ω,1-enchainment) (ω-position, where ω is the number of carbon atoms) results in a "chain straightened" segment with repeated methylene sequences (Scheme 3.2). In contrast, 1,2-insertion followed by complete chain-walking and insertion (ω,2-enchainment) leads to the formation of a methyl branch (Scheme 3.2), while the

longer alkyl branches are likely due to the predominant 1,2-enchainment and/or a 2,1-enchainment (Scheme 3.2).

It was assumed that 1,2-insertions mainly installed branches (*i.e.,* methyl branches through ω,2-enchainment or longer branches through 1,2-enchainment) and 2,1-insertions installed mainly linear segments (ω,1-enchainment). Coates *et al*.[38] have demonstrated that 2,1-insertions installed also alkyl branches (Scheme 3.2).

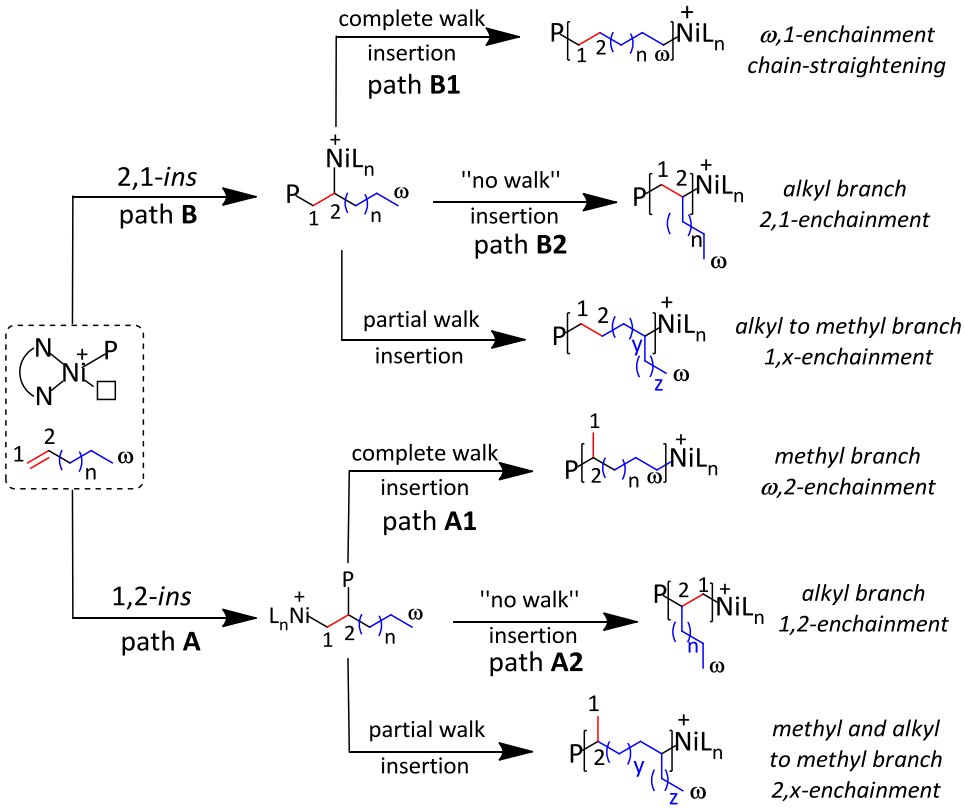

Scheme 3.2. *Possible insertion for α-Olefins using α-Diimine Nickel* catalysts.

However, as anticipated by Coates, it is impossible to distinguish these two paths since both 1,2- and 2,1-enchainment result in the same branching defect.[38] These new findings introduced by Coates increase the complexity of the polymerization mechanism, requiring the use of monomers with ^{13}C-labeled carbon atoms and mathematical models able of capturing the complexity of the system.[38]

3.2 α–Diimine ligand structures

Since Brookhart's initial work (Chart 1, I),[12] impressive efforts have been made to control the regiochemistry of olefin insertion, mainly through the *ortho*- (Chart 1, I–III) and *para*-aryl positions modification including steric tuning and electronic perturbations [39-41] and ligand backbone adjustments (Chart 1, V and VI).[42,43]

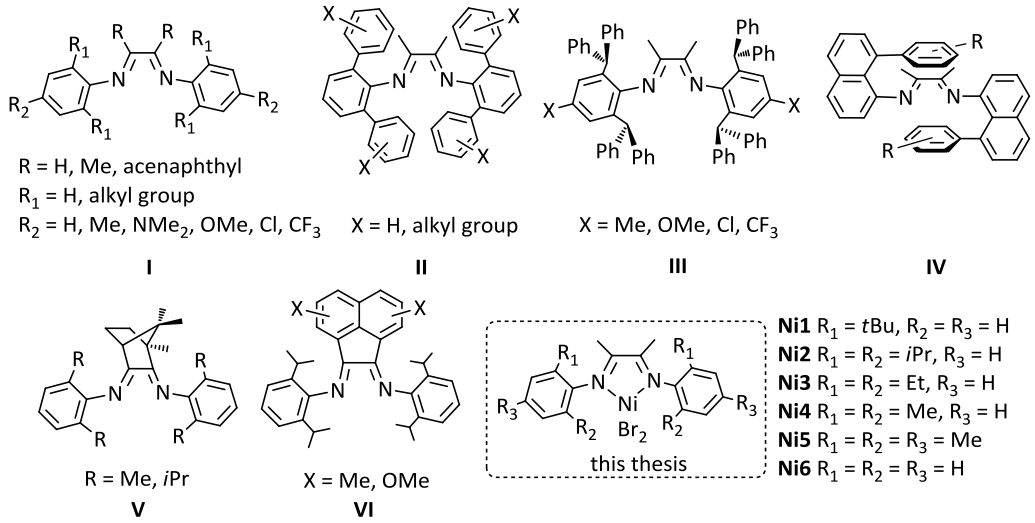

***Chart 1**. Some α-Diimine ligand structures reported in the literature and α-diimine Ni(II) complexes used in this work.*

The *ortho*-aryl groups are prone to easy chemical modification and exert a significant influence on the polymerization activities as well as on the thermal stability. [41,42,44] In addition, the alkyl substitution of N–aryl groups exerts a precise control over both the regiochemistry of olefin insertion and the location of the incoming monomer after chain-walking. By modifying the ligand structure, the various combinations of monomer insertion and chain-walking give rise to highly branched polymers with low melting temperature and crystallinity (Scheme 3.2) or chain-straightened PE-like materials with high melting temperature and crystallinity (Scheme 3.2). [37,40]

A series of α-diimine Ni(II) complexes with a variety of electron-donating and electron-withdrawing substituents on the *para* positions of the *bis*-aryl ligand have been also synthesized and used for the polymerization of olefins.[24,27,33,34] The presence of substituents on the *para* positions strongly perturbs the metal electronics and exerts a significant impact on the catalyst stability and lifetime, and polymer molecular weight and topology.

More recently, complexes of type IV, in which 8-arylnaphthyl-α-diimine positions the aryl groups over the axial sites to form "sandwich" type complexes, have been reported.[34,38,40] It has been demonstrated that these bulky substituents are more effective in shielding the axial sites than the *ortho*-isopropyl groups in complexes of type I (Chart 1). These sandwich catalysts produced highly branched ultrahigh molecular weight PEs[34] and chain-straightened poly(α-olefin)s with the highest melting temperatures reported to date. [38,40] The evolution of α-diimine Ni(II) complexes has been accompanied by a progressive increase of steric bulk and number of *ortho*-substituents. This is because the *ortho*-substituents offer steric crowding both above and below the metal center and this steric hindrance at the axial sites is critical for suppressing the associative chain-transfer process.[20,33]

It has been demonstrated that by modifying the *ortho*-substituents from methyl to isopropyl, the complex bearing the bulkier isopropyl group affords much higher molecular weight polymers at significantly higher polymerization activity than the corresponding methyl-substituted complexes.[20,45-48]

Thus, it is generally accepted that a key feature for producing high polymers with high turnover frequencies lies in the suppression of chain transfer by the steric bulk of the *ortho*-aryl substituents.

References

[1] Bubeck , R. A. *Mater. Sci. Eng.: R: Rep*. **2002** , *39* , 1.

[2] Lohse, D. J.; Milner, S. T.; Fetters, L. J.; Xenidou, M.; Hadjichristidis, N.; Mendelson, R. A.; Garcia-Franco, C. A.; Lyon, M. K. *Macromolecules* **2002**, *35*, 3066.

[3] Liu, W.; Liu, P.; Wang, W.J.; Li, B.G.; Zhu, S. *Macromol. React. Eng*. **2016**, *10*, 180-200.

[4] Peacock, A. J. In Handbook of polyethylene; Marcel Dekker: New York, 2000; pp 43−53.

[5] Chum, P. S.; Kruper, W. J.; Guest, M. J. *Adv. Mater.* **2000**, *12*, 1759−1767.

[6] Barnhart, R. W.; Bazan, G. C.; Mourey, T. *J. Am. Chem. Soc.* **1998,** *120*, 1082−1083.

[7] Komon, Z. J. A.; Bu, X.; Bazan, G. C. *J. Am. Chem. Soc.* **2000**, *122*, 1830−1831.

[8] Kim, J.; Pawlow, J. H.; Wojcinski, L. M.; Murtuza, S.; Kacker, S.; Sen, A. *J. Am. Chem. Soc.* **1998**, *120*, 1932−1933.

[9] Murtuza, S.; Harkins, S. B.; Long, G. S.; Sen, A. *J. Am. Chem. Soc*. **2000,** *122*, 1867−1872.
[10] Möhring, V. M.; Fink, G. *Angew. Chem. Int. Ed. Engl.* **1985**, *24*, 1001−1003.
[11] Schubbe, R.; Angermund, K.; Fink, G.; Goddard, R. *Macromol. Chem. Phys.* **1995**, *196*, 467−478.
[12] Johnson, L. K.; Killian, C. M.; Brookhart, M. *J. Am. Chem. Soc.* **1995**, *117,* 6414−6415.
[13] Johnson, L. K.; Mecking, S.; Brookhart, M. *J. Am. Chem. Soc.* **1996**, *118*, 267−268.
[14] Mecking, S.; Johnson, L. K.; Wang, L.; Brookhart, M. *J. Am. Chem. Soc.* **1998,** *120*, 888−899.
[15] Killian, C. M.; Tempel, D. J.; Johnson, L. K.; Brookhart, M. *J. Am. Chem. Soc*. **1996**, *118*, 11664−11665.
[16] Tempel, D. J.; Johnson, L. K.; Huff, R. L.; White, P. S.; Brookhart, M. *J. Am. Chem. Soc.* **2000,** *122*, 6686−6700.
[17] Shultz, L. H.; Tempel, D. J.; Brookhart, M. *J. Am. Chem. Soc*. **2001,** *123*, 11539−11555.
[18] Chen, Y.; Wang, L.; Yu, H.; Zhao, Y.; Sun, R.; Jing, G.; Huang, J.; Khalid, H.; Abbasi, M. Akram, N.M. *Prog. Polym. Sci.* **2015**, *45*, 23-43.
[19] Guan, Z.; Cotts, P. M.; McCord, E. F.; McLain, S. J. Chain Walking: *Science* **1999**, *283*, 2059−2062.
[20] Ittel, S. D.; Johnson, L. K.; Brookhart, M. Late-Metal Catalysts for Ethylene Homo- and Copolymerization *Chem. Rev.* **2000,** *100*, 1169−1203.
[21] Gibson, V. C.; Spitzmesser, S. K. *Chem. Rev.* **2003**, *103*, 283−316.
[22] Guan, Z. *Chem. Eur. J.* **2002**, *8*, 3086−3092.
[23] Guan, Z. J. *Polym. Sci., Part A: Polym. Chem*. **2003**, *41*, 3680−3692.
[24] Dong, Z.; Ye, Z. *Polym. Chem.* **2012**, *3,* 286−301.
[25] Takeuchi, D. *Macromol. Chem. Phys*. **2011,** *212*, 1545−1551.
[26] Ye, Z.; Xu, L.; Dong, Z.; Xiang, P. Designing Polyethylenes of Complex Chain Architectures via Pd-Diimine-Catalyzed "Living" Ethylene Polymerization. *Chem. Commun.* **2013,** *49*, 6235−6255.
[27] Takeuchi, D. *Polym. J.* **2012**, *44*, 919−928.
[28] Guo, L. H.; Chen, C. L. *Sci. China: Chem.* **2015,** *58*, 1663−1673.
[29] Arriola, D. J.; Carnahan, E. M.; Hustad, P. D.; Kuhlman, R. L.; Wenzel, T. T. *Science* **2006**, *312*, 714−719.
[30] Ye, Z.; Feng, W.; Zhu, S.; Yu, Q. *Macromol. Rapid Commun*. **2006***, 27,* 871−876.

[31] Rose, J. M.; Cherian, A. E.; Lee, J. H.; Archer, L. A.; Coates, G. W.; Fetters, L. J. *Macromolecules* **2007**, *40*, 6807−6813.
[32] Okada, T.; Park, S.; Takeuchi, D.; Osakada, K. *Angew. Chem., Int. Ed*. **2007**, *46*, 6141−6143.
[33] Camacho, D. H.; Guan, Z. *Chem. Commun.* **2010,** *46,* 7879−7893.
[34] Zhang, D.; Nadres, E. T.; Brookhart, M.; Daugulis, O. *Organometallics* **2013**, *32*, 5136−5143.
[35] Leone, G.; Mauri, M.; Bertini, F.; Canetti, M.; Piovani, D.; Ricci, G. *Macromolecules* **2015**, *48,* 1304−1312.
[36] Leone, G.; Mauri, M.; Pierro, I.; Ricci, G.; Canetti, M.; Bertini, F. *Polymer* **2016**, *100*, 37−44.
[37] O'Connor, K. S.; Watts, A.; Vaidya, T.; LaPointe, A. M.; Hillmyer, M. A.; Coates, G. W. *Macromolecules* **2016**, *49*, 6743−6751.
[38] O'Connor, K. S.; Lamb, J. R.; Vaidya, T.; Keresztes, I.; Klimovica, K.; LaPointe, A. M.; Daugulis, O.; Coates, G. W. *Macromolecules* **2017**, *50,* 7010−7027.
[39] Meinhard, D.; Wegner, M.; Kipiani, G.; Hearley, A.; Reuter, P.; Fischer, S.; Marti, O.; Rieger, B. *J.Am. Chem. Soc.* **2007**, *129*, 9182−9191.
[40] Vaidya, T.; Klimovica, K.; LaPointe, A. M.; Keresztes, I.; Lobkovsky, E. B.; Daugulis, O.; Coates, G. W. *J. Am. Chem. Soc.* **2014,** *136*, 7213−7216.
[41] Rhinehart, J. L.; Brown, L. A.; Long, B. K. *J. Am. Chem. Soc.* **2013**, *135*, 16316−16319.
[42] Liu, F.-S.; Hu, H.-B.; Xu, Y.; Guo, L.-H.; Zai, S.-B.; Song, K.-M.; Gao, H.-Y.; Zhang, L.; Zhu, F.-M.; Wu, Q. *Macromolecules* **2009,** *42*, 7789−7796.
[43] Zou, W.; Chen, C. *Organometallics* **2016**, *35*, 1794−1801.
[44] Zhong, L.; Li, G.; Liang, G.; Gao, H.-Y.; Wu, Q. *Macromolecules* **2017**, *50*, 2675−2682.
[45] Wang, F.; Tanaka, R.; Cai, Z.; Nakayama, Y. M.; Shiono, T. *Polymers* **2016**, *8*, 160.
[46] Peleška, J.; Hoštàlek, Z.; Hasalíkovà, D.; Merna, J. *Polymer* **2011**, *52*, 275−281.
[47] Merna, J.; Hoštàlek, Z.; Peleška, J.; Roda, J. *Polymer* **2009**, *50,* 5016−5023.
[48] Gates, D. P.; Svejda, S. A.; Ońate, E.; Killian, C. M.; Johnson, L. K.; White, P. S.; Brookhart, M. *Macromolecules* **2000,** *33,* 2320−2334.

Chapter IV

Chain-Walking Polymerization of α-Olefins by α-Diimine Ni(II) Complexes

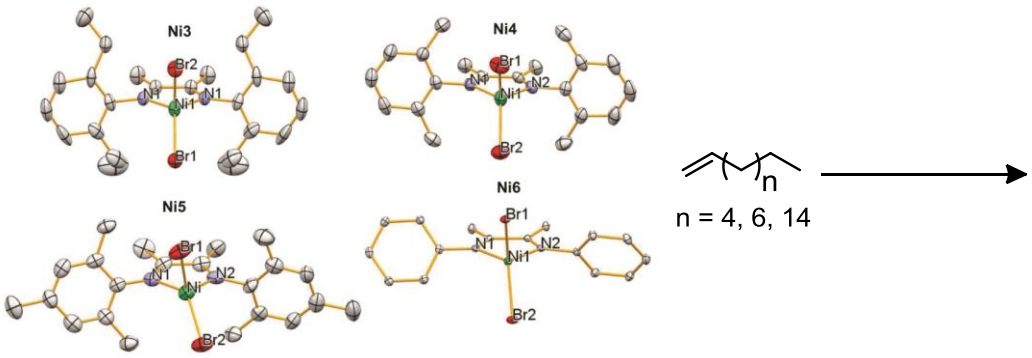

Introduction

In this Chapter, I report a systematic investigation on the chain-walking polymerization of higher linear α-olefins catalyzed by traditional α-diimine Ni(II) complexes with methyl α-diimine backbone and different aryl *ortho*- (H, Me, Et, ^{i}Pr, ^{t}Bu) and *para*-(H, Me) substituents (**Ni1–Ni6** in Figure 4.1). I focused my attention on this class of complexes because, in comparison with those having acenaphthyl α-diimine backbone, α-diimine Ni(II) complexes with methyl α-diimine backbone gave higher molecular weight polymers and enhanced activity.[1]

In particular, I focused on :

1) the polymerization of 1-octene[2] catalyzed by an α-diimine Ni(II) complex (**Ni2**) (Figure 4.1), in combination with different aluminum alkyls (Et_2AlCl, MAO and MMAO). The results of this work have been taken from: Pierro I. *et al*. *Polymer* **2016**, *100*, 37–44 ;

2) the synthesis and the characterization of copolymers of 1-octene with 1-decene and cyclopentene[3] catalyzed by **Ni2** (Figure 4.1). The results of this work have been taken from: Pierro I. *et al*. *Eur. Polym. J.* **2017**, *93*, 200−211;

3) the synthesis and the characterization of 1-octene, 1-decene, and 1-octadecene polymers catalyzed by the series **Ni1–Ni6** [4] (Figure 4.1). The effect of ligand steric and electronic perturbation on the catalytic behavior, monomer enchainment, and polymer properties is discussed. The results of this work have been taken from: Pierro I. *et al. Macromolecules* **2018,** *51,* 801−814.

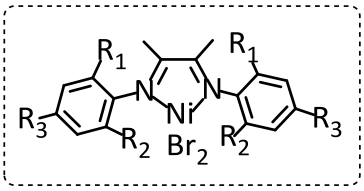

Ni1 R1 = ^{t}Bu, R2 = R3 = H
Ni2 R1 = R2 = ^{i}Pr, R3 = H
Ni3 R1 = R2 = Et, R3 = H
Ni4 R1 = R2 = Me, R3 = H
Ni5 R1 = R2 = R3 = Me
Ni6 R1 = R2 = R3 = H

Figure 4.1. *α-diimine Nickel(II) complexes synthesized in this work.*

4.1 Polyolefins from 1-octene chain-walking polymerization [2]

First, I focused on the polymerization of 1-octene catalyzed by an α-diimine Ni(II) complex [(ArN)C(CH_3)-(CH_3)C(NAr)]$NiBr_2$ [Ar = 2,6-(*i*Pr)$_2C_6H_3$] (**Ni2** Figure 4.1). The effect of monomer concentration, reaction temperature, Al/Ni mole ratio and aluminum alkyl type (*i.e*., Et_2AlCl, MAO and MMAO) on productivity, selectivity of monomer insertion and polymer structure/properties is discussed. The mechanical behavior of the obtained polymers was investigated by uniaxial stretching until failure and step-cycle tensile tests.

4.1.1 Polymerization of 1-octene

Leone *et al.*[5] screened Et_2AlCl in combination with **Ni2** complex (Figure 4.1) for the polymerization of 1-hexene, 1-octene and 1-dodecene at different monomer concentration. The polymerization gave branched, semicrystalline PE-like materials with narrow molecular weight distribution. Herein, I report extension of these studies about the Ni(II)-catalyzed 1-octene polymerization by expanding the range of monomer feedstock concentration from 0.2 to 3.0 mol/L. Additional polymerizations were carried out modifying the Al/Ni mole ratio, the polymerization temperature and using **Ni2** in combination with different aluminoxanes (*i.e*., MAO and MMAO). The polymerization results are reported in Table 4.1.

Table 4.1. *Polymerization of 1-octene catalyzed by* ***Ni2****.* [a]

Entry	OCT (mol/L)	Al-alkyl	Al/Ni (mol/mol)	T (°C)	Yield (g)	Conv (%)	TOF [b] (h^{-1})	M_n [c] (kg/mol)	M_w/M_n [c]	$[\eta]_w$ [d] (dL/g)
1	0.2	Et_2AlCl	200	22	0.19	54	59	36.6	1.16	0.34
2	0.4	Et_2AlCl	200	22	0.40	56	118	74.0	1.20	0.62
3	0.6	Et_2AlCl	200	22	0.59	55	175	90.8	1.29	0.69
4	0.8	Et_2AlCl	200	22	0.82	58	244	101.8	1.32	0.65
5	1.0	Et_2AlCl	200	22	1.10	58	324	105.6	1.36	0.94
6	1.5	Et_2AlCl	200	22	1.73	65	514	109.1	1.68	0.95
7	2.0	Et_2AlCl	200	22	2.43	68	722	132.6	1.64	1.34
8	2.5	Et_2AlCl	200	22	2.99	67	888	175.0	1.73	1.36
9	3.0	Et_2AlCl	200	22	3.16	59	862	230.0	1.84	1.60
10	1.0	Et_2AlCl	10	22	1.20	67	328	100.4	1.37	0.86
11	1.0	Et_2AlCl	50	22	1.24	69	338	114.7	1.40	0.93
12	1.0	Et_2AlCl	500	22	1.31	73	358	87.6	1.89	0.92
13	1.0	Et_2AlCl	200	0	0.33	18	90	80.5	1.23	0.67
14	1.0	Et_2AlCl	200	50	1.24	69	338	132.1	1.78	0.90
15	1.0	MMAO	200	22	0.74	42	202	142.7	1.65	0.81
16	1.0	MAO	200	22	0.72	40	197	167.5	1.51	1.07

[a] *Polymerization conditions: toluene, total volume,18mL;* ***Ni2****,10 μmol; time, 180 min.*

[b] *Turnover frequency (TOF),calculated by the equation:* mol_{pol} *x* mol_{Ni}^{-1} *x* h^{-1}.

[c] *Molecular weight (M_n) and molecular weight distribution (M_w/M_n) from SEC.*

[d] *Weight-average intrinsic viscosity ($[\eta]_w$) by SEC using the online viscometer.*

Catalyst **Ni2**/Et_2AlCl displayed good activity for 1-octene polymerization. Although turnover frequency (TOF) was strongly affected by mass transfer limitations, the calculated TOFs increased with increasing the monomer concentration. The monomer conversion does not vary much with the increase of 1-octene feedstock concentration. This behavior can be accounted to the higher exothermic character at the beginning of the reaction and to the increased viscosity of the reaction mixture.

The effect of Al/Ni ratio was investigated for **Ni2**/Et_2AlCl at monomer concentration of 1.0 mol/L. The activity did not increase with Al/Ni ratio from 10 to 500, meaning that formation of the active species is apparently complete (but not necessarily quantitative) and sufficient for Al/Ni = 10. The molecular weight distribution of the obtained polymers was monomodal and ranged from 1.37 (Table 4.1 entry 10, Al/Ni = 10) to 1.89 (Table 4.1 entry 12, Al/Ni=500), indicating a single site catalytic system.

The aluminium alkyl plays an important role, strongly influencing the polymerization activity, and the polymer molecular weight and molecular weight distribution. The system **Ni2**/Et_2AlCl was generally more active than **Ni2**/MAO and **Ni2**/MMAO. This result could be likely due to the fact that cationic nickel-alkyl species, formed by **Ni2** and Et_2AlCl, may stay in equilibrium between chloro-bridged and cationic alkyl species due to the less steric bulk and stronger nucleophilic nature of Et_2AlCl [6,7] (Scheme 4.1).

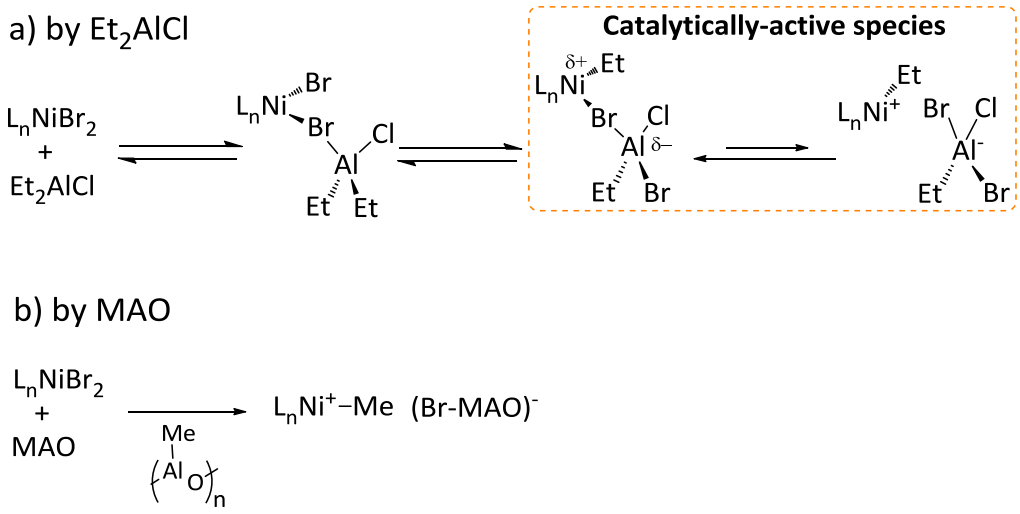

Scheme 4.1. *Different catalytically active species generated in different catalyst system.*

Such a close interaction would stabilize the catalytically active species, leading to a higher monomer conversion. In addition, the polymers from **Ni2**/MAO and **Ni2**/MMAO had higher molecular weight and broader molecular weight distribution.

The effect of polymerization temperature was investigated in the case of **Ni2**/Et_2AlCl. Increasing the temperature from 0 to 22°C yielded a threefold monomer conversion increase, while a further temperature rise to 50°C had no significant influence on the activity (Table 4.1, entry 5, 13, 14). Increasing the reaction temperature, the obtained polymers had higher molecular weight, meaning that chain transfer and termination reactions are reduced as compared to the chain propagation at elevated temperature.[8-10]

Thermal and structural analysis

The DSC curves of poly(1-octene)s obtained at different monomer concentration, keeping constant the other polymerization conditions, are reported in Figure 4.2. The values of melting and crystallization temperatures and enthalpies are reported in Table 4.2.

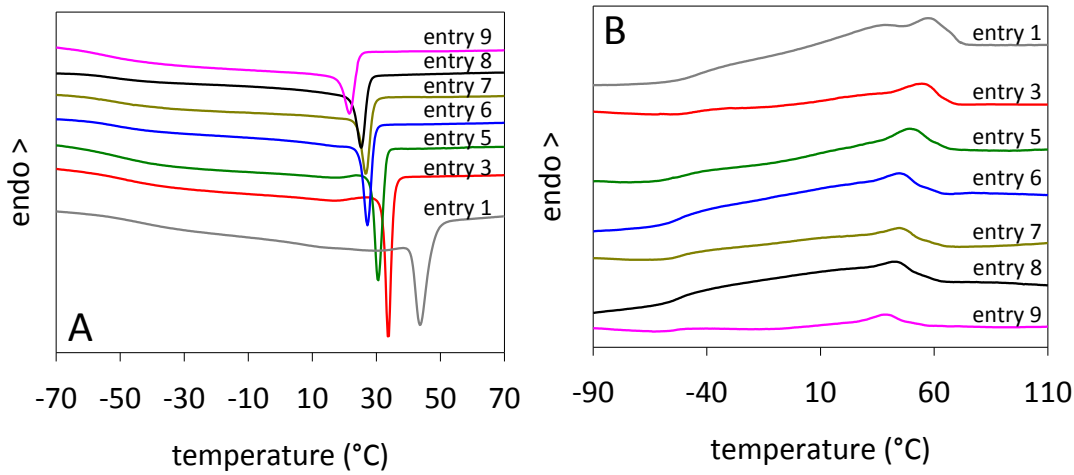

Figure 4.2. *DSC cooling scans (A) and DSC successive heating scans (B) of selected poly(1-octene)s obtained at different monomer feedstock concentration.*

The crystallization behavior (Figure 4.2 A) of all the polymers exhibits characteristic bimodal exotherms that are similar to those displayed by ethylene/α-olefin copolymers with a wide distribution of short chain branching.[11,12] The cooling DSC trace shows a relative sharp crystallization exotherm followed by a wide tail. The first peak corresponds to the crystallization

of the linear portions of the less branched macromolecular chains that usually crystallize at higher temperatures, while the low temperature tail corresponds to the crystallization of the shorter linear portions of chains. The crystallization temperature (T_c) taken at the maximum of the sharp peak decreases with the increase of the monomer concentration (Table 4.2).

The heating curves of the non-isothermal crystallized poly(1-octene)s are reported in Figure 4.2 B. Glass transition events at low temperature and very broad melting endotherms can be observed. The glass transition temperature (T_g) ranges from –55 to –42°C and decreases with increasing the monomer concentration (Table 4.2).

The melting event begins at subambient temperatures and may extend over a 80°C temperature range. The broad endothermic event reflects the crystallization behavior pointing out the non-homogeneous distribution of the crystallisable units along the polymer chains. In general, as the monomer concentration increases, the melting event of the obtained polymer shifts to a lower temperature range and the melting point taken at peak maximum decreases (T_m in Table 4.2). Analogously, the melting enthalpy (ΔH_m) decreases with monomer concentration, going from 36 J/g for [1-octene] = 0.2 mol/L to 14 J/g for [1-octene] = 3 mol/L, reflecting the reduced crystallinity.

Table 4.2. *Microstructural data and thermal properties*

Entry	Branches/ 1000C[a]	8,1[b] (%)	CH_3/1000C[c]		Total CH_3[c]	T_g[d] (°C)	T_c[d] (°C)	T_m[d] (°C)	ΔH_m[d] (J/g)	X_{DSC}[e] (%)
			Me	Lg						
1	74	48	35	22	59	-42	43	57	36	12.4
2	68	52	34	26	61	-45	34	55	29	10.0
3	59	58	32	27	60	-45	33	54	26	9.9
4	61	57	33	29	63	-46	33	53	25	8.6
5	66	53	27	32	60	-49	31	49	22	7.6
6	64	55	22	37	60	-51	27	45	19	6.6
7	62	56	20	42	63	-50	26	44	18	6.2
8	65	54	18	41	60	-50	25	43	18	6.2
9	71	50	16	49	66	-55	22	39	14	4.8
10	58	58	32	26	60	-44	38	56	33	11.4
11	53	62	29	28	58	-46	36	54	31	10.7
12	67	53	32	31	63	-49	30	48	22	7.6
13	60	57	14	50	64	-56	23	44	19	6.6
14	61	57	38	24	62	-44	34	51	28	9.7
15	67	53	24	43	68	-53	18	36	10	3.4
16	69	51	21	48	70	-55	14	31	8	2.8

[a] *From ^{1}H NMR (see equation (1) in Appendix).*

[b] *Percentage of 8,1-insertion (see equation (2) in Appendix).*

[c] *From ^{13}C NMR. A small amount (never exceeding $2CH_3$/1000C) of propyl branches was observed.*

[d] *From DSC.*

[e] *Crystallinity from melting enthalpy, $X_{DSC} = (\Delta H_m/\Delta H^0_m) \times 100$, $\Delta H^0_m = 290$ J/g.*

The influence of Al/Ni ratio on the thermal properties of poly(1-octene)s is analogous with previous observations deduced from monomer concentration effect. Indeed, an increase in the Al/Ni ratio from 10 to 200 produced a corresponding decrease in T_g, T_c, T_m, and ΔH_m of the polymer (Figure 4.3). A further increase in Al/Ni ratio did not result in modifying the thermal properties of the polymer (Table 4.2 entry 12).

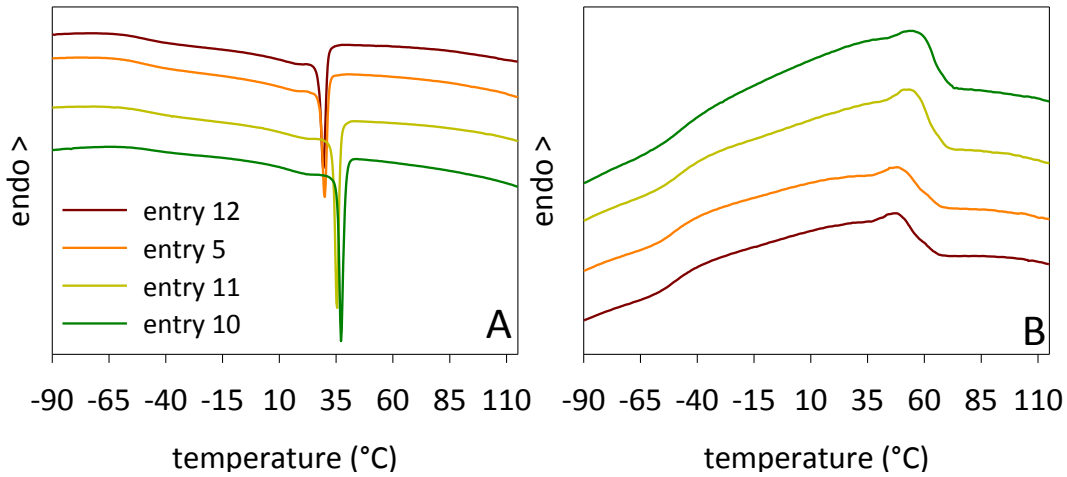

Figure 4.3. *DSC cooling scans (A) and DSC successive heating scans (B) of poly(1-octene)s obtained by varying the Al/Ni ratio (entries 5, 10, 11 and 12, Table 4.1).*

The thermal properties of the poly(1-octene)s obtained by varying the polymerization temperature are markedly different (Figure 4.4).

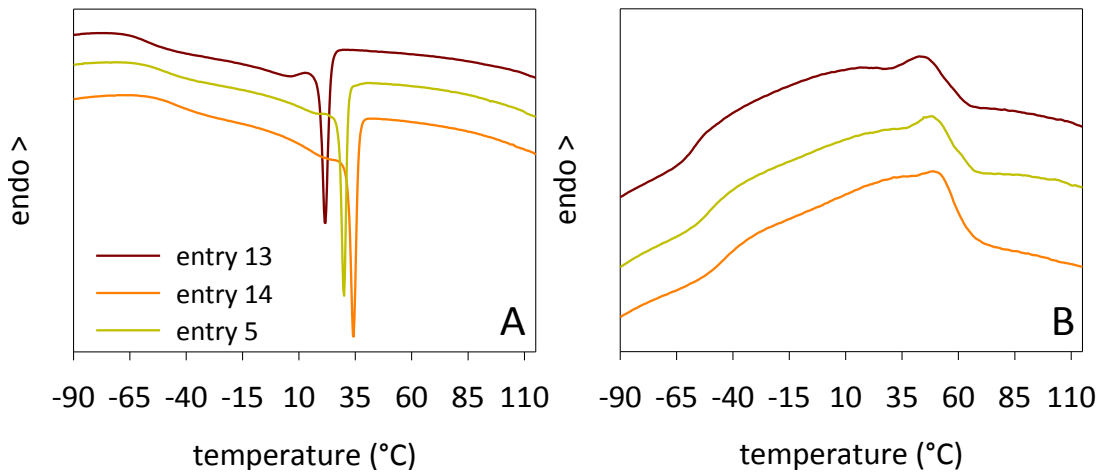

Figure 4.4. *DSC cooling scans (A) and DSC successive heating scans (B) of poly(1-octene)s obtained by varying the polymerization temperature (entries 5, 13, and 14, Table 4.1).*

The polymer prepared at 0°C (entry 13) exhibits a broad T_m at 44°C with a crystallinity of 6.6%, while the polymer obtained at 50°C (entry 14) exhibits a T_m at 51°C with a crystallinity of 9.7%. In general, the reduction of the polymerization temperature results in a decrease in T_g, T_c, T_m, and ΔH_m of the polymer (Table 4.2 entry 5, 13, 14). Polymerizations carried out in the presence of MAO or MMAO, at [1-octene] = 1 mol/L, lead to polymers with a very low crystallinity (Table 4.2 entry 15, and 16). The melting range of these poly(1-octene)s was very broad and located at a much lower temperature, beginning at about –25°C and ending near 60°C, as compared to the polymers prepared by **Ni2**/Et_2AlCl (Figure 4.5).

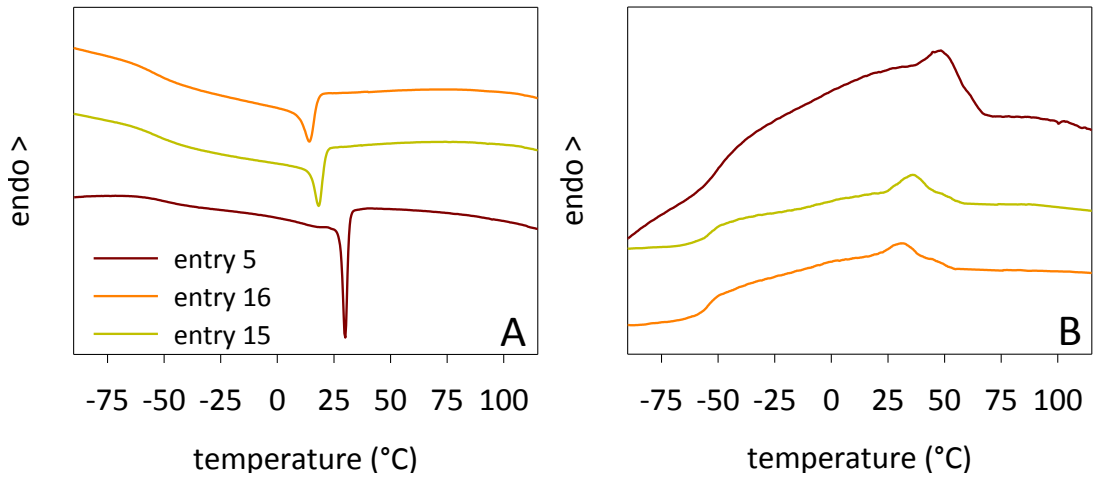

Figure 4.5. *DSC cooling scans (A) and DSC successive heating scans (B) of poly(1-octene)s obtained by varying the aluminum alkyl activator (entries 5, 15, and 16, Table 1).*

The exclusive 1,2-enchainment would result in a poly(1-octene) with 125 branches/1000C, but the observed trend is that the branching content was almost half of the theoretic value, which is a result of nickel migration on polymer chain.[13] All the polymers were also characterized by ^{13}CNMR for quantification of total methyl groups and branch-type distribution.[14] The results are reported in Table 4.2. Typical spectrum of a branched polymer obtained with **Ni2**/Et_2AlCl (Table 4.1 entry 1) is shown in Figure 4.6.

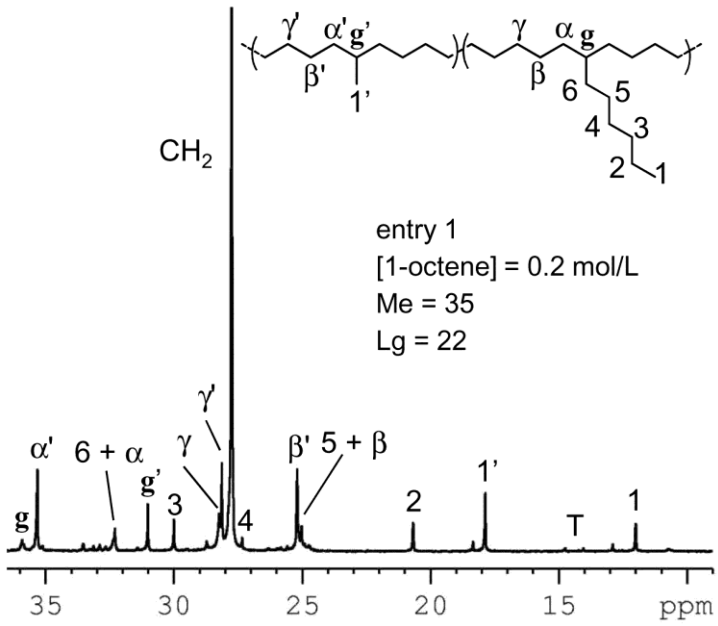

Figure 4.6. *^{13}C NMR spectrum and assignment of a selected poly(1-octene) (Table 4.1, entry 1). The polymer was dissolved in $C_2D_2Cl_4$, and HDMS was used as internal chemical shift reference.*

The interpretation of the ^{13}C NMR spectra was performed on the basis of previously assignments.[5] The nomenclature used for isolated branches is that of Usami and Takayama.[15] All the investigated polymers have predominantly methyl and longer than butyl branches (Me and Lg in Table 4.2, respectively): the intense signal at 27.7 ppm of long methylene sequences and signals due to methyl ($1B_1$ at 17.8 ppm) and longer branches ($1B_n$ at 12.0 ppm and $2B_n$ at 20.6 ppm) are safely identified in the ^{13}C NMR spectra. Carbons of ethyl and butyl branch ($1B_2$ and $2B_4$ at 9.0 and 21.1 ppm, respectively) are absent, while a very weak signal due to a propyl branch ($1B_3$ at 12.8 ppm) is observed and ascribed to a small fraction of 1,2-monomer insertion into a secondary Ni-alkyl bond.[10] Propyl branches are present in less than 3.0 mol %. In addition, after a careful analysis of the ^{13}C NMR spectra, the occurrence of methyl signals were registered in the region spanning from 14 to 15 ppm (marked as T in Figure 4.6). Sivaram assigned all of these peaks to carbons of adjacent methyl branches,[16] while Brookhart observed how some of these signals could also be ascribed to methyl groups adjacent to longer branches.[9] The overall trend was that the 8,1-enchainment, which gave linear polymer chain segments (Scheme 3.2 Chapter III), ranged from 48 to 62% without any apparent relation with respect to the polymerization conditions and the

aluminum alkyl employed. This suggests that the catalyst system do not have a significant selectivity for 2,1- and 1,2-insertion.

With respect to the results obtained by varying the concentration of 1-octene, the overall trend is that increasing the monomer concentration results in relatively constant total methyls. In contrast, monomer concentration significantly determines the branch-type distribution. The formation of a longer than methyl branch was favoured by increasing the 1-octene feedstock concentration, while methyl branches dominated at low monomer concentration. The fact that decreasing the monomer concentration resulted in a larger number of methyl branches, may be due to a favoured 1,2-insertion followed by chain-walking (ω,2-enchainment), but also due to a 2,1-insertion off a secondary penultimate carbon (Figure 4.7). [17]

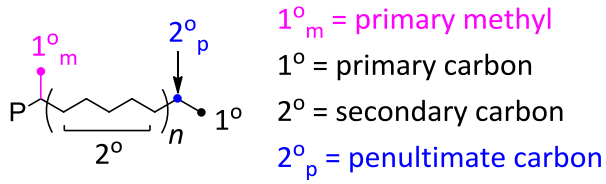

Figure 4.7. *Possible positions where a Nickel complex can insert monomer on a growing polymer chain.*

Comparison of the polymers obtained at different polymerization temperatures shows that the content of methyl branches increases from 14 to 39 CH_3/1000C when the temperature was increased, while longer branches decreased from 50 to 22 CH_3/1000C. This indicates that an increase in reaction temperature accelerates ω,2-enchainment with respect to 1,2-enchainment/or 2,1-enchainment, while the 8,1-enchainment percentage ranges from 53 to 57, confirming that **Ni2**/Et_2AlCl catalyst system did not have a selectivity for 1,2- and 2,1-insertion.

When MAO or MMAO was used, the 8,1-enchainment (2,1-insertion followed by chain-walking) content was almost the same found for Et_2AlCl. This means that the selectivity for 1,2- and 2,1-insertion was relatively independent from the aluminum alkyl employed. However, the resulting polymers had a different branch-type distribution. In particular, **Ni2**/MAO and **Ni2**/MMAO catalysts gave polymers with a larger fraction of long branches (Table 4.2), while **Ni2**/Et_2AlCl gave polymers with a larger fraction of methyl ones. This means that **Ni2**/MAO

and **Ni2**/MMAO catalysts show a higher selectivity for 1,2-insertion/or 2,1-insertion followed by a new monomer insertion (1,2-enchainment/or 2,1-enchainment), while **Ni2**/Et_2AlCl shows a higher selectivity for 1,2-insertion followed by chain-walking to give a methyl branch (ω,2-enchainment), or to a 2,1-insertion off a secondary penultimate carbon.

Such differences may be also due to the nature of the ion pairing species generated from the two aluminum alkyls. Indeed, the anion generated from the reaction of **Ni2** with Et_2AlCl is smaller than that from MAO or MMAO, validating a closer interaction with the active center, and forcing the 1,2-interted unit to chain-walk before a new 1,2-insertion.[6]

As well known, the thermal properties and crystallinity of polymers are strongly influenced by microstructure. Indeed, the poly(1-octene)s exhibit differences in melting temperature and crystallinity even comparing polymers with the same content of total branching. Figure 4.8 plots T_m versus the sum of all the branches longer than methyl for the polymers under investigation.

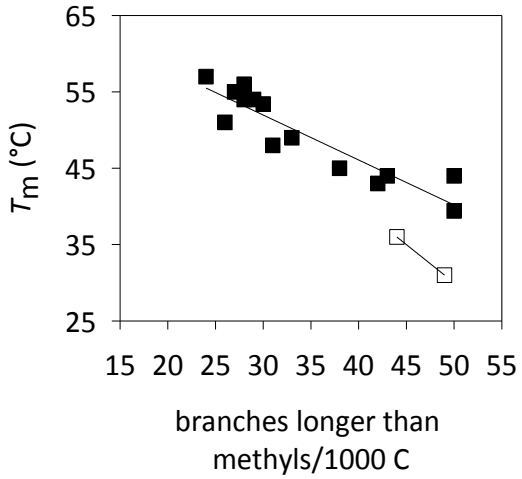

Figure 4.8. *Plot of melting temperature (T_m) as a function of the total branching longer than methyl. Polymers from* ***Ni2****/Et_2AlCl (■) and from* ***Ni2****/MAO and* ***Ni2****/MMAO (□). The solid lines are guides to the eye and illustrate the overall trend.*

A relationship between the two data was found, and increasing the content of longer side groups the melting temperature decreases. An analogous trend was observed for melting enthalpy. It is worth noting that, with the same branches longer than methyl content, the polymers produced by **Ni2**/MAO and **Ni2**/MMAO exhibit lower T_m and crystallinity than those obtained by **Ni2**/Et_2AlCl. These

features could be attributed to a different distribution of longer than methyl branches.

The synthesized poly(1-octene)s were structurally characterized by X-ray techniques. WAXD patterns show a diffuse peak centered at about $2\theta = 20°$, while the typical diffractions of the orthorhombic poly(ethylene) crystalline phase are not evidenced (Figure 4.9).

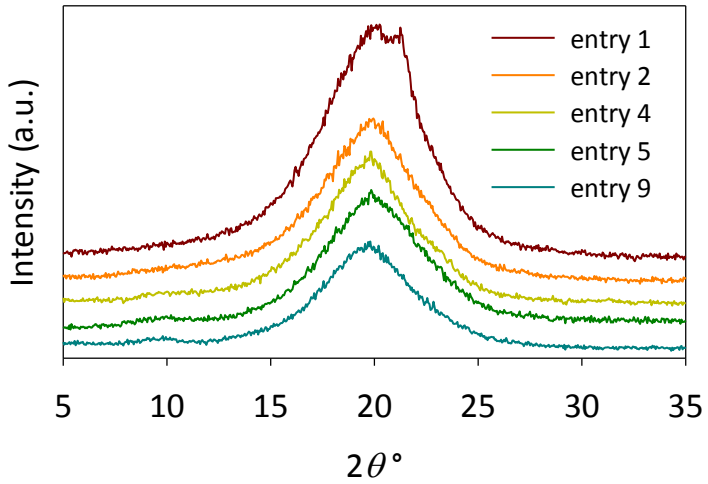

Figure 4.9. *WAXD patterns of selected poly(1-octene)s obtained at different 1-octene feedstock concentration.*

Therefore, the low melting temperature and broad melting range of poly(1-octene)s are attributed to the fringed-micellar crystal structure with a broad size distribution that come from the statistical distribution of crystallizable chain lengths.[18,19]

An important parameter, strictly related to the polymer topology, is the intrinsic viscosity ($[\eta]_w$ in Table 4.1). The $[\eta]_w$ generally increases as a function of the polymer molecular weight. Nonetheless, the $[\eta]_w$ values for the polymers obtained from **Ni2**/MAO and **Ni2**/MMAO resulted lower than those from **Ni2**/Et_2AlCl with comparable molecular weight, indicating a different polymer topology.[20]

Mechanical properties

The mechanical behavior of the obtained polymers was investigated by uniaxial stretching until failure. The polymers exhibit elastomeric features with a low modulus, a uniform deformation to high strain and an instantaneous strain

recovery after fracture. The tensile properties are reported in Table 4.3 and selected stress-strain curves are shown in Figure 4.10.

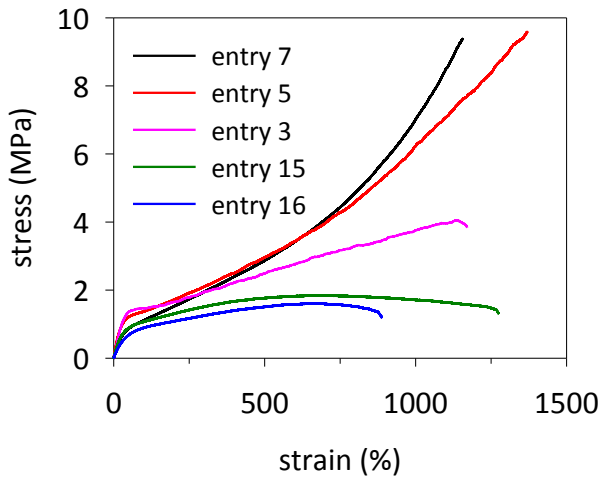

Figure 4.10. *Stress-strain curves of selected poly(1-octene)s during monotonic tensile deformation.*

Comparing the tensile behavior of polymers obtained by **Ni2**/Et_2AlCl varying the polymerization parameters, *i.e.*, monomer feedstock concentration, reaction temperature and Al/Ni ratio, one can notice some remarkable differences. The initial modulus depends only on the crystallinity of the polymer ranging from 9.3 to 2.3 MPa with decreasing the crystallinity. Most of the polymers show high and comparable ultimate strain (about 1250 ± 150%), independent of the crystallinity.

In Figure 4.10, for entry 3, 5 and 7 (obtained by **Ni2**/Et_2AlCl at different 1-octene concentration), a strain-hardening is observed while, for entry 15 and 16 (obtained by **Ni2**/MAO and **Ni2**/MMAO) a more uniform deformation associated to viscous flow at high deformation is observed. This could be due to the fact that, for entry 15 and 16, the formation of a longer than methyl branch was favoured.

The elastic modulus of both polymers is low in agreement with their very low crystallinity (Table 4.3).

Table 4.3 *Mechanical properties*

Entry	E [a] (MPa)	σ [a] (MPa)	ε [a] (%)	SR_I [b]	SR_X [c]	$SR_{1200\%}$ [d]
1	9.3 ± 0.2	1.4 ± 0.1	30 ± 4	-	-	-
2	6.8 ± 0.8	2.3 ± 0.2	560 ± 35	50	35	n.d.
3	6.5 ± 0.3	4.1 ± 0.3	1179 ± 62	60	46	45
4	5.7 ± 0.4	5.1 ± 0.3	1148 ± 30	61	48	50
5	5.1 ± 0.3	8.6 ± 0.8	1350 ± 12	66	54	59
6	4.7 ± 0.1	9.1 ± 0.7	1282 ± 91	74	64	69
7	3.8 ± 0.3	8.6 ± 0.7	1198 ± 55	81	71	73
8	3.7 ± 0.3	9.4 ± 0.3	1284 ± 32	82	74	74
9	3.3 ± 0.1	8.0 ± 0.4	1300 ± 66	86	78	78
10	7.8 ± 1.3	13.8 ± 1.8	1337 ± 88	56	43	48
11	5.9 ± 0.1	11.8 ± 0.5	1173 ± 26	57	45	52
12	4.9 ± 0.2	8.6 ± 1.5	1388 ± 89	66	54	61
13	2.3 ± 0.3	0.9 ± 0.1	146 ± 21	-	-	-
14	5.7 ± 0.3	9.4 ± 0.9	1200 ± 54	57	43	53
15	3.5 ± 0.7	1.9 ± 0.3	1210 ± 60	81	69	n.d.
16	2.3 ± 0.2	1.7 ± 0.4	800 ± 42	85	75	n.d.

[a] *E = Young's modulus, σ = ultimate tensile strength, ε = elongation at break.*

[b] *Strain recovery measured after the first step in a step cycle test type at 300% strain.*

[c] *Strain recovery measured after the last step in a step cycle test type at 300% strain.*

[d] *Strain recovery measured after the strain at 1200% in a step cycle test type at increasing strains.*

[e] *The specimens break before the strain at 1200% in a step cycle test type at increasing strains.*

The elasticity of poly(1-octene)s, *i.e.* the capability to return to the initial state once the force is removed, was evaluated from step cycle tensile tests. In the first set of experiments, the samples were cyclically loaded and unloaded ten times to 300% strain. For example, the cyclic curve of sample 8 is shown in Figure 4.11 A.

In the second set of cyclic experiments, the samples were extended step by step up to different strains. As a typical example, the stress-strain curve during cyclic tensile deformation of sample 8 is shown in Figure 4.11 B.

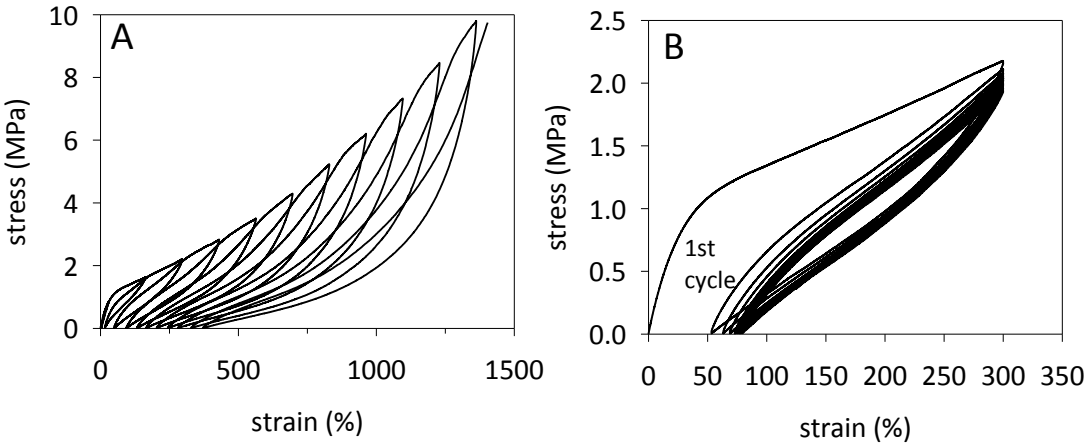

***Figure 4.11**. (A) Stress-strain curve of poly(1-octene) (Table 1, entry 8) in the hysteresis experiments for as train of 300%. (B) Stress-strain curve of poly(1-octene) (Table 4.1, entry 8) during step cycle tensile deformation at different strain.*

All the poly(1-octene)s exhibit a certain amount of unrecovered strain after the 1st cycle with only a small increase in the unrecovered strain on each subsequent cycle. For all the polymers, a permanent structural change took place during the 1st cycle, and a material with better elastomeric properties was created. The main difference between the cyclic deformation behavior of the poly(1-octene)s is in the amount of unrecovered strain after the 1st cycle. From the stress-strain curve the strain recovery (SR) can be calculated as equation 3 in Appendix.

The recovery strain after the first load cycle ranges from 50 to 86% and increases with decreasing the polymer crystallinity (SR_I in Table 4.3). All the polymers show as light decreasing trend in the strain recovery with the load cycle times, while the order of the strain recovery remains unchanged (Figure 4.12 A). In Figure 4.12 B the strain recovery is plotted as a function of the applied strain.

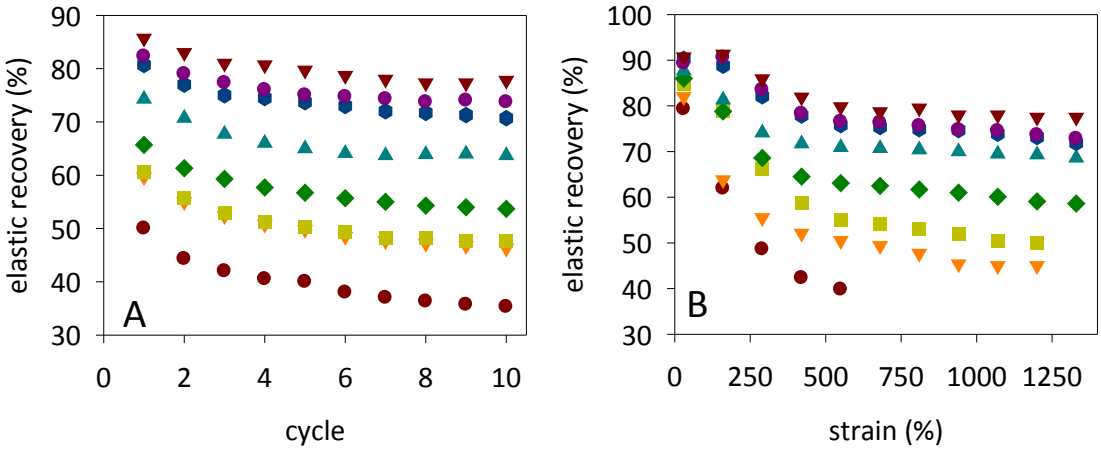

Figure 4.12. *(A) Strain recovery as a function of cycle times of the poly(1-octene)s obtained at different monomer concentration (entries 2-9 from bottom to top). (B) Strain recovery as a function of the applied strain of the poly(1-octene)s obtained at different monomer concentration (entries 2-9 from bottom to top).*

The more amorphous poly(1-octene)s displayed excellent elastic recoveries of about 75% after the last load cycle (SR_X in Table 4.3). It is worth pointing out that for the hysteresis test performed at fixed 300% strain, the polymers produced by **Ni2**/MAO and **Ni2**/MMAO behave in-line with those obtained by **Ni2**/Et_2AlCl, exhibiting a similar strain recovery trend.

For all the materials obtained by **Ni2**/Et_2AlCl, the strain recovery decreases rapidly at lower applied strains and then levels off at higher applied strains. Generally, the elastic recovery over the whole range of deformations decreases with increasing the crystallinity of the polymer. Entry 9, *i.e.* the more amorphous polymer produced by **Ni2**/Et_2AlCl at [1-octene]= 3 mol/L, exhibits the highest elastic recovery (about 78%) for the whole range of applied strains. The dependence of strain recovery on the applied deformation was somewhat different for the polymers obtained by **Ni2**/MAO and **Ni2**/MMAO. For entry 15 and 16, the strain recovery decreased linearly with increasing the applied strain over the entire cyclic test (Figure 4.13).

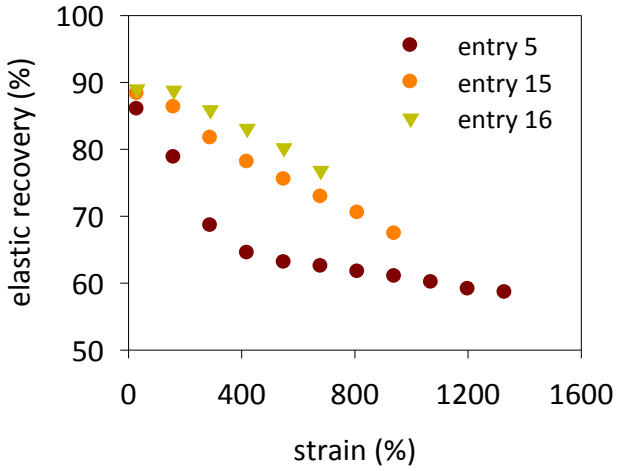

Figure 4.13. *Strain recovery as a function of the applied strain of poly(1-octene)s obtained by varying the aluminum alkyl activator (entries 5, 15, and 16, Table 4.1).*

Overall, the tensile tests showed that the investigated polymers behave as thermoplastic elastomers with properties close to those reported for block and random poly(ethylene-*co*-1-octene)[21-24] and generally outperform the 1-dodecene/ethylene di- and tri-block copolymers in terms of elastic recovery.[5] Moreover, it is worth emphasizing that these materials retain excellent mechanical properties even after being melted and reprocessed several times (Figure 4.14).

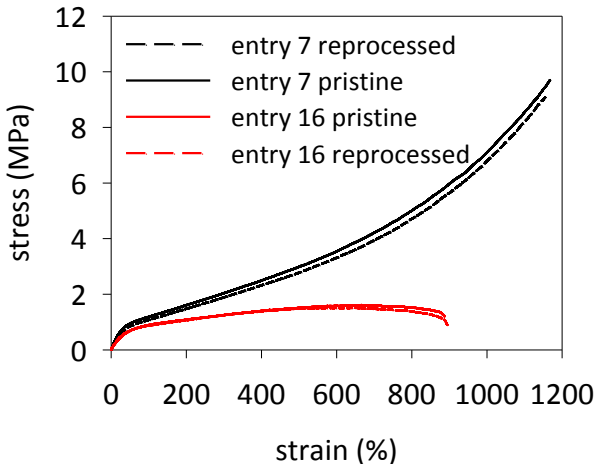

Figure 4.14. *Stress-strain curves of selected poly(1-octene)s during monotonic tensile deformation: comparison between pristine and reprocessed samples.*

4.2 Polyolefins from 1-octene copolymerization with 1-decene and cyclopentene [3]

Here the synthesis, the characterization and the mechanical properties of new polyolefin TPEs are reported. A facile procedure is employed, through the chain-walking polymerization, to fabricate random copolymers of 1-octene (OCT) with 1-decene (DE) and cyclopentene (CPE). The effect of the type and the feedstock comonomers concentration on the microstructure, the total branching and the branch-type distribution is studied. Moreover, a comprehensive investigation on the mechanical behavior by uniaxial stretching until failure, step-cycle and creep tensile tests is carried out.

The present work extends our previous studies with the aim to find alternatives to finely modulate the structure and properties of polymers from of 1-octene, allowing access to TPEs with valuable mechanical properties from readily accessible and potential biorenewable starting materials.

4.2.1 Copolymerization of 1-octene with 1-decene

A series of experiments was carried out at different comonomers feedstock compositions (OCT/DE from 4.0 to 0.25) while the total concentration was kept at 1.0 mol/L, this concentration being optimal to obtain high yield and polymers with valuable mechanical properties.[2,5] The results are summarized in Table 4.4.

Table 4.4. *Polymerization of 1-octene (OCT), 1-decene (DE) and copolymerization of OCT with DE catalyzed by* ***Ni2****/Et_2AlCl* [a]

Entry	OCT (mol/L)	DE (mol/L)	OCT/DE (mol/mol)	M [b] (mol/L)	Yield (g)	Conv (%)	M_n [c] (kg/mol)	M_w/ M_n [c]	Branches/1000C [d]
1	1.0			1.0	1.1	58	105.6	1.36	66
2		1.0		1.0	0.9	43	115.3	1.42	55
3	0.8	0.2	4.0	1.0	1.1	58	117.5	1.51	69
4	0.5	0.5	1.0	1.0	1.2	61	126.4	1.43	63
5	0.2	0.8	0.25	1.0	1.3	62	126.8	1.46	62

[a] *Polymerization conditions: toluene, total volume, 16 mL;* ***Ni2****, 10 µmol; Al/Ni molar ratio, 200; temperature, 22 °C; time, 3 h.*

[b] *M is the total (co)monomers feedstock concentration.*

[c] *Molecular weight (M_n) and molecular weight distribution (M_w/M_n) from SEC.*

[d] *From ^1H NMR.*

Ni2/Et_2AlCl shows good activities for the polymerization of 1-octene and 1-decene, the former being consumed slightly faster (Table 4.4, entry 1 vs 2) to give branched PE–like materials with high molecular weight and narrow molecular weight distribution. The exclusive 1,2-enchainment would result in a poly(1-octene) with 125 branches/1000C, and a poly(1-decene) with 100 branches/1000C. However, the effective branching level of the resulting homopolymers is almost half of the theoretic value (*i.e.,* 66 and 55/1000C for 1-octene and 1-decene polymers, respectively) which is the result of the fact that the nickel walks along the growing polymer chain, rendering branches of various lengths.[13] This result confirms that **Ni2** is poorly regioselective. [5]

Good activities were also obtained for the copolymerization of 1-octene with 1-decene with product obtained in the order of grams. The resulting copolymers have high molecular weight, narrow molecular weight distribution from 1.43 to 1.51, and branches/1000C of 69 at OCT/DE = 4, 63 at OCT/DE = 1 and 62 at OCT/DE = 0.25 (Table 4.4, entries 3–5).

Structural and thermal analysis

The polymers were analyzed by ^{13}C NMR (Figure 4.15). Total methyls and branching distribution are quantitatively calculated on the basis of previous resonance assignments,[14] and reported in Table 4.5.

Sample 3, obtained at OCT/DE = 4, exhibits the highest content of branching. The basic trend is that the total methyls of the resulting copolymers decrease with increasing the 1-decene feedstock concentration, thus confirming that the density of branches is primarily controlled by the monomer length.[5] All the polymers have predominantly methyl and longer than butyl branches (Me and Lg in Table 4.5, respectively): the intense signal at 27.73 ppm of long $–CH_2–$ sequences and signals due to methyl ($1B_1$ at 17.8 ppm is 1' in Figure 4.15) and longer branches ($1B_n$ at 12.0 ppm and $2B_n$ at 20.6 ppm are 1 and 2 in Figure 4.15, respectively) are safely identified in the ^{13}C NMR spectra (Figure 4.15). Other very weak signals of carbons of ethyl, propyl and butyl branches ($1B_2$, $1B_3$ and $2B_4$ at 9.0, 12.6 and 21.1 ppm, respectively) are detected. Moving 1-octene concentration from 0.8 to 0.2 mol/L, the content of methyls decreases from 31 to 23/1000C and, likewise, the content of longer branches drops from 33 to 30/1000C (Table 4.5, entries 3–5). It is worth mentioning that the predominance of longer branches means that successive 1,2-

insertions (1,2-enchainment) or 2,1-insertions (2,1-enchainment) are faster than a 1,2-insertion followed by chain-walking (ω,2-enchainment).[25]

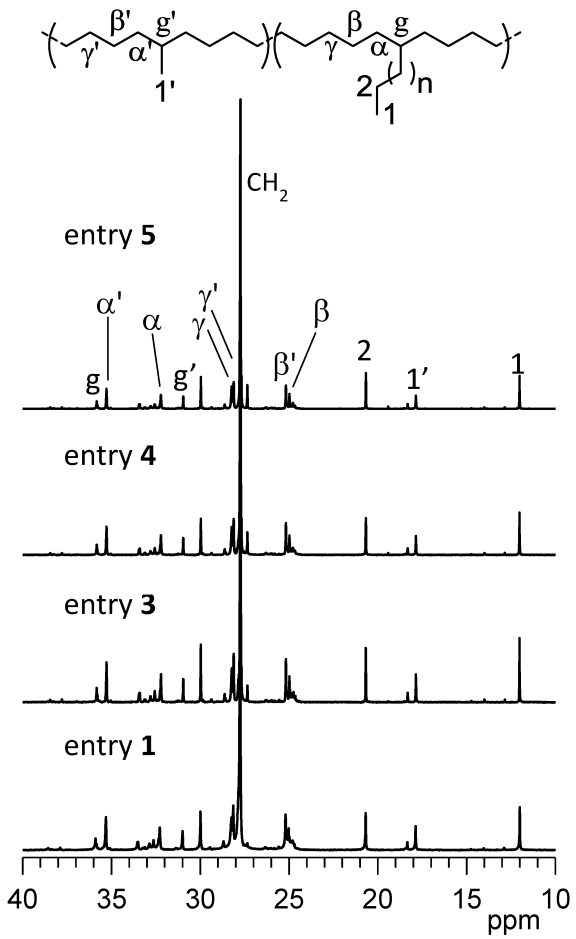

Figure 4.15. *^{13}C NMR spectra and assignment of OCT/DE copolymers (n = 4 to 6).*

Table 4.5. *Microstructural data and thermal properties for OCT/DE copolymers.*

Entry	CH_3/1000C [a]		Total CH_3 [a]	T_g [b]	T_c [b]	T_m [b]	ΔH_m [b]	X_{DSC} [c]
	Me	Lg		(°C)	(°C)	(°C)	(J/g)	(%)
1	27	32	60	-49	32	49	29	10.0
2	21	30	51	-45	35	55	34	11.7
3	31	33	65	-48	32	49	30	10.3
4	23	31	55	-46	33	53	33	11.4
5	23	30	54	-45	35	56	34	11.7

[a] From ^{13}C NMR. A small amount (never exceeding 1 CH_3/1000C) of alkyl branches was observed; [b] From DSC; [c] Crystallinity from melting enthalpy, $X_{DSC} = (\Delta H_m/\Delta H^0_m) \times 100$, $\Delta H^0_m = 290$ J/g.

DSC of OCT/DE copolymers revealed a thermal behavior similar to those displayed by polyolefins made by **Ni2**/Et_2AlCl.[2,5] The cooling DSC trace shows a relative sharp crystallization exotherm followed by a wide tail (Figure 4.16 A). The crystallization temperature (T_c) taken at the maximum of the sharp peak increases progressively with the increasing of 1-decene feedstock concentration (Table 4.5). The heating curves of the non-isothermal crystallized OCT/DE copolymers exhibit a glass transition event at low temperature, ranging from –48 to –45 °C, and a broad melting endotherm (Figure 4.16 B). In general, with increasing the 1-decene feedstock concentration, the melting point and the melting enthalpy of the obtained copolymers increase (T_m and ΔH_m in Table 4.5, respectively). These data are strictly related to the copolymers microstructure. Indeed, a decrease in the content of longer than methyl branches produces a corresponding increase in T_c, T_m, and ΔH_m of the copolymer (Table 4.5). In this regard, it is worth noting that poly(1-decene) and the copolymer obtained at low OCT/DE ratio, which have similar total branching and longer side groups content, exhibit very similar T_c, T_m and crystallinity (Table 4.5, entry 2 and 5, respectively).

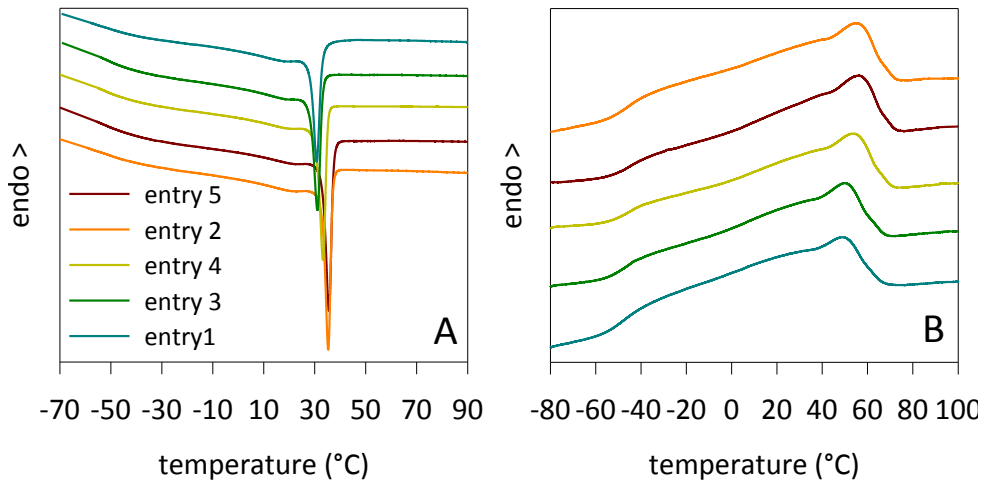

Figure 4.16. *(A) DSC cooling scans of OCT/DE copolymers and reference homopolymers and (B) DSC successive heating scans.*

4.2.2 Copolymerization of 1-octene with cyclopentene

Copolymerizations of 1-octene with cyclopentene were performed at three different OCT/CPE ratio from 1.4 to 0.5, keeping constant the 1-octene feedstock concentration of 1.0 mol/L. The results are summarized in Table 4.6.

Table 4.6. *Copolymerization of 1-octene (OCT) with cyclopentene (CPE) catalysed by* ***Ni2****/Et_2AlCl [a].*

Entry	OCT (mol/L)	CPE (mol/L)	OCT/CPE (mol/mol)	*M* [b] (mol/L)	Time (h)	Yield (g)	Conv (%)	CPE [c] (mol%)	M_n [d] (kg/mol)	M_w/ M_n [d]
6	1.0	1.4	0.7	2.4	3	0.40	12	0.8	78.4	1.29
7	1.0	0.7	1.4	1.7	22	1.75	69	4.2	159.0	1.62
8	1.0	1.4	0.7	2.4	22	1.50	45	5.6	174.7	1.41
9	1.0	2.1	0.5	3.1	22	1.50	37	6.5	165.8	1.36

[a] *Polymerization conditions: toluene, total volume, 16 mL;* ***Ni2****, 10 µmol; Al/Ni molar ratio, 200; temperature, 22 °C.*

[b] *M is the total (co)monomers feedstock concentration.*

[c] *From ^{13}C NMR.*

[d] *Molecular weight (M_n) and molecular weight distribution (M_w/M_n) from SEC.*

Under the employed conditions, **Ni2**/Et_2AlCl exhibits no activity toward the cyclopentene homopolymerization. The productivities of OCT/CPE copolymerizations are modest, but markedly increase with increasing the polymerization time (Table 4.6, entry 6 vs 8). Indeed, the presence of cyclopentene in the polymerization mixture shuts down the polymerization rate, and hence the overall productivity (entry 7 in Table 4.6 vs entry 2 in Table 4.5), as found by Ye *et al*.[26] and Zhu *et al*.[27] for the copolymerization of ethylene with CPE. All the copolymers obtained at longer polymerization time (Table 4.6, entries 7–9) have molecular weights greater than 150 kg/mol, narrow molecular weight distribution (from 1.36 to 1.62), excellent solubility in common organic solvents, and low CPE incorporation. The CPE content in the copolymers increases only from 4.2 to 6.5 mol% by increasing the comonomer concentration from 0.7 to 2.1 mol/L (Table 4.6, entries 7–9), thus suggesting the incorporation of CPE is generally disadvantaged.

Structural and thermal analysis

The copolymers were studied by ^{13}C NMR. According to the assignments by Müller,[28] the predominant copolymers microstructure is sketched in Figure 4.17. The OCT/CPE copolymers show all the NMR peaks exhibited by the ^{13}C NMR of the homopolymer, meaning the presence of the same branched structures in the copolymers. In addition, some new peaks are also found in the spectra of the copolymers, whose intensity increases by increasing the CPE incorporation. These peaks can be attributed to the carbon atoms of the five-membered CPE isolated unit in the *cis*-1,3-enchained form, namely at 38.8 (C2), 38.3 (C1, C3) and 29.9 ppm (C4, C5),[26,27] and carbons of ethylene units in the vicinity of the rings, *i.e.*, α'', β'', γ'' at 34.7, 26.9 and 27.9 ppm, respectively (Figure 4.17).[29]

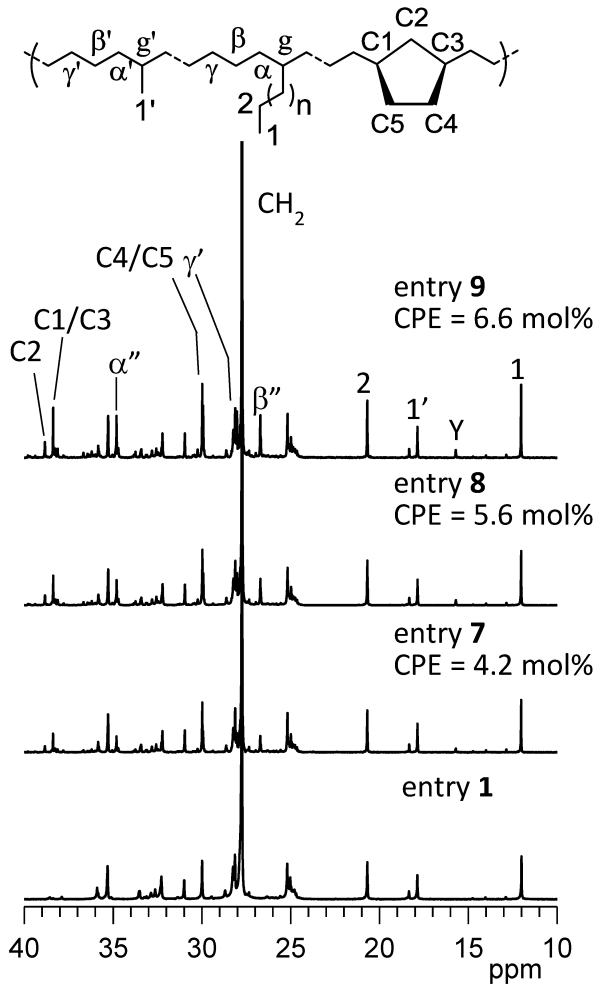

Figure 4.17. *^{13}C NMR spectra and assignment of OCT/CPE copolymers (n =4).*

In contrast, no resonances are observed in regions that would clearly identify 1,2-enchained CPE units: the 1,3-enchainment of CPE is attributed to the rapid isomerization of the last 1,2-inserted CPE unit by a β–H elimination–reinsertion process (Scheme 4.2).[30,31]

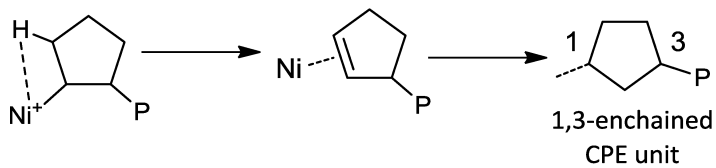

Scheme 4.2. *Isomerization mechanism for the generation of a 1,3-enchained CPE unit.*

In addition, a peak at about 15.6 ppm (marked as Y in Figure 4.17), whose intensity slightly increases with increasing the CPE content in the copolymers, was registered in the ^{13}C NMR spectra of OCT/CPE copolymers. Peak Y should be assigned to the CH_3 carbon of a new branching structure in the vicinity of the last-inserted CPE unit. By comparison with the chemical shift of propylene/CPE copolymers,[32] peak Y has been assigned to a methyl branch close to the repeating ring unit likely formed through the 1,2-insertion of 1-octene on the last-inserted CPE followed by chain-walking (8,2-enchainment in Scheme 4.3).

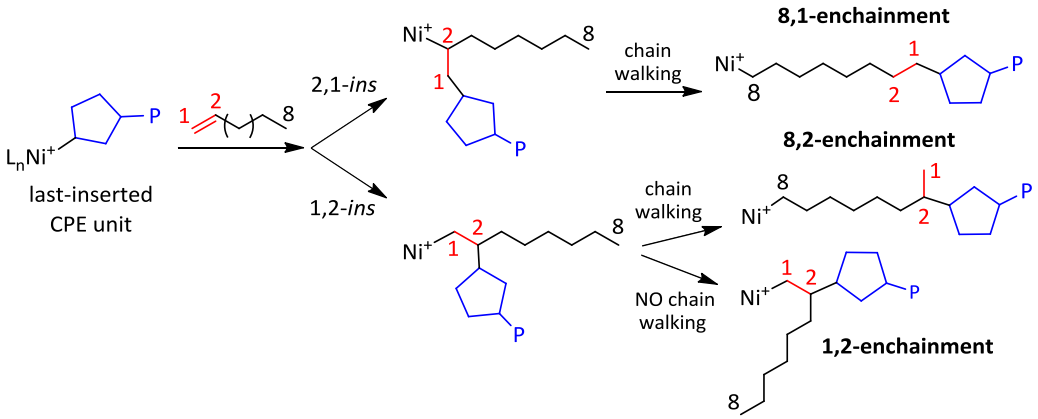

Scheme 4.3. *Modes of enchainment for 1-octene insertion on the last-inserted CPE unit.*

The obtained copolymers are moderately branched with a total branching which drops from 72 to 62/1000C with increasing the CPE content in the copolymers. Table 4.7 lists the branch distribution of the copolymers.

Table 4.7 *Microstructural data and thermal properties for OCT/CPE copolymers.*

Entry	CH_3/1000C [a]		Total CH_3 [a]	CPE [a]	T_g [b]	T_c [b]	T_m [b]	ΔH_m [b]	X_{DSC} [c]
	Me [d]	Lg [e]		(mol%)	(°C)	(°C)	(°C)	(J/g)	(%)
7	33	38	72	4.2	-45	25	43	23	7.9
8	26	36	63	5.6	-44	24	42	22	7.6
9	25	36	62	6.5	-43	22	39	20	6.9

[a] *From ^{13}C NMR. A small amount of alkyl branches (1 CH_3/1000C) was observed.*

[b] *From DSC.*

[c] *Crystallinity from melting enthalpy, $X_{DSC} = (\Delta H_m/\Delta H_m^0)\times 100$, $\Delta H_m^0 = 290$ J/g.*

[d] *Me branches are calculated as the sum of isolated methyls as sketched in Figure 4.18 and methyl branches adjacent to the repeating unit from CPE (Scheme 4.3, 8,2-enchainement).*

[e] *Lg includes isolated longer branches as sketched in Figure 4.18 and longer branches close to the CPE ring (Scheme 4.3, 1,2-enchainement).*

Generally, the copolymers exhibit two major branch lengths, namely methyl and longer than butyl branches (Me and Lg in Table 4.7, respectively). By increasing the CPE incorporation, methyl branches decrease from 33 to 25/1000C and longer branches from 38 to 36/1000C. Currently, a conclusive mechanistic rationale is not possible. A plausible explanation of the fact that methyl branches decrease much more than longer branches is that when CPE is the last-inserted unit, the formation of a methyl adjacent to the ring (8,2-enchainement in Scheme 4.3) may be disfavoured with respect to the formation of a longer branch close to the CPE (1,2-enchainement in Scheme 4.3). This is because to give a methyl branch close to the CPE, the nickel center has to walk through a CH carbon, which could disallow the nickel from walking through.[33]

The thermal behavior of OCT/CPE copolymers was investigated by DSC and the thermograms are reported in Figure 4.18.

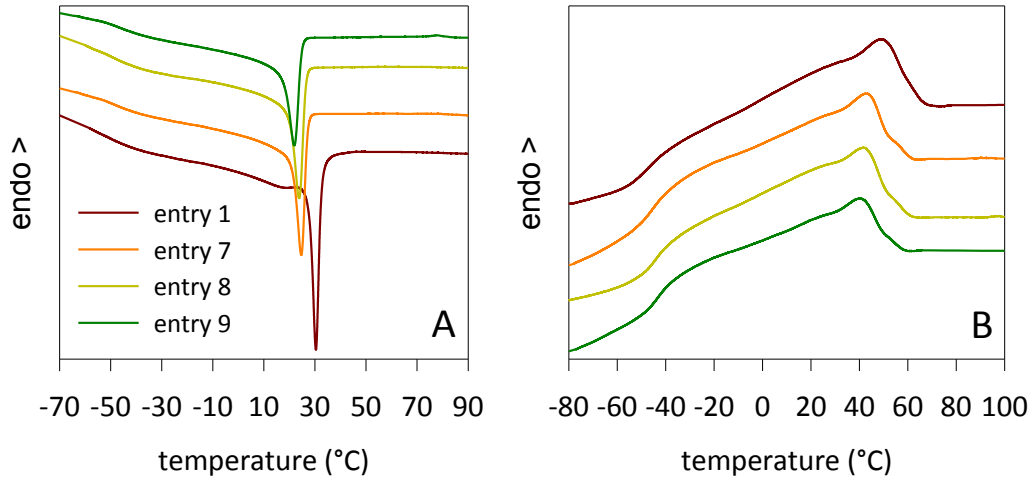

Figure 4.18. *(A) DSC cooling scans of OCT/CPE copolymers and poly(1-octene) and (B) DSC successive heating scans.*

The DSC curves of the copolymers show similar features as found for poly(1-octene) prepared at the same 1-octene feedstock concentration (1.0 mol/L). In particular, all the copolymers exhibit a sharp crystallization peak in the cooling scan (Figure 4.18 A) and a broad endothermic transition beginning at subambient temperatures in the heating scan (Figure 4.18 B). Nevertheless, OCT/CPE copolymers exhibit reduced T_c, T_m and melting enthalpy with respect to poly(1-octene) (entry 1 in Table 4.5). Increasing the CPE incorporation in the copolymers, T_c and T_m shift to lower temperatures and the ΔH_m value decreases, which is the result of the reduced crystallinity due to the CPE ring incorporation. The presence

of rigid CPE moiety ensures higher T_gs than that obtained for reference poly(1-octene) (T_g= –49 °C, entry 1 in Table 4.5), and the T_g value slightly increases with increasing the CPE content.

The synthesized copolymers were structurally characterized by X-ray techniques. WAXD patterns show a diffuse peak centred at about 20 2θ°, while the typical diffractions of the poly(ethylene) orthorhombic crystalline phase were not evidenced (Figure 4.19 A). Therefore, the low melting temperature and broad melting range of the copolymers can be likely due to the fringed-micellar crystal structure with a broad size distribution that comes from the statistical distribution of crystallizable chain lengths. In this respect, Bensason *et al.*[34] and Peeters *et al*.[35] showed that the crystallinity of ethylene/1-octene copolymers is influenced by the comonomer content and the decrease in the crystallinity degree determines a gradual change from a completely lamellar morphology to a granular crystals morphology, where the crystalline regions are described as fringed micelles.

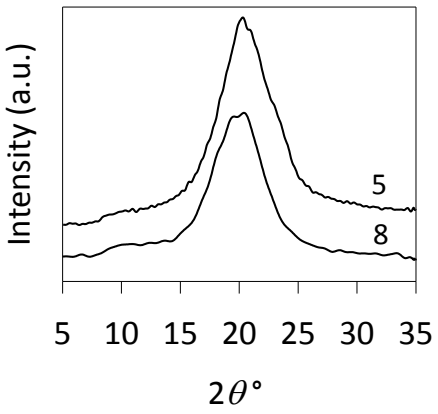

Figure 4.19. *WAXD profiles of selected copolymers.*

Table 4.8. *Supermolecular parameters and mechanical properties.*

Entry	E^a (MPa)	σ^a (MPa)	ε^a(%)	SR_I [b]	SR_X [c]	$SR_{1200\%}$ [d]
1	5.4 ± 0.2	10.2 ± 1.0	1398 ± 61	65	54	59
2	7.5 ± 0.3	15.5 ± 0.4	1388 ± 29	59	47	53
3	5.7 ± 0.4	12.5 ± 0.4	1375 ± 73	64	52	59
4	6.1 ± 0.4	15.1 ± 1.5	1291 ± 33	61	49	56
5	7.3 ± 0.2	16.0 ± 1.3	1310 ± 27	58	46	53
7	3.8 ± 0.4	9.4 ± 0.6	1260 ± 85	69	57	66
8	3.7 ± 0.2	9.1 ± 0.2	1324 ± 70	69	57	64
9	3.2 ± 0.1	8.0 ± 0.3	1424 ± 41	69	56	61

[a] *Young's modulus (E), ultimate tensile strength (σ) and elongation at break (ε).*

[b] *Strain recovery measured after the first step in a step cycle test type at 300% strain.*

[c] *Strain recovery measured after the last step in a step cycle test type at 300% strain.*

[d] *Strain recovery measured after the strain at 1200% in a step cycle test type at increasing strains.*

4.2.3 Mechanical properties of 1-octene copolymers with 1-decene and cyclopentene

First investigation on the mechanical behavior of the copolymers was performed at 19 °C by uniaxial stretching until failure. Representative stress-strain curves are depicted in Figure 4.20 and the tensile properties are reported in Table 4.8.

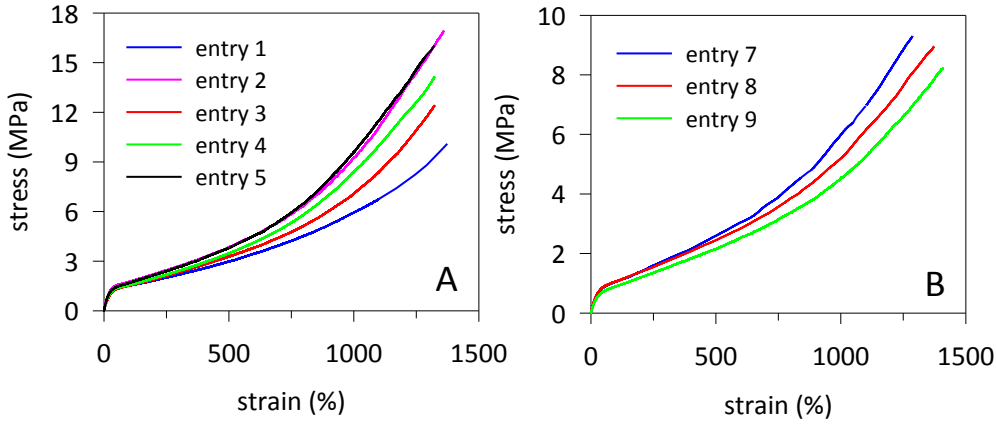

Figure 4.20. *Stress-strain curves of (A) OCT/DE copolymers and reference homopolymers and (B) OCT/CPE copolymers during monotonic tensile deformation.*

All samples show stress-strain curves with typical features of elastomers, *i.e.*, low modulus, strain hardening at high strain and an instantaneous strain recovery. Comparing the tensile behavior of OCT/DE copolymers and reference homopolymers (entry 1 and 2), one can notice some differences (Figure 4.20 A). The initial modulus depends only on the crystallinity of the polymer ranging from 5.4 to 7.5 MPa with increasing the crystallinity. A stress upswing, characterized by an increasing slope in the stress-strain curve, is observed for all the materials and the onset of strain hardening occurs at different strain as a function of the copolymer composition. Sample 5, prepared at higher feedstock concentration of 1-decene, and poly(1-decene) (entry 2) exhibit stronger strain hardening with ultimate tensile strength of about 16 MPa. The OCT/DE copolymers and the homopolymers show high and comparable ultimate strain around 1350%. Taking into account that the investigated polymers have similar molecular weight and narrow molecular weight distribution, the differences in stress-strain behavior can be likely attributed to the differences in microstructure and composition.

The copolymer obtained at OCT/DE = 4 (entry 3) exhibits tensile properties close to those of poly(1-octene) (entry 1), whereas the copolymer obtained at

OCT/DE = 0.25 (entry 5) shows a tensile behavior very similar to that of poly(1-decene) (entry 2). Moreover, the stress-strain behavior of sample 4 (OCT/DE =1) is intermediate between that of sample 3 and 5. The stress-strain curves of OCT/CPE copolymers and reference poly(1-octene) (entry 1) are shown in Figure 4.20 B. Compared to sample 1, the copolymers have lower Young's modulus between 3.2 and 3.8 MPa and lower ultimate tensile strength in the range from 8.0 to 9.4 MPa. The lower modulus and tensile strength of the copolymers are related to the reduced crystallinity due to the CPE incorporation in the polymer backbone. As regards the elongation at break, the copolymers present high strain fractures similar to that of reference homopolymer. The elongation at break value slightly increases with increasing the CPE content (Table 4.8). All the investigated materials were also subjected to step cycle tensile tests to determine the elastic recovery. In the first set of experiments, the samples were cyclically loaded and unloaded ten times to 300% strain, based on the initial gauge length. All the samples exhibit a certain amount of unrecovered strain after the 1^{st} cycle with only a small increase in the unrecovered strain on each subsequent cycle (Figure 4.21 A). Therefore, a permanent structural change takes place during the first conditioning cycle, and a material with better elastomeric properties is created. From the stress-strain curve the strain recovery (SR) can be calculated with equation 3 in Appendix. For OCT/DE copolymers, the recovery strain after the first load cycle ranges from 58 to 64% and increases with decreasing the polymer crystallinity (SR_I in Table 4.8). The OCT/DE copolymers show a slight decreasing trend in the strain recovery with the load cycle times, whereas the order of the strain recovery remains unchanged (Figure 4.21 B). The OCT/CPE copolymers display similar recovery over the whole cycle tensile test and the highest elastic recovery of about 57% after the last load cycle (SR_X in Table 4.8).

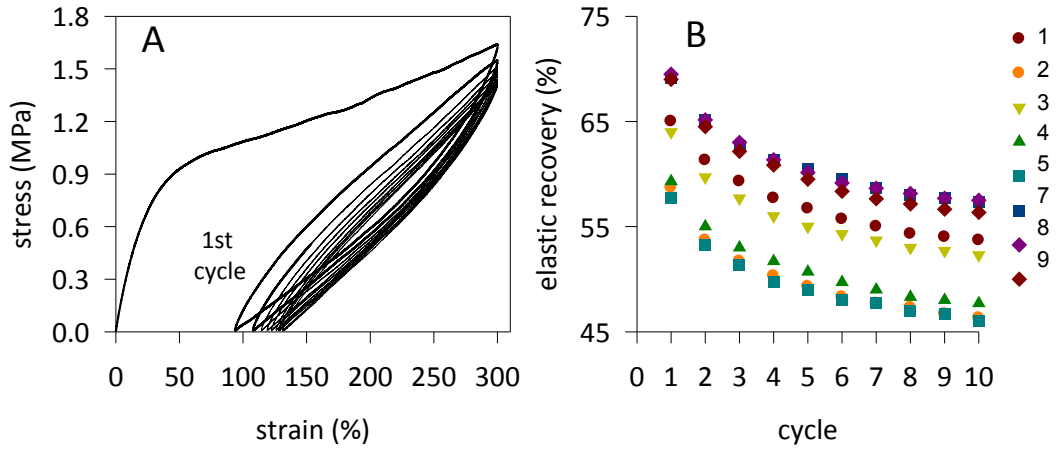

Figure 4.21. *(A) Stress-strain curve of OCT/CPE copolymer (Table 4.6, entry 9) in the hysteresis experiments for a strain of 300%; (B) Strain recovery as a function of cycle times.*

In the second set of cyclic experiments, the samples were extended step by step up to different strains. As a typical example, the stress-strain curve during cyclic tensile deformation of sample 9 is shown in Figure 4.22 A. The strain recovery decreases rapidly at lower applied strains and then levels off at higher applied strains (Figure 4.22 B). For OCT/DE copolymers, the elastic recovery over the whole range of deformations decreases with increasing the copolymers crystallinity. In particular, sample 3, obtained from the highest 1-octene feedstock concentration, exhibits strain recoveries close to that of poly(1-octene), whereas sample 5 generated from the experiment at the lowest 1-octene feedstock concentration, shows a behavior comparable to that of poly(1-decene). All the OCT/CPE copolymers exhibit strain recovery higher than the reference poly(1-octene), sample 7, with a CPE content of 4.2 mol%, presenting the highest elastic recovery (about 66%) for the whole range of applied strains.

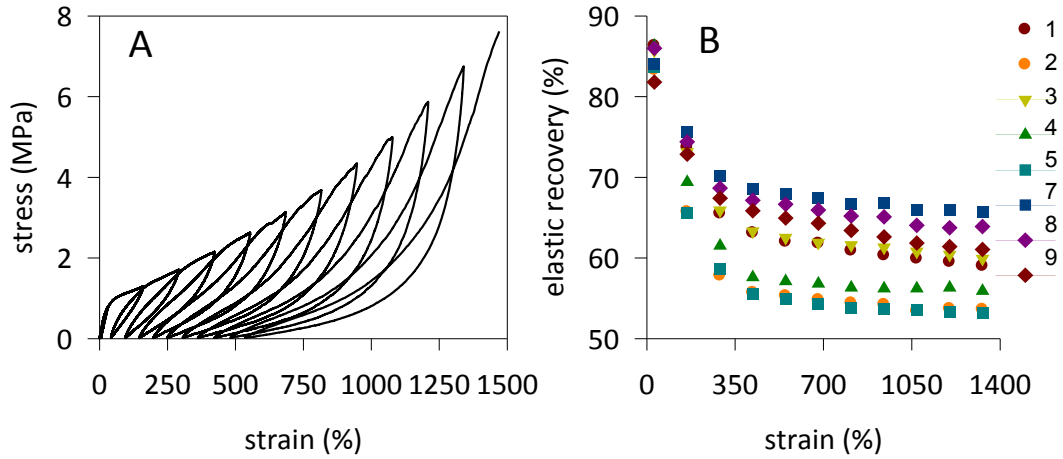

Figure 4.22. *(A) Stress-strain curve of OCT/CPE copolymer (Table 4.6, entry 9) during step cycle tensile deformation at different strain; (B) train recovery as a function of the applied strain.*

Copolymers were subjected to creep experiments in order to evaluate their resistance to permanent deformation. Samples were elongated to 300% strain and held at a constant stress for 3 h. It is worth pointing out that every sample required typical stress value in order to achieve 300% strain (from 1.5 to 2.8 MPa). Selected strain-time curves are shown in Figure 4.23 A.

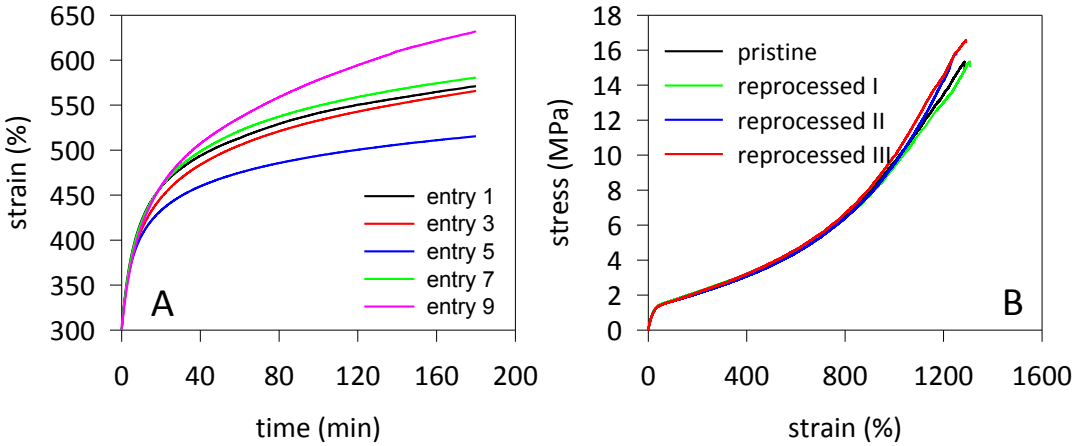

Figure 4.23. *(A) Creep experiments of selected samples and (B) stress-strain curves of OCT/DE copolymer (Table 1, entry 5) during monotonic tensile deformation: comparison between pristine and reprocessed samples.*

The OCT/CPE copolymers exhibit the higher deformation over time, particularly sample 9 with the highest CPE content and the lowest crystallinity. The OCT/DE copolymers show improved resistance to strain-induced deformation compared to

OCT/CPE copolymers, sample 5, obtained from copolymerization with the highest feedstock concentration of 1-decene, exhibiting the least amount of deformation. The creep behavior of reference poly(1-octene) is intermediate between that of the two copolymer series.

Altogether, the tensile tests show that the investigated copolymers behave as elastomers with properties close to those reported for TPEs of random ethylene/α-olefin copolymers.[21-24,36]

Finally, it is worth emphasizing that these materials retain excellent mechanical properties, *i.e.* high elongation at break and ultimate tensile strength, and good strain recovery, even after being molted and reprocessed several times (Figure 4.23 B).

4.3 Chain-Walking polymerization of 1-octene, 1-decene and 1-octadecene by α-Diimine Ni(II) complexes [4]

In the last the investigation about the chain-walking of higher α-olefins, a systematic investigation on the polymerization of 1-octene, 1-decene, and 1-octadecene catalyzed by the series α-diimine **Ni1**–**Ni6** complexes (Figure 4.1) was carried out. The crystal structures of **Ni3**–**Ni6** are reported for the first time. As above mentioned, I focused my attention on such complexes because in comparison with those having acenaphthyl α-diimine backbone, α-diimine Ni(II) complexes with methyl α-diimine backbone gave higher molecular weight polymers and better activity.[1] The effect of ligand steric and electronic perturbation on the catalytic behavior, monomer enchainment, and polymer properties is discussed. In addition, the mechanical properties of the resulting polymers are thoroughly explored.

4.3.1 Synthesis and X-ray Crystallography of Nickel Complexes

Nickel complexes were synthesized following a procedure reported in the literature for analogous compounds.[17] The reaction of ligands with 1 equiv of (DME)$NiBr_2$ (DME = 1,2-dimethoxyethane) in CH_2Cl_2 afforded the desired **Ni1**–**Ni6** complexes as mustard and brown solids at 80–93% yields. Crystallization of **Ni3**–**Ni6** from CH_2Cl_2 at low temperature afforded crystals suitable for single crystal X-ray diffraction. X-ray crystal structure for these four compounds is depicted in Figure 4.24. Numerous attempts to obtain single crystals of **Ni1** suitable for X-ray

diffraction analysis failed, while the molecular structure of **Ni2** is published in ref. [37].

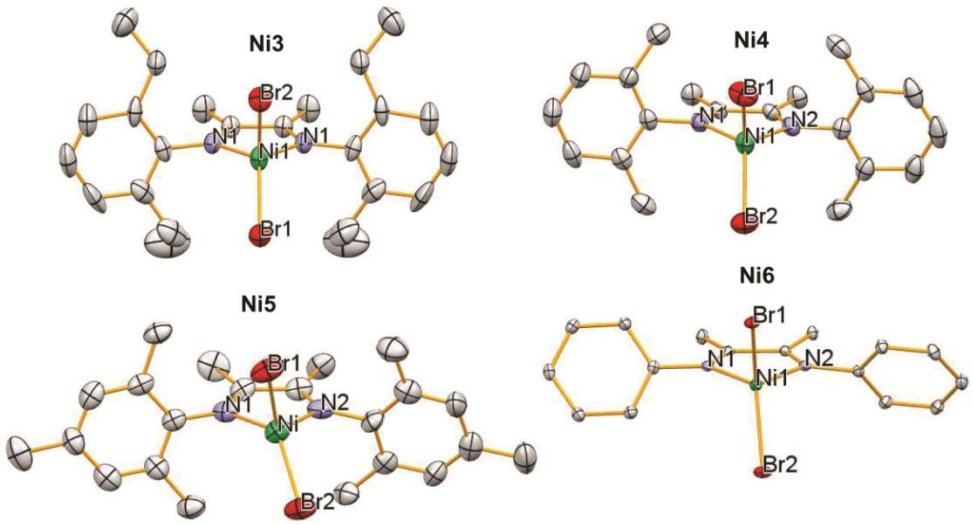

***Figure 4.24**. X-ray crystal structure for **Ni3–Ni6**. Hydrogen atoms are omitted for clarity. Atoms are drawn at the 30% probability level.*

Complex **Ni3** crystallized in the orthorhombic space group *Pnma*, as that reported in the literature for **Ni2**,[37] while **Ni4** crystallized in the monoclinic space group *C*2/*c*, Ni5 in the monoclinic space group $P2_1/c$, and Ni6 in the orthorhombic space group $P2_12_12_1$. As shown in Figure 4.24, all the complexes have similar structure; that is, the distorted tetrahedral geometry at the nickel center is composed of the two nitrogen atoms and two bromine atoms. The observed bond lengths are typical for α-diimine Ni(II) complexes.[37-39] The C=N imine (1.27(1)Å for Ni3, 1.30(1)Å for Ni4, 1.25(2) and 1.28(2)Å for Ni5, 1.290(5) and 1.291(5)Å for Ni6) and the N–Caryl bonds (1.43(1)Å for Ni3, 1.454(9) and 1.441(9)Å for Ni4, 1.46(3) and 1.42(2)Å for Ni5, 1.425(5) and 1.435(5) Å for Ni6) are in agreement with the expected lengths for this type of bond.[40] For disubstituted complexes, the dihedral angle formed by the planes containing the atoms N1–Ni–N2 and Br1–Ni–Br2 is 90° for **Ni3**, 86.67° for Ni4, and 86.62° for **Ni6**. Thus, the plane of the aryl ring becomes more rigidly locked perpendicular to the coordination plane with increasing the steric bulk of the *ortho* substituents.[41] In addition, the X-ray structure analysis of **Ni5** shows that the presence of a methyl in the para position has a significant influence on the coordination geometry, changing the dihedral angle formed by the planes containing the atoms N1–Ni–N2 and Br1–Ni–Br2 to 78.76°, thus suggesting that the introduction of groups in the para position causes

repulsive interactions between substituents. Similar characteristics were observed in similar Ni(II) complexes bearing 4,5-*bis*(arylimino)pyrenylidenes.[42] The dihedral angle formed by the two imino-phenyl rings is 20.61° for Ni3, 11.66° for **Ni4**, 22.23° for **Ni5**, and 65.38° for **Ni6**. This confirms that the absence of *ortho* substituents has a strong influence on the steric environment, allowing a higher degree of freedom for the rotation of the aniline moieties, and hence no steric hindrance at the axial sites of the nickel center. As it will be discussed later, this is the reason why **Ni6** is not active in the polymerization.

4.3.2 Polymerization of 1-octene, 1-decene and 1-octadecene

All the complexes were used, in combination with Et_2AlCl, in the polymerization of 1-octene, 1-decene, and 1-octadecene. A short polymerization time was chosen for the initial screening in order to maintain homogeneous conditions, avoiding mass transfer limitation due to the formation of insoluble polymer, and insufficient mixing. In this way, the observed differences in turnover frequencies (TOFs) can only be ascribed to the different type of ligand. The results are summarized in Table 4.9.

Table 4.9. *Polymerization of 1-Octene, 1-Decene, and 1-Octadecene Using* ***Ni1–Ni6*** *and a Reaction Time of 10 min*[a]

entry	complex	Yield (mg)	Conv (%)	TOF[b] (h^{-1})	M_n[c] (kg/mol)	M_w/M_n[c]
1-octene						
1	**Ni1**	–				
2	**Ni2**	58	3	304	14.9	1.5
3	**Ni3**	187	10	980	37.4	1.2
4	**Ni4**	308	17	1614	52.8	1.3
5	**Ni5**	424	24	2220	57.9	1.2
6	**Ni6**	–				
1-decene						
7	**Ni1**	–				
8	**Ni2**	66	3	277	26.7	1.2
9	**Ni3**	197	9	826	50.5	1.2
10	**Ni4**	356	16	1493	56.0	1.3
11	**Ni5**	421	19	1766	59.0	1.4
12	**Ni6**	–				
1-octadecene						
13	**Ni1**	–				
14	**Ni2**	50	1	213	31.8	1.4
15	**Ni3**	80	2	342	55.8	1.4
16	**Ni4**	417	10	972	66.4	1.3
17	**Ni5**	534	13	1244	73.8	1.3
18	**Ni6**	–				

[a]*Polymerization conditions: toluene, total volume, 16 mL; Ni, 10μmol; Al/Ni molar ratio, 200; temperature, 22 °C; monomer concentration, 1.0 mol/L; time, 10 min.* [b]*Turnover frequency (TOF), calculated by the equation* $mol_{pol}/(mol_{Ni} \times h)$. [c]*Molecular weight* (M_n) *and molecular weight distribution* (M_w/M_n) *from SEC.*

Ni2–**Ni5** were highly active in the polymerization of higher α-olefins, TOF being in the range of 200–2200 h^{-1}. In contrast, **Ni1** and **Ni6** were not active under the same conditions, confirming that the absence of *ortho*-aryl substituents or monosubstitution in *ortho*-aryl positions is not efficient in protecting active centers from chain-transfer (Figure 4.24).[1,13]

A correlation exists between the activity, the ligand hindrance, and the monomer length (Figure 4.25). Specifically, the TOF increases with decreasing the bulk of the *ortho*-substituents (Figure 4.25). For disubstituted complexes, TOF increases in the following order **Ni2 < Ni3 < Ni4**. A similar trend in TOF was observed by Chen *et al*. for the polymerization of 1-hexene with α-diimine Pd(II)

complexes.[43] Consistently with the trend of TOF, the molecular weight of the resulting polymers increase with decreasing the bulk of the *ortho*-substituents. Additionally, we found that **Ni5**, with a methyl group on the *para*-aryl position, was considerably more active than its para-hydrogen **Ni4** counterpart. This suggests that the presence of an electron-donating methyl group in the *para*-position has a positive effect on the activity.[46] Likewise, the introduction of methyl group in *para*-position led to an increase in polymer molecular weight. These effects can be ascribed to the perturbation of the metal electronics and steric environment on the nickel center, as also revealed by the molecular structure of **Ni5** (Figure 4.24). In other words, the positive effect of the presence of the electron-donating methyl groups in the *para*-position is due to the stabilization of the electron-deficient and coordinatively unsaturated active intermediate.[42,44-46]

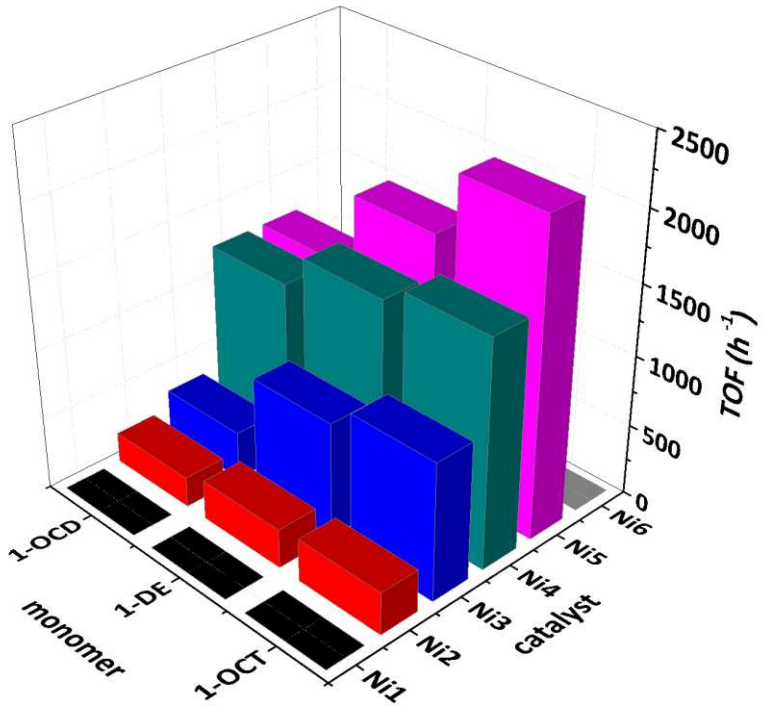

Figure 4.25. *TOF vs the nickel complex employed.*

On the other hand, the TOF decreases with increasing the monomer length likely due to steric reasons (Figure 4.25). By increasing the monomer size, the steric hindrance of the growing polymer chain increases, thus retarding the new monomer insertion and limiting the chain propagation rate.

We also carried out the same experiments at longer polymerization times in order to collect enough material to make a thorough characterization; shorter polymerization times were chosen for less bulky and more active complexes (*i.e.*, **Ni3**–**Ni5**) and 1-octadecene to limit changes in mixing of the solution when running polymerization at this scale.[47] The results are summarized in Table 4.10.

Table 4.10. *Polymerization of 1-octene, 1-decene and 1-octadecene using* ***Ni1–Ni5****.*[a]

entry	complex	time (h)	Yield (g)	Conv (%)	M_n[b] (kg/mol)	M_w/M_n[b]	branches/ 1000C[c]	ω,1[c] (%)
1-octene								
19	**Ni1**	5	0.2	12	79.3	1.5	53	62
20	**Ni2**	3	1.1	62	105.6	1.3	66	53
21	**Ni3**	3	1.5	82	124.4	1.6	70	51
22	**Ni4**	3	1.7	94	118.3	1.7	75	48
23	**Ni5**	3	1.8	100	101.1	1.8	73	49
1-decene								
24	**Ni1**	22	0.2	8	68.5	1.7	49	55
25	**Ni2**	3	1.0	43	115.3	1.4	55	53
26	**Ni3**	3	1.8	80	159.6	1.7	58	48
27	**Ni4**	3	2.2	98	128.1	1.7	61	46
28	**Ni5**	2	2.2	99	120.1	1.7	61	46
1-octadecene								
29	**Ni1**	485	0.2	5	105.5	1.8	23	60
30	**Ni2**	3	0.5	13	134.7	1.5	25	57
31	**Ni3**	1	1.1	27	152.5	1.3	31	47
32	**Ni4**	1	1.7	43	146.2	1.6	32	49
33	**Ni5**	1	2.5	62	117.9	1.8	31	47

[a] *Polymerization conditions: toluene, total volume, 16 mL; Ni, 10 μmol; Al/Ni molar ratio, 200; temperature, 22 °C; monomer concentration, 1.0 mol/L;* [b] *Molecular weight (M_n) and molecular weight distribution (M_w/M_n) from SEC;* [c] *From ^{1}H NMR. The term ω,1 implies that an olefin has inserted and then chain-walked to give an insertion that is through the ω and 1 carbon atoms.* ***Ni6*** *is not active.*

The polymers have molecular weights in the range from 68.5 to 159.6 kg/mol, and the molecular weight distributions increase slightly with respect to the experiments at short reaction time (Table 4.9) but still remain below 2.

The total branching level was calculated by ^{1}H NMR (Table 4.10). As expected, all the obtained polymers are less branched than it would correspond to a regular and exclusive 1,2-enchainment, *i.e*., 125 branches/1000C for poly(1-octene), 100 branches/1000C for poly(1-decene), and 56 branches/1000C for poly(1-octadecene). This is because nickel walks along the growing polymer chain, rendering branches of various lengths (Scheme 3.2, Chapter III) and long methylene units through the ω,1-enchainment (Scheme 3.2, Chapter III). The overall trend is that the fraction of ω,1-enchainment ranges from 46 to 62%, thus confirming that this class of complexes exhibits regiorandom insertion of α-olefins (Table 4.10).[2,5]

Generally, **Ni1** gives less branched polymers with the highest degree of *ω*,1-rearrangement (lowest % of 1,2-insertion). Energetically less favourable, 2,1-insertion is more favored for **Ni1**. This is because, before a 2,1-insertion, the alignment between the C=C double bond of the monomer and the Ni–alkyl bond results in an interaction of the monomer chain with an *ortho* hydrogen atom, thus giving transition states that are less sterically congested than in the case in which both the *ortho* positions are substituted.[9,10] For the disubstituted complexes **Ni2**–**Ni4**, reducing the steric bulk of the ligand from the *ortho*-isopropyl to *ortho*-methyl groups resulted in a more branched polymer, although the differences became less pronounced with increasing the monomer size (Table 4.10). In the case of 1-octadecene, the branching level of the resulting polymers ranged from 23 to 32/1000C, narrower than that usually found for the polymers obtained using ethylene as the feedstock.[13,49] Chen *et al*. found the same trend in the case of 1-hexene and attributed these results to the low coordination capability of 1-hexene and, in general, to the difficulty for α-olefins to trap the secondary metal–alkyl species.[43] The polymers were further characterized by ^{13}C NMR for quantification of individual branch levels.[14] The results are summarized in Table 4.11.

Table 4.11. *Microstructural data and thermal properties.*

entry	total CH_3 [a]	CH_3/1000C [b]					T_g [c]	T_m [c]	ΔH_m [c]	X_{DSC} [c]
		Me (%)	Et (%)	Pr (%)	Bu (%)	Lg (%)	(°C)	(°C)	(J/g)	(%)
1-octene										
19	53	26 (49)	2 (3)	1 (2)	0.4 (1)	24 (45)	–41	63	60	21
20	60	27 (45)				32 (53)	–47	49	34	12
21	68	30 (44)				37 (55)	–49	37	23	8
22	68	31 (45)				36 (53)	–50	36	22	8
23	69	33 (48)				35 (51)	–49	38	23	8
1-decene										
24	51	20 (39)	4 (8)	2 (4)	1 (2)	24 (47)	–43	72	55	19
25	52	21 (40)				30 (58)	–46	54	40	14
26	59	22 (37)				36 (61)	–46	48	31	10
27	62	27 (43)				34 (55)	–46	47	31	10
28	60	24 (40)				35 (58)	–47	47	30	10
1-octadecene										
29	26	11 (42)				15 (58)		96	113	39
30	30	11 (37)				19 (63)		85	97	33
31	35	9 (26)				26 (74)		65	78	27
32	36	10 (28)				26 (72)		63	73	25
33	34	9 (26)				25 (74)		64	74	25

[a] total methyls by ^{13}C NMR;

[b] distribution of the main branch levels by ^{13}C NMR;

[c] from DSC (second heating, T_m at peak maximum).

The polymers made with **Ni2**–**Ni5** show two major branch lengths. The most abundant branches are methyl and longer than butyl branches (Lg): typical signals of methyl ($1B_1$ at 17.8 ppm) and longer branches ($1B_n$ at 12.0 ppm and $2B_n$ at 20.6 ppm) are safely identified in the ^{13}C NMR spectra (Figure 4.26 C–E). Only very weak signals of carbons of ethyl, propyl, and butyl branches are detected.

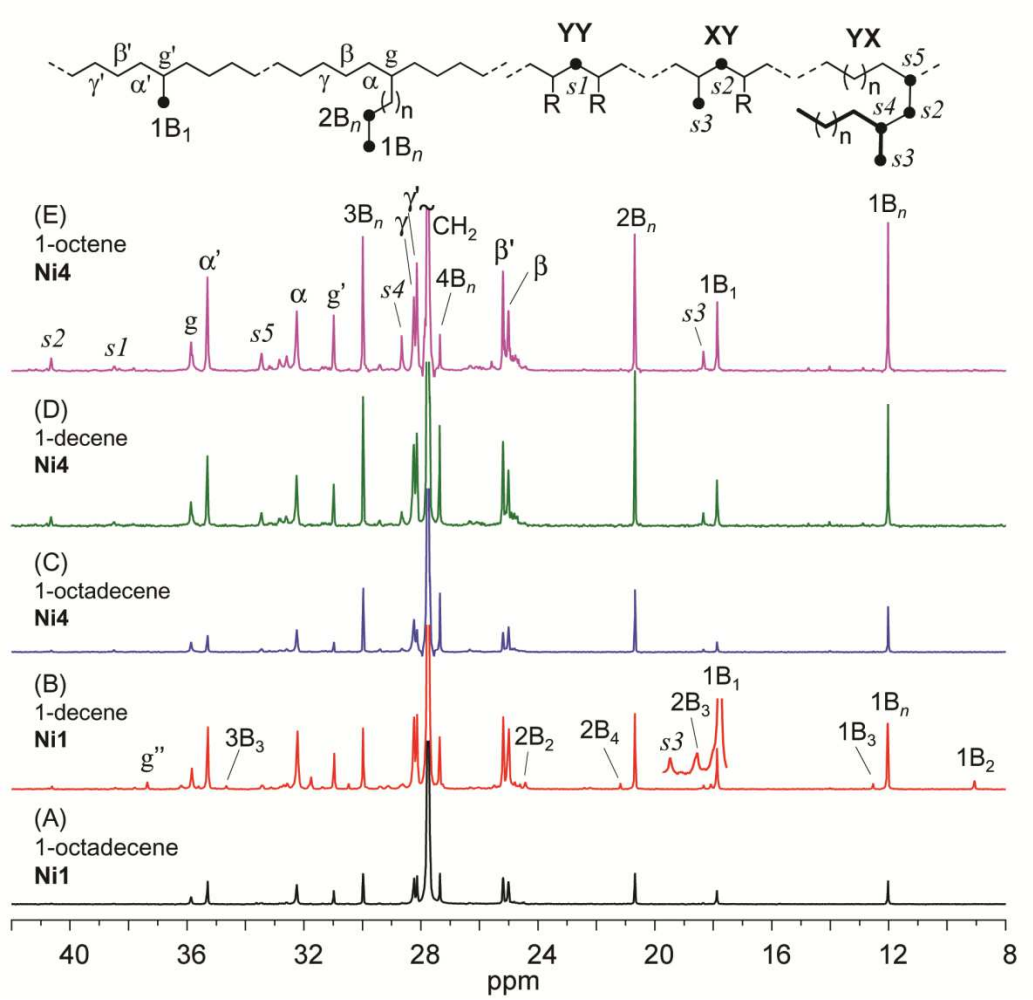

Figure 4.26. *^{13}C NMR spectra of (A) entry 29, (B) entry 24, (C) entry 32, (D) entry 27 and (E) entry 22. R is a branch longer than butyl. Refer to Scheme 4.4 for signals ascribed to butyl ($2B_4$), propyl ($1B_3$, $2B_3$ and $3B_3$) and ethyl isolated branches ($1B_2$, $2B_2$ and g", see Scheme 4.4).*

In contrast, 1-octene and 1-decene polymers generated with **Ni1** result in more rearranged structures. The ^{13}C NMR spectra clearly show signals due to carbons of

ethyl ($1B_2$ at 9.0 ppm), propyl ($1B_3$ at 12.5, $2B_3$ at 18.0 ppm and $3B_3$ at 34.6 ppm), and butyl branches ($2B_4$ at 21.1 ppm) (Figure 4.26 B).[50] Although these signals are small in comparison to the others, their presence indicates that insertion paths, different from those shown in Scheme 3.2 in Chapter III, become more competitive. The presence of these branches reflects a significant extent of chain-walking and the high propensity of **Ni1** to promote 2,1-insertion.

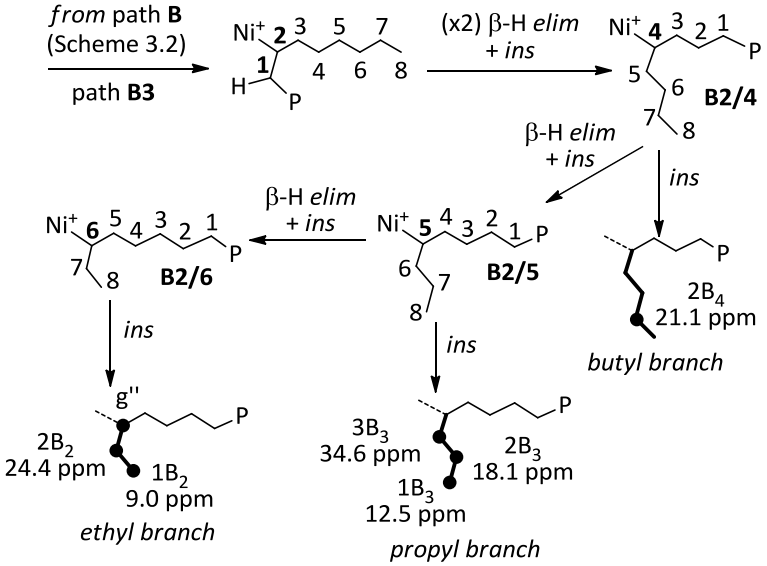

Scheme 4.4. *Mechanism for the formation of butyl, propyl and ethyl branch (β–H elim + ins = β–H elimination and insertion; ins = monomer insertion) for 1-octene polymerization (g'' at 37.4 ppm).*

We found that 1-octene polymer includes a 3% of ethyl branch, 2% of propyl branch, and 1% of butyl branch, while the 1-decene polymer includes a 8% of ethyl branch, 4% of propyl branch, and 2% of butyl branch (Table 4.11). These results indicate that the intermediate B2/6 in Scheme 4.5, formed when the metal is at C6 position (C8 for 1-decene), which installs an ethyl branch in the polymer chain, is stable enough (and most favored) to allow further monomer insertion, followed by the intermediate B2/5 formed when the metal is at C5 (which installs a propyl branch; C7 for 1-decene) and B2/4 formed when the metal is at C4 (which installs a butyl branch; C6 for 1-decene).

On the other hand, the 1-octadecene sample generated with **Ni1** show only methyl and long branches (Figure 4.26 A). This suggests that insertion of 1-octadecene into a secondary Ni–alkyl bond do not occur with **Ni1** and that the

metal prefers to migrate to ω carbon: the 2,1-insertion of 1-octadecene preferentially evolves into a 18,1-enchainment to give long methylene sequences (Scheme 3.2, path B1, Chapter III).

The length of the monomer significantly affects the branch type distribution, long branches being increasingly predominant as the α-olefin size increases (Table 4.11). The higher percentage of longer than butyl branches with respect to methyl branches indicates that after a 1,2-insertion (or 2,1-ins) a further 1,2 insertion (or 2,1-ins) without chain-walking is favored (Scheme 3.2, path A2 or B2, Chapter III). The amount of ω,2-enchainment, which installs a methyl in the polymer chain (Scheme 3.2, path A1, Chapter III), decreases in favor of 1,2-enchainment (or 2,1-enchainment) (which installs a long branch) with increasing the monomer size. This is likely due to the fact that the probability of migration up to the terminal ω carbon of the last-inserted monomer unit decreases for longer α-olefins.[51]

On the whole, chain-walking occurs more frequently in the polymerization of α-olefins catalyzed by **Ni1** and the formation of ethyl, propyl, and butyl branches also indicates that insertion into a secondary Ni–alkyl bond, particularly for 1-octene and 1-decene, occurs. Therefore, the fact that **Ni1** spends most time walking along the polymer chain, rendering linear PE-like units (much more favorable ω,1-enchainment) and alkyl branching of different lengths may contribute also to its low turnover rate, which in turn limits the molecular weight of the polymers that can be achieved (Table 4.10).[25]

Further information comes from ^{13}C NMR spectrum (Figure 4.26). All the polymers show weak signals at 38.4 and 40.6 ppm ascribed to α,α-methylene carbons (s1 and s2, respectively) and at 18.3 ppm ascribed to a methyl carbon (s3 of structure YX, Figure 4.26).[52] According to previous assignment,[9] s1 at 38.4 ppm corresponds to the α,α-methylene carbon of the structure YY–CH(R)CH_2CH(R)– (R > butyl), while s2 at 40.6 ppm to the α,α-methylene carbon of the structure XY–CH(R)CH2CH(Me)– (R > butyl). We can relate these signals to the mechanistic pathways. Indeed, on the basis of the chain-walking coordination/insertion mechanism model, the structure YY comes from two successive 1,2-insertions without chain-walking (Scheme 4.5, path C1a), while structures XY and YX come from a 1,2-insertion on the last 1,2-enchained unit followed by chain-walking: XY if nickel gives chain-walking to ω′ (Scheme 4.5, path C1b), YX if nickel gives chain-walking to ω (Scheme 4.5, path C1c).

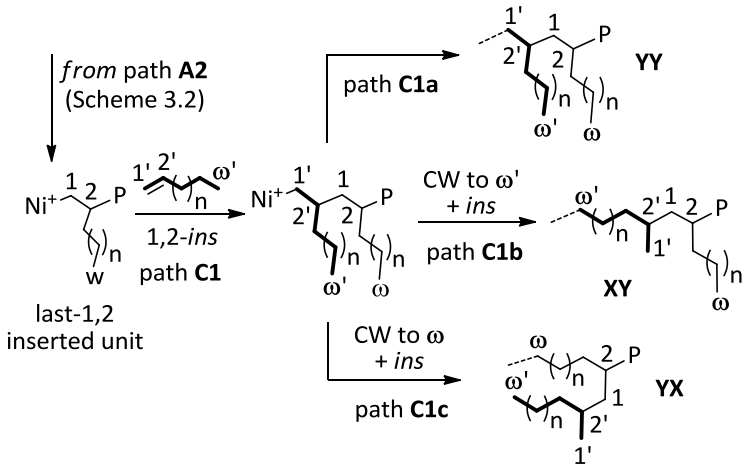

Scheme 4.5. *Modes of monomer enchainment before the last 1,2-inserted unit (CW = chain-walking; ins = new further insertion; 1,2-ench = 1,2-enchainment).*

Changes in the branching density and distribution affect the thermal properties of the polymers. The thermal behavior of the polymers was investigated by DSC, and the results are reported in Table 4.11. Figure 4.27 A shows the thermograms of the polymers synthesized with **Ni2**. Glass transition events at low temperature and broad melting endotherms can be observed. Generally, T_g, T_m, and ΔH_m of the resulting polymers increase with increasing the monomer length. Despite comparable ω,1 fraction (Table 4.10), the length of linear segments increases with the monomer chain length, resulting in higher melting points.

Figure 4.27 B compares the thermograms of all the 1-decene polymers. The polymer from **Ni1** (Table 4.11, entry 24) exhibits the highest T_m (72 °C) and crystallinity (19%). Among the other investigated complexes, **a Ni2** bearing bulky isopropyl group gives the polymer with the highest T_m (54 °C) and crystallinity (14%). DSC analysis of 1-decene polymers by less bulky complexes, *i.e.*, **Ni3**–**Ni5**, shows comparable broad endotherms with similar melting point and enthalpy. A similar trend of melting behavior as a function of nickel complex was observed for 1-octene and 1-octadecene polymers. The thermal data are strictly related to the polymer microstructure, T_m and ΔH_m increasing with the increase of crystallizable methylene sequences generated from the ω,1-enchainment. Figure 4.27 C plots ΔH_m versus the number of branches longer than methyl. A relationship between the two data was found and enhancing the content of longer than methyl side groups the melting enthalpy decreases. An analogous trend was observed for T_m.

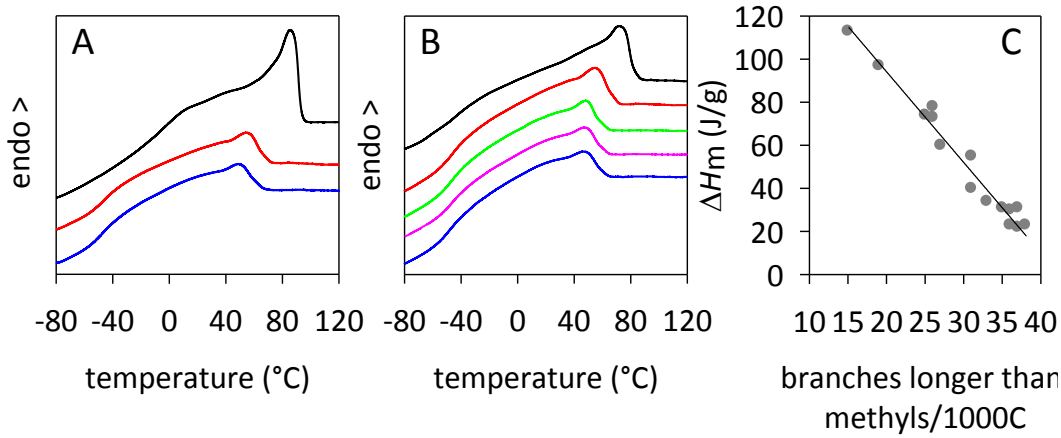

Figure 4.27. *DSC traces of (A) 1-octene, 1-decene and 1-octadecene polymer from* ***Ni2*** *(entry 20, 25 and 30, from bottom to top), (B) 1-decene polymers obtained from* ***Ni1–Ni5*** *(entries 24–28 from top to bottom). (C) Plot of melting enthalpy (ΔH_m) as a function of the total branching longer than methyl. The line is a guide to the eye and illustrates the overall trend.*

The synthesized polymers were structurally characterized by X-ray techniques. WAXD patterns of 1-octene and 1-decene polymers obtained with **Ni2**–**Ni5** show a diffuse peak centered at about 2θ = 20°, while the patterns of the polymers from **Ni1** show a weak peak at about 2θ = 21.5° followed by a broad shoulder, thus confirming an increase in the crystalline content (Figure 4.28 A). The WAXD data together with the low T_ms and broad melting range suggest the existence of a fringed-micellar crystal structure with a broad size distribution that comes from the statistical distribution of crystallizable chain lengths.[18,19] WAXD diffractograms of 1-octadecene polymers show the typical diffractions of poly(ethylene) orthorhombic crystalline structure: sharp patterns were collected for entries 29 and 30 (from **Ni1** and **Ni2**) while the profiles result less definite for entries 31, 32, and 33 (from **Ni3**–**Ni5**) characterized by lower crystallinity degree (Figure 4.28 B).

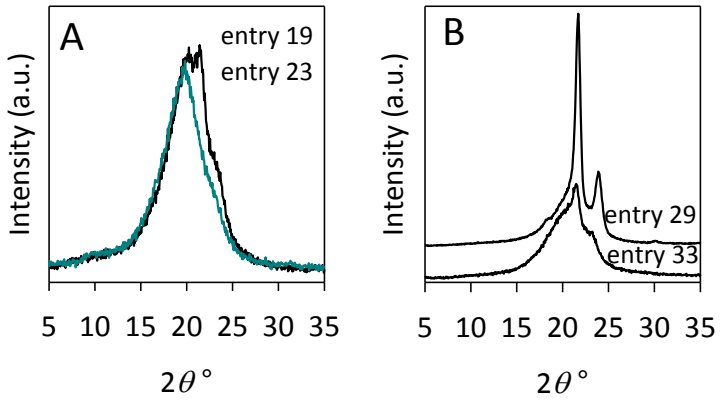

***Figure 4.28**. WAXD profiles of (A) 1-octene polymers from **Ni1** and **Ni5** (entry 19 and 23) and (B) 1-octadecene polymers from **Ni1** and **Ni5** (entry 29 and 33).*

Mechanical Properties

First investigation on the mechanical behavior of 1-octene, 1-decene and 1-octadecene polymers obtained with **Ni2**–**Ni5** was carried out at 20 °C by uniaxial stretching until failure. The tensile properties are summarized in Table 4.12 and selected stress-strain curves are shown in Figure 4.29.

Figure 4.29 A shows the tensile strength curves of the polymers obtained with **Ni2**. 1-Octene and 1-decene polymers show stress-strain curves with typical features of elastomers, *i.e.*, low modulus, and high elongation at break. Compared to these polymers, 1-octadecene polymer exhibits different tensile behavior due to longer crystallizable methylene sequences in the polymer backbone, with higher modulus and ultimate strength, but lower elongation at break. The stress−strain curve of 1-octadecene polymer exhibits more evident yielding phenomena and a steady increase of the stress (Figure 4.29 A).

Figure 4.29 B compares the tensile strength curves of 1-decene polymers generated using **Ni2**–**Ni5**. The strain deformation of the more crystalline polymer from **Ni2** (Table 4.12, entry 25) proceeds with the highest Young's modulus (7.5 MPa) and stress at break (15 MPa). 1-Decene polymers from **Ni3**–**Ni5**, which have similar crystallinity, exhibit comparable tensile behaviour with a Young's modulus of about 4 MPa and ultimate tensile strength, in the range from 9.0 to 10.5 MPa.

Table 4.12. *Mechanical properties.*

entry	E [a] (MPa)	σ [a] (MPa)	ε [a] (%)	SR_I [b]	SR_X [c]	$SR_{550\%}$ [d]	$SR_{1200\%}$ [e]
1-octene							
20	5.8±0.7	10.6±1.0	1420±90	65	54	63	59
21	2.1±0.4	5.4±0.6[f]	>1900[g]	79	67	76	71
22	1.9±0.4	3.6±0.5[f]	>1900[g]	80	66	75	68
23	2.1±0.3	2.8±0.3[f]	>1900[g]	75	61	71	63
1-decene							
25	7.5±0.3	15.5±0.4	1388±29	59	47	56	53
26	4.1±0.5	10.6±1.6	1397±87	67	54	65	63
27	3.8±0.9	9.6±1.0	1503±65	64	50	61	59
28	3.6±0.4	9.0±1.2	1476±77	62	48	60	57
1-octadecene							
30	48.7±1.5	22.9±1.0	670±48	27	16	16	n.d.[h]
31	38.4±1.9	17.4±1.4	638±72	20	12	14	n.d.[h]
32	32.1±2.0	20.7±1.3	774±69	23	13	15	n.d.[h]
33	30.5±2.2	20.4±1.6	799±50	22	13	16	n.d.[h]

[a] Young's modulus (E), ultimate tensile strength (σ), and elongation at break (ε); [b] Strain recovery measured after the first step in a step cycle test type at 300% strain; [c] Strain recovery measured after the last step in a step cycle test type at 300% strain; [d] Strain recovery measured after the strain at 550% in a step cycle test type at increasing strains; [e] Strain recovery measured after the strain at 1200% in a step cycle test type at increasing strains; [f] Stress at 1900%; [g] Instrument detection limit; [h] The specimens break before the strain at 1200% in a step cycle test type at increasing strains.

All the 1-decene polymers showed high and similar ultimate strain (about 1450±50%), regardless of crystallinity. A similar trend of Young's modulus as a function of the crystallinity was found for 1-octene polymers. However, it is worth emphasizing that the low crystallinity 1-octene polymers, *i.e.*, entries 21–23, display impressive strain at break values approaching 2000%. The 1-octadecene polymers differ mainly in Young's modulus, which ranges from 49 to 30 MPa with decreasing the polymer crystallinity (from 33 to 25%, Table 4.11).

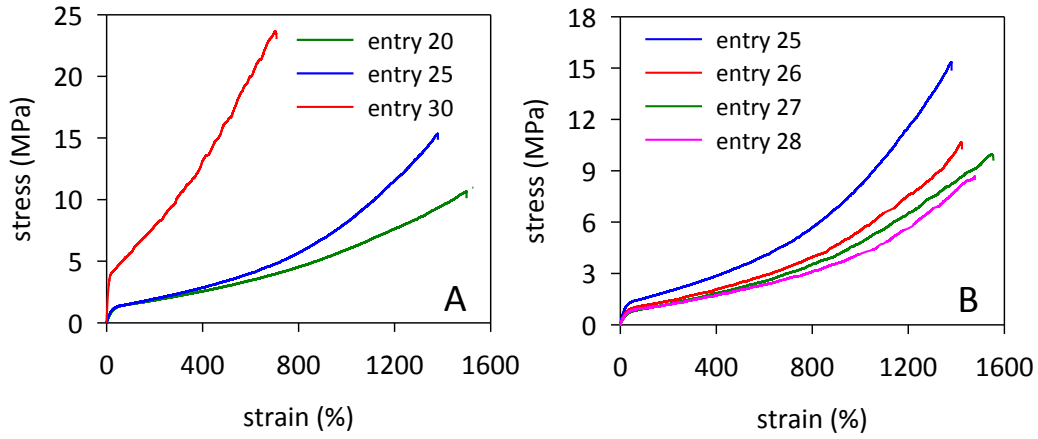

Figure 4.29. *Stress-strain curves of (A) 1-octene, 1-decene and 1-octadecene from* ***Ni2*** *(entry 20, 25 and 30) during monotonic tensile deformation and (B) 1-decene polymers from* ***Ni2–Ni5*** *(entries 25–28) during monotonic tensile deformation.*

The elasticity of the polymers was evaluated from step cycle tensile tests. In the first set of experiments, the samples were subjected to ten repetitive stress−strain cycles with a maximum of 300% strain, and the elastic recovery in specimen length was measured after removal of the strain for each cycle. The first cycle results in the most significant amount of permanent deformation, followed by minimal increase in the unrecovered strain on subsequent cycles (Figure 4.30).

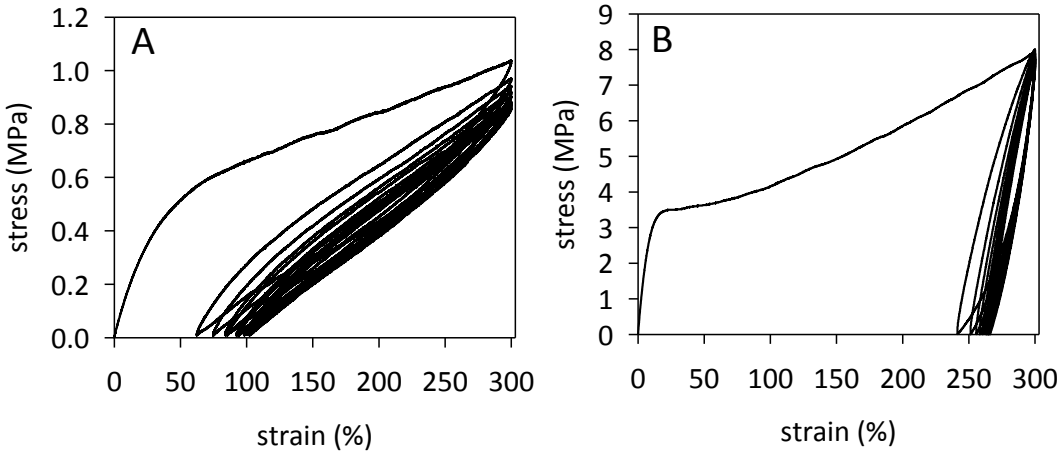

***Figure 4.30**. Stress-strain curve of (A) 1-octene polymer from **Ni3** (entry 21) and (B) 1-octadecene polymer from **Ni3** (entry 31) in the hysteresis experiment for ten cycles at 300% strain.*

The main difference between the cyclic deformation behavior of the investigated polymers is in the amount of unrecovered strain after the first cycle. For 1-octene and 1-decene polymers the strain recovery after the first load cycle ranges from 59 to 80% and increases with decreasing the polymer crystallinity (SR_I in Table 4.13). The more amorphous poly(1-octene)s (Table 4.12, entries 21–23) display similar recovery over the whole cycle tensile test and the highest elastic recovery of about 67% after the last load cycle (SR_X in Table 4.12, Figure 4.30 A). In contrast, 1-octadecene polymers exhibit high amount of permanent deformation after the first cycle with SR_I values ranging from 20 to 27% and very low strain recovery (ca. 15%) after the last cycle (Figure 4.30 B). These data indicate that the 1-octadecene polymers are not elastomers and permanently deform upon stretching.

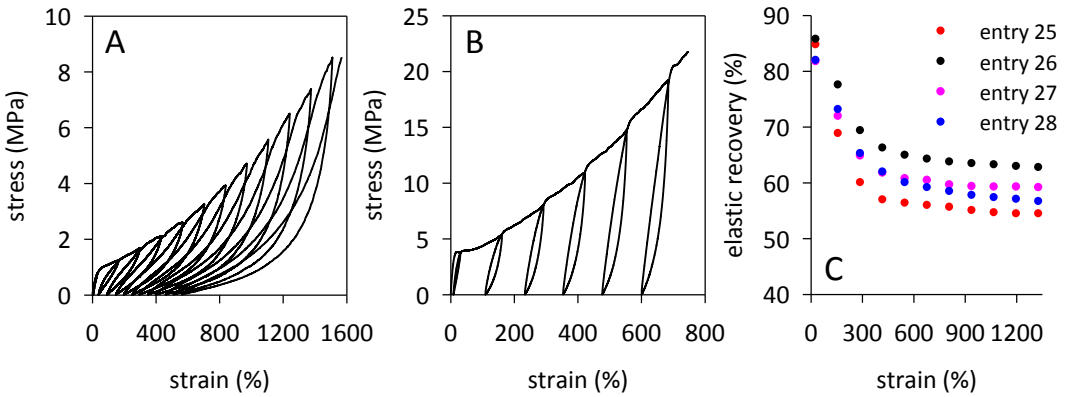

Figure 4.31. *Stress-strain curve of (A) 1-decene polymer from* ***Ni3*** *(entry 26) and (B) 1-octadecene polymer from* ***Ni3*** *(entry 31) during step cycle tensile deformation at different strain. (C) strain recovery as a function of the applied strain for 1-decene polymers from* ***Ni2–Ni5*** *(entries 25–28).*

In the second set of cyclic experiments, the samples were extended step by step up to different strains until fracture. As typical examples, the stress-strain curve during cyclic tensile deformation of 1-decene polymer (entry 26) and 1-octadecene polymer (entry 31) are shown in Figure 4.31 A and 4.31 B, respectively. Based on the curves, the strain recovery values were obtained (Table 4.12).

Generally, the strain recovery decreases rapidly at lower applied strains and then tends to level off at higher applied strains. As a typical example, the strain recovery as a function of the applied strain for 1-decene polymers is reported in Figure 4.31 C. 1-Octene and 1-decene polymers exhibit similar behavior with comparable and high SR values for the whole range of applied strains ($SR_{550\%}$ and $SR_{1200\%}$ in Table 4.12), whereas the 1-octadecene polymers present very low recovery of 15% when the strain was equal to 550%.

As a further experiment, the 1-octene and 1-decene polymers were subjected to creep test in order to evaluate their resistance to permanent deformation. Samples were elongated to 300% strain and held at a constant stress for 3 h. It is worth pointing out that every sample required typical stress value in order to achieve 300% strain (from 1.2 MPa for the low crystallinity 1-octene polymers to 2.8 MPa for the highest crystallinity 1-decene polymer). Selected strain-time curves are shown in Figure 4.32. The low crystallinity 1-octene and 1-decene polymers exhibited great deformation over time, particularly those generated with **Ni3**–**Ni5**.

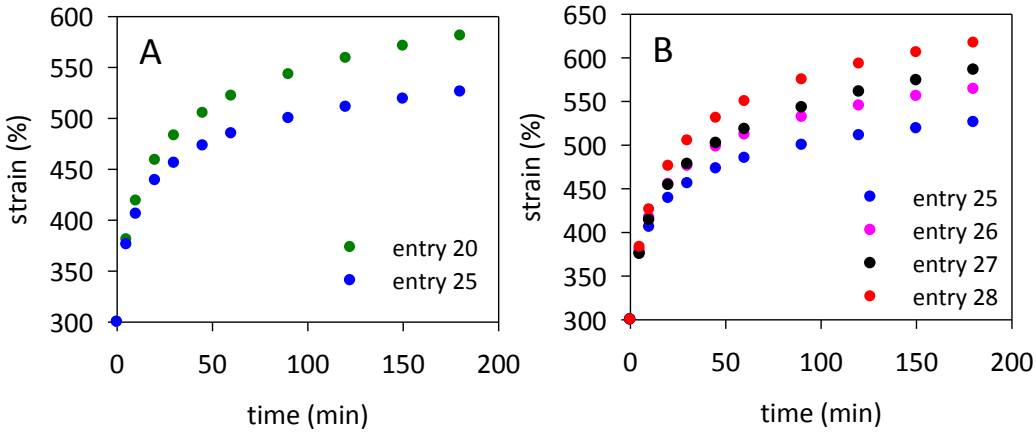

Figure 4.32. *Creep experiments of (A) 1-octene, 1-decene from* ***Ni2*** *(entry 20 and 25) and (B) 1-decene polymers from* ***Ni2–Ni5*** *(entries 25–28).*

Overall, the resulting polymers exhibited a broad spectrum of tensile properties, strongly depending on the crystallinity, that is the monomer length and the type of α-diimine ligand. The tensile tests show that 1-octene and 1-decene polymers behaved as elastomers with properties close to those reported in the literature for analogous polyolefin TPEs. [18,36,53] In contrast, 1-octadecene polymers behaved as plastomers, exhibiting properties intermediate between those of an elastomer and a LLDPE–like material.[35,54]

References

[1] Camacho, D. H.; Guan, Z. *Chem. Commun*. **2010,** *46*, 7879−7893.

[2] Leone, G.; Mauri, M.; Pierro, I.; Ricci, G.; Canetti, M.; Bertini, F. *Polymer* **2016**, *100,* 37–44.

[3] Pierro, I.; Leone, G.; Zanchin, G.; Canetti, M.; Ricci, G.; Bertini, F. *Eur. Polym. J.* **2017**, *93*, 200−211.

[4] Pierro, I.; Zanchin, G.; Parisini, E.; Martì-Rujas, J.; Canetti, M.; Ricci, G.; Bertini, F.; Leone, G. *Macromolecules* **2018**, *51*, 801−814.

[5] Leone, G.; Mauri, M.; Bertini, F.; Canetti, M.; Piovani,D.; Ricci, G. *Macromolecules* **2015**, *48*, 1304–131.

[6] Gao, H.Y.; Liu, X.F.; Tang, Y.; Pan, J.; Wu, Q. *Polym.Chem*. **2011**, *2*, 1398-1403.

[7] De Souza, R.F.; Simon, L.C.; Alves, M.D.C.M. *J.Catal*. **2003**, *214*, 165-168.

[8] Meinhard, D.; Wegner, M.; Kipiani, G.; Hearley, A.; Reuter, P.; Fischer, S.; Marti, O.; Rieger, B. *J. Am. Chem. Soc*. **2007**, *129*, 9182−9191.

[9] McCord, E. F.; McLain, S. J.; Nelson, L. T. J.; Ittel, S. D.; Tempel, D.; Killian, C. M.; Johnson, L. K.; Brookhart, M. *Macromolecules* **2007**, *40*, 410−420.
[10] Merna, J.; Hoštálek, Z.; Peleška, J.; Roda, J. *Polymer* **2009**, *50*, 5016−5023.
[11] Canetti, M. ; Leone, G.; Ricci, G.; Bertini, F. *Eur. Polym. J.* **2015,** *73*, 423-432.
[12] Liu, W.; Wang, W.J.; Fan, H.; Yu, L.; Li, B.G.; Zhu, S. *Eur. Polym. J.* **2014**, *54*, 160-171.
[13] Ittel, S. D.; Johnson, L. K.; Brookhart, M. *Chem. Rev.* **2000**, *100*, 1169−1204.
[14] Azoulay, J. D.; Bazan, G. C.; Galland, G. B. *Macromolecules* **2010**, *43*, 2794−2800.
[15] Usami, T.; Takayama, S. *Macromolecules* **1984**, *17,* 1756-1761.
[16] Subramanyam, U.; Rajamohanan, P.R.; Sivaram, S. *Polymer* **2004,** *45,* 4063-4076.
[17] O'Connor, K. S.; Lamb, J. R.; Vaidya, T.; Keresztes, I.; Klimovica, K.; LaPointe, A. M.; Daugulis, O.; Coates, G. W. *Macromolecules* **2017**, *50,* 7010−7027.
[18] Wang, H.P.; Chum, S.P.; Hiltner, A.; Baer, E. *J. Polym. Sci. Part B Polym. Phys.* **2009,** *47*,1313-1330.
[19] Alizadeh, A.; Richardson, L.; Xu, J.; McCartney, S.; Marand, H.; Cheung, Y. W.; Chum, S. *Macromolecules* **1999**, *32*, 6221−6235.
[20] Cotts, P. M.; Guan, Z.; McCord, E.; McLain, S. *Macromolecules* **2000***, 33,* 6945−6952.
[21] Wang, H.P.; Chum, S.P., Hiltner, A.; Baer, E. *J. Appl. Polym. Sci.* **2009,***113*, 3236-3244.
[22] Liu, W.; Zhang, X.; Bu, Z.; Wang, W.J.; Fan, H.; Li, B.G.; Zhu, S. *Polymer* **2015,** *72,* 118-124.
[23] Hölzer, S.; Menzel, M.; Zia, Q.; Schubert, U.S.; Beiner, M.; Weidisch, R. *Polymer* **2013**, *54*, 5207-5213.
[24] Burger, C.; Chen, X.; Mao, Y.; Hsiao, B.; Chen, H.; Marchand, G.R.; Lai, S.Y.; Chiu, D. *Macromolecules* **2010**, *43*, 1922-1929.
[25] Vaidya, T.; Klimovica, K.; LaPointe, A.M.; Keresztes, I.; Lobkovsky, E.B.; Daugulis, O.; Coates, G.W. *J. Am. Chem. Soc.* **2014**, *136*, 7213-7216.
[26] Morgan, S.; Ye, Z.; Subramanian, R.; Wang, W.-J.; Ulibarri, G. *Polymer* **2010,** *51*, 597–605
[27] Zou, H.; Zhu, F.; Wu, Q. *J. Polym. Sci.: Part A Polym. Chem.* **2008**, *46,* 2186–2192.
[28] Jerschow, A.; Ernest, E.; Hermann, W.; Muller, N. *Macromolecules* **1995**, *28*, 7095–7099.

[29] Naga, N.; Imanishi, Y. *Macromol. Chem. Phys.* **2002,** *203*, 159–165.
[30] Collins, S.; Kelly, W.M. *Macromolecules* **1992***, 25*, 233–237.
[31] McLain, S.J.; Feldman, J.; McCord, E.F.; Gardner, K.H.; Teasley, M.F.; Coughlin, E.B.; Sweetman, B.J.; Johnson, L.K.; Brookhart, M. *Macromolecules* **1998,** *31,* 6705–6707.
[32] Naga, N.; Imanishi, Y. *Polymer* **2002**, *43,* 2133–2139.
[33] Xiang, P.; Ye, Z.; Morgan, S.; Xia, X.; Liu, W. *Macromolecules* **2009,** *42*, 4946–4949.
[34] Bensason, S.; Minick, J.; Moet, A.; Chum, S.; Hiltner, A.; Baer, E. *J. Polym. Sci. Part B: Polym. Phys.* **1996**, *34*, 1301–1315.
[35] Peeters, M.; Goderis, B.; Reynaers, H.; Mathot, V. *J. Polym. Sci. Part B: Polym. Phys.* **1999,** *37,* 83–100.
[36] O'Connor, K.S.; Watts, A.; Vaidya, T.; LaPointe, A.M.; Hillmyer, M.A.; Coates, G.W. *Macromolecules* **2016,** *49*, 6743–6751.
[37] Gomes, C. S. B.; Gomes, P. T.; Duarte, M. T. *J. Organomet. Chem*. **2014**, *760,* 101−107.
[38] Wang, F.; Tanaka, R.; Cai, Z.; Nakayama, Y. M.; Shiono, T. *Polymers* **2016***, 8*, 160.
[39] Rhinehart, J. L.; Brown, L. A.; Long, B. K. *J. Am. Chem. Soc.* **2013**, *135*, 16316−16319.
[40] Allen, F. H. *Acta Crystallogr., Sect. B: Struct. Sci.* **2002**, *58*, 380−388.
[41] Tempel, D. J.; Johnson, L. K.; Huff, R. L.; White, P. S.; Brookhart, M. *J. Am. Chem. Soc.* **2000**, *122*, 6686−6700.
[42] Song, K.; Yang, W.; Li, B.; Liu, Q.; Redshaw, C.; Li, Y.; Sun, W.-H. *Dalton Trans.* **2013,** *42*, 9166−9175
[43] Dai, S.; Zhou, S.; Zhang, W.; Chen, C. *Macromolecules* **2016**, *49*, 8855−8862.
[44] Popeney, C. S.; Guan, Z. *Macromolecules* **2010***, 43*, 4091−4097.
[45] Xiao, L.; Gao, R.; Zhang, M.; Li, Y.; Cao, X.; Sun, W.-H. *Organometallics* **2009,** *28*, 2225−2233.
[46] Zhang, M.; Wang, K.; Sun, W.-H. *Dalton Trans*. **2009**, 6354−6363.
[47] Radlauer, M. R.; Day, M. W.; Agapie, T. *Organometallics* **2012**, *31*, 2231−2243.
[48] Gates, D. P.; Svejda, S. A.; Oñate, E.; Killian, C. M.; Johnson, L. K.; White, P. S.; Brookhart, M. *Macromolecules* **2000**, *33,* 2320−2334.
[49] Johnson, L. K.; Killian, C. M.; Brookhart, M. *J. Am. Chem. Soc*. **1995**, *117*, 6414−6415.

[50] Sheldrick, G. M. *SHELXTL Reference Manual; Siemens Analytical X-ray Systems, Inc.: Madison, WI*, **1996.**
[51] Rose, J. M.; Cherian, A. E.; Coates, G. W. *J. Am. Chem. Soc.* **2006**, *128*, 4186−4187.
[52] Hu, H.; Gao, H.; Chen, D.; Li, G.; Tan, Y.; Liang, G.; Zhu, F.; Wu, Q. *ACS Catal.* **2015**, *5*, 122−128.
[53] Wang, H. P.; Khariwala, D. U.; Cheung, W.; Chum, S. P.; Hiltner, A.; Baer, E. *Macromolecules* **2007,** *40*, 2852−2862.
[54] Wang, H. P.; Khariwala, D. U.; Cheung, W.; Chum, S. P.; Hiltner, A.; Baer, E. *Macromolecules* **2007**, *40*, 2852−2862.

Concluding remarks

Novel olefin homo- and co-polymers were prepared following two different synthetic strategies:

1) the first one is related to the synthesis of highly stereoregular poly(1,3-diene)s having different structures and their successive hydrogenation with diimide, formed in situ by thermal decomposition of *p*-toluenesulfonyl hydrazide (*p*-TsNH);

2) the second one regards the synthesis of branched and hyperbranched polyolefins through the chain-walking (co)polymerization of long chain α-olefins.

All the obtained polymers were fully characterized, in order to establish correlations between their structures and properties, and to evaluate their possible applications as thermoplastic and/or elastomeric materials.

As concern the first synthetic strategy highly stereoregular poly(1,3-diene)s having different structures (*i.e.*, *cis*-1,4; *trans*-1,4; 1,2; 3,4; iso-and syndiotactic) were synthesized by polymerizing various 1,3-dienes with catalytic systems based on transition metal and lanthanide organometallic compounds. The polymers obtained were successively hydrogenated obtaining *i)* highly stereoregular polyolefins from 1,2 and 3,4 polydienes and *ii)* perfectly alternating ethylene/α-olefin copolymers from 1,4 (*cis* and *trans*) poly(1,3-diene)s.

In particular, highly isotactic perfectly alternating ethylene/2-butene copolymers (E/2B), along with other ethylene/2-butene copolymers (E/2B) with a lower stereoregularity, were prepared by hydrogenation of the following stereoregular polydienes: diisotactic *trans*-1,4 poly(*E,E*-2,4-hexadiene), isotactic *cis*-1,4 poly(*E*-3-methyl-1,3-pentadiene), syndiotactic *cis*-1,4 poly(*E*-3-methyl-1,3-pentadiene), *cis*-1,4 poly(2,3-dimethyl-1,3-butadiene). The spectroscopic NMR characterization of the E/2B copolymers, and the schemes of polymerization and hydrogenation, allowed defining the different molecular structures of the four E/2B copolymers. The *racemo*-di-isotactic alternating E/2B copolymer obtained by hydrogenation of the di-isotactic *trans*-1,4 poly(*E,E*-2,4-hexadiene) is a novel polymer never reported before. Contrary to the *meso*-di-isotactic alternating E/2B copolymer prepared with Ziegler–Natta catalysts, which is crystalline, the *racemo*-di-isotactic E/2B copolymer is not able to crystallize, notwithstanding the regular relative configurations of two adjacent tetrahedral stereoisomeric centers (*racemo*), and the regular succession of configurations, diisotactic, of successive

monomeric units along the chain. All the alternating E/2B copolymers are amorphous. This is what expected for the four copolymers due to their predominantly atactic structure. All samples show mechanical properties with low values of the Young modulus, and low values of the stress at any strain, easy deformability and viscous flow at very high deformation.

Perfectly alternating ethylene/propylene (E/P) copolymers having isotactic, syndiotactic and atactic structures have been obtained by means of hydrogenation of highly stereoregular isotactic *cis*-1,4 poly(1,3-pentadiene), syndiotactic *cis*-1,4 poly(1,3-pentadiene) and *cis*-1,4 poly(isoprene), respectively. The copolymers were fully characterized by NMR (^{1}H, ^{13}C and 2D), XRD, and their thermal and mechanical properties were investigated. Despite their high stereoregularity, as clearly evidenced by the NMR analysis, all the copolymers were found to be amorphous, exhibiting low mechanical properties.

The following alternating copolymers were also prepared and characterized: *i*) alternating isotactic ethylene/1-butene copolymer, obtained by hydrogenation of isotactic *cis*-1,4 poly(1,3-hexadiene); *ii*) alternating ethylene/1-pentene copolymers, iso- and syndiotactic, obtained by hydrogenation of *cis*-1,4 poly(1,3-heptadiene)s, iso- and syndiotactic; *iii*) alternating ethylene/1-hexene copolymers, iso- and syndiotactic, obtained by hydrogenation of *cis*-1,4 poly(1,3-octadiene)s, iso- and syndiotactic. All these samples are amorphous.

By polymerizing 3-methyl-1,3-pentadiene with the catalyst $CoCl_2(PRPh_2)_2$/MAO (R = methyl, ethyl, *n*-propyl, isopropyl and cyclohexyl), the isotactic 1,2 poly(*E*-3-methyl-1,3-pentadiene) (iP3MPD) was obtained. iP3MPD is a new crystalline polymer that could not be synthesized with the classic stereospecific Ziegler-Natta catalysts but can be synthesized with catalysts based on cobalt complexes with various phosphines in combination with methylaluminoxane. The mechanical tests show that the elasticity of iP3MPD is an unusual case of a polymer that shows rubbery elastomeric properties below the glass-transition temperature.

As mentioned above, highly stereoregular polyolefins were instead obtained by hydrogenation of several 1,2 (or 3,4) polydienes.

Syndiotactic poly(3-methyl-1-butene) (sP3MB) has been obtained for the first time by hydrogenation of syndiotactic 3,4-poly(isoprene), which in turn had been synthesized by polymerizing isoprene with the catalyst system $FeCl_2$(2,2'-bipyridine)$_2$/MAO. The chains of sP3MB assume in the crystalline phase a 3/1 helical conformation, providing the first example of a syndiotactic polymer with 3-fold helical chains.

The synthesis and characterization of (*i*) syndiotactic poly(5-methyl-1-hexene), obtained by hydrogenation of syndiotactic *trans*-1,2 poly(5-methyl-1,3-hexadiene); (*ii*) syndiotactic 1,2 poly(heptene), obtained by hydrogenation of syndiotactic *trans*-1,2 poly(1,3-heptadiene); *(iii*) syndiotactic 1,2 poly(octene), obtained by hydrogenation of syndiotactic *trans*-1,2 poly(1,3-octadiene), were also reported.

Most of these polymers were completely new, being hardly obtainable by simple stereospecific polymerization of the corresponding α-olefins.

Some of the polymers obtained exhibited interesting properties for possible application as thermoplastic and elastomeric materials; however, being most of the monomers used for the preparation of the stereoregular poly(1,3-diene)s particularly expensive, they will hardly be able to find an industrial application, or, in any case, their possible use should be carefully assessed. However, their use as model polymers, useful for evaluating similar polymers, remains extremely significant.

As concern the second synthetic strategy the branched polyolefins were obtained by using a series of traditional α-diimine Ni(II) complexes with methyl ligand backbone and different substituents in *ortho*- and *para*- aryl positions as catalyst components, in combination with different aluminium alkyls.

In particular, I focused on the polymerization of 1-octene catalyzed by a traditional α–diimine Ni(II) complex (**Ni2**), in combination with different aluminum alkyls. I obtained the poly(1-octene)s with high yield, which are branched poly(ethylene)-like materials with high molecular weight. The polymers show two major branch lengths, *i.e.,* methyl and longer. The extent of chain-walking can be easily tuned by varying the polymerization conditions and reagents. The thermal properties and crystallinity of the poly(1-octene)s are strongly determined by their microstructure. The tensile tests showed that the poly(1-octene)s behave as thermoplastic elastomers exhibiting a low modulus, strain-hardening and an instantaneous strain recovery after fracture.

Three sets of 1-octene/1-decene (OCT/DE) and 1-octene/cyclopentene (OCT/CPE) random copolymers were synthesized with the use of α–diimine Ni(II) complex (**Ni2**). The resulting copolymers are mainly composed of long methylene segments, methyl branches and longer than methyl branches. The thermal properties and crystallinity of the resulting copolymers are strongly determined by their microstructure: the presence of long branches and rigid ring units interferes on the crystallization and melting behavior. The tensile tests show that the 1-

octene copolymers behave as TPEs exhibiting a low modulus, strain hardening at high strain and an instantaneous strain recovery. The OCT/CPE copolymers are found to have better strain recovery than homopolymers and OCT/DE copolymers, while the latter are more resistant to deformation.

Finally, I report an investigation on the polymerization of 1-octene, 1-decene and 1-octadecene catalyzed by a series of α-diimine Ni(II) complexes with methyl ligand backbone and different substituents in *ortho*- and *para*- aryl positions. The effect of ligand steric and electronic perturbation on the catalytic behavior, monomer enchainment, and polymer properties was discussed. We demonstrate that two methyl substituents on the *ortho*-positions of the α-diimine ligand are bulky enough to exhibit a certain steric effect, retarding the free rotation of aniline moieties, and hence decreasing the β–H elimination and subsequent chain-transfer. This feature allows the synthesis of high molecular weight polymers, more branched than those obtained with bulky *iso*-propyl and *tert*-butyl substituents, while maintaining high turnover frequencies. In addition, **Ni5**, with two methyl groups on the *ortho*-positions and a methyl on the *para*-position, was more active than its *para*-hydrogen **Ni4** complex suggesting that the presence of the methyl in the *para* position has a further positive effect on the turnovers/h due to the stabilization of the reactive, electron-deficient and coordinatively unsaturated alkyl agostic intermediate. Moreover, it is pointed out that under short polymerization time, *i.e.,* assuming no complications due to mass transfer limitations and insufficient mixing, modifying the *ortho* substituents from methyl to *iso*-propyl groups, the complexes bearing less bulky methyl groups afford higher molecular weight polymers at significantly higher turnovers/h. The thermal properties and crystallinity of the polymers vary depending on the extent of branching and the branch-type distribution. The tensile tests show that the 1-octene and 1-decene polymers behave as elastomers exhibiting low modulus, high elongation at break and good elastic recovery, while 1-octadecene polymers show evident yielding phenomena and plastic deformation.

These systems prove great prospect due to the low cost and accessibility of starting reagents and monomer feedstocks, the high turnovers/h together with the reusability of the resulting polymers that retain excellent mechanical properties even after being melted and reprocessed several times.

Other projects

In parallel to the PhD project on the hydrogenation of stereoregular poly(1,3-diene)s and chain-walking polymerization, I was also involved in other research projects that involve the ISMAC laboratory with which I collaborated, namely:

- Some aspects concerning the $TiCl_4$–promoted polymerization of dicyclopentadiene (DCPD) have been studied. The results prove that the presence of the double bond in the cyclopentene ring, the peculiar spatial disposition of the cyclopentene in the *endo*-DCPD and the oligomerization conditions play a key role in the formation of a unique crystalline polymer. Hydrogenation and epoxidation of the obtained products are reported as well.

The results have been published on *Macromol. Chem. Phys*. **2017**, *218*, 1600602.

- A wide library of V(III) and V(IV) complexes was synthesized, allowing the comprehension of the influence of the different steric and electronic properties of the employed ligand on the catalytic behavior and polymerization mechanism. The V–catalyzed copolymerization of ethylene with various cyclic olefins brought to mainly alternating copolymers. In addition, the study on vanadium complexes allowed us to get more insight into some drawbacks correlated with vanadium catalysis, such as the facile reduction to V(II), and the compositional drift that takes place during copolymerization experiments.

The results have been published on *Organometallics* **2018**, *37*, 3181−3195; *Journal of Organometallic Chemistry*, **2018**, *861,* 142-150; *Journal of Molecular Catalysis A: Chemical*, **2016**, *424*, 220-231.

- Some V complexes, in combination with MAO, were active in the polymerization of 1,3-butadiene, affording poly(1,3-butadiene)s with different microstructure (*cis*-1,4, *trans*-1,4 or 1,2) depending on the type of ligand.

The results have been published on *Catalysts*, **2017**, *7,* 369.

Appendix

Experimental Section

Manipulations of air- and/or moisture-sensitive materials were carried out under an inert atmosphere using a dual vacuum/ni-trogen line and standard Schlenk-line techniques.

Materials

Toluene (Fluka, ≥99.7% pure) and heptane (Aldrich, >99% pure) were refluxed over Na for about 8 h and then distilled and stored over molecular sieves under nitrogen. *o*-Xylene (Aldrich, anhydrous grade), *p*-toluenesulfonyl hydrazide (*p*-T*s*NH, Aldrich), acetone (Aldrich, anhydrous grade), were used as purchased.

Diethylaluminium chloride (Et_2AlCl, Fluka), triisobutylaluminum [$Al(^iBu)_3$, Aldrich, 98% pure], methylaluminoxane (MAO) (10 wt % solution in toluene, Aldrich), and modified-methylaluminoxane (MMAO, 7 wt % solution in heptane, Akzo Nobel) were used as received.

The monomers used in the Chapter II are: 3-Methyl-1,3-pentadiene (Fluka, 96% pure, mixture of (*E*) and (*Z*) isomers), (*E,E*)-2,4-hexadiene (Aldrich, 98% pure), 2,3-dimethyl-1,3-butadiene (Aldrich, 98% pure), (*E*)-1,3-pentadiene (96% pure, Fluka), isoprene (98% pure, Aldrich), 1,3-hexadiene (Aldrich, 99% pure, mixture of (*E*) and (*Z*) isomers), 1,3-heptadiene (Chemsampco, 99% pure; predominantly *E* isomer), 1,3-octadiene (Chemsampco, 99% pure; predominantly *E* isomer), 5-methyl-1,3-hexadiene (Chemsampco, 80% pure; predominantly *E* isomer). These monomers were refluxed over calcium hydride for about 4 h, then distilled trap-to-trap, and stored under nitrogen.

$Nd(OCOC_7H_{15})_3$ (Strem Chemicals, Bischheim, France) was used as received. $Ni(acac)_2$ (Aldrich, 95%) was used as received. $CoCl_2(P^nPrPh_2)_2$ was prepared as described in ref. [1] $CoCl_2(P^tBu_2Me)_2$ was prepared as described in ref. [2] $CoCl_2(P^iPrPh_2)_2$ and $FeCl_2(bipy)_2$ were prepared as described in refs. [3,4], respectively.

The monomers used in the Chapter IV are: 1-Octene (Aldrich, 98% pure), 1-decene (DE) (Aldrich, 95% pure) and cyclopentene (Aldrich, 96% pure). These monomers were refluxed over CaH_2 for 4 h, then distilled via trap-to-trap and

finally stored under nitrogen and kept at -15°C. 1-Octadecene (Aldrich, ≥95%) was degassed under vacuum then by bubbling nitrogen, kept over molecular sieves and used without any further purification.

The α-diimine Ni(II) complexes **Ni1–Ni6**, were synthesized using a known procedure.[5] Single crystal, suitable for X-ray structure determination, were obtained for **Ni3–Ni6** from a cold CH_2Cl_2 solution.

Deuterated solvent for NMR measurements ($C_2D_2Cl_4$) (Cambridge Isotope Laboratories, Inc.) was used as received.

Polymerization

The experimental conditions for the dienes polymerizations and for the hydrogenated polymers are reported in Chapter II.

The (co)polymerizations synthesized with α-diimine Ni(II) complexes-based catalysts were carried out in a 25 mL round-bottomed Schlenk flask. The reactor was first dried by heating at 110°C and then vacuum was applied for 1 h. Toluene, (co)monomers, Et_2AlCl and a toluene solution of catalyst (2 mg/mL) were transferred into the reactor vessel in that order. Polymerization was quenched with methanol containing a small amount of hydrochloric acid. The precipitated polymers were collected by filtration, repeatedly washed with fresh methanol and then dried to constant weight. 1-Octadecene polymers were then extracted with acetone through the Soxhlet method for 12 h to remove the unreacted monomer.

Hydrogenation procedure

The hydrogenation was carried out in a round-bottom flask equipped with a magnetic stirring, a reflux condenser, nitrogen inlet port, and temperature controller. Typically, the specified amount of the unsaturated polymer was dissolved in *o*-xylene. The reaction mixture was continuously stirred at room temperature until the polymer was completely dissolved. *p*-T*s*NH was added, and the mixture was brought to reflux by slowly heating to 120 °C. After 3 days, the mixture was allowed to cool spontaneously to room temperature and further *p*-T*s*NH was added. This operation was repeated once again. Upon completion of the reaction, the hydrogenated sample was hot-filtered, the volume of the filtered solution was reduced under vacuum, and the dissolved polymer precipitated by adding methanol and collected by filtration. The polymer was dried under vacuum at room temperature, and then it was extracted with acetone through a Soxhlet

method for 10 h in order to remove any excess *p*-T*s*NH and byproducts of the *p*-T*s*NH decomposition. The residual fraction was finally dried under vacuum, dissolved in toluene, precipitated with methanol, and dried again under vacuum at room temperature to a constant weight.

Characterization

^{13}C and ^{1}H NMR measurements were carried out on a Bruker Avance 400 spectrometer. The spectra were obtained in $C_2D_2Cl_4$ at 103 °C (hexamethyldisiloxane, HMDS, as internal standard). The concentration of polymer solutions was about 10wt %. The ^{13}C parameters were the following: spectral width 17 kHz; 90° pulse 11.0 μs PL1-5.0 dB, with a delay of 16 s. The 2D spectra were acquired on a Bruker AVANCE DRX 600 MHz (14.1 T) at 330 K. The g-HSQC experiment was performed by applying a coupling constant $^{1}J_{CH}$ = 130 Hz; data matrix 2K × 256; number of scans 128, 90° pulse calculated for each sample, PL1-2.2 dB.

Proton broad-band decoupling was achieved with a 1D sequence using bi_waltz_16_32 power-gated decoupling. ^{1}H NMR spectroscopy was used to determine overall branching.[6] The fraction of ω,1-insertions (reported in Chapter IV) was calculated from the equation reported by Brookhart.[7] ^{13}C NMR spectroscopy was used to examine the types of branches. The quantitative analysis was based on the equations reported by Galland.[8] ^{1}H NMR spectroscopy was used to examine the total branching, according to Rieger *et al*.[6] by equation (1) :

$$(1) \quad total\,\frac{branching}{1000C} = \frac{\frac{1}{3}I_{CH_3}}{\frac{\left(I_{CH_2}-\left(\frac{1}{3}I_{CH_3}\right)\right)}{2}+\frac{1}{3}I_{CH_3}} \times 1000$$

The fraction of ω,1-insertions was calculated using the equation (2) reported by Brookhart et al.[7]

$$(2) \quad \omega, 1 = \frac{1000-a\mathrm{B}}{1000+2\mathrm{B}}$$

where B is the total branching calculated by equation (1), and *a* = (number of carbon atoms in the monomer – 2).

The molecular weight averages (M_w) and the molecular weight distribution (M_w/M_n) were obtained by a high temperature Waters GPCV2000 size exclusion chromatography (SEC) system using two online detectors: a differential

viscometer and a refractometer. The experimental conditions consisted of three PL Gel Olexis columns, *o*-DCB as the mobile phase, 0.8 mL min^{-1} flow rate, and 145 °C temperature. Universal calibration of the SEC system was performed using 18 narrow M_w/M_n polystyrene standards with molar weights ranging from 162 to 5.6 × 106 g mol^{-1}. For the analysis, about 12 mg of the polymer was dissolved in 5 mL of *o*-DCB with 0.05% of BHT as the antioxidant.

Structural, thermal and mechanical analysis for poly(1,3-diene)s and hydrogenated polymers

X-ray powder diffraction profiles were obtained with Ni-filtered Cu K_α radiation with an automatic diffractometer X-Pert by Panalytical. Thermal analysis was performed with a differential scanning calorimeter Mettler-DSC30/2285, equipped with a liquid nitrogen cooling system for measurements at low temperature. The scans were recorded in flowing nitrogen atmosphere at heating or cooling rates of 10 °C/min. Compression-molded samples were prepared by heating the dry precipitated powders at 120 °C for 10 min under a press at very low pressure and cooling to room temperature by circulating cold water inside the press plates.

Mechanical tests have been performed at room temperature on compression-molded films with a universal mechanical tester Zwicky by Zwick Roell, following the standard test method for tensile properties of thin plastic sheeting ASTM D882-83. Rectangular specimens 10 mm long, 5 mm wide, and 0.3 mm thick have been stretched up to the break or up to a given deformation $\varepsilon = 100 \times (L_f - L_0)/L_0$, where L_0 and L_f are the initial and final lengths of the specimen, respectively. Two benchmarks have been placed on the test specimens and used to measure elongation. For some samples the elastic properties have been quantified by performing at least three mechanical cycles of stretching and relaxation at room temperature on the compression-molded films and recording the corresponding hystereses. In the first cycle specimens of compression-molded films of initial length L_0 have been stretched up to a final lengths L_f, that is, up to a deformation $\varepsilon = 100 \times (L_f - L_0)/L_0$ lower than that at which viscous flow begins, and then relaxed at controlled rate. The final length of the relaxed specimens L_r is measured 10 min after the end of the relaxation step. This value of the specimen length corresponds to the initial length L_i of the specimen in the successive cycle. In each cycle the specimen is stretched always up to the same final length L_f, that is, at the

same final deformation ε = 100 × (L_f −L_0)/L_0, to avoid viscous flow. After each cycle, the values of the tension set, that is, the residual deformation after recovery, has been calculated as t_s = [(L_r − L_i)/L_i] × 100, where L_i is the initial length of the specimen at the beginning of the cycle and L_r is the length of the relaxed sample at the end of the cycle. The percentage of dissipated energy (E_{diss}) has been evaluated as the area of the hysteresis, that is, the difference between the area under curves of the stretching and relaxation steps. In the mechanical tests the ratio between the drawing rate and the initial length was fixed equal to 0.1 mm/(mm × min) for the measurement of Young's modulus and 10 mm/(mm × min) for the measurement of stress−strain curves and the determination of the other mechanical properties (stress and strain at break and tension set). The reported stress−strain curves and the values of the mechanical properties are averaged over at least five independent experiments. From the stress-strain curve the strain recovery (SR) can be calculated by equation:

$$(3) \quad SR = \frac{\varepsilon_a - \varepsilon_r}{\varepsilon_a} \times 100$$

where ε_a is the applied strain and ε_r is the strain in the cycle at zero load after the applied strain.

Structural, thermal and mechanical analysis for (co)polymers synthesized by α-diimine Ni(II) complexes

Differential scanning calorimetry (DSC) measurements were performed on a Perkin–Elmer DSC 8000 instrument equipped with a liquid nitrogen device. The scans were carried out from -100 to 130 °C under nitrogen atmosphere using heating and cooling rates of 20 °C/min. The crystallinity (X_{DSC}) was calculated from the DSC scans as follows: $X_{DSC} = (\Delta H_f/\Delta H_0) \times 100$, where ΔH_f is the enthalpy associated with the melting of the sample and ΔH_0 is the melting enthalpy of a 100% crystalline poly(ethylene) taken equal to 290 J/g.[9]

Wide angle X-ray diffraction (WAXD) data were obtained at 18 °C using a Siemens D-500 diffractometer equipped with a Siemens FK 60-10 2000W tube (Cu K_α radiation, λ = 0.154 nm). The operating voltage and current were 40 kV and 40 mA, respectively. The data were collected from 5 to 35 $2\theta^\circ$ 0.02 $2\theta^\circ$ intervals.

The materials for structural and mechanical characterization were molded in a press at 90 °C (1-octene and 1-decene polymers) or 110 °C (1-octadecene

polymers) and 50 bar for 5 min, then the press plates were cooled at 20 °C/min to room temperature. Films with a thickness of about 150 μm were produced. Tensile dog-bone-shaped specimens (length overall 75 mm, gauge length 25 mm, and width of narrow section 4 mm) were analyzed at 20 °C using a Zwick Roell ProLine Z010 mechanical tester equipped with a XforceP (50 N) load cell at a constant crosshead rate of 15 mm/min. In the hysteresis experiments performed at the fixed strain of 300% or a gradually increased strain between 30 and 1750%, the specimens were cyclically loaded and unloaded in uniaxial tension. The strain recovery (SR) was calculated as SR = 100 $(\varepsilon_a-\varepsilon_r)/\ \varepsilon_a$, where ε_a is the applied strain and ε_r is the strain in the cycle at zero load after the applied strain. For each material, at least five samples were tested for extension experiments and two samples for strain recovery tests.

For single crystal X-Ray diffraction, the diffraction data were collected at room temperature for Ni3−Ni5 and at 100 K for Ni6 using a Bruker X8 Prospector APEX-II/CCD diffractometer equipped with a focusing mirror (Cu Kα radiation, λ = 1.54178 Å). The structures were determined using direct methods and refined (based on F2 using all independent data) by full-matrix least-squares methods (SHELXTL 97).[10,11]

All non-hydrogen atoms were located from different Fourier maps and refined with anisotropic displacement parameters. Hydrogen atoms were added in riding positions.

References

[1] Ricci, G.; Forni, A.; Boglia, A.; Sommazzi, A.; Masi, F. *J. Organomet. Chem*. **2005***, 690*, 1845

[2] Ricci, G.; Forni, A.; Boglia, A.; Motta, T. *J. Mol. Catal. A: Chem*. **2005**, *226*, 235-241

[3] Ricci, G.; Forni, A.; Boglia, A.; Motta, T.; Zannoni, G.; Canetti, M.; Bertini, F. *Macromolecules* **2005**, *38*, 1064-1070.

[4] Ricci, G.; Morganti, D.; Sommazzi, A.; Santi, R.; Masi, F. *J. Mol. Cat A:* Chemicals **2003**, *204/205*, 287-293.

[5] O'Connor, K. S.; Lamb, J. R.; Vaidya, T.; Keresztes, I.; Klimovica, K.; LaPointe, A. M.; Daugulis, O.; Coates, G. W. *Macromolecules* **2017**, *50,* 7010−7027.

[6] Meinhard, D.; Wegner, M.; Kipiani, G.; Hearley, A.; Reuter, P.; Fischer, S.; Marti, O.; Rieger, B. *J. Am. Chem. Soc*. **2007**, *129*, 9182−9191.

[7] McCord, E. F.; McLain, S. J.; Nelson, L. T. J.; Ittel, S. D.; Tempel, D.; Killian, C. M.; Johnson, L. K.; Brookhart, M. *Macromolecules* **2007**, *40*, 410−420.

[8] Azoulay, J. D.; Bazan, G. C.; Galland, G. B. *Macromolecules* **2010**, *43*, 2794−2800.

[9] Simanke, A.G.; Alamo, R.G.; Galland, G.B.; Mauler, R.S. *Macromolecules*, **2001**, *34* 6959–6971.

[10] Sheldrick, G. M. *SHELXTL Reference Manual; Siemens Analytical X-ray Systems, Inc.: Madison, WI*, **1996**.

[11] Sheldrick, G. M. A Short History of SHELX. *Acta Crystallogr.,Sect. A: Found. Crystallogr.* **2008**, *64*, 112−122

PhD Course Activity Summary

CANDIDATE: IVANA PIERRO
SUPERVISOR: PROF. CLAUDIO DE ROSA (UNINA)
CO-SUPERVISOR: DR. GIOVANNI RICCI (CNR-ISMAC)

1) Attended Courses:

- *Structural Analysis of Materials at Nanometer Length Scale with Small Angle X-ray Scattering* (12h) – Prof. Finizia Auriemma
- *Application of the Conformational Analysis to the Structural Studies of Synthetic Polymers* (8h) – Prof. Beniamino Pirozzi
- *Advanced Mass Spectrometry Course* (10h) – Prof. Pietro Pucci
- *Nanostructures and nanotechnologies* (6h) – Prof. Claudio De Rosa
- *Morphology of polymers* (24h) – Dr. Rocco di Girolamo
- *The techniques of solid-liquid extraction used in the preparation of the sample for chemical analysis and production of extracts for industrial uses* (8h) – Prof. Daniele Naviglio

2) Pubblications:

- De Rosa C., Malafronte A., Scoti M., Auriemma F., Pierro I., Leone G., Ricci G. "Synthesis and structure of syndiotactic poly(3-methyl-1-butene): a case of 3/1 helical conformation for syndiotactic polymers" *Macromolecules* **2018**, *51*, 8574-8584.
- Zanchin, G. , Vendier, L., Pierro, I., Bertini, F., Ricci, G., Lorber, C., Leone, G. "Homo- and co-polymerization of ethylene with cyclic olefins catalyzed by phosphine adducts of (innido)vanadium(IV) complexes" *Organometallics* **2018**, *37*, 3181−3195.
- Zanchin G., Pierro I., Parisini E., Marti-Rujas J., Ricci G., Leone G. "Synthesis, structure and behavior of vanadium(III) diphosphine complexes in the homo- and co-polymerization of ethylene with norbornene: the ligand donor strength and bite angle make the difference" *Journal of Organometallic Chemistry*, **2018**, *861,* 142-150.

- Pierro I., Zanchin G., Parisini E., Marti-Rujas J., Canetti M., Ricci G., Bertini F., Leone G. "Chain-walking polymerization of α-olefins by α-diimine Ni(II) complexes: the effect of reducing the steric hindrance of *ortho*- and *para*-aryl substituents on the catalytic behavior, monomer enchainment and polymer properties" *Macromolecules*, **2018,** *51*, 801-814.
- De Rosa C., Scoti M., Auriemma F., Malafronte A., Santillo C., Zanchin G., Pierro I., Leone G., Ricci G. "Mechanical Properties of Isotactic 1,2-Poly(*E*-3-methyl-1,3-pentadiene): An Example of Rubbery Elasticity below Glass Transition Temperature" *Macromolecules*,**2018**, *51*, 488-496.
- Leone G., Zanchin G., Pierro I., Sommazzi A., Forni A., Ricci G. "Synthesis, Structure and 1,3-Butadiene Polymerization Behavior of Vanadium (III) Phosphine Complexes" *Catalysts*, **2017**, *7,* 369.
- Pierro I., Leone G., Zanchin G., Canetti M., Ricci G., Bertini F. " Polyolefin thermoplastic elastomers from 1-octene copolymerization with 1-decene and cyclopentene" *European Polymer Journal*, **2017**, *93*, 200-211.
- De Rosa C., Auriemma F., Santillo C., Scoti M., Malafronte A., Zanchin G., Pierro I., Leone G., Ricci G. "Crystal Structure and Properties of Isotactic 1,2-Poly(*E*-3-Methyl-1,3-Pentadiene)" *Macromolecules*, **2017**, *50*, 5412-5424.
- Zanchin G., Leone G., Pierro I., Rapallo A., Porzio W., Bertini F., Ricci G. ''Addition Oligomerization of Dicyclopentadiene: Reactivity of *Endo* and *Exo* Isomers and Post modification'' *Macromol. Chem. Phys***. 2017**, *218*, 1600602.
- Ricci G., Boccia A.C., Leone G., Pierro I., Zanchin G., Scoti M., Auriemma F., De Rosa C. "Isotactic and Syndiotactic Alternating Ethylene/Propylene Copolymers Obtained Through Non-Catalytic Hydrogenation of Highly Stereoregular *cis*-1,4 Poly(1,3-diene)s" *Molecules*, **2017**, *22*, 755.
- Ricci G., Leone G., Boccia A.C., Pierro I., Zanchin G., Mauri M., Scoti M., Malafronte A., Auriemma F., De Rosa C. "Perfectly Alternating Ethylene/2-Butene Copolymers by Hydrogenation of Highly Stereoregular 1,4-Poly(1,3-diene)s: Synthesis and Characterization" *Macromolecules*, **2017**, *48*, 1304-1312.
- Leone G., Pierro I., Zanchin G., Forni A., Bertini F., Rapallo A., Ricci G. "Vanadium (III)-catalyzed copolymerization of ethylene with norbornene: Microstructure at tetrad level and reactivity ratios" *Journal of Molecular Catalysis A: Chemical*, **2016**, *424*, 220-231.

- Leone G., Mauri M., Pierro I., Ricci G., Canetti M., Bertini F. "Polyolefin thermoplastic elastomers from 1-octene chain-walking polymerization"" *Polymer*, **2016**, *100*, 37-44.

3) Attended congresses/workshops:

Attended congresses and contributions:

- Poster and Oral Presentation "*Polyolefins by hydrogenation of stereoregular poly(1,3-diene)s and chain-walking mechanism polymerization: synthesis, structure and mechanical properties*" Macrogiovani 2017, Trento 22-23 June 2017 (Italy) Pierro I.
- Poster Presentation "*Polyolefins by hydrogenation of stereoregular poly(1,3-diene)s and chain-walking mechanism polymerization: synthesis, structure and mechanical properties*" Milan Polymer Days 14^{th}-16^{th} February 2018 (Italy) Pierro I.
- Poster Presentation "*1-Octene copolymers with 1-Decene and cyclopentene by an α-diimine Ni(II)/$AlEt_2Cl$ catalyst: synthesis, thermal and mechanical behavior*" Milan Polymer Days 15^{th}-16^{th} February 2017 (Italy) Pierro I., Leone G., Zanchin G., Ricci G., Canetti M., Bertini F.
- Poster contribution "*Cr(II) and Cr(III) complexes with pyridine-imine ligands: synthesis and application in the polymerization of olefins*" Milan Polymer Days 15^{th}-16^{th} February 2017 (Italy) Zanchin G., Leone G., Pierro I., Bertini F., Ricci G.
- Poster Presentation "*Thermoplastic elastomers from 1-octene polymerization catalyzed by α- diimine nickel based catalysts*" Blue Sky Conference, Sorrento (Italy) 27^{th} June – 1 July 2016 Pierro I., Leone G., Ricci G., Canetti M., Bertini, F.
- Poster Presentation "*Synthesis, structure and ethylene/norbornene copolymerization behaviour of $VCl_3(PMePh_2)_2$*" Blue Sky Conference, Sorrento (Italy) 27^{th} June – 1 July 2016 Leone G., Pierro I., Zanchin G., Forni A., Bertini F., Rapallo A., Ricci, G.
- Poster contribution "*Ti(IV)-Catalyzed Polymerization of Dicyclopentadiene: a study on endo/exo-isomers reactivity and post-polymerization modification*" Blue Sky Conference, Sorrento (Italy) 27^{th} June – 1 July 2016 Zanchin G., Pierro I., Leone G., Rapallo A., Porzio W., Ricci, G.

Workshops:

- Poster Presentation "*Syndiotactic poly(α-olefin)s by hydrogenation of highly stereoregular 1,2 (3,4) syndiotactic polydienes*" - Workshop on Italian-Nordic Polymer Future - Pisa (Italy) 14 – 15 September 2017 Ricci G., Leone G., Pierro I., Zanchin G., Consiglio S., Boccia A.C., Scoti M., Malafronte A., Auriemma F., De Rosa C.
- Poster Presentation "*Perfectly alternating olefin copolymers by hydrogenation of stereoregular cis-1,4 iso- and syndiotactic polydienes*" - Workshop on Italian-Nordic Polymer Future, Pisa (Italy) 14th–15th September 2017 Ricci G., Leone G., Pierro I., Zanchin G., Consiglio S., Boccia A.C., Scoti M., Malafronte A., Auriemma F., De Rosa C.
- Poster contribution "*Vanadium (III) phosphine complexes: synthesis, characterization and behavior in the polymerization of 1,3-butadiene*" - Workshop on Italian-Nordic Polymer Future, Pisa (Italy) 14th–15th September 2017 Ricci, G., Sommazzi, A., Zanchin G., Pierro I., Forni A., Leone G.
- Poster contribution "*Polymerization of butadiene and isoprene with bis-imine, pyridil-imine and keto-imine vanadium complexes based catalysts*", Workshop on Italian-Nordic Polymer Future (Italy) 14th–15th September 2017 Ricci, G., Sommazzi, A., Zanchin G., Pierro I., Guelfi M., Pampaloni G., Leone G.